

# **Mitochondrial dysfunction as a therapeutic target in Parkinson's Disease**

**Thomas Payne**

MBChB, MRCP

**Department of Neuroscience**

A thesis submitted to the University of Sheffield for the degree  
of Doctor of Philosophy

Submitted April 2022

***The problem is not to find the best or most efficient method to proceed to a discovery, but to find any method at all.***

Richard P. Feynman

## Contents

Contents.....	3
Acknowledgements .....	7
Abstract .....	8
Abbreviations .....	9
List of Figures.....	13
List of Tables.....	15
Chapter 1: Introduction.....	16
Parkinson's Disease .....	16
Epidemiology .....	17
Clinical Features.....	17
Current Treatments.....	20
Pathological features .....	21
Pathogenesis.....	22
Genetics .....	22
Mitochondria in health .....	23
Mitochondrial dysfunction in Parkinson's Disease .....	25
Lysosomal Dysfunction.....	28
Alpha-synuclein .....	28
Neuroinflammation .....	30
Bile acids and gastrointestinal dysbiosis .....	30
Developing Neuroprotective therapies in Parkinson's Disease .....	32
Common challenges to neuroprotective trial design in Parkinson's .....	32
Cohort stratification .....	33
Clinical endpoint design.....	34
Stratification of Parkinson's Disease according to mitochondrial dysfunction .....	38
Genetic stratification .....	38
Stratification using blood, urine and cerebrospinal fluid biomarkers .....	39
Stratification of mitochondrial dysfunction in patient derived peripheral tissue ..	42
Stratification of bioenergetic function in the brain using <sup>31</sup> Phosphorous Magnetic Resonance Spectroscopy .....	44
Methodological basis of spectroscopy .....	45
Acquisition of MR signal and methodological considerations .....	47
Localisation in Magnetic Resonance Spectroscopy .....	51
Quantitation of Magnetic Resonance Spectroscopy Signal .....	52
Considerations in <sup>31</sup> Phosphorus Magnetic Resonance Spectroscopy .....	55

Previous <sup>31</sup> P-MRS studies to assess mitochondrial dysfunction in Parkinson's disease and related disorders .....	56
Previous studies to assess lysosomal dysfunction in Parkinson's Disease ....	61
Identifying mitochondrial Rescue therapies .....	66
Drug screens to identify mitochondrial rescue agents .....	66
Ursodeoxycholic acid.....	66
Aims and Objectives .....	68
Aims.....	68
Objectives.....	69
Chapter 2: Methods.....	70
The Ursodeoxycholic acid in Parkinson's Study (The UP Study).....	70
Contributions to published paper .....	70
Published Paper: Ursodeoxycholic acid as a novel disease-modifying treatment for Parkinson's disease: protocol for a two-centre, randomised, double-blind, placebo-controlled trial, The 'UP' study.....	71
Additional Methodological Detail.....	72
Clinical Assessment.....	72
Genetic Analysis .....	74
<sup>31</sup> Phosphorous Magnetic Resonance Spectroscopy Acquisition .....	74
<sup>31</sup> Phosphorous Magnetic Resonance Spectroscopy Analysis .....	78
Quantification of partial volume effects .....	83
Serum bile acid profiling .....	84
Statistical Analysis .....	84
Mechanistic stratification of Parkinson's disease using <sup>31</sup> Phosphorus Magnetic Resonance Spectroscopy and patient derived tissue fibroblasts .....	87
Participants, Recruitment, Consent and schedule of activities .....	87
<sup>31</sup> Phosphorus Magnetic Resonance Spectroscopy and morphometric analysis	90
Clinical Assessment.....	90
Skin biopsy and establishment of fibroblast cell lines .....	91
Assessment of mitochondrial function in fibroblast cell lines .....	92
Mitochondrial Membrane Potential, mitochondrial morphology and lysosomal morphology.....	92
Intracellular ATP.....	94
Cross-sectional statistical Analysis .....	94
<sup>31</sup> Phosphorus magnetic resonance spectroscopy statistical analysis.....	94
Patient-derived fibroblast cell assay statistical analysis.....	95
Assessing relationships between <sup>31</sup> Phosphorus magnetic resonance spectroscopy and fibroblast cell assays .....	96

Cross-sectional sample size sample size calculations.....	97
Longitudinal <sup>31</sup> Phosphorus Magnetic Resonance Spectroscopy statistical analysis .....	97
Chapter 3: The UP study confirms the neuroprotective potential of ursodeoxycholic acid in Parkinson's disease .....	99
Introduction to chapter .....	99
Contributions to published paper .....	99
Manuscript in preparation for submission .....	100
<b>Abstract</b> .....	102
<b>Introduction</b> .....	103
<b>Methods</b> .....	105
<b>Results</b> .....	119
<b>Discussion</b> .....	139
Chapter 4: Combining <sup>31</sup> Phosphorus magnetic resonance spectroscopy and patient derived peripheral tissue to mechanistically stratify Parkinson's disease.....	145
Introduction to chapter .....	145
Phospholipids in <sup>31</sup> P-MRS.....	145
Contributions to published paper .....	146
Manuscript in preparation for submission .....	147
<b>Abstract</b> .....	149
<b>Introduction</b> .....	150
<b>Methods</b> .....	152
<b>Results</b> .....	160
<b>Discussion</b> .....	175
<b>Supplementary Figures</b> .....	179
Chapter 5: Longitudinal assessment of <sup>31</sup> Phosphorus magnetic resonance spectroscopy and relationships to clinical progression.....	181
Introduction to chapter .....	181
Contributions to paper.....	181
Paper in preparation for submission .....	181
<b>Abstract</b> .....	183
<b>Introduction</b> .....	184
<b>Methods</b> .....	186
<b>Results</b> .....	190
<b>Discussion</b> .....	199
Chapter 6: Discussion .....	204
The UP Study and early phase neuroprotective trial design .....	204
Previous neuroprotective trials targeting mitochondrial dysfunction .....	204

Quantification of motor impairment .....	207
Target engagement .....	208
Cohort stratification .....	209
Limitations of The UP Study .....	210
Future directions .....	211
<sup>31</sup> P-magnetic resonance spectroscopy and the assessment of patient derived peripheral tissue as tools for mechanistic stratification of Parkinson's Disease .....	216
Relationships between <sup>31</sup> P-MRS measured brain bioenergetics and the <i>in vitro</i> assessment of mitochondria in patient derived peripheral tissue .....	216
Longitudinal changes in <sup>31</sup> P-MRS and the relationship to clinical progression	217
Limitations of <sup>31</sup> P-Magnetic Resonance Spectroscopy .....	218
Limitations of tissue fibroblasts .....	219
Future directions .....	220
Conclusions .....	221
References .....	223
Appendices .....	239
Appendix 1: Development of analysis protocol for <sup>31</sup> P-Magnetic Resonance Spectroscopy .....	239
Appendix 2: List of R packages used in data analysis .....	241

## Acknowledgements

I would first like to thank all the organisations and charities that have supported the work included in this thesis. I am forever grateful to The Cure Parkinson's Trust, The Jon Moulton Charity Trust, The Michael J Fox Foundation, and the NIHR Sheffield Biomedical Research Centre.

I am grateful to all in my supervisory team who have taught me the scientific skills needed to succeed in my projects. It is hard to believe that it was over a decade ago that I first met my primary supervisor Professor Oliver Bandmann, who took an eager medical student under his wing and has supported me in all my academic endeavours since. I would not be where I am today without him. Dr Thomas Jenkins, my secondary supervisor, has helped guide my developing skills in neuroimaging and has always provided a thoughtful and keen eye for detail. Professor Heather Mortiboys has provided me the opportunity to develop my knowledge and understanding of mitochondria and guided all my forays into fibroblast tissue culture. I would also like to thank the late Professor Iain Wilkinson, who ignited my interest in magnetic resonance physics as I was starting upon my PhD journey.

I like to extend my sincere gratitude to all the participants who kindly took part in these research studies, both people with Parkinson's and healthy volunteers. Without their enthusiasm to take part in research, none of this would have been possible. Everyone I have encountered in my research studies has genuinely made translational research a joy to work in. I hope that in my future career I can contribute to developing treatments to slow down or stop Parkinson's Disease altogether.

I would also like to thank Liam Haslam, the research nurse who supported these studies, the staff of the radiographers and support staff of the Academic Unit of Radiology and the NIHR Sheffield Biomedical Research Centre team who all helped facilitate and support this research and have always been welcoming of me.

Finally, I would like to give my everlasting thanks to my wife Daisy and our cat Rosa. The life of a clinical academic is filled with trials and tribulations that I never would have been able to get through without their unconditional support.

## Abstract

**Introduction:** Mitochondrial dysfunction is a key pathogenic mechanism leading to neuronal cell death in Parkinson's disease (PD). Ursodeoxycholic acid (UDCA) has shown great promise in preclinical models of PD. This thesis investigates the safety and tolerability of UDCA in PD in a phase IIa/proof of concept clinical trial, the UP study. In parallel, <sup>31</sup>P Phosphorus Magnetic Resonance Spectroscopy (<sup>31</sup>P-MRS) and patient derived tissue fibroblasts were utilised to mechanistically stratify PD for future PD neuroprotection trials.

**Methods:** *UP study:* 30 participants were randomized in a 2:1 fashion to UDCA 30 mg/kg vs placebo. Standard clinical rating scales were complemented by sensor-based gait analysis. Midbrain target engagement of UDCA was assessed applying <sup>31</sup>P-MRS. *Mechanistic stratification:* <sup>31</sup>P-MRS measures of bioenergetic dysfunction in the putamen and midbrain were correlated with the assessment of the mitochondria and lysosomes in fibroblasts in 35 patients with recent onset PD and 25 controls.

**Results:** *UP study:* UDCA was safe and extremely well tolerated in PD. Gait impairment deteriorated less or improved in the UDCA group compared to placebo. <sup>31</sup>P-MRS detected an improvement in the efficiency of ATP hydrolysis in the UDCA group, suggesting target engagement. *Mechanistic stratification:* Midbrain phosphocreatine levels correlated inversely with predicted risk of rapid disease progression. Low <sup>31</sup>P-MRS putaminal ATP was associated with changes in mitochondria and lysosomes consistent with impaired mitophagy. Longitudinal <sup>31</sup>P-MRS revealed reduced phospholipid membrane synthesis in the putamen of PD which could be consistent with the ongoing neurodegenerative process.

**Conclusion:** The UP study results can be used to aid the design of future phase IIb/III clinical trials to investigate further the neuroprotective potential of UDCA. <sup>31</sup>P-MRS may be a useful tool for disease stratification for future PD neuroprotection trials according to mitochondrial dysfunction.

## Abbreviations

1-Methyl-4-phenylpyridinium ion	MPP+
<sup>31</sup> P Phosphorous Magnetic Resonance Spectroscopy	<sup>31</sup> P-MRS
8-hydroxy-2-deoxyguanosine	8-OHdG
8-Hydroxyguanosine	8-OHG
Adenosine Diphosphate	ADP
Adenosine Triphosphate	ATP
Advanced method for accurate, robust and efficient spectral fitting	AMARES
Analysis of variance	ANOVA
B1 insensitive selective train to obliterate signal	BISTRO
Catechol-O-methyltransferase	COMT
Cerebrospinal fluid	CSF
Chemical shift imaging	CSI
Chenodeoxycholic acid	CDCA
Cholic acid	CA
Creatine	Cr
Deoxycholic acid	DCA
Depth-resolved surface-coil spectroscopy	DRESS
Dihyronicotinamide adenine dinucleotide	NADH
Dimethylsulfoxide	DMSO
Eagles Minimum Essential Media	EMEM
Echo time	TE
Farnesoid X receptor	FXR
Fetal bovine serum	FBS
Fibroblast growth factor 21	FGF-21
Free induction decay signal	FID
Gibbs free energy of ATP hydrolysis	$\Delta G_{ATP}$
Glucocerebrosidase	GCase
Glycerophosphorylcholine	GPC
Glycerophosphorylethanolamine	GPE
Glycoursodeoxycholic acid	GUDCA
Grey matter	GM

Growth differentiation factor 15	GDF-15
Hazard ratio	HR
High energy phosphates	HEPs
Hoehn and Yahr	H&Y
Image-selected <i>In Vivo</i> spectroscopy	ISIS
l-Methyl-4-phenyl-1,2,5,6-tetrahydropyridine	MPTP
Induced neuronal progenitor cells	iNPCs
Inorganic phosphate	Pi
Insulin receptor substrate 1	IRS-1
Levodopa equivalent dosage	LED
Likelihood ratios	LR
Lithocholic acid	LCA
Magnetic resonance imaging	MRI
Magnetic resonance spectroscopy	MRS
Mild cognitive impairment	MCI
Minimal clinically important difference	MCID
Mini Mental State Examination	MMSE
Mitochondrial DNA	mtDNA
Mitochondrial membrane potential	MMP
Monoamine oxidase B inhibitors	MAO-B
Montreal Cognitive Assessment	MoCA
Movement Disorders Society	MDS
Movement Disorders Society Unified Parkinson's Disease Rating Scale	MDS-UPDRS
Multiple System Atrophy	MSA
Net magnetisation vector	NMV
Nicotinamide Adenine Dinucleotide	NAD
Non-motor symptoms rating scale	NMSS
Nuclear overhauser enhancement	NOE
Oxidative phosphorylation	OXPHOS
Parkinson's Disease dementia	PDD
Parkinson's Disease	PD
Parkinson's Disease Questionnaire	PDQ-39

Patient information sheet	PIS
Peroxisome proliferator-activated receptor- $\gamma$	PPAR- $\gamma$
Peroxisome proliferator-activated receptor-gamma coactivator-1 $\alpha$	PGC-1 $\alpha$
Phosphoglycerate kinase 1	PGK1
Phosphocholine	PC
Phosphocreatine	PCr
Phosphodiesterases	PDE
Phosphoethanolamine	PE
Phosphomonoesters	PME
Phosphatidylcholine	PtdCho
Phosphatidylethanolamine	PtdEth
Physical activity monitor	PAM
Point resolved spectroscopy	PRESS
Postural instability gait disorders	PIGD
Potassium buffered saline	PBS
PTEN-induced putative kinase 1	PINK1
Radiofrequency	RF
Reactive oxygen species	ROS
Region of interest	ROI
Rapid eye movement	REM
Rapid eye movement sleep behaviour disorder	RBD
Repetition time	TR
Signal-to-noise ratio	SNR
Single nucleotide polymorphisms	SNPs
Schwab and England Activities of Daily Living scale	SEADL
Sphingosine-1-phosphate receptor 2	S1PR2
Stimulated echo acquisition mode	STEAM
Takeda G-protein-coupled receptor 5	TGR5
Tauroursodeoxycholic acid	TUDCA
Tetramethylrhodamine	TMRM
Tremor-dominant	TD
Tyrosine hydroxylase	TH

Ubiquitin-specific protease 30	USP-30
Ultra-performance liquid chromatography linked to mass spectrometry	UPLC-MS
Ursodeoxycholic Acid	UDCA
White matter	WM

## List of Figures

Figure 1.1: The electron transport chain and oxidative phosphorylation. ....	26
Figure 1.2: Stratification of Parkinson's Disease to facilitate precision medicine approaches in neuroprotective trials .....	40
Figure 1.3: The basis of Magnetic Resonance Spectroscopy .....	48
Figure 1.4: Image-selected In Vivo spectroscopy (ISIS).....	54
Figure 2.1: Localisation of <sup>31</sup> P-MRS 2D CSI acquisition sequences .....	77
Figure 2.2: AMARES quantification of <sup>31</sup> P-MRS.....	80
Figure 3.1: The UP Study Assessment overview. ....	107
Figure 3.2: Gait analysis equipment and data processing.....	111
Figure 3.3: The Dynaport MoveMonitor+ .....	113
Figure 3.4: <sup>31</sup> Phosphorus Magnetic Resonance voxel localisation, example spectra and results.....	116
Figure 3.5: Consort flowchart of enrollment, allocation and follow-up assessments performed.....	120
Figure 3.6: Impact of UDCA upon serum bile acid profiles.....	123
Figure 3.7: Changes in core gait parameters across all participants.....	133
Figure 3.8: Individual changes in key gait and spectroscopic parameters.....	134
Figure 3.9: Changes in <sup>31</sup> P-MRS derived measures acquired from the mean posterior putamen baseline to week 48 between treatment groups. ....	138
Figure 4.1: <sup>31</sup> Phosphorus magnetic resonance spectroscopy methodology.....	155
Figure 4.2: <sup>31</sup> P-MRS in PD compared to controls.....	163
Figure 4.3: <sup>31</sup> P-MRS measured phospholipids acquired from the mean midbrain, mean posterior putamen and mean anterior putamen. ....	166
Figure 4.4: Fibroblast assay results in PD compared to controls .....	168
Figure 4.5: Fibroblast measures of mitochondrial and lysosome function/morphology; correlations between measures for both PD and controls.....	170
Figure 4.6: Correlations between <sup>31</sup> P-MRS measures and fibroblast assay data... ..	172
Figure 4.7: <sup>31</sup> P-MRS measured putaminal inorganic phosphate and relationships to fibroblast assay results.....	173
Figure 4.8: <sup>31</sup> P-MRS measured midbrain ATP and inorganic phosphate and relationships to fibroblast assay results.....	174
Supplementary Figure 4.1: Fibroblast assay results in each media type.....	179

Figure 5.1: Key <sup>31</sup> P-MRS spectroscopy at each time point and by disease group.	195
Figure 5.2: Change in each individual across all key <sup>31</sup> P-MRS parameters in the mean posterior putamen. ....	196
Figure 5.3: <sup>31</sup> P-MRS midbrain bioenergetics and phospholipid measures at baseline and follow-up. ....	197
Figure 5.4: Correlation of <sup>31</sup> P-MRS midbrain phosphocreatine and semantic fluency score. ....	198

## List of Tables

Table 1.1: Movement Disorders Society Unified Parkinson's Disease Rating Scale	36
Table 1.2: Previous studies of <sup>31</sup> P Magnetic Resonance Spectroscopy in Parkinson's Disease	65
Table 2.1: Modified Hoehn and Yahr Scale	74
Table 2.2: Prior knowledge used for the AMARES method of spectral quantification for both midbrain and putamen	81
Table 2.3: Inclusion and Exclusion Criteria	88
Table 2.4: Schedule of Assessments	89
Table 3.1. The UP Study: Demographic and clinical features	121
Table 3.2. The UP Study: Details of Adverse Treatment Reactions	126
Table 3.3. Results of secondary outcomes	130
Table 3.4: Summary results of 7-day physical activity monitoring	135
Table 4.1: Demographic and clinical features of the study cohort	161
Table 4.2: <sup>31</sup> P-MRS summary results	165
Table 4.3 Fibroblast assay summary statistics for the entire study cohort in both media conditions	169
Table 5.1: Demographic features of the study cohort	190
Table 5.2: Clinical features of participants with PD	191
Table 5.3: Summary of key <sup>31</sup> P-MRS parameters in the mean midbrain, mean posterior putamen and mean anterior putamen	193
Appendix Table 1: means and ranges of manually defined <sup>31</sup> P-MRS peaks in and linewidths in 10 healthy controls	240
Appendix Table 2: R packages used in analysis and presentation of all thesis data	241

# Chapter 1: Introduction

## Parkinson's Disease

Parkinson's disease (PD) is the second most common neurodegenerative condition after Alzheimer's disease.<sup>1</sup> PD is not only a movement disorder comprising progressive gait and motor disturbance, but can also lead to cognitive impairment, neuropsychiatric complications and autonomic dysfunction.<sup>2</sup> It is relentlessly progressive and incurable. There are no disease-modifying treatments for PD. The lack of disease-modifying therapy has substantial financial implications, with costs of £25-60K per patient per year in advanced PD.<sup>3</sup> Therefore, there is a great unmet need in developing neuroprotective treatments to both slow down disease progression for those with PD and reduce the associated socioeconomic impact as a whole.

PD was first described by James Parkinson in 1817, even to this day the description of several cases he offered still bear striking resemblance to what is observed in clinic today.<sup>4</sup> Over 200 years since the description of the 'Shaking Palsy' much has been learnt of PD and the broad pathological and clinical features that define the disease.

It is becoming increasingly clear that there is considerable heterogeneity between individual patients in the pathogenic mechanisms causing PD. This marked heterogeneity is likely to have been a key reason for the failure of previous attempts to identify disease-modifying treatment for PD.

The design of successful neuroprotective trials in the future will depend on a 'personalised medicine' approach. To facilitate such trials, tools need to be developed to successfully stratify patients according to their individual pathogenic mechanisms. Ideally, these tools should then also be able to confirm target engagement of the putative neuroprotective compound and objectively quantify disease progression.

Mitochondrial dysfunction is a key pathogenic mechanism that has been implicated in the pathogenesis of PD since decreased mitochondrial complex I activity was reported in post mortem brain tissue of patients with sporadic PD.<sup>5</sup> Mitochondrial dysfunction has been identified as a highly promising therapeutic target for disease modification in PD.<sup>6,7</sup>

## Epidemiology

PD is an age-related disorder with increasing prevalence with age and affects men slightly more than woman. The majority of patients have onset in later life and typically over 65 years of age, although approximately 25% of patients will have onset before this age.<sup>8</sup> PD is a disorder rapidly increasing in prevalence with 6.1million people globally affected by the disease in 2016 compared to 2.5million in 1990.<sup>9</sup> This is not simply due to a globally ageing population as age-standardised rates still increased by 21.7%.<sup>9</sup>

There are several risk factors and prodromal features to PD, which are of great interest in the context of designing future neuroprotective trials as identifying and intervening in the neurodegenerative process earlier would potentially be of great benefit. The Movement Disorders Society (MDS) has produced detailed information on the definition of prodromal PD based upon several risk factors and additional clinical features (discussed in greater detail below) all expressed as likelihood ratios.<sup>10</sup> Likelihood ratios (LR) express the ratio of the probability of finding a feature in those with a certain disease (in this case PD) to the probability of finding that feature in those without the disease. These can be expressed as both LR positive (LR+, how much the presence of a feature increases probability of disease) and LR negative (LR-, how much the absence of a feature decreases probability of disease).<sup>11</sup> Risk factors for PD include male sex (LR+ 1.2), regular pesticide exposure (LR+ 1.5), occupational solvent exposure (LR+ 1.5), non-use of caffeine (LR+ 1.35), first-degree relative with PD (LR+ 2.5), type II Diabetes mellitus (LR+ 1.5) and physical inactivity (LR+1.3). Smoking history is generally protective with lifelong non-smokers increasing the risk of PD (LR+ 1.2), and both active and previous smokers having a reduced risk of PD (LR- 0.51 and 0.91 respectively).<sup>10</sup>

## Clinical Features

The classical components of PD clinically are those of bradykinesia (slowness or poverty of movement), rigidity (an abnormal increase in muscle tone over the entire radius of joint movement), rest tremor (classically a 4-6 Hz pill rolling tremor), and gait impairment. Gait impairment classically presents early with reduced arm swing, reduced stride length, a stooped posture and eventually progresses to the classical festinant gait.<sup>2</sup> As the disease progresses the development of several neuropsychiatric

features such as cognitive impairment, hallucinations or psychosis can cause significant morbidity.

The clinical features were formally collected into a diagnostic criteria, the UK Parkinson's Disease Society Brain Bank Clinical Criteria, and proved to be an effective and accurate criteria to follow.<sup>12</sup> A clinico-pathological study assessing retrospective correlation of the clinical criteria with post mortem findings in 100 cases diagnosed as PD determined an accuracy of 82%, with the non-PD cases consisting of Alzheimer's disease (n=6), progressive supranuclear palsy (n=6), multiple system atrophy (n=5) and vascular basal ganglia disease (n=3).<sup>13</sup> This study was replicated by the same authors over a subsequent 10-year period finding that the sensitivity of clinical diagnosis had improved to 91.1% for PD, in a sample of 143 cases of parkinsonism including MSA and PSP.<sup>14</sup>

The described features may be found in any patient presenting with PD although the magnitude of each feature can vary greatly between. For example, bradykinesia should always be present to some degree, but tremor can be absent in some patients. Those presenting with particularly tremor dominant PD are felt to have the most favourable prognosis with regards to developing cognitive impairment.<sup>15</sup>

The axial and gait impairment of PD is particularly important as previous studies have demonstrated that the strongest evidence to predict an adverse prognosis is a higher age of onset and a greater involvement of axial and gait features, such as postural instability and freezing of gait.<sup>16</sup> Further, greater axial involvement at presentation has previously been used in a prognostic model to predict an adverse outcome of PD, defined by either postural instability or dementia at 5 years.<sup>17</sup> In contrast to some motor features, such as the variable presence of tremor, changes in postural stability and gait can be seen even in recently diagnosed and untreated PD.<sup>18</sup>

PD is well recognised to have several common non-motor symptoms that can be extremely debilitating. Constipation is by far the most common non-motor symptom, it is estimated that around 40-50% of PD patients experience constipation, as defined by less than 3 bowel movements per week.<sup>19</sup> Constipation can precede the onset of motor symptoms by many years and is recognised to increase the risk of PD (LR+ 2.5).<sup>10,20</sup>

Some non-motor symptoms are well recognised as prodromal features of PD, for example rapid eye movement sleep behaviour disorder (RBD) is now essentially seen as a clear prodromal phase to PD. RBD is characterised by dream enactment and incomprehensible vocalisations during rapid eye movement (REM) sleep, this is due to the loss of the normal physiological atonia that accompanies REM sleep. RBD is estimated to have a prevalence of around 24% in PD compared to just 3% in the healthy population.<sup>21</sup> In the largest prospective cohort study to date 1,280 individuals with idiopathic RBD were monitored for conversion to PD, they found an average age of onset for RBD of 66.3 years and the conversion rate to PD was 6.3% annually, with 73.5% of converting to PD after 12 years of follow-up.<sup>22</sup> Polysomnography confirmed RBD (the gold standard of RBD diagnosis) has a particularly large effect on the risk of developing PD (LR+ 130), as does questionnaire-screened probable RBD (LR+ 2.8).<sup>10</sup> Olfactory loss is a well-recognised prodromal feature with many patients reporting a reduced sense of smell leading up to the diagnosis of PD, certainly it's presence has a marked impact on the risk of developing PD (LR+ 6.4).<sup>10</sup>

Other non-motor symptoms reported at presentation by many drug-naïve patients include urinary symptoms (urgency, frequency and nocturia), orthostatic hypotension, depression and anxiety.<sup>23</sup> Depression and anxiety can be particularly common in PD with up to 19.6% of those with PD exhibiting anxiety and 24% of those with PD exhibiting depression as diagnosed with common clinical depression rating scales.<sup>24</sup>

Advanced PD is associated with the development of several neuropsychiatric complications. Early in the disease course many patients describe perception abnormalities, this frequently manifests as a false sense of a presence around the individual or the sense of something passing nearby, these are surprisingly common with up to 50% of patients experiencing these phenomena.<sup>25</sup> As PD progresses more frank and disabling hallucinations can develop with potentially 60% of patients experiencing hallucinations, which can be in multiple domains (visual, auditory, tactile or olfactory).<sup>26</sup> Psychotic delusions were seen in 16% of PD patients in a previous observational study with a mean disease duration of approximately 8 years.<sup>27</sup>

Mild cognitive impairment (MCI) is seen in around a third of newly diagnosed PD patients.<sup>28</sup> There is a high rate of conversion of PD-MCI to frank Parkinson's Disease dementia (PDD) with a previously reported annual conversion rate of 11%.<sup>29</sup> Overall,

PDD is estimated to have a prevalence of around 30% in PD.<sup>30</sup> Subjective cognitive impairment is also common in PD and also carries a risk, a previous longitudinal study of 43 PD patients with a mean age of 50 years and disease duration of 8 years found that after approximately 8 years follow-up 50% of those with PD-MCI had converted to PDD, and 33% of those with subjective memory complaints had converted to PDD compared to 14% in those with no cognitive complaints at enrolment.<sup>31</sup> PDD is associated with substantially greater care costs at around 3 times the costs per year of survival compared to those without dementia.<sup>32</sup>

Mortality is increased in PD relative to the healthy population by a factor of roughly 1.5.<sup>33</sup> Absolute reduction in life expectancy is highly dependent upon the age of diagnosis with patients diagnosed at age 65 showing a reduced life expectancy of 6.7 years whereas in those diagnosed at 85 the reduced life expectancy was only 1.2 years which is somewhat expected as the age at diagnosis approaches natural life expectancy.<sup>34</sup>

As such, many of these features of advanced features of PD carry significant morbidity and highlight the need for disease modifying therapy to reduce the rate of progression and thus the development of these highly disabling neuropsychiatric features.

### Current Treatments

The current treatments available for PD provide symptomatic relief only. The 'gold standard' treatment is levodopa, an amino acid that is converted to dopamine within the striatum. Many PD patients exhibit an excellent treatment response to this in the early stages of the disease. It is administered in combination with a dopa-decarboxylase inhibitor that prevents peripheral conversion of levodopa and improves central nervous system bioavailability.<sup>35</sup> Although levodopa has been shown to have an excellent symptomatic effect it does not demonstrate any positive disease-modifying qualities, with data now from two separate large randomised double-blind placebo-controlled trials, with no differences in the rate of progression between placebo and levodopa, or early initiation of levodopa versus delayed start levodopa. Although disappointing, they do lend evidence favouring the early commencement of levodopa for symptomatic therapy as there was no difference in levodopa related dyskinesia or fluctuations between any treatment groups in either trial. These complications were historically felt to occur sooner with early initiation of levodopa.<sup>36,37</sup>

Other commonly used medications are dopamine agonists. These exert their effect directly upon the dopaminergic receptors, however they have a less favourable side effect profile such as fatigue, hallucinations and impulse control disorder.<sup>38</sup> Enzyme inhibitors such as Monoamine oxidase B inhibitors (MAO-B) and Catechol-O-methyltransferase (COMT) inhibitors are also used in the treatment of PD and essentially modify the pharmacokinetics of levodopa, although rasagiline monotherapy can also have modest symptomatic effect in PD. MAO-B inhibitors reduce the degradation of dopamine in the central nervous system thus increasing the availability of dopamine in the synapse. COMT inhibitors increase and prolong the systemic availability of levodopa.

### Pathological features

Principally PD is a progressive neurodegenerative disorder characterised by the loss of dopaminergic neurons in the substantia nigra pars compacta and functionally leads to striatal dopamine deficiency, this is marked even in the early stages of the disease.<sup>39</sup>

The second histopathological hallmark is that of the abnormal accumulation of  $\alpha$ -synuclein, a pre-synaptic protein the function of which is not entirely clear. The aggregation of alpha-synuclein can be seen in the form of Lewy neurites, which are thread-like and located in cellular processes, or in Lewy bodies, as clear globular inclusion bodies in the neuronal perikarya. Lewy bodies also include phosphorylated neurofilaments and ubiquitin. Initially this pathology is found within the medulla oblongata but subsequently spreads to the midbrain (including the substantia nigra) and can eventually be found to have spread outside of the nigrostriatal system and even cortically.<sup>40</sup>

There is evidence that  $\alpha$ -synuclein most likely has a role in regulating synaptic vesicles with evidence that it co-localises with synaptic vesicles in the presence of calcium, it also promotes their clustering to maintain a vesicle pool as would be expected in active synaptic termini.<sup>41,42</sup> More recently it has been demonstrated that  $\alpha$ -synuclein has a high affinity for the inner pre-synaptic membrane and can also anchor to synaptic vesicles. Further, the ability of  $\alpha$ -synuclein to bind to the inner membrane was modulated by lipid composition. It is therefore postulated that  $\alpha$ -synuclein has multiple roles, one in which it stabilises synaptic vesicle docking at the inner pre-synaptic membrane, and a further one where it binds to synaptic vesicles to promote clustering.

The disruption of this balance may be a key step in the pathological process to the generation of Lewy bodies.<sup>43</sup>

Although the neuropathology is well described it is difficult to relate this to the clinical presentation. A post-mortem study by Parkkinen *et al*<sup>44</sup> screened material from 904 elderly patients, regardless of cause of death, for  $\alpha$ -synuclein in the dorsal motor nucleus of the vagus nerve, the substantia nigra and the basal forebrain nuclei. Of these 106 cases that met these criteria; 9 were diagnosed with DLB, 9 with PD and 2 with PDD. It was not possible to predict the presence of extrapyramidal symptoms based upon neuropathology and found widespread  $\alpha$ -synuclein pathology in some asymptomatic individuals. Furthermore, only 20% of their cases with cortical  $\alpha$ -synuclein pathology were diagnosed with either PDD or DLB.<sup>44</sup> It should be noted that there was a tendency for those with extrapyramidal symptoms to have a greater  $\alpha$ -synuclein disease load. Therefore, despite being pathologically well characterised with respect to PD,  $\alpha$ -synuclein pathology is not necessarily specific to PD and can be seen in asymptomatic individuals, likely as a result of aging. Additionally,  $\alpha$ -synuclein pathology does not seem to correlate with key clinical features. These findings have been replicated in neurologically asymptomatic individuals by other groups.<sup>45</sup>

### Pathogenesis

The current pathogenesis of PD is poorly understood. However, there are several consistent features that appear to play a key role in the development of the disease. As discussed above it is felt that Lewy body pathology appears to spread in a stereotypical fashion to several anatomical structures over time. It is unclear exactly how this leads to neuronal cell death or exactly how Lewy bodies form.

### Genetics

The identification of monogenic forms of familial PD has revealed some of the pathogenic mechanisms that may be significant in PD. The identification of *SNCA* (encoding  $\alpha$ -synuclein) in a family exhibiting a typical PD phenotype but of earlier onset in an autosomal dominant inheritance showed clear evidence of PD being a 'synucleinopathy'.<sup>46</sup> Mutations in *SNCA* are either from missense mutations resulting in misfolded alpha-synuclein or multiplication mutations that display a clear dosage effect with an earlier onset disease with increasing multiplications.<sup>47</sup> *SNCA* mutations

can result in a relatively typical PD presentation although there is a tendency towards earlier age of onset and early cognitive decline.<sup>48</sup>

*LRRK2* associated PD is the most common autosomal-dominant genetic form of the disease worldwide with the G2019S mutation being the most common variant. *LRRK2* PD demonstrates some typical features of PD pathology such as the presence of Lewy Bodies.<sup>49</sup> *LRRK2* presents in a similar manner to sporadic PD with a median age of onset of 57 years and exhibits a good response to levodopa.<sup>48</sup> *LRRK2* are not necessarily fully penetrant and therefore in some situations could be viewed as a risk factor for PD, this is variable and ranges from a LR+ of 2.5 at age 50-54 up to 11.6 in those aged 70-74 for the G2019S.<sup>10</sup>

Several genes have been identified in autosomal recessive PD. The three most common mutations associated with early onset PD are *PARK2* (parkin), *PINK1* and *PARK7* (DJ-1). *LRRK2*, parkin, *PINK1* and DJ-1 all appear to be involved in mitochondrial function and will be discussed in greater detail later.

Mutations in *GBA1* are the most common genetic risk factor for PD with a large international multi-centre study finding an odds ratio of 5.43 of developing Parkinson's disease if heterozygous for a *GBA* mutation compared with controls.<sup>50</sup> The phenotype of *GBA* associated PD (*GBA*-PD) is that of typical PD but with a higher risk of rapid progression and development of dementia.<sup>51</sup> *GBA1* encodes for the lysosomal protein glucocerebrosidase (GCCase). GCCase has reduced catalytic activity and protein expression in the brains of patients with *GBA*-PD mutations. Sporadic PD patients with non-mutant *GBA* also show a decrease in GCCase activity.<sup>52</sup>

### *Mitochondria in health*

Mitochondria are responsible for ATP production via oxidative phosphorylation (OXPHOS). Mitochondria contain their own circular genome of mitochondrial DNA (mtDNA) which is roughly 16kilobases in length. Several important genes for mitochondrial function and regulation with are nuclear encoded. The 13 proteins encoded by mtDNA are key components of respiratory complexes I-IV of the inner mitochondrial membrane that facilitate OXPHOS. The core function of complexes I-IV are to generate an electrochemical gradient generated by the transfer of protons from the mitochondrial matrix to the inter membrane space, the pumping of protons is coupled with the transfer of electrons to oxygen throughout the respiratory complexes.

The generation of this gradient (the mitochondrial membrane potential, MMP) is essential for the functioning of complex V, ATP synthase, that utilises this proton motive force to generate ATP (**Figure 1**).<sup>53</sup>

Complex I utilises the dihydronicotinamide adenine dinucleotide (NADH) generated from the Krebs cycle which reduces Nicotinamide Adenine Dinucleotide (NAD) into NADH. The oxidation of NADH by complex I allows the release of electrons which are then mobilised through complexes II-IV and alongside the movement of four protons into the intermembrane space from the mitochondrial matrix.<sup>53,54</sup>

Complex II has no subunits encoded by mtDNA and oxidises succinate to fumarate and transfers the electrons released from this reaction to ubiquinone which are then passed to complex III. Complex II also differs from complexes I, III and IV in that it does not move any protons into the intermembrane space to increase the proton motive force, it only facilitates the transfer of electrons through complexes III and IV. Complex I and II are the two independent entry points to oxidative phosphorylation.<sup>55</sup>

Complex III oxidises ubiquinone to ubiquinol which transports four protons to the intermembrane space and transfers the electrons to cytochrome c.<sup>50,53</sup> Complex IV then oxidises cytochrome c and converts oxygen to water, as a result of this two protons are moved into the intermembrane space.<sup>56</sup>

Finally, complex V (ATP synthase) uses the proton motive force created by the electrochemical gradient to channel protons across the membrane back into the mitochondrial matrix. As protons move through the proton channel of complex V it causes several conformational changes in the complex that ultimately catalyses the synthesis of ATP from ADP and phosphate.<sup>53,54</sup>

Mitochondrial health is tightly regulated through mitophagy and the balance of mitochondrial fission and fusion. Mitophagy is a form of macroautophagy removing damaged or dysfunctional mitochondria. There are several important mechanisms by which this is mediated. In health, PTEN-induced putative kinase 1 (PINK1) is imported into the mitochondria via the translocases of the outer mitochondrial membrane complex and the inner mitochondrial membrane complex, where it undergoes cleavage and is then translocated back into the cytosol for degradation. If there is a loss of the normal MMP though this cleavage does not occur and PINK1 will stabilise on the outer mitochondrial membrane leading to the phosphorylation of ubiquitin

located on the outer mitochondrial membrane. In turn, this recruits Parkin and activates its ubiquitin E3 ligase activity to poly-ubiquitinate several proteins that leads to the recruitment of autophagy receptors such as optineurin and induce mitophagy of the mitochondria.<sup>57</sup>

Mitochondrial fission and fusion are paired processes that are essential to maintain overall mitochondrial health and regulates the morphology of mitochondria. Mitochondrial fusion facilitates the generation of connected mitochondrial networks to share constituents of each individual component, such as proteins, metabolites, mtDNA and maintains a homogenous MMP to support OXPHOS.<sup>58</sup>

Fission is a key driver for both the degradation and proliferation of the total number of mitochondria. This is dependent upon the site of fission within a mitochondrion, be it at the periphery of the length of the mitochondria (generally mediated by Fis1) or the midzone (mediated by Drp1). Peripheral fission is generally preceded by an increase in ROS and calcium and a decrease in MMP, this leads to a small and a large daughter mitochondrion. The small daughter mitochondria are those that will generally be marked for degradation via mitophagy and they will cease to undergo further fusion or fission events. Mitochondria undergoing midzone fission can be thought to be more representative of the usual turnover of the healthy mitochondria in a healthy connected network where fission allows the proliferation and motility of mitochondria and the distribution of mtDNA throughout the network.<sup>53,59</sup>

#### *Mitochondrial dysfunction in Parkinson's Disease*

Mitochondrial dysfunction in PD was first formally identified in the post-mortem substantia nigra of nine patients with sporadic PD. In this landmark study mitochondrial complex I activity was significantly reduced compared to nine controls.<sup>5</sup>

Prior to this discovery several case reports had emerged where individuals had inadvertently injected themselves with a new 'synthetic heroin' that actually contained 1-Methyl-4-phenyl-1,2,5,6-tetrahydropyridine (MPTP). All of these individuals had developed Parkinsonism almost indistinguishable from sporadic PD. They were administered the same treatments of levodopa and dopamine agonists with therapeutic benefit.<sup>60</sup>

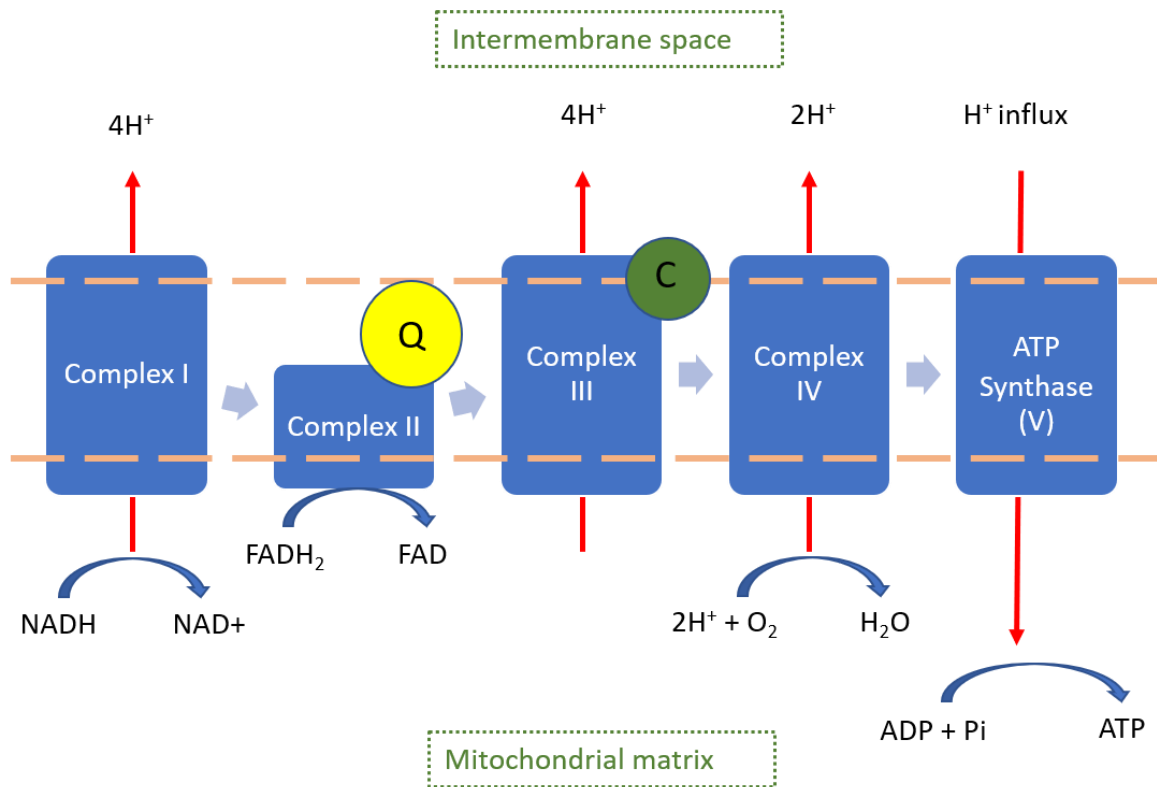


**Figure 1.1: The electron transport chain and oxidative phosphorylation.**

The electron transport chain is composed of five complexes located in the inner mitochondrial membrane that generate an electrochemical gradient and a protonmotive force to facilitate the generation of ATP via ATP synthase (complex V). There are two separate entry points into the electron transport chain, either via Complex I or II. Important molecules also required are the electron transporters ubiquinone (Q) and cytochrome c (C). Complex II does not pump any protons across the membrane. NADH is produced the citric acid cycle and along with FADH act as electron donors to complex I and II for electrons to enter the transport chain. The numbers of protons pumped into the intermembrane space are per pair of electrons utilised by the respective complex.

Subsequently, MPTP was used to induce primate models of PD successfully. The active and neurotoxic metabolite of MPTP was then identified to be 1-Methyl-4-phenylpyridinium ion (MPP<sup>+</sup>) which is a highly specific complex I inhibitor.<sup>61</sup>

Several genes causing familial PD (*Parkin*, *PINK1*, *DJ-1* and *LRRK2*) have been identified that are crucially important in the functioning of mitochondria, either through mitophagy (the recycling and regulation of damaged mitochondria), mitochondrial fission or in protecting against oxidative stress.<sup>6</sup> *PINK1* and *parkin* have clear roles in mitophagy as discussed earlier.<sup>62</sup> *LRRK2* may have a regulatory role in mitochondrial fission and exhibits a clear phenotype of mitochondrial dysfunction in primary fibroblast

cultures.<sup>63,64</sup> DJ-1 is felt to be cytoprotective against oxidative stress and regulates Nrf2, a transcription regulator for cellular antioxidant responses.<sup>65</sup>

Post-mortem abnormalities in the respiratory chain complexes have been noted across multiple studies with evidence of reduced levels and activity of complex I in the substantia nigra and midbrain, reduced levels of complex II, III, IV and complex V in the midbrain. Reduced complex I activity has also been observed in frontal cortex whereas for complexes II-IV there generally aren't abnormalities outside of the midbrain.<sup>66</sup>

Alpha-synuclein aggregation, a hallmark of PD pathology, induces mitochondrial dysfunction in primary neuronal cultures *in vitro*.<sup>67</sup> Post-mortem studies have found that Lewy body pathology frequently contains dysmorphic and fragmented organelles such as mitochondria.<sup>68</sup>

Oxidative stress is a key feature of mitochondrial dysfunction, reactive oxygen species (ROS) are naturally generated through OXPHOS, primarily through complex I and III. In health ROS are handled by antioxidants to prevent any deleterious effects of ROS production. Glutathione, one of the most abundant antioxidants is depleted in PD at post-mortem indicating increased oxidative stress.<sup>69</sup> Oxidative stress leads to increased DNA and RNA damage in the substantia nigra.<sup>70</sup> A greater burden of somatic mtDNA mutations are found in PD, specifically in the substantia nigra and particularly in genes encoding cytochrome c oxidase (complex IV).<sup>71</sup> Further, an overall reduction in mtDNA copy numbers has been seen in PD and has been proposed even as a potential biomarker.<sup>72</sup>

As discussed earlier, PINK1/Parkin are key genes in the process of mitophagy, and mitophagy deficits are clearly an underlying mechanism in the development of PINK1/Parkin related PD and there is evidence that these deficits only manifest in cell types extremely dependent upon OXPHOS such as neuronal populations.<sup>73</sup> Increased levels of phosphorylated ubiquitin associated with PINK1/Parkin have been found in sporadic PD implying a greater accumulation of mitochondria being targeted for degradation and implicating impaired mitophagy in sporadic PD.<sup>74</sup>

### *Lysosomal Dysfunction*

Lysosomal dysfunction has also been implicated in the pathogenesis of PD. It is, in many ways, intrinsically linked to mitochondrial dysfunction as lysosomes are a crucial part of mitophagy and macroautophagy.

Much of our knowledge regarding lysosomal dysfunction PD comes from the autosomal recessive condition Gaucher's disease, the most common lysosomal storage disorder resulting from an insufficiency in activity of the enzyme GCCase, encoded by the gene GBA1.<sup>75</sup> GCCase is responsible for the conversion of glucocerebroside to glucose and ceramide. When this fails it results in an accumulation of glucocerebroside within lysosomes, impairing lysosomal activity.<sup>76</sup>

Individuals with GBA1 haploinsufficiency have a higher risk of developing PD, with a large international multi-centre genome wide association study finding an odds ratio of 5.43 compared to controls.<sup>50</sup>

GCCase catalytic activity and protein expression is reduced in the brains of both GBA-PD and sporadic PD, *in vitro* models of PD with non-mutant GBA1 also show a decrease in activity of GCCase.<sup>52</sup> Functional GCCase deficiency in primary cultures of iPS neurons resulted in compromised lysosomal activity and an accumulation of  $\alpha$ -synuclein resulting in neurotoxicity. Interestingly,  $\alpha$ -synuclein further inhibits lysosomal activity and normal GCCase activity forming a positive feedback loop.<sup>76</sup> This has also been demonstrated in tissue fibroblast lines, echoing a reduction in both GCCase protein levels and activity in both GBA-PD and sporadic PD, there was also an observed increase in cytosolic reactive oxygen species.<sup>77</sup> Furthermore, mutant GCCase is significantly associated with  $\alpha$ -synuclein inclusion both in homozygous and heterozygous GBA1 mutation carriers, suggesting an association between mutant GCCase and the aggregation of  $\alpha$ -synuclein leading to Lewy Body disease.<sup>78</sup>

### *Alpha-synuclein*

As discussed earlier the presence of Lewy bodies and Lewy neurites in the nigrostriatal pathways is the pathological hallmark of PD. Lewy bodies and Lewy neurites are principally composed of aggregated  $\alpha$ -synuclein with a single phosphorylation at Ser-129 being the most abundant modification.<sup>79</sup>

There are several mutations in *SNCA* that result in an autosomal-dominant familial PD. Some point-mutations (G51D and H50Q) have been predicted to have a much

higher propensity to aggregate.<sup>80</sup> Further, point mutations such as G51D demonstrate increased neurotoxicity in murine models of PD compared to wild-type  $\alpha$ -synuclein when injected into the substantia nigra.<sup>81</sup> It may be that aggregation and formation of fibrillary  $\alpha$ -synuclein alone is not the only pathogenic step as the A30P and A53T mutations of SNCA have also demonstrated cytotoxicity following the formation of prefibrillar oligomers.<sup>82</sup>

Host-to-graft transmission of  $\alpha$ -synuclein has been observed in both humans and mice. In humans, three individuals who underwent fetal ventral mesencephalic transplants demonstrated Lewy-body pathology in the transplanted neurons at post-mortem, the range of survival following transplantation was 11-16 years.<sup>83,84</sup> This host-to-graft transmission has been further examined in transgenic murine models expressing human  $\alpha$ -synuclein where 15% of grafted mouse cortical neuronal stem cells demonstrated the presence of  $\alpha$ -synuclein 4-weeks post-graft.<sup>85</sup>

In wild-type mice the pathological spread of  $\alpha$ -synuclein was triggered by the injection of both recombinant human and murine pre-formed fibrils of  $\alpha$ -synuclein into the striatum with the development of dopaminergic cell loss in the substantia nigra and impaired motor function. These features were absent in mice injected with soluble forms of  $\alpha$ -synuclein.<sup>86</sup>

This has culminated in a theory as to whether  $\alpha$ -synuclein behaves similar to a prion disorder with the cell-to-cell transmission of pathological forms of  $\alpha$ -synuclein leading to aggregation and neurodegeneration. This could start from sites outside of the central nervous system such as the enteric nervous system where  $\alpha$ -synuclein has been found in the GI tract of prodromal PD in two separate cohorts with the earliest alpha-synuclein positive prodromal pathological samples being up to 20 years prior to diagnosis. It should be noted that although the presence of  $\alpha$ -synuclein in the GI tract is not present in all those with PD it does appear to be highly specific to PD compared to controls.<sup>87,88</sup>

In two separate rodent models the exogenous injection of alpha-synuclein into the GI tract has demonstrated retrograde transmission of  $\alpha$ -synuclein along the vagus nerve to the dorsal motor nucleus of the vagus nerve where it propagates further to structures such as the locus coeruleus and the substantia nigra.<sup>89,90</sup> In one model truncal

vagotomy ameliorated these features entirely in response to the exogenous injection of alpha-synuclein.<sup>90</sup>

### *Neuroinflammation*

There is growing evidence that inflammatory processes may play a part in the pathogenesis of PD. Epidemiological evidence has shown a reduced risk of developing PD for those taking non-steroidal anti-inflammatory drugs and for those on immunosuppression.<sup>91,92</sup> Reactive microglia have been found at post-mortem in PD and confirmed *in vivo* using PET imaging and the microglia activated associated ligand <sup>11</sup>C-PK11195.<sup>93,94</sup> Further, pro-inflammatory cytokine profiles from peripheral blood in PD have shown to increase the rate of both motor and cognitive impairment.<sup>95</sup> This has now culminated in a randomised double-blind placebo-controlled phase II trial in PD using Azathioprine, a widely used and well tolerated immunosuppressant that is a purine analogue that inhibits nucleic acid synthesis, hence reducing proliferation of both B and T lymphocytes. The primary outcome is the change between groups in the MDS-UPDRS axial score over 12 months.<sup>96</sup>

### *Bile acids and gastrointestinal dysbiosis*

Described earlier the gastrointestinal system is of increasing interest in PD with respect to  $\alpha$ -synuclein. However, there is increasing evidence of multiple pathogenic processes which may contribute to PD originating in the gastrointestinal system.

The appendix is a particularly rich  $\alpha$ -synuclein deposition site prompting a previous study assessing if appendicectomy reduced the risk of PD. A Canadian population-based study identified 42,999 individuals undergoing appendicectomy and matched two further cohorts of those had undergone cholecystectomy ( $n=42,995$ ) and healthy controls ( $n=42,999$ ). They found appendicectomy increased the risk of PD in the first 5 years post-procedure, but this risk did not persist and ultimately there was no evidence of risk reduction following appendicectomy. Interestingly, the highest rates of PD were in the cholecystectomy group with incidence rates per 100,000 person-years of 31 in the appendicectomy group, 21 in the control group and 40 in the cholecystectomy group. This was not formally statistically tested in their analysis.<sup>97</sup>

Subsequently, cholecystectomy has been associated with an increased risk of PD in a Korean population-based cohort study of 161,838 individuals who underwent cholecystectomy and 286,135 matched healthy controls. There was a statistically

significant increase in the adjusted hazard ratio (HR) for the development of PD in the whole cohort at 1.14, although this relationship seemed to be stronger in men (HR 1.22). In women the HR was 1.03 and was not significant.<sup>98</sup>

Following cholecystectomy there are several changes in bile acid composition. Multiple studies have demonstrated that the greatest changes are an increase in the secondary bile acids deoxycholic acid (DCA) and lithocholic acid (LCA) accompanied with a reduction in the primary bile acid cholic acid (CA), although one of these studies found these changes relatively modest at longer follow-up (5-8 years).<sup>99-101</sup> LCA and DCA are both hydrophobic bile acids which are associated with pro-inflammatory responses and can be cytotoxic at high concentrations.<sup>102,103</sup>

Bile acids can also demonstrate nuclear receptor mediated signalling. Although many of these receptors are most abundant in the intestine and liver, many are also expressed in the brain such as farnesoid X receptor (FXR), membrane receptors Takeda G-protein-coupled receptor 5 (TGR5) and sphingosine-1-phosphate receptor 2 (S1PR2).<sup>104</sup> FXR deletion in mice has been associated with neurotransmitter disturbances resulting in memory and motor impairment.<sup>105</sup> TGR5 activation is neuroprotective and anti-inflammatory in a mouse model of hepatic encephalopathy, whereas S1PR2 is pro-inflammatory.<sup>106,107</sup>

Gastrointestinal dysbiosis has also been observed in PD with several studies noting changes in the composition of the gut microbiome. A recent meta-analysis using ten publicly available datasets found an increase in bacterial species of the *Lactobacillus*, *Akkermansia*, and *Bifidobacterium* genera alongside a depletion of *Lachnospiraceae* and *Faecalibacterium* genus. *Lachnospiraceae* and *Faecalibacterium* are important short-chain fatty acid producers and a reduction in them are hypothesised to lead to increased inflammation in the GI tract.<sup>108</sup>

Gastrointestinal dysbiosis can also markedly affect bile acid composition and has also been associated with elevated levels of the secondary bile acids (i.e. those generated by the conversion of primary bile acids by the gut microbiome). An elevation of the *Burkholderiales* genus which encodes the rate limiting enzyme for secondary bile acid synthesis was associated with increased DCA and LCA.<sup>109</sup> A further study also identified elevated levels of both DCA and the glyco- and tauro- conjugates of DCA between drug naïve PD patients and healthy controls.<sup>110</sup> Further, a reduction in

potentially neuroprotective bile acids, ursodeoxycholic Acid (UDCA, discussed in greater detail below) and tauroursodeoxycholic acid (TUDCA) has also been observed.<sup>111</sup>

### Developing Neuroprotective therapies in Parkinson's Disease

Previous neuroprotective trials in PD have generally delivered disappointing results. Many trials have focused on clinically-defined endpoints utilising common clinical rating scales or commencement of dopaminergic medication in drug-naïve participants. Cohorts have typically focused only on drug-naïve or very early PD with no attempts at stratification of the trial cohort according to a particular pathogenic mechanism being target. Further, there has generally been few attempts focusing on demonstrating the target engagement of these compounds to confirm physiological effect independent of clinical response.<sup>112-116</sup>

### Common challenges to neuroprotective trial design in Parkinson's

Identifying individuals most likely to respond to a specific therapy that, for instance, targeted mitochondrial dysfunction would be desirable and represent a shift towards 'precision medicine' approaches. This would increase the likelihood of demonstrating a disease modifying effect as the trial cohort would include a greater proportion of individuals likely to respond to that drug.

Additionally, with respect to the clinical heterogeneity of PD, there is a clear desire to identify common clinical characteristics that may prove beneficial when designing disease-modifying trials. This could include identifying those at highest risk of fast disease progression to increase the likelihood of detecting a clinically meaningful response to a putative neuroprotective compound over a short trial length in relation to the usual progression rate of PD.

Aside from cohort stratification there are challenges with how to measure disease progression in PD. At present this has largely relied on subjective clinical rating scales which, although thoroughly validated, present several challenges when attempting to detect a disease modifying effect. Another issue, particularly with early Phase I and II clinical trials, is the confirmation of target engagement. Target engagement is the demonstration that an investigative compound is having the desired effect on the molecular pathway and/or the cellular mechanism which is being targeted.

### *Cohort stratification*

Attempts at stratification by clinical phenotype include using the Movement Disorders Society Unified Parkinson's Disease Rating Scale (MDS-UPDRS) to classify individuals into either tremor-dominant (TD), postural instability gait disorders (PIGD) or indeterminate.<sup>117,118</sup> It was initially felt that those with PIGD-PD at disease onset had the more aggressive disease course with a greater risk of cognitive impairment.<sup>117,119</sup> Further studies then demonstrated that there was significant instability between these clinical subtypes with many patients moving between subtypes as measured at 12 months follow-up, with 18% of TD and 39% of PIGD changing classification to a different subtype, this effect was independent of dopaminergic medication.<sup>120</sup> These subtypes became more distinct and consistent in longitudinal studies with greater duration which again demonstrated that PIGD-PD generally has a less favourable prognosis.<sup>121</sup> Regardless, the significant instability in clinical subtype at disease onset poses large challenges for any studies wishing to enrich their cohorts with particular features, such as aggressive disease or a greater risk of cognitive impairment.

A more recent study has attempted to accurately predict the risk rapid disease progression through the development and external validation of a prognostic model across two large incident longitudinal cohorts of PD to predict the onset of either dementia or postural instability at 5 years. This demonstrated that the key features associated with a greater risk of this unfavourable outcome were increasing age, reduced semantic fluency and the axial sub-score of the UPDRS. The axial sub-score includes the items pertaining to postural instability, posture, gait and rising from a chair in the UPDRS. This provides a more concise assessment that is less susceptible to large changes in clinical features on examination.<sup>17</sup>

Mechanistic stratification of PD would be desirable as it would enable precision medicine approaches to deliver target therapies against specific pathogenic mechanisms identified in an individual. Several biomarkers and techniques had been investigated previously, with particular attention on mitochondrial dysfunction, discussed in greater detail below.

## *Clinical endpoint design*

### *Clinical Rating Scales*

The most widely utilised clinical scale in all PD studies is the MDS-UPDRS, which was revised from the UPDRS and in which many aspects remain very similar (extremely so in the motor examination), is the current most utilised and validated clinical tool to quantify the disease state of an individual with PD.<sup>122</sup>

The MDS-UPDRS is composed of four parts. Part I is assess the non-motor experiences of daily living such as cognition, depression and hallucinations. Part I is split into IA (administered by the examiner) and IB (completed by the patient). Part II is completed by the patient and assess their motor experiences of daily living, such as tremor, handwriting, performing personal hygiene care and eating tasks for example. Part III is the motor examination completed by the examiner and covers speech, facial expression, rigidity (in the neck and all four limbs), bradykinesia in all four limbs, gait and tremor, both rest (in all four limbs and the lip) and action and postural tremor in the upper limbs only. Part IV assess treatment related complications such as 'ON' and 'OFF' state fluctuations, painful 'OFF' state dystonia and dyskinesias. For each item it is possible to score across five descriptors with '0' being normal examination or a problem not experienced by the patient to a maximum of '4' which generally indicates severe examination findings or functional dependence. The full list of examination items for all parts can be seen in **Table 1.1**.<sup>122</sup>

As with any clinical rating scale relying upon subjective clinical examination the MDS-UPDRS demonstrates both inter- and intra-rater variability. One study assessing the inter- and intra-rater variability among specialist nurses, neurology residents and movement disorder specialist found motor examination ratings differed by a mean of up to 5.4 points between some raters. A senior movement disorders specialist demonstrated 95% intra-rater repeatability limits of -8.3 to 7.1 when assessing the same cases 6 weeks later.<sup>123</sup> This study used the UPDRS prior to the MDS revision but given that the motor examination section remained extremely similar these findings are likely representative of the MDS-UPDRS.

Other common clinical rating scales include the non-motor symptoms rating scale (NMSS) that assesses a wide variety of non-motor symptoms and scores them in a multiplicative fashion between the severity (scored as none (0), mild (1), moderate (2)

or severe (3)) and the frequency (rarely (1), often (2), frequent (3) or very frequent (4)). Although comprehensive in assessing the non-motor state of PD it is somewhat held back from being widely utilised as a clinical endpoint in trials due to the multiplicative nature of the scoring system making total scores difficult to interpret.<sup>124</sup>

The most widely used patient reported outcome measure in PD is the Parkinson's Disease Questionnaire (PDQ-39) that assess patient reported responses within several dimension, namely mobility, activities of daily living, emotional well-being, stigma, social support, cognition, communication and bodily discomfort. Each item within each dimension is then scored according to the frequency with which the patient has encountered that particular problem within the last month, either never, occasionally, sometimes, often or always (or cannot perform the task stated. Items are framed around the question "How often during the last month have you..." and example items include "Had problems walking half a mile?", "Had difficulty washing yourself?" and "Felt depressed?". Each dimension can be scored separately or combined into a summary index score that reflects the overall impact of an individual's PD on their health status. PDQ-39 is the most common patient reported outcome utilised in PD clinical trials.<sup>125</sup>

<b>Part I</b>		<b>Part III (continued)</b>	
1.1	Cognitive impairment	3.3e	Rigidity– LLE
1.2	Hallucinations and psychosis	3.4a	Finger tapping– Right hand
1.3	Depressed mood	3.4b	Finger tapping– Left hand
1.4	Anxious mood	3.5a	Hand movements– Right hand
1.5	Apathy	3.5b	Hand movements– Left hand
1.6	Features of DDS	3.6a	Pronation- supination movements– Right hand
1.7	Sleep problems	3.6b	Pronation- supination movements– Left hand
1.8	Daytime sleepiness	3.7a	Toe tapping– Right foot
1.9	Pain and other sensations	3.7b	Toe tapping– Left foot
1.10	Urinary problems	3.8a	Leg agility– Right leg
1.11	Constipation problems	3.8b	Leg agility– Left leg
1.12	Light headedness on standing	3.9	Arising from chair
1.13	Fatigue	3.10	Gait
<b>Part II</b>		3.11	Freezing of gait
2.1	Speech	3.12	Postural stability
2.2	Saliva and drooling	3.13	Posture
2.3	Chewing and swallowing	3.14	Global spontaneity of movement
2.4	Eating tasks	3.15a	Postural tremor– Right hand
2.5	Dressing	3.15b	Postural tremor– Left hand
2.6	Hygiene	3.16a	Kinetic tremor– Right hand
2.7	Handwriting	3.16b	Kinetic tremor– Left hand
2.8	Doing hobbies and activities	3.17a	Rest tremor amplitude– RUE
2.9	Turning in bed	3.17b	Rest tremor amplitude– LUE
2.10	Tremor	3.17c	Rest tremor amplitude– RLE
2.11	Getting out of bed	3.17d	Rest tremor amplitude– LLE
2.12	Walking and balance	3.17e	Rest tremor amplitude– Lip/jaw
2.13	Freezing	3.18	Constancy of rest
<b>Part III</b>		<b>Part IV</b>	
3.1	Speech	4.1	Time spent with dyskinesias
3.2	Facial expression	4.2	Functional impact of dyskinesias
3.3a	Rigidity– Neck	4.3	Time spent in the OFF state
3.3b	Rigidity– RUE	4.4	Functional impact of fluctuations
3.3c	Rigidity– LUE	4.5	Complexity of motor fluctuations
3.3d	Rigidity– RLE	4.6	Painful OFF-state dystonia

**Table 1.1: Movement Disorders Society Unified Parkinson’s Disease Rating Scale**

*This does not include the additional non-scoring items captured such as who is completing the patient completed questionnaire (patient, caregiver, or both), whether the Part II examination is in the ‘OFF’ state and when the last levodopa dose was, whether dyskinesias were present and affected Part III ratings and the Hoehn & Yahr Stage. Each item can be rated as normal (0), slight (1), mild (2), moderate (3), and severe (4), each item has additional guidance for scoring and descriptors for each rating. It is not advised to use total MDS-UPDRS scores and instead present the score of each individual part when used in clinical studies.*

## Objective quantification of motor impairment

Given the importance of clinical endpoint design and accurately quantifying disease progression in PD there has been a recent shift to developing further technologies to assist with the quantification of the disease state of PD. This has predominantly focused on the objective quantification of motor impairment using wearable digital motion sensors comprising a gyroscope and accelerometer but has also been performed using 3D motion capture technology and instrumented walkways. This can be assessed in either clinic-based assessments or in free-living environments, such as monitoring patients at home.

Wearable accelerometry based systems have been used to predict conversion to PD, a study of 696 healthy had their gait assessed four times at 2-yearly intervals using a lower-back placed wearable device and utilising simple walking tasks at different speeds under single and dual tasking situations. In the cohort 16 participants developed PD and demonstrated that pace tended to slow around 4 years prior to diagnosis. Cox regression identified higher step time variability and asymmetry across multiple parameters all predicted conversion to PD.<sup>126</sup>

Wearable sensors have also offered the ability to detect differences in gait between PD and controls and offer benefits over instrumented walkways in that they are more accessible and don't have the same real-world spatial constraints of a walkway system. Additionally, accelerometers allow the quantification of further signal parameters outside of the usual spatiotemporal features described above. This includes movement intensity, regularity and the symmetry of movement. One study assessing upper body accelerometry in 70 patients with PD and 64 healthy controls found that these measures moderately outperformed traditional spatiotemporal measures in differentiating PD from controls.<sup>127</sup> This was replicated in larger study by the same authors.<sup>128</sup>

Gait impairment in PD is not entirely dopaminergic responsive and the cortical cholinergic system is also implicated. A previous study assessing gait impairment using an instrumented walkway to capture spatiotemporal gait parameters such as the step time, step length, swing time and the variability of these features 99 patients with PD and 47 controls found that poorer performance in gait assessments correlated with a smaller volume of the nucleus basalis of Meynert, a key structure in the cholinergic

basal forebrain implicated in gait impairment. Additionally, at baseline patients with PD demonstrated a reduced step length and step velocity alongside an increase in step time and stance time. Additionally, the variability of many of these features across all steps was much greater in PD compared to controls. Over 36 months step length and step time continued to deteriorate with an associated increase in the variability of each measurement across steps in PD compared to controls.<sup>129</sup>

A further study by the same group using the same instrumented walkway system in 109 newly diagnosed patients with PD and 130 healthy controls tracked changes in gait parameters at 18-month intervals up to a maximum of 6 years. Similar gait parameters changed over this time in both groups with reductions in both step time and velocity with an associated increase in their variability seen in both groups although in PD these changes were more marked. Several features seemed to be more specific to PD as opposed to natural aging with a significantly greater reduction in step width and length being noted with a significantly greater increase in both step time and step length variability in PD.<sup>130</sup>

These techniques may lend themselves well as an alternative clinical endpoint in trials to quantify disease progression. Further, there is already data on expected changes and rate of change in PD in some of these parameters.

### Stratification of Parkinson's Disease according to mitochondrial dysfunction

The stratification of PD can be approached from the perspective of the multiple pathogenic mechanisms implicated, this paradigm is visualised in **Figure 1.2**. This thesis will focus on mitochondrial dysfunction as a target for mechanistic stratification. As discussed earlier there is a large amount of supporting literature for mitochondrial dysfunction being a key driver of PD and, as will be discussed below, some potentially promising approaches to identifying mitochondrial dysfunction *in vivo*.

#### Genetic stratification

Genetic stratification of PD would allow the delivery of precision medicine approaches targeting the specific molecular pathway affected. This approach has been explored with *Parkin*, *LRRK2* and *GBA* so far.

*Parkin* is the most common autosomal recessive form of PD and so far, no drug has made it trial specifically targeting the *Parkin* pathways. However, one promising target could be the inhibition of ubiquitin-specific protease 30 (USP-30). USP-30 that de-

ubiquitinates the same substrates that Parkin ubiquitinates and thus opposes its action. Inhibiting USP-30 could compensate for reduced Parkin activity, so far though this has only been demonstrated *in vitro*.<sup>131</sup> There are further trials targeting genetically stratified Parkin-PD based upon optimising mitochondrial function given the distinct phenotype of mitochondrial dysfunction that Parkin-PD exhibits. One such trial, discussed in greater detail below, is trialling co-enzyme Q10 in a cohort of genetically and phenotypically screened PD.<sup>132</sup>

#### Stratification using blood, urine and cerebrospinal fluid biomarkers

Multiple candidate biomarkers have been assessed in the urine, blood and CSF of patients with PD. 8-Hydroxyguanosine (8-OHG) and 8-hydroxy-2-deoxyguanosine (8-OHdG) are generated from reactive oxygen species hydroxylating deoxyguanosine or guanosine in DNA and RNA, first identified in the post-mortem tissue. Oxidative stress is closely related to mitochondrial dysfunction.<sup>70</sup> This has been assessed in urine, serum and CSF. CSF did reveal elevated levels in PD but this was also the case in Multiple System Atrophy and Alzheimer's Disease.<sup>133</sup> CSF and serum levels seem to correlate poorly.<sup>134</sup> Urine and serum analysis has not revealed any consistent replicated trend in between multiple studies that have only shown conflicting results.<sup>135</sup>

Glutathione is a reducing agent that undergoes oxidation in the presence of oxidative stress. PD patients demonstrated increased oxidised glutathione in the CSF compared to controls, but total glutathione was similar between PD, controls, MSA and Alzheimer's Disease.<sup>136,137</sup>

DJ-1 protein was shown to be upregulated in early PD but not late PD compared to controls when assessed in the CSF, further studies however found a reduction in DJ-1 in the CSF but overall there were many similarities between PD, Alzheimer's Disease and Multiple System Atrophy.<sup>138-140</sup> In serum and whole blood results have again been conflicting limiting the utility of DJ-1 as a biomarker, one study in found elevated levels in Pd compared to controls whereas two further studies did not, one of which controlled for the presence of platelets and haemolysis which would lead to falsely high levels of DJ-1.<sup>141-143</sup>

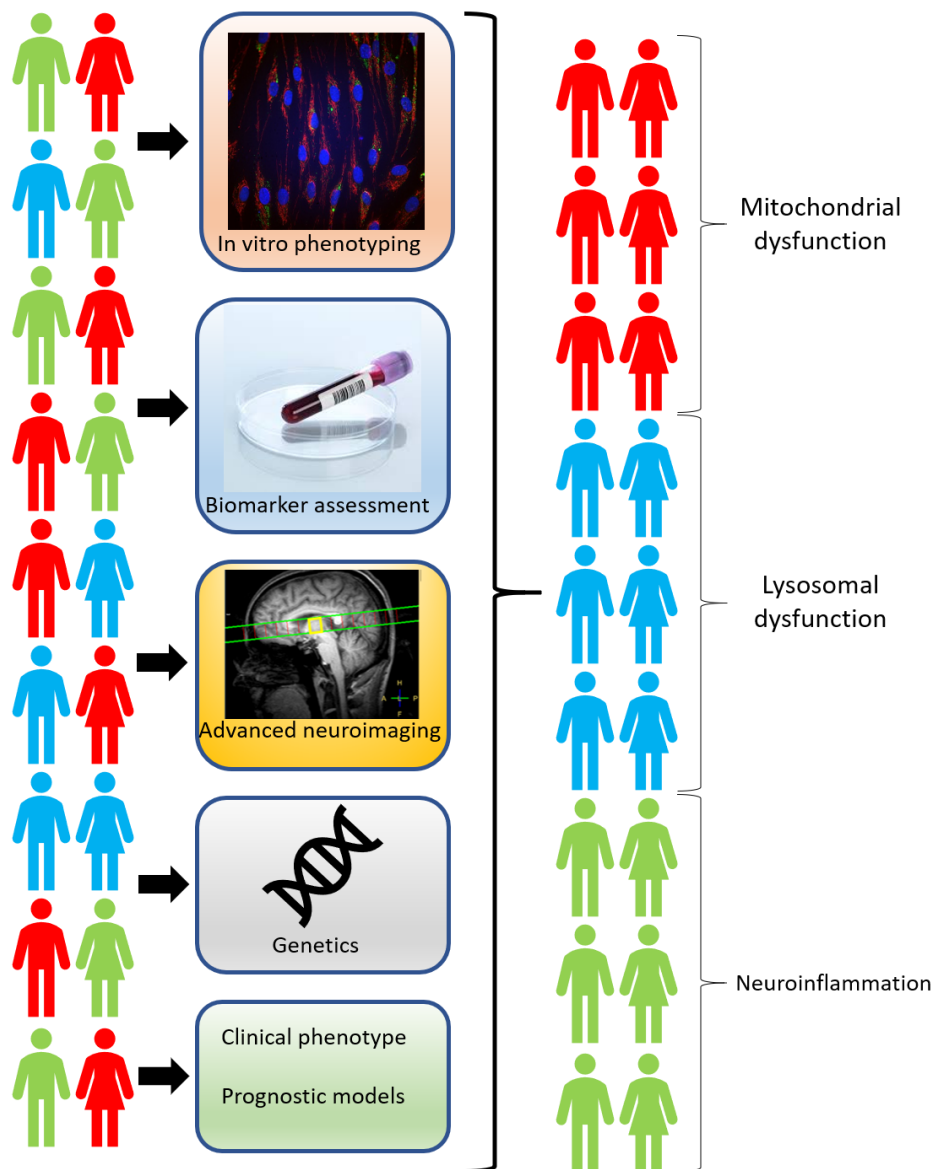


**Figure 1.2: Stratification of Parkinson's Disease to facilitate precision medicine approaches in neuroprotective trials**

Currently the challenge to developing successful neuroprotective trials is both the clinical and pathogenic heterogeneity of PD. Therefore, techniques need to be developing to stratify PD pathogenic phenotypes to target with specific compounds based upon their mechanism of action. On the left of the figure is an unstratified cohort which represents a population with a mix of multiple possible pathogenic mechanisms, for simplicity three are presented; mitochondrial dysfunction (red), lysosomal dysfunction (blue) and neuroinflammation (green). Next potential stratification techniques are proposed to help distinguish these pathogenic subtypes this could include techniques such as advanced neuroimaging e.g. PET, spectroscopic techniques etc, patient derived tissue in vitro modelling or more classical possible blood biomarkers. These techniques then stratify our original cohort into subtypes with which to target with specific drugs, such as mitochondrial rescue therapies for mitochondrial dysfunction or immunosuppression for neuroinflammatory driven PD.

Metabolomics has revealed some changes in lipid peroxidation related to reactive oxygen species, malondialdehyde is the most researched with a clear elevation in serum and plasma compared to controls that correlated inversely with disease progression.<sup>144</sup> This however was not replicated in the CSF.<sup>145</sup> Many other changes in various lipids have been detected but the utility of these abnormalities in the context of biomarker development is unclear at the moment.<sup>146</sup>

Further studies have since assessed cell-free circulating mtDNA in both serum and CSF as a potential biomarker. In 56 PD patients from a UK cohort (with 10 age matched controls), CSF was taken following comprehensive clinical assessment and in 30 patients repeated after 18 months. qPCR was performed for the genes *MTND1* and *MTND4*. There was a significant reduction in both *MTND1* and *MTND4* in the CSF of patients compared to controls. There was no correlation with clinical phenotype, age or gender. Longitudinal analysis did not reveal a significant change over the observed time period of 18 months.<sup>147</sup> Unfortunately this has also been observed in Alzheimer's Disease, however this was in both symptomatic patients and preclinical patients with abnormal CSF phosphorylated tau. In the PD study there was no significant correlation with tau and all patients met the UK PD Brain Bank diagnostic criteria.<sup>147,148</sup> Interestingly *LRRK2* associated PD had the greatest elevation in cell free circulating mtDNA.<sup>149</sup>

In peripheral blood mitochondrial DNA copy has been assessed in a study of 363 PD patients who had undergone cognitive assessment and genotyping for common genetic variants associated with cognitive impairment. Again, *MTND1* and *MTND4* were assessed using qPCR in peripheral blood cells. There was a significant reduction in mtDNA copy number between patients and controls (163±89 vs 195±129), this was independent of age and gender. There was no correlation with any cognitive assessments and mtDNA copy number. The same study confirmed these findings in post mortem samples from the substantia nigra pars compacta.<sup>72</sup>

The adaptation of biomarkers typically associated with mitochondrial disease has also yielded conflicting results. Fibroblast growth factor 21 (FGF-21) and growth differentiation factor 15 (GDF-15) have both shown promise as mitochondrial biomarkers in primary mitochondrial disease in the serum.<sup>150,151</sup> In a Chinese cohort comparing GDF-15 levels between patients with idiopathic PD (n=104) and healthy

controls (n=88) they found GDF-15 had a diagnostic sensitivity of 71.2%, specificity of 82.5%.<sup>152</sup> However, this was not replicated in a slightly larger UK cohort of 121 PD patients and 103 healthy volunteers, which found no clinical or diagnostic utility to GDF-15 or FGF-21.<sup>153</sup>

Urate is an important endogenous antioxidant and increased levels have been found to be associated with a reduced risk of PD. A previous meta-analysis identified high serum urate (defined as a serum urate above 6.8 mg/dL) reduced risk of PD by around 33% in a dose dependent manner.<sup>154</sup> A subsequent prospective case-control study drawing participants from a collective pool of 90,214 participants from three separate US based cohorts. 388 cases of PD were identified in this cohort with a previous recording of serum urate, these were matched with 1,267 controls. They identified again that particularly high urate levels were associated with a reduced risk of PD, although this was only seen in men.<sup>155</sup> Previous data from the DATATOP study assessing serum and CSF samples from over 700 participants revealed that elevated levels of urate in serum and CSF were associated with a reduced rate of clinical progression.<sup>156</sup> However, data the Michael J Fox Foundation led Parkinson's progression markers initiative, has failed to replicate a clear association between PD and urate levels, although urate may be reduced more in GBA-PD, likely limiting it's utility as a biomarker.<sup>157,158</sup>

#### Stratification of mitochondrial dysfunction in patient derived peripheral tissue

Mitochondrial function and morphology can be directly interrogated in fibroblasts which are readily grown from skin biopsies obtained by skin biopsy. Tissue fibroblasts have been used successfully in modelling genetic forms of PD such as *Parkin* and *LRRK2* and *GBA* related PD.<sup>64,77,159,160</sup>

Tissue fibroblasts have been used for mechanistic stratification in sporadic PD with one study using fibroblast cell lines generated from skin biopsies of 50 healthy volunteers and 100 sporadic PD patients. Mitochondrial and lysosomal phenotyping was performed through the assessment of MMP, cellular ATP and lysosomal number. Initial phenotyping did not identify any difference in group means between these measures but there was a significantly greater variability in the sporadic PD fibroblasts with respect to ATP and MMP with 12/100 and 4/100 PD patients having ATP levels more than two and three standard deviations below the control mean respectively.

Similar results were found with respect to lysosome number with 15/100 PD patients having lysosome counts greater than two standard deviations from the control mean. Reduced protein levels of complex I and complex IV were found in a mitochondrial subgroup of five patients with the lowest cellular ATP values.<sup>161</sup> This mirrors post-mortem abnormalities in the mitochondrial complexes discussed earlier. Reduced cathepsin D activity per lysosome, was found in a lysosomal subgroup of five patients with the highest lysosomal counts, suggesting lysosomal dysfunction. Subsequently in 3 sporadic PD cases and 3 healthy volunteer lines, they utilised a direct reprogramming of patient fibroblasts into induced neuronal progenitor cells (iNPCs) for conversion into tyrosine hydroxylase (TH) positive neurons. This hold several advantages over classical induced pluripotent stem cell models as iNPCs are never converted to an embryonic cell type and therefore maintain their epigenetic phenotype, which is crucial in PD where age is the greatest risk factor for the development of the disease.<sup>162,163</sup> The mitochondrial and lysosomal abnormalities observed in the fibroblasts were further exacerbated with marked reductions in cellular ATP and MMP in TH positive neurons and an increased lysosome count compared to healthy volunteers.<sup>161</sup> Finally, UDCA, a potential mitochondrial rescue agent, was administered to six sporadic PD lines with mitochondrial abnormalities greater than two but less than 3 standard deviations from the control mean. UDCA restored the reduced levels of MMP, ATP and complex I activity to similar levels as control lines.<sup>161</sup>

One prior study examined fibroblasts derived from 47 patients with sporadic PD and 21 matched controls specifically to determine if markers of clinical severity were related to any underlying pattern of mitochondrial dysfunction. All lines underwent in-depth mitochondrial phenotyping and they used a classification and regression tree analysis to determine if mitochondrial phenotype could classify subgroups according to scores on clinical rating scales. They found that higher MDS-UPDRS III scores were associated with lower ATP/ADP levels and greater superoxide production, this was only in galactose containing media, which does not contain glucose and therefore forces mitochondria to rely on oxidative phosphorylation for ATP production. It was unclear why this may be the case but may represent that in PD under normal conditions where glycolysis can be used to meet energy demand that OXPHOS is suppressed to reduce oxidative stress. Therefore, when the ability to utilise glycolysis

is reduced in galactose only culture conditions OXPHOS must be used to produce ATP and reveals the mitochondrial deficits with increased ROS production.<sup>164</sup>

Tissue fibroblasts offer an easily accessible tissue to obtain from patients for mechanistic stratification, of note no previous studies have attempted to assess mitochondrial dysfunction in the peripheral tissue in tandem with assessments of bioenergetic function in the central nervous system which would be of great interest.

### Stratification of bioenergetic function in the brain using <sup>31</sup>Phosphorous Magnetic Resonance Spectroscopy

<sup>31</sup>Phosphorous Magnetic Resonance Spectroscopy (<sup>31</sup>P-MRS) offers the ability to assess brain bioenergetics in pathologically relevant anatomical sites to PD *in vivo*. This is a distinct advantage over the biomarkers discussed above.

<sup>31</sup>P-MRS will form a key part of this thesis. I will therefore first describe basic aspects of this imaging technique in some detail. These sections use the following references, unless specifically referenced otherwise, from chapters of highly regarded and established reference texts by de Graaf, 2019<sup>165-170</sup> and Stagg and Rothman, 2014<sup>171-176</sup>.

Magnetic resonance spectroscopy (MRS) is a non-invasive technique using similar principles underpinning standard magnetic resonance imaging (MRI), the latter of which has been utilised extensively in clinical practice for decades. However, instead of producing anatomical images, MRS detects resonant frequencies and allows quantification of metabolites within the specific tissue examined.<sup>177</sup> Analogous to standard proton (<sup>1</sup>H) based clinical anatomical imaging, proton spectroscopy is the most widely used form of spectroscopy both clinically, for example in the diagnosis and monitoring of brain tumours, and in research.<sup>178</sup>

In <sup>31</sup>P-MRS, the nuclei of interest are phosphorous (<sup>31</sup>P) rather than hydrogen (<sup>1</sup>H) based and this provides an opportunity to investigate key metabolites in energy production such as ATP (which has three resonances;  $\beta$ ,  $\alpha$  and  $\gamma$ ), phosphocreatine (PCr) and inorganic phosphate (Pi) which all correspond to clear spectroscopic signals (**Figure 1F**). It is therefore an ideal approach to assess brain bioenergetics

### *Methodological basis of spectroscopy*

Certain atomic nuclei that demonstrate a clear magnetic moment (referred to as “spin”) exhibit a natural phenomenon known as precession, the angular momentum of a nuclei about an axis. These nuclei can then exhibit resonant behaviour. Magnetic resonance occurs with the input of external energy into a spin system to change the energy state of those nuclei. This input of energy is at a frequency near the precession frequency of a nucleus and is proportional to the strength of the external magnetic field  $B_0$  and the gyromagnetic ratio  $\gamma$ , a nucleus-specific constant. This relationship is described using the Larmor equation, shown in equation 1.1. The required frequency to induce nuclear resonance is termed the Larmor frequency.

$$\omega = \gamma B_0$$

#### **Equation 1.1: The Larmor frequency**

When MR-sensitive nuclei are placed within an external magnetic field (referred to as  $B_0$ ), the spins of these nuclei will precess with respect to the axis of  $B_0$ , and the net magnetisation vector (the averaged angular momentum of all nuclei) will be aligned with  $B_0$ , it should be noted though that only a certain proportion of spins will be preferentially aligned with  $B_0$ . The direction of  $B_0$  is in the z-axis by convention in MRS. For these spins, the direction of this alignment can either parallel or antiparallel in the case of dipolar nuclei, such is the case for  $^1\text{H}$  and  $^{31}\text{P}$  (**Fig 1.3A**). This property can be exploited by applying a radiofrequency (RF) pulse (termed  $B_1$ ) at the Larmor frequency which will lead to the nuclei spins' to absorb energy and transition from a lower energy state to a higher energy state e.g. from antiparallel to parallel to  $B_0$ . This RF pulse is applied at an angle relative to  $B_0$  in the xy axis to rotate the spins of those nuclei so that the net magnetization vector of the system is now aligned with the direction of  $B_1$  in the transverse plane, and these spins are now in alignment with each other (phase coherence). However, once the RF pulse has finished the spins of the nuclei will then relax back from the higher energy state to the lower energy state, and this dispersed energy is released as electromagnetic radiation.

This energy is dispersed to the local environment around the nuclei and is largely measured by the recovery of the longitudinal net magnetisation vector in the direction

of  $B_0$  and is termed  $T_1$  relaxation. The total time taken for the nuclei to fully relax back to its original state with respect to  $B_0$  and restore the net magnetisation vector is the  $T_1$  constant (or time). The other key process occurring after the termination of an RF pulse is the loss of the transverse components of magnetisation in the  $xy$  axis as the phase coherence of the nuclei decays or dephases. This is termed  $T_2$  relaxation, and the time taken for a nuclei to lose all transverse magnetisation and relax in the  $x$  and  $y$  axis is the  $T_2$  constant (or time). In reality the transverse magnetisation relaxes much faster than anticipated and this is due to  $T_2^*$  effects where transverse magnetisation relaxation is affected by local magnetic field inhomogeneities either be it from the magnet itself, local field distortions caused by different tissue compositions or other materials placed within the magnetic field.  $T_2^*$  is always of shorter duration than  $T_2$  and can be thought of as the effective  $T_2$  once the above factors in magnetic field inhomogeneities have been taken into account.

The dispersion of energy in the form of electromagnetic radiation following the termination of an RF pulse is detected as an oscillating voltage by magnetic induction in a receiver coil and is the basis of generating an MRS signal.

However, nuclei are not examined in isolation and in the human body all MR sensitive nuclei will have subtly varying resonant frequencies. This is based upon several factors in the local chemical environment that the nuclei are present in. For example, when a greater number of electrons are in close proximity to an MR sensitive nucleus due to the molecular composition then the magnetic field that nucleus experiences is slightly less than another nucleus with fewer electrons in close proximity. This is called electron shielding and causes a 'shift' in the resonant frequencies of the nuclei being examined due to the molecular composition that the nuclei exist in. This 'chemical shift' is the key physical principle underpinning MRS, because the resonant frequencies of a nucleus will change depending on its molecular environment. Therefore, the varying frequencies detected by a receiver coil can be assigned to different molecules containing MR sensitive nuclei based upon their chemical shift.

In addition to chemical shift, J-coupling can also alter the detected resonant frequency. J-coupling is independent of  $B_0$  and is the result of the indirect interaction between two spins via the intervening electron structure of the molecule. This can be either homo-nuclear (between nuclei of the same species) or hetero-nuclear (between nuclei of

different species such as proton and phosphorus nuclei). This is generally a weak scalar interaction (e.g. affects the precessional frequency but not the direction of the angular momentum) and further modulates the MRS signal as it will split the resonance of a molecular structure into several similar resonances, represented by several resonant peaks within a spectra (a multiplet).

Following a single RF pulse, the detected signal is termed a free induction decay signal (FID) that is composed of multiple sinusoidal waves, each representing differing resonant frequencies. The differing Larmor frequencies of a nucleus are the result of chemical shift and J-coupling providing a unique 'fingerprint' to each molecule. Through Fourier transformation, an FID in the time-domain is decomposed into the individual frequency components and amplitudes in the frequency domain (see **Figure 1.3**).

#### *Acquisition of MR signal and methodological considerations*

Although the above discussed principles apply to any derived MRS signal, there are many different methods available to acquire an MRS signal, and several parameters that must be taken into account when designing an MRS acquisition. Additionally, the method of spectral localisation must also be chosen as many MRS experiments require derivation of an MRS signal from a specific anatomical structure.

In standard clinical MRI the three main parameters that determine image contrast are the  $T_1$ ,  $T_2$  and  $T_2^*$  times of the nuclei being examined in the tissue (discussed in greater detail earlier). The  $T_1$ ,  $T_2$  and  $T_2^*$  times of a specific nuclei differ based upon the molecular composition of the tissue examined. These properties are most important when determining the repetition time (TR) and echo time (TE) to use in an MRS acquisition. TR is the time between each successive RF pulse. TE is the time from the middle of the RF pulse sequence to the middle of the echo.

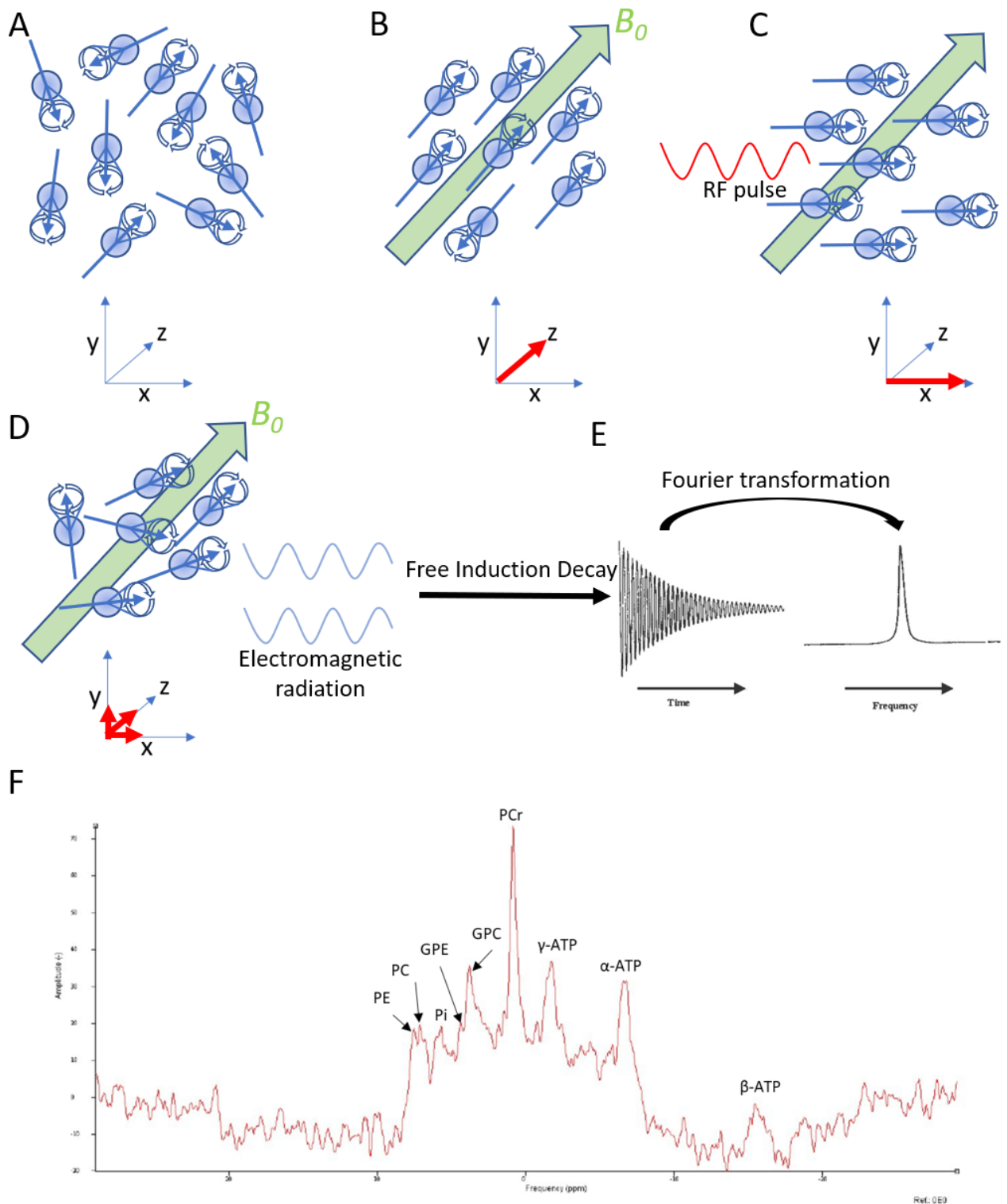


**Figure 1.3: The basis of Magnetic Resonance Spectroscopy**

*This figure depicts the methodological basis of MR spectroscopy. (A) Depicts the random Brownian motion of a group of MR sensitive nuclei. These nuclei exhibit a ‘spin’ with associated angular momentum, the direction of which is denoted by the blue arrows. Below the net magnetisation vector (NMV), at this point there is no NMV in any direction due to the changing random Brownian motion of these nuclei and their associated molecules. (B) When placed in a strong external magnetic field ( $B_0$ ) denoted by the large green arrow these dipolar*

nuclei will align in either a parallel or antiparallel state, as a result the NMV is now in the same direction as  $B_0$  which is the z-axis by convention. (C) A radiofrequency (RF) pulse applied at the Larmor frequency of the nuclei moves the spins into the xy-axis by a certain degree (flip angle), the NMV is reflected on the axis below. (D) following the cessation of the RF pulse these nuclei will relax back to alignment with  $B_0$ , this emits electromagnetic radiation due to the changing magnetic field that will induce a current in the receiver coil and is detected as free induction decay (FID). This relaxation is both in the z-axis ( $T_1$ , the time taken for recovery in the longitudinal axis) and in the xy-axis ( $T_2$  and  $T_2^*$  effects, the time taken for transverse magnetisation to relax in the x and y axis). (E) This FID is composed of multiple sinusoidal waves which can be converted into spectral peaks through Fourier transformation to identify the frequency components in the time domain. (F) A typical  $^{31}\text{P}$ -MRS acquired spectra, in this case from the midbrain of a healthy control. This spectrum has been phased appropriately to ensure absorptive line shapes (all resonances of interest are in the same direction) for all resonances of interest and undergone 10Hz Gaussian apodisation (this removes the sampled signal at the edges of the acquisition to improve visualisation of each peak at the expense of broadening each peak) to aid visualisation. Here there are clear peaks represented the key molecules that can be quantified in  $^{31}\text{P}$ -MRS. PE=phosphoethanolamine, PC=phosphocholine, Pi=inorganic phosphate, GPE=glycerophosphoethanolamine, GPC=glycerophosphocholine, PCr=phosphocreatine and the three ATP resonances  $\gamma$ -,  $\alpha$ -, and  $\beta$ -ATP.  $\gamma$ -ATP and  $\alpha$ -ATP are both represented by doublet peaks due to the J-coupling of their neighbouring phosphorus nuclei and  $\beta$ -ATP is a triplet peak due to J-coupling as it neighbours both the  $\alpha$ - and  $\gamma$ -ATP phosphorus nuclei. PE and PC represent the phosphomonoesters (precursors to phospholipid membrane synthesis) and GPE and GPC represent the phosphodiester (phospholipid membrane breakdown products).

The selection of parameters such as TR and TE affect the acquired signal-to-noise ratio (SNR). Noise is the random background signal arising from things such as radiofrequency coil resistance or electronic noise in certain MRI components. The strength of the acquired signal in the region of interest can be used to express the SNR, higher values are desirable for any experiment.

TR selection is important in any MRS acquisition and accounts for  $T_1$  effects. To maximise signal strength with respect to the  $T_1$  relaxation effects a TR time 5 times greater than  $T_1$  time should be chosen. In this situation maximum SNR will be achieved by applying the RF pulse at  $90^\circ$  to  $B_0$ . In reality, using such a long TR results in prohibitively long acquisition times and therefore the selection of a shorter TR is necessary. This means that between each RF pulse the net magnetisation in the direction of  $B_0$  (termed  $M_z$ ) has not fully recovered. Eventually after a number of RF pulses a new steady state of  $M_z$  will be reached, this effect is called partial saturation. A higher steady-state  $M_z$  will result in a better SNR. In instances of partial saturation, a  $90^\circ$  flip angle is not optimal and will lead to signal loss in the FID following further

RF pulses. A smaller angle is therefore required, the optimal flip angle to achieve the greatest SNR given a certain  $T_1$  is called the Ernst angle. Certain Ernst angles and short TR times can be used to maximise the SNR of certain molecular species  $T_1$  times at the expense of a much greater variation in the signal of other molecular species.

The effects of  $T_2$  and (more importantly)  $T_2^*$  can never be eliminated and will always affect an MRS signal. Generally, the macroscopic inhomogeneities contributing to  $T_2^*$  can be minimised by using spin-echo pulse sequences. Selection of TE is most relevant in these spin-echo acquisitions (rather than an FID acquisition), where two RF pulses are applied in sequence, a  $90^\circ$  pulse followed by a  $180^\circ$  pulse at a time of  $TE/2$ . This  $180^\circ$  pulse refocuses the spins of certain nuclei which have dephased (out of phase coherence) due to magnetic field inhomogeneities back into phase to improve the acquired signal and reduce  $T_2^*$  effects. This generally results in an improved SNR, with greater gains with an increasingly short TE.

Given that within a spectra there are several resonances each with slightly different  $T_1$  times (e.g. the  $T_1$  time of PCr is different to that of Pi) the SNR of a particular resonance will be dictated by the choice of TR, TE and the Ernst angle. Optimisation of these parameters is key to improving the sensitivity of an MRS experiment.

In a perfect MRS experiment the external magnetic field,  $B_0$ , used would be completely homogenous so that all nuclei in an examined tissue would experience an identical field. In practice, this is not the case and the magnetic field is subtly distorted by magnetic susceptibility of different tissues and the surrounding air. This therefore creates magnetic field inhomogeneities and results in a distribution of Larmor frequencies observed for a nucleus rather than a single frequency that results in a broadened spectral peak. This can be compensated by  $B_0$  'shimming', where a supplemental corrective magnetic field can be applied to remove the inhomogeneities in the region of interest (ROI). This ensures that the selected ROI will experience as homogenous a  $B_0$  field as possible. The drawback of this though is that outside the shimmed ROI there is reduced  $B_0$  homogeneity that can profoundly affect signal quality. Inadequate shimming for multi-voxel spectroscopic techniques can also impact spatial encoding if the  $B_0$  field changes over time.

### *Localisation in Magnetic Resonance Spectroscopy*

Spatial localisation techniques broadly fall into single-voxel and multivoxel techniques. In the event that precise spatial localisation is not required, then a pulse-acquire sequence can be used, which apply a single RF pulse and then capture the resultant FID signal. These are rapid to acquire but tend to have much greater line broadening in the resultant spectra due to the magnetic field inhomogeneities across the whole excited volume resulting in a greater range of chemical shifts for each spectral resonance of interest.

Non-localised spectroscopy is generally undesirable given that, in many *in vivo* experiments, the MRS signal in a specific brain region is of pathological interest. Single voxel spectroscopy allows a single spectrum to be derived from a single voxel placed in a region of interest. Single voxel techniques generally employ three orthogonal slice-selective pulses to select a signal from the intersection of all three slices, such as seen in Image-Selected In Vivo Spectroscopy (ISIS) techniques. ISIS is the spectral localisation technique of choice in  $^{31}\text{P}$ -MRS as it acquires an FID signal that is almost devoid of  $T_2$  weighting, this is useful as it limits the effects of magnetic field inhomogeneities inherent across different tissues. This is in contrast to other techniques more commonly used in proton spectroscopy such as stimulated echo acquisition mode (STEAM) or point resolved spectroscopy (PRESS) which generate a stimulated echo using three  $90^\circ$  pulses in the case of STEAM and a spin-echo created by one  $90^\circ$  and two  $180^\circ$  refocusing pulses in the case of PRESS. STEAM and PRESS translate poorly to  $^{31}\text{P}$ -MRS as the minimum TE that these acquisitions can employ is still too long for the relatively short  $T_2$  times of phosphorus nuclei to generate an appropriate echo signal.

ISIS can be used in 1D, 2D and 3D configurations. In the case of 1D ISIS It utilises a frequency selective inversion pulse in a specific gradient followed by the non-selective excitation of the whole volume. This inversion pulse is captured in the on and off state generating an FID for each acquisition that starts in the opposite direction along an axis. The localised signal is the calculated difference between the two experiments, leaving an FID representative of the slice obtained by the frequency selective gradient. This can be expanded to both 2D and 3D configurations where increased combinations of gradients in orthogonal directions are captured in the on/off state

where the resulting differences between all acquired signals will result in a single localised volume (**Figure 1.4**).

Chemical shift imaging (CSI) is the most utilised multi-voxel technique. This utilizes a non-selective (broadband) RF pulse with phase-encoding localization and recording of FIDs. Phase encoding is typically performed with ISIS, discussed above, to enable localisation of the acquired FID. This can be obtained in 1D, 2D or 3D configurations to generate a grid of voxels covering the region of interest.

#### *Quantitation of Magnetic Resonance Spectroscopy Signal*

The amplitude of a specific spectral peak is proportional to the number of nuclei resonating at that specific frequency and can therefore be thought of as the concentration of that molecule in the tissue. However, the amplitude of a peak can also be affected by multiple other technical factors, such as the TE and TR used, coil loading (change in impedance of transmit/receive coils given varying body shape and size), receiver gain (the calibration of the receiver amplifier with respect to the maximum MR signal being detected) and the external magnetic field strength. Further, it is extremely difficult to completely measure variances due to coil loading and receiver amplifier gain, thus making the determination of absolute concentrations of MR visible metabolites extremely challenging. Several techniques that attempt to quantify absolute quantifications are generally still prone to these challenges.

One method is to use phantoms containing known quantities of certain metabolites to generate a reference peak of known concentration and calculate the concentrations of all other spectral resonances relative to this. A small phantom placed in the coil with the patient being scanned can create a reference peak within the same acquisition. However, this has several disadvantages. Typically, the phantom must be placed in an area in which is difficult to guarantee a homogenous magnetic field through shimming during the acquisition (for example, at the edge of the field of view) and the presence of the phantom induces further magnetic field inhomogeneities and changes in coil loading in the examined *in vivo* tissue. An alternative approach is that the phantom is placed instead in the same position as the tissue examined either before or after the *in vivo* data has been acquired. This avoids the negative impact upon the magnetic field homogeneity that scanning a phantom simultaneously introduces and therefore preserves signal quality in the subject. However, when the phantom is

scanned separately to the subject it is extremely difficult to replicate the same coil loading effects and resultant magnetic field to ensure that the phosphorus signal detected was done so in an identical environment to the subject, thus limiting the comparison of phosphorus resonances across the two mediums (phantom and brain).

Given the difficulties in ascertaining true absolute metabolite concentrations in MRS, many studies elect to express metabolite peaks as a ratio to another reference peak within the same spectrum. For example, choline or creatine may be used as the denominator in proton spectroscopy or phosphocreatine in  $^{31}\text{P}$ -MRS. This is a useful approach, because technical confounds cancel out, but assumes that the reference peak is expected to be constant across both health and disease and can be less reliable if this assumption is not met. Alternatively, the integrals of each peak can instead be normalised to the total phosphorus signal detected, giving normalised values that can be compared across subjects.<sup>179</sup> This approach has been used widely in  $^{31}\text{P}$ -MRS previously and is likely more resilient to partial volume effects (e.g. the effects upon detected signal caused by varying tissue composition within the region of interest, ROI).<sup>179-181</sup>

Following acquisition of a spectrum, several post-processing steps are necessary prior to quantification of the signal. Zero-filling the data by appending zero value data points to the end of the FID, to generally double the original number of data points, improves the frequency resolution of the spectra to allow better identification of peaks but does not improve the accuracy of the quantification of each peak.

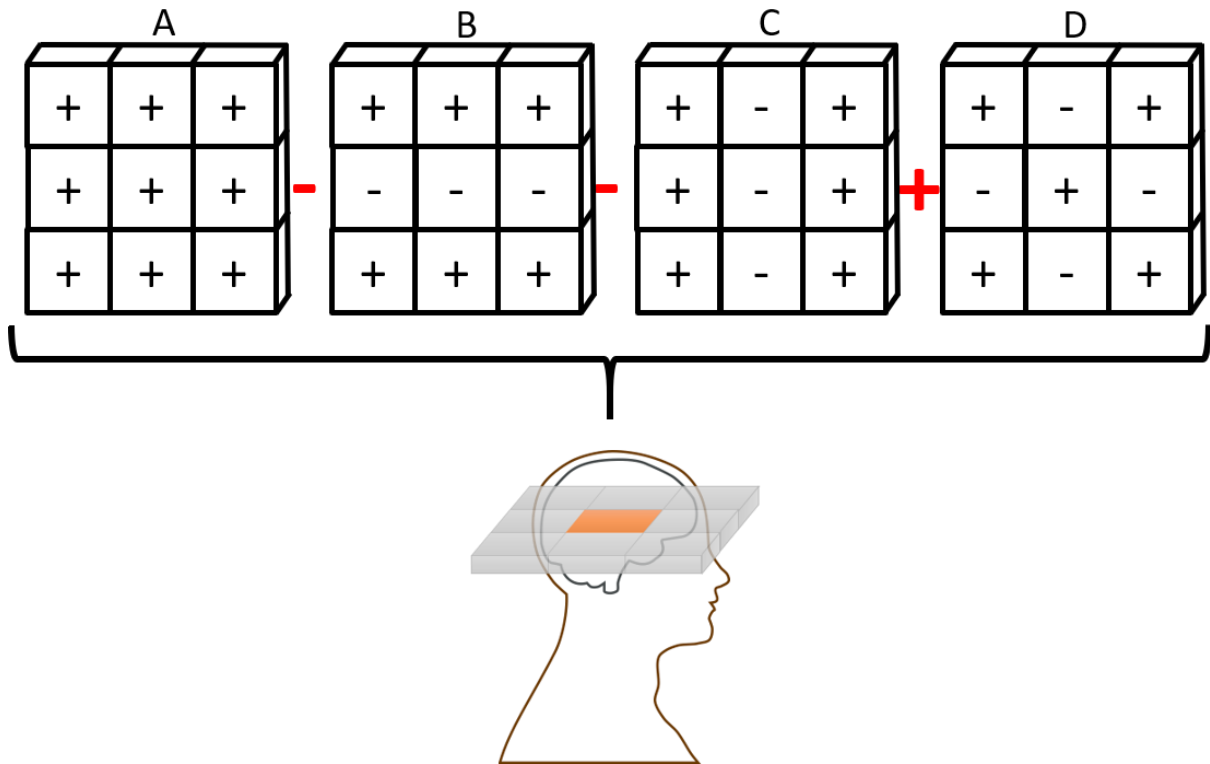


**Figure 1.4: Image-selected In Vivo spectroscopy (ISIS)**

*An example of how a 2D ISIS acquisition is acquired, using a plane acquired from the brain as an example with the orange shaded area being the resultant voxel of interest. Initially a radiofrequency (RF) pulse captures a 90° flip angle acquisition of the whole field of view (denoted by '+'). Subsequent acquisitions in B and C then utilise a single inversion gradients at 180° (denoted by '-') in two additional planes. The fourth acquisition is D which utilises the same inversion gradients from B and C but simultaneously so that the point of overlap becomes a non-inverted area of acquisition. The subtraction of B and C from A with the addition of D leaves the resultant acquired signal representative of the single shaded voxel of interest. For a full 3D ISIS acquisition a total of 8 acquisitions are needed. ISIS was initially developed for single voxel spectroscopy but is now used commonly as a multivoxel method using the same approach as detailed above.*

All spectra must be appropriately phased prior to quantification. Following Fourier transformation of an FID the resultant resonances of interest in a spectrum may not be in the absorptive phase (purely positive). This is because the initial spectrum is calculated using an arbitrary initial phase detected by the hardware that may not be ideal for the spectrum acquired. Phasing is a transformation that rotates the sinusoidal waves of the FID by a certain amount in degrees. This is done using both zero order (affecting the whole spectrum) and first order (with reference to a single point, generally a particularly dominant peak, with the correction factor varying in relation to

distance from that peak in frequency) phasing to show purely absorptive line shapes. This ensures all peaks for quantification are all pointing in the same direction, to ensure consistent quantification. Apodisation is a function to smoothly reduce a sampled signal down to zero, generally where data has been zero filled, to prevent a sharp ending of the signal before zero-filling. This is used to prevent truncation artifacts but can result in broadened peaks which may affect quantification. Apodization is a step that can be performed but is not always done as it alters underlying FID prior to quantification.

Following post-processing the relative intensity (area under the peak) can be calculated using one of several methods, LCModel is the most commonly used software algorithm used for spectral peak fitting and quantification in proton spectroscopy.<sup>182</sup> In <sup>31</sup>P-MRS the AMARES (advanced method for accurate, robust and efficient spectral fitting) algorithm is frequently utilised as it allows a highly customisable set of prior knowledge to be imbued to the algorithm prior to quantification. This prior knowledge can be used to constrain peak widths, to guide peak identification in multiplet peaks due to J-coupling, and constrain the location of peaks in the spectra based upon previous work, to ensure that signal rather than noise is fitted.<sup>183</sup> These constraints can be classed as 'hard' or 'soft' constraints. Hard constraints will fix a parameter of the analysis to a single value, for example fix the J-coupling constants between the ATP multiplets to a single value. Soft constraints will allow certain parameters to fall within a range. These are generally used for the selection of peaks, as each peak position varies slightly between each individual. AMARES can also perform weighting which is the multiplication of the first points of the FID, with a quarter-sine wave. This is particularly useful in the quantitation of a spectrum with a large background signal or and improves the quantitation in these circumstances.

### *Considerations in <sup>31</sup>Phosphorus Magnetic Resonance Spectroscopy*

Despite the relative popularity of proton spectroscopy, much of the developed technology with respect to acquisition and quantification does not necessarily translate well to <sup>31</sup>P-MRS for several reasons. The  $T_2$  times of many phosphorus metabolites are much shorter than metabolites detected in proton spectroscopy and therefore impacts the choice of acquisition sequence. Echo based acquisitions such as PRESS and STEAM, widely used in proton spectroscopy due their high SNR, are unsuitable

for phosphorus spectroscopy as the minimum TE achievable is still much greater than the  $T_2$  times of phosphorus metabolites. This would mean that many phosphorus metabolites would be profoundly underestimated and results in a reduced SNR. Therefore  $^{31}\text{P}$ -MRS typically relies upon the generation of FIDs, where the short time to from RF pulse to signal acquisition results in a greater SNR. Although STEAM can utilise a relatively short TE, the resultant SNR is generally poor compared to ISIS in  $^{31}\text{P}$ -MRS.

$^{31}\text{P}$ -MRS demonstrates both prominent hetero- and homonuclear coupling. Proton coupling is particularly problematic for detection of phosphomonoesters and phosphodiesteres. This can be accounted for by using proton decoupling techniques utilising RF pulses to disrupt heteronuclear J-coupling during acquisition. In  $^{31}\text{P}$ -MRS, the three resonances of ATP (one for each phosphate group) demonstrate clear J-coupling between phosphorus nuclei with characteristic doublet peaks to represent  $\alpha$ -ATP and  $\gamma$ -ATP and a triplet peak for  $\beta$ -ATP. This is not problematic given an appropriately designed spectral quantification algorithm. Somewhat similar to J-coupling, which is the interaction between nuclei through bonds, there can also be dipolar interactions between  $^{31}\text{P}$  and  $^1\text{H}$  spins through space, which can result in poorer peak definition. This effect can be reduced by using nuclear Overhauser enhancement (NOE). This applies a selective RF pulse at a frequency to saturate the  $^1\text{H}$  resonance in the tissue prior to acquisition of the  $^{31}\text{P}$ -MRS spectra and reduces the dipolar interaction between  $^{31}\text{P}$  and  $^1\text{H}$  spins. This results in an improved SNR of the  $^{31}\text{P}$ -MRS spectra.

#### *Previous $^{31}\text{P}$ -MRS studies to assess mitochondrial dysfunction in Parkinson's disease and related disorders*

$^{31}\text{P}$ -MRS has been used to assess for bioenergetic defects in the brains of patients with mitochondrial cytopathy. One study assessed ten patients with mitochondrial cytopathy (four with chronic progressive external ophthalmoplegia, five with Leber's hereditary optic neuropathy and one with neurogenic muscle weakness, ataxia and retinitis pigmentosa) and thirty-six age-matched healthy controls. Patients with mitochondrial cytopathy were also treated with coenzyme Q10 for 6 months and were scanned pre- and post-treatment.  $^{31}\text{P}$ -MRS was obtained from the occipital lobes using a pulse-acquire sequence of TR 5000ms and localised using depth-resolved surface-coil spectroscopy (DRESS). Patients with mitochondrial cytopathy displayed high ADP

and Pi and low PCr compared to controls, implying impaired ATP production via oxidative phosphorylation. Additionally, the authors calculated the Gibbs free energy of ATP hydrolysis ( $\Delta G_{ATP}$ ). This term expresses the amount of useful energy released to a system upon hydrolysis of ATP. The value is negative as the hydrolysis of ATP is an exergonic reaction, and more negative values indicate greater useful energy for work generated by the hydrolysis of ATP. The authors found a higher  $\Delta G_{ATP}$  (i.e. less negative values) in mitochondrial cytopathy compared to controls, although this improved (became more negative) after treatment with coenzyme Q10 and approached control values.<sup>184</sup>

The first study applying  $^{31}P$ -MRS to people living with PD assessed differences between Multiple System Atrophy (MSA) (n=15), PD (n=13) and healthy controls (n=16) in the occipital lobe using a surface coil and DRESS localisation at 1.5T. MSA demonstrated reduced PCr and Pi compared to the control group (3.6mM $\pm$ 0.28 vs 4.41mM $\pm$ 0.20 and 1.56mM $\pm$ 0.33 vs 1.29mM $\pm$ 0.13, respectively, both p<0.05). Pi was increased in PD compared to controls (1.63mM $\pm$ 0.21 vs 1.29mM $\pm$ 0.13, p<0.0001). Cytosolic Mg<sup>2+</sup> was reduced in PD compared to controls (143mM $\pm$ 11 vs 181mM $\pm$ 23, p<0.0001). Between the PD and MSA groups, only PCr was significantly lower in MSA compared to PD, and Mg<sup>2+</sup> was lower in PD compared to MSA. Using the two parameters of PCr and Mg<sup>2+</sup> the authors were able to classify 86% of patients correctly according to diagnosis.<sup>185</sup>

Another early study utilised a combined multimodal imaging methodology with both  $^{31}P$ -MRS and FDG-PET.<sup>181</sup> This study included ten PD patients and nine age-matched controls. The disease duration covered a large range of 2.2-15 years although no patients had clinically evident dementia.  $^{31}P$ -MRS was obtained using a 3D CSI technique at 1.5T with a dual-tuned  $^1H/^{31}P$  head coil. Voxel size in this study was 40x40x40mm giving a voxel size of 64cm<sup>3</sup> which by current imaging standards would be considered large, although was appropriate for the time of the study. Three voxels were placed within right and left temporoparietal regions and occipital cortex, and a fourth central voxel encompassed the thalamus, globus pallidus and substantia nigra. There was a significant increase in Pi/ $\beta$ -ATP ratio implying impaired oxidative phosphorylation in both right and left temporoparietal regions and the central voxel (1.07 $\pm$ 0.24 vs 0.66 $\pm$ 0.22, 0.96 $\pm$ 0.27 vs 0.62 $\pm$ 0.24, 1.00 $\pm$ 0.32 vs 0.56 $\pm$ 0.14 respectively, all p values <0.05). Elevations in Pi/ $\beta$ -ATP ratio in the temporoparietal

regions were inversely correlated with cognitive testing performance. FDG-PET revealed reduced metabolism bilaterally in the temporoparietal regions, the same regions which demonstrated an increase in Pi/ $\beta$ -ATP ratio. Concomitant FDG-PET hypometabolism and increased Pi/ $\beta$ -ATP ratio was considered to imply deficits in both glycolysis and oxidative phosphorylation. It should be noted that different tissues in the brain have varying dependency on glycolysis with neuronal populations having a much greater reliance on oxidative phosphorylation compared to astrocytes, which are much more dependent upon glycolysis and are abundant within the white matter.<sup>186</sup>

Bioenergetic function represents a dynamic equilibrium and functional assessment of *in vivo* bioenergetics can be difficult when assessed in a static situation. A dynamic functional study of occipital lobe bioenergetics in PD has been previously used to demonstrate impaired function in PD.<sup>187</sup> This study used a <sup>31</sup>P-MRS surface coil placed over the occipital lobe in 20 PD patients and 20 healthy controls. Dynamic testing was provided by recording spectra in the resting state, during visual activation in the form of 8Hz flashing lights and in the recovery phase. There were no spectroscopic differences between groups during rest and activation. However, during the recovery phase, high energy phosphates (HEPs, a combination of PCr and  $\beta$ -ATP), fell significantly (36% relative to levels at rest) in PD, implying impairment of oxidative phosphorylation to restore  $\beta$ -ATP levels.<sup>187</sup> The same group used the same functional <sup>31</sup>P-MRS protocol in 10 early-onset PD patients with *PINK1* mutations, 10 early-onset sporadic PD patients and 20 healthy controls. The *PINK1* patients demonstrated low HEPs at baseline with a subsequent fall during activation whereas the sporadic PD patients demonstrated normal HEPs at baseline but a sharp reduction during recovery similar to the previous study. Overall, bioenergetic dysfunction was much more marked in the early-onset *PINK1* PD patients as would be expected given the impaired mitophagy observed in *PINK1* PD.<sup>188</sup>

The most extensive previous high-quality study of <sup>31</sup>P-MRS was carried out in 2009.<sup>189</sup> This was a cross-sectional study in which <sup>31</sup>P-MRS was applied to 29 people with PD and 19 age matched controls. The PD cases had a wide range of disease duration (2-20 years) and severity, with 16 Hoehn and Yahr (H&Y) stage I-II and 13 at stage III-IV. The study was performed with a dedicated dual tuned <sup>1</sup>H/<sup>31</sup>P head coil at 3T. The researchers performed 2D <sup>31</sup>P-MRS CSI imaging with two acquisitions, an axial acquisition capturing the putamen in the basal ganglia and a coronal acquisition

aligned to capture the substantia nigra. The voxel size was 30x30x25mm<sup>2</sup>. The authors calculated absolute metabolite concentrations using an independent spherical reference phantom with a set concentration of 20mmol/L phosphate using the phantom, replacement method. There was a significant reduction in PCr, ATP and HEPs in the putamen in PD compared to controls, with a trend for a greater reduction in the putamen contralateral to the most clinically affected side. In the midbrain, ATP and HEPs were reduced in the midbrain voxel contralateral to the worst clinically affected side in PD compared to controls. Abnormalities were also found in phospholipid metabolism with reduced PE and GPE in the contralateral and ipsilateral putamen of H&Y stage I-II PD compared to controls. Reduced PE and GPE was also reduced in the contralateral midbrain in H&Y stage III-IV PD compared to controls.<sup>189</sup>

Of note, the reported ATP concentrations are far lower than values previously reported. This could be explained by differing methodologies and the challenges of absolute quantification of phosphorus metabolite concentrations using phantom replacement methods.<sup>190</sup>

Subsequently the same group utilised the same acquisition parameters to assess two *PINK1* homozygous PD patients, nine *PINK1* heterozygous patients without PD and twenty-three controls. The two *PINK1* PD patients demonstrated values for GPE, GPC, PCr and HEPs two standard deviations higher than the control mean in the putamen.<sup>191</sup>

A further cross-sectional study of 20 H&Y stage I-II PD patients and 15 healthy controls used a 2D CSI acquisition focused on the striatum (rostral putamen and head of the caudate nucleus) and the cortical grey matter in the temporoparietal region at 3T. A voxel size of 30x30x30mm<sup>2</sup> was obtained and the spectra were analysed with in-house software. This study found no significant differences in any measure obtained by <sup>31</sup>P-MRS. This study had a large proportion of very recently diagnosed and untreated PD with mild disease severity. The MRS protocol used a much shorter TR than is standard which, although useful for proton spectroscopy, is less optimised for <sup>31</sup>P-MRS metabolites which have comparatively much longer  $T_1$  times and may explain a lack of differences between groups.<sup>192</sup> Published separately, the same 20 PD participants exhibited some possible sex-differences with women showing higher ATP and HEPs

relative to men in the striatum and cortex of the hemisphere contralateral to their worse clinically affected side.<sup>193</sup>

A 12-week clinical trial of terazosin utilised <sup>31</sup>P-MRS as a novel outcome measure to assess whether enhanced glycolysis led to an increase in ATP in the brain. Terazosin is an  $\alpha$ -1 adrenergic antagonist prescribed commonly used for benign prostatic hyperplasia and has been associated with a reduced risk of PD in epidemiological studies. Terazosin activates Phosphoglycerate kinase 1 (PGK1) to promote glycolysis and improve ATP levels, possibly to compensate for mitochondrial dysfunction.<sup>194</sup> In this 12-week trial 13 participants were randomised to receive either terazosin (n=8) or placebo (n=5). Terazosin was titrated from 1mg initially to 5mg by 1mg/week. Three participants taking terazosin withdrew due to dizziness or orthostatic hypotension (a recognised side effect of terazosin). The authors used a 7T MRI system with a <sup>31</sup>P/<sup>1</sup>H dual tuned birdcage head coil and obtained an FID sequence of the whole brain following shimming. This sequence utilised a TR of 2000ms, a spectral bandwidth of 10,000Hz and 128 signal averages. It was found that terazosin increased the  $\beta$ -ATP/Pi ratio interpreted as an increase in total ATP in the brain; the researchers reported no other <sup>31</sup>P-MRS measures. It should be noted that this study comprised a small sample size (n=5 for each group for the longitudinal <sup>31</sup>P-MRS data) and the analysis protocol included apodization of the spectra prior to analysis. The analysis also used a non-standard algorithm defining each spectral peak of interest purely by the maximal amplitude within a given range of ppm, and the metabolite concentrations were then calculated using the sum of all points within a range of 25ppm.<sup>195</sup> Additionally, although the acquisition likely will have provided good SNR, the fact that the signal is derived from whole brain limits the utility of the technique as it would be desirable to examine changes in ATP in more anatomically relevant areas of the brain in PD.

An open-label pilot-study of UDCA in five PD patients over 6 weeks starting at 15mg/kg and ascending to 50mg/kg used <sup>31</sup>P-MRS to assess target engagement.<sup>196</sup> The researchers took a novel approach by utilising the magnetization transfer technique to calculate the rate of ATP synthesis. The magnetization transfer technique captures a fully relaxed spectra (i.e. with a TR greater than longest  $T_1$  of any of the metabolites being measured) and then applies a B1 insensitive selective train to obliterate signal (BISTRO) pulse for frequency-selective saturation on  $\gamma$ -ATP resonance. By saturating the  $\gamma$ -ATP resonance, the differences in Pi and  $\gamma$ -ATP concentrations between fully

relaxed spectra and  $\gamma$ -ATP saturated spectra can be used to infer the rate of ATP synthesis. When  $\gamma$ -ATP is fully saturated in principle any changes in the concentration of ATP through ATP hydrolysis will result in a transfer in the longitudinal magnetisation of  $\gamma$ -ATP to Pi. This uses both the change in Pi amplitude as a function of the saturation time of  $\gamma$ -ATP and the apparent  $T_1$  of Pi when  $\gamma$ -ATP is fully saturated to calculate the rate of this reaction.<sup>197</sup>

Although interesting, this technique has several limitations. It relies heavily on surface coils to capture the signal (which can be particularly susceptible to  $B_1$  field inhomogeneities), which limits application to less pathologically relevant areas in early PD, such as the occipital lobe. Of note, the previous reported protocol used an intermediate TR, rather than a true TR greater than the longest  $T_1$  which may result in an incompletely saturated system and therefore lead to a loss of accuracy in the measurements. Previously, the technique has been used in muscle which is much more suited to interrogation by surface coils. Additionally, the assumption that the differences in the peak amplitude between relaxed and saturated spectra are only due to chemical transfer between Pi and ATP may not always necessarily hold true. For example, in muscle it has been observed that the differences were actually more likely to be due to  $^{31}\text{P}$ - $^{31}\text{P}$  nuclear Overhauser effects (i.e. the dipolar interaction between  $^{31}\text{P}$  nuclei rather than the transfer of Pi to ATP).<sup>198</sup>

However, strengths of this study include utilisation of a 7T MRI system and the interesting finding emerged that UDCA led to a slight increase in ATP concentration and a reduction in rate of ATP synthesis, with an increase in the rate of the CK reaction. However, it must be stressed  $^{31}\text{P}$ -MRS data was only available for three participants and the study was not powered to detect meaningful changes in any clinical or spectroscopic parameters.<sup>196</sup>

#### *Previous studies to assess lysosomal dysfunction in Parkinson's Disease*

$^{31}\text{P}$ -MRS can also be used to assess for potential indicators of lysosomal dysfunction.  $^{31}\text{P}$ -MRS is able to measure various phospholipids involved in membrane metabolism such as phosphocholine (PC) phosphoethanolamine (PE), glycerophosphorylcholine (GPC) and glycerophosphorylethanolamine (GPE). PE and PC represent the phosphomonoesters (precursors to phospholipid membrane synthesis) and GPE and GPC represent the phosphodiester (phospholipid membrane breakdown products).

One study has been conducted assessing  $^{31}\text{P}$ -MRS in GBA-PD. 13 PD patients heterozygous for *GBA* mutations and 19 age and sex matched healthy controls underwent  $^{31}\text{P}$ -MRS. In this study, there was no significant difference between GBA-PD and controls with regards to energy metabolism measurements in the form of ATP, PCr, ADP and Pi. GPE was found to be significantly elevated in the putamen of GBA-PD compared to controls (1.40 vs 1.31,  $p < 0.05$ ). The authors postulated that, as GPE is typically a degradation product of phospholipid membrane metabolism, it may be increased due to greater synthesis of the membrane phospholipid phosphatidylcholine. This may be due to increased activation of the enzyme cytidyltransferase, which has been observed in Gaucher disease (which homozygous *GBA* mutations cause). This study used a 3T MRI system and a dedicated dual tuned  $^1\text{H}/^{31}\text{P}$  head coil with voxels of interest placed within the mesostriatum and used a previously published protocol.<sup>189</sup> The absolute difference observed is relatively small, and this study did not compare GBA-PD with PD so it is difficult to draw conclusions as to whether the findings represent a specific spectroscopic signature for GBA-PD or not.

For a summary of the  $^{31}\text{P}$ -MRS studies in PD and their key technical features please refer to **Table 1.2**. Of note, there have been no studies applying  $^{31}\text{P}$ -MRS longitudinally in PD patients to date, and there is limited data on how and whether abnormalities in  $^{31}\text{P}$ -MRS relate to cross-sectional clinical features or longitudinal progression.

Study	Population	Acquisition details	TR, TE and field strength	Analysis	Results
Barbiroli, et al 1999	MSA=15 PD=13 Controls=16	FID acquired DRESS using <sup>31</sup> P surface coil localised to occipital lobe.	Field = 1.5T TR = 5000ms	GE supplied peak fitting algorithm on 4Hz line broadened data	MSA: ↓Pi and ↓PCr vs controls. ↓PCr vs PD PD: ↑Pi and ↓Mg <sup>2+</sup> vs controls
Hu et al, 2000	PD=10 Controls=9	3D CSI at 1.5T, dual tuned <sup>1</sup> H/ <sup>31</sup> P head coil, central voxel and bilateral temporoparietal voxels of size 40x40x40mm <sup>3</sup>	Field = 1.5T TR = 5000ms	NMR1@ spectral processing software.	↑ Pi/β-ATP in all voxels of PD Pi/β-ATP ratio inversely correlated with cognitive performance
Rango et al, 2006	PD=20 Controls=20	FID acquired DRESS using <sup>31</sup> P surface coil localised to occipital lobe. Absolute metabolite quantification using phantom placed within coil simultaneously with patient data	Field = 1.5T TR = 2000ms	Levenberg–Marquardt frequency domain fitting method using custom analysis software.	No differences at rest ↓HEP's during recovery phase
Hattingen et al, 2009	PD=16 H&Y I-II and 13 H&Y III-IV Controls=19	3D CSI, dual tuned <sup>1</sup> H/ <sup>31</sup> P head coil, of basal ganglia and substantia nigra with decoupling with acquired voxel size 30x30x25mm and reconstructed on a 20x20x16 matrix for a voxel size of 15x15x12.5mm <sup>3</sup> . Absolute metabolite quantification using phantom replacement method	Field = 3T TR = 2000ms TE = 2.3ms	jMRUI v3.0 and AMARES for spectral peak fitting	↓PCr, HEP and ATP in all PD groups in putamen ↓ATP in midbrain in contralateral side to symptoms in all PD groups
Brockmann et al, 2012	GBA-PD = 13 Controls = 19	As per Hattingen et al, 2009	As per Hattingen et al, 2009	As per Hattingen et al, 2009	No differences in bioenergetics (ATP, PCr or Pi) between groups. Putaminal GPE was increased in GBA-PD
Hilker et al, 2012	<i>PINK1</i> homozygous PD = 2 <i>PINK1</i> heterozygous = 9 Controls =23	As per Hattingen et al, 2009	As per Hattingen et al, 2009	As per Hattingen et al, 2009	↑GPE, GPC, PCr and HEPs above two standard deviations in putamen in <i>PINK1</i> PD compared to other groups

Weiduschat et al, 2014	Male, PD = 10 Female, PD= 10 Mean disease duration 3 years	2D FID CSI with acquisition covering striatum and temporal grey matter. Voxel size 30x30x30mm <sup>3</sup> , reconstructed on a 14x14 matrix	Field = 3T TR=1000ms	In-house Levenberge-Marquardt non-linear least-squares IDL minimization routine for peak fitting. Metabolites expressed as a ratio relative to the root mean square of the background noise	↑ striatal and cortical ATP and HEPs in women vs men. Only seen in contralateral hemisphere to symptoms
Weiduschat et al, 2015	PD= 20 H&Y stage I-II, mean disease duration 3 years Controls=15	As per Weiduschat, Mao et al. 2014	As per Weiduschat, Mao et al. 2014	As per Weiduschat, Mao et al. 2014	No differences observed.
Schultz et al, 2022	RCT of Terazosin in PD Terazosin = 8 Placebo = 5	Dual tuned <sup>1</sup> H/ <sup>31</sup> P head coil used to acquire whole-brain FID	Field = 7T TR = 2000ms	Each spectral peak of interest defined purely by the maximal amplitude within a given range of ppm, each peak was then quantified as the sum of all points within ± 25ppm	In the 5 terazosin participants completing the trial, terazosin ↑β-ATP/Pi ratio
Sathe et al, 2020	Open-label, prospective, multiple-ascending-dos of UDCA 5 PD patients	Surface coil acquired 3D CSI localised to occipital lobes and a cylindrical voxel size of 4.1cm <sup>3</sup> . Magnetisation transfer experiment also performed using BISTRO sequence to quantify ATPase and CK reaction rates.  Absolute metabolite quantification using phantom replacement method	Field = 7T TR = 1200ms	jMRUI v5.0 and AMARES algorithm for spectral peak fitting	Imaging data was only available for 3 participants. 2 participants showed ~10% and 48% reduction in ATPase reaction with an increase of ~5% and 8% in the CK reaction respectively

**Table 1.2: Previous studies of <sup>31</sup>Phosphorus Magnetic Resonance Spectroscopy in Parkinson's Disease**

*TR= repetition time, TE = echo time, MSA=Multiple system atrophy, PD = Parkinson's disease, Pi= inorganic phosphate, PCr= phosphocreatine, CSI= chemical shift imaging, FID= free induction decay, DRESS= depth resolved surface coil spectra, HEPs= high energy phosphates, GPE= glycerophosphoethanolamine, GPC= glycerophosphocholine, H&Y= Hoehn & Yahr stage, BISTRO= B1-insensitive train to obliterate signal, UDCA=ursodeoxycholic acid, CK= creatine kinase*

## Identifying mitochondrial Rescue therapies

### Drug screens to identify mitochondrial rescue agents

Small scale drug screens of previously identified compounds that may be neuroprotective in other *in vivo* and *in vitro* models have been tested in human pluripotent stem cell derived dopaminergic neurons which subsequently undergo induced mitochondrial dysfunction using MPTP exposure. Out of the 44 compounds tested, 16 showed a positive benefit on measures of cell viability but there were no robust measures of mitochondrial function performed in the study.<sup>199</sup>

The first large scale high-throughput drug screen in PD derived tissue was performed in *parkin* mutant fibroblast cell lines and used a compound library of 2000 drugs. The primary screening assay assessed the effect on MMP. Out of 2000 compounds initially screened, 60 were identified to improve MMP by more than two standard deviations. 49 were then taken forward after assessment of toxicity and dose-response effects and subsequently assessed for ability to restore cellular ATP levels in a dose responsive manner. This left 15 candidates that were assessed for feasibility based upon current literature to take forward into further studies. This left two top compounds, ursocholic acid and dehydro(11,12)ursolic acid lactone. These then went through further assessment analysing in-depth respiratory chain function that demonstrated an effect of 200-500% increase on the activity of complexes I-IV for both compounds.<sup>200</sup>

Based upon this drug screen the authors identified a similar compound based upon the structure of ursocholic acid that was not included in the initial compound screen. This compound, UDCA, was structurally very similar but already a licensed medication for primary biliary cirrhosis, and exhibited a similar effect upon mitochondrial dysfunction observed in *parkin* fibroblast cell lines.<sup>200</sup>

### Ursodeoxycholic acid

After the initial drug screen described above, UDCA was subsequently tested in *LRRK2* mutant fibroblast cell lines with similar clear mitochondrial rescue effects shown on cellular ATP levels. This rescue effect was also demonstrated in transgenic *LRRK2* flies.<sup>201</sup> UDCA was also shown to suppress cell death and reduce reactive oxygen species in SH-SY5Y cells using sodium nitroprusside as an agent to induce mitochondrial dysfunction.<sup>202</sup> Other groups have also demonstrated the neuroprotective effect of UDCA in the MPTP mouse model and the rotenone model of

PD.<sup>203,204</sup> The current mode of action appears to be related to activation of the protein kinase Akt.<sup>202</sup> Akt signalling results in phosphorylation of a number of downstream targets involved in proliferation, differentiation, survival and metabolism. Reduced Akt signalling has been found in sporadic PD brains post-mortem in the substantia nigra and in many animal models of familial forms of PD.<sup>205</sup>

UDCA has been in clinical use for decades, predominantly in primary biliary sclerosis but also in other conditions such as intrahepatic cholestasis of pregnancy and primary sclerosing cholangitis. UDCA is usually administered at a dose of approximately 15mg/kg with excellent safety and tolerability reported previously.<sup>206</sup>

UDCA accounts for around 4% of the normal bile acid composition in humans. UDCA is a secondary bile acid synthesised from chenodeoxycholic acid (CDCA) in the colon by bacterial 7 $\beta$  epimerization. Following oral administration, around 30-60% is absorbed within the GI tract, predominantly in the small intestine. Following absorption into the portal circulation, UDCA is taken up by hepatocytes and can be conjugated into either glycooursodeoxycholic acid (GUDCA, the far more common conjugate) or tauroursodeoxycholic acid (TUDCA). UDCA reaches peak concentration in the systemic circulation around 1-3 hours following oral administration and will enrich bile acid composition of UDCA to around 40%.<sup>207</sup>

UDCA has also shown promise in *in vitro* models of Alzheimer's disease demonstrating a mitochondrial rescue effect in patient-derived fibroblasts.<sup>208</sup> The taurine conjugate, TUDCA, has also demonstrated possible neuroprotective properties in rodent MPTP-induced models of PD with TUDCA reducing dopaminergic degeneration; this effect is considered likely mediated by Akt signalling, similar to UDCA.<sup>204</sup>

UDCA has been trialled at doses of up to 50mg/kg in motor neuron disease with a similar side effect profile as when used at lower doses. The main side effects are diarrhoea and a change in the colour of the participants' stools. In the trial of UDCA in amyotrophic lateral sclerosis, using doses of 15mg/kg, 30mg/kg and 50mg/kg, researchers found 3/21 (14.2%) participants experienced diarrhoea (1/4 in 15mg/kg group and 2/7 in 50mg/kg group) and 1/21 (4.8%) participants (in the 15mg/kg group) experienced nausea.<sup>209</sup>

CSF pharmacokinetics demonstrated that the compound crossed the blood-brain barrier in a dose dependent manner with CSF levels sampled 2 hours after administration correlating strongly to serum concentrations 1 hour after administration with an  $R^2=0.7815$ .<sup>209</sup>

UDCA has only very recently been tested in PD (discussed in greater detail earlier) in an open-label pilot-study of five PD patients over 6 weeks starting at 15mg/kg and ascending to 50mg/kg. With respect to side effects, 3/5 participants noted intestinal discomfort. Pharmacokinetically, UDCA demonstrated accumulation over time with pre-dose levels of UDCA much greater than baseline levels prior to commencing UDCA. Following administration, and over 6 hours, absorption was highly variable between subjects and demonstrated multiple peaks (likely due to enterohepatic circulation); in some people, UDCA clearly led to a large increase in serum UDCA.<sup>196</sup>

## Aims and Objectives

### Aims

My thesis will focus on the translation of a putative neuroprotective compound (UDCA) identified in an academically led drug screen into a phase II double-blind, randomised controlled trial. Several endpoints will be used, targeted at addressing some of the previously discussed issues currently challenging clinical trial design in PD, including <sup>31</sup>P-MRS, motion sensor-based gait analysis and serum biomarkers.

Cohort stratification is of great importance to future trial design and in tandem I will be assessing the ability of both <sup>31</sup>P-MRS and patient-derived tissue to mechanistically stratify individuals with PD. This approach applies both *in vivo* and *in vitro* techniques concurrently allowing the assessment of brain bioenergetics and peripheral tissue within the same individuals.

**Hypothesis 1:** *“Ursodeoxycholic acid will be both safe and tolerable in PD in a phase II randomised double-blind placebo-controlled trial and exert an effect suggestive of neuroprotection as assessed using novel secondary endpoints”*

**Hypothesis 2:** *“Measures of mitochondrial function obtained from PD patients using <sup>31</sup>P-MRS will correlate with measures of mitochondrial function obtained from fibroblast cell lines. These correlations will reflect plausible underlying pathogenic mechanisms and demonstrate meaningful relationships to clinical assessments.”*

## Objectives

1. Assess the safety and tolerability of UDCA in a phase II randomised controlled trial (The UP Study)
2. Assess the utility of several novel secondary endpoints in the UP study to either objectively quantify disease progression or target engagement.
3. Correlate measures of mitochondrial function obtained by  $^{31}\text{P}$ -MRS with measures of mitochondrial function from fibroblast cell lines and clinical assessments.
4. Perform the first ever longitudinal study of  $^{31}\text{P}$ -MRS in PD to determine whether changes in  $^{31}\text{P}$ -MRS measures of mitochondrial function correlate with clinical progression.

## Chapter 2: Methods

### The Ursodeoxycholic acid in Parkinson's Study (The UP Study)

As discussed earlier in Chapter 1 UDCA has significant potential as a mitochondrial rescue agent and has therefore culminated into the design of a phase II, randomised, double-blind placebo-controlled trial. The primary endpoint of this study is to determine the safety and tolerability of high dose UDCA in PD. Secondary endpoints focus on detecting early evidence of disease modification and using  $^{31}\text{P}$ -MRS is being utilised to detect evidence of target engagement of UDCA.

This section will focus on the published trial protocol, authored by myself and the wider team involved with The UP Study. Additional methodological detail, outside the scope of the initial paper is also included in this chapter, this includes the addition of serum bile acid analysis using the stored samples taken from participants at each visit.

### Contributions to published paper

With regards to the study itself I was responsible for the recruitment, consenting and blinded clinical assessment of all Sheffield recruited participants during the length of the study. I was not involved in active AE or safety review. I was responsible for the analysis of all  $^{31}\text{P}$ -MRS data throughout the whole study and the statistical analysis of both clinical and biomarker data in conjunction with a co-author who was the statistician associated with the trial (Miss Rosie Taylor). The acquisition and analysis of the sensor-based gait analysis was performed by co-authors in the Institute for In-silico Medicine, The University of Sheffield.

I drafted the manuscript with the exception of any sections regarding the sensor-based gait analysis which was done by a co-author (Dr Ellen Buckley). The manuscript was drafted under the guidance of my primary supervisor (and co-author Professor Oliver Bandmann).

Published Paper: Ursodeoxycholic acid as a novel disease-modifying treatment for Parkinson's disease: protocol for a two-centre, randomised, double-blind, placebo-controlled trial, The 'UP' study

This paper was published as open-access in the BMJ Open, the citation is the following:

*Payne T, Sassani M, Buckley E, Moll S, Anton A, Appleby M, Maru S, Taylor R, McNeill A, Hoggard N, Mazza C, Wilkinson ID, Jenkins T, Foltynie T, Bandmann O. Ursodeoxycholic acid as a novel disease-modifying treatment for Parkinson's disease: protocol for a two-centre, randomised, double-blind, placebo-controlled trial, The 'UP' study. BMJ Open. 2020 Aug 5;10(8):e038911.*

doi: 10.1136/bmjopen-2020-038911

PMID: 32759251

PMCID: PMC7409998

## Additional Methodological Detail

Below, further methodological information is provided on the secondary and exploratory endpoints described in the schedule of assessments.

### Clinical Assessment

**Montreal Cognitive Assessment (MoCA):** This is a widely used tool to assess cognition and was used as both a screening criterion (excluding those with possible dementia with a score <25) and an exploratory endpoint. The MoCA has been shown to be more effective at detecting both mild cognitive impairment in PD and predicting progression to PDD than similar screening tools such as the Mini Mental State Examination (MMSE).<sup>210</sup>

**Levodopa equivalent dosage (LED):** Given the wide range of PD medications it is desirable to derive a single measure with which to express the amount of dopaminergic medication an individual is taking. Given levodopa remains the most efficacious and commonly prescribed dopaminergic medication the preference is to express non-levodopa medications relative to the amount of levodopa that would be required to confer a similar clinical benefit.<sup>211</sup>

**Predicted risk of rapid clinical progression:** As described earlier Velseboer *et al*, 2016<sup>17</sup> developed a prognostic model to calculate the risk of rapid disease progression in PD as defined by either the development of dementia or postural instability. This was developed and validated across two large cohorts of PD. This risk is calculated using the model shown in **Equation 2.1**. Strong factors predictive of an unfavourable outcome were increasing age, greater UPDRS axial sub-score (this uses the original UPDRS items “Arising from chair”, “Posture”, “Gait” and “Postural Stability”) and poor semantic fluency. Semantic Fluency is tested by asking the participant to name as many animals in one minute as possible. Given this model was developed for a cohort in the Netherlands and externally validated in a UK cohort there is a language correction factor (denoted as  $L_c$  in equation 2.1) for testing semantic fluency that is already calculated for both Dutch (a factor of 1) and English (a factor of 1.267) and can be calculated for any language if a mean semantic fluency score for a health population in a given language is already known.

$$P_{\text{unfavourable outcome}} = \frac{1}{1 + e^{-(\text{age} \times 0.0059 + \text{UPDRS axial sub-score} \times 0.3794 + \text{semantic fluency} \times L_c \times -0.0684 - 3.1246)}}$$

**Equation 2.1: Prognostic model calculating the risk of either postural instability or dementia at 5 years from diagnosis with Parkinson’s disease.**

*L<sub>c</sub> represents language correction factor.*

**MDS-UPDRS:** This has already been described in greater detail earlier in the section ‘Clinical Endpoint Design’. Part I assesses the non-motor experiences in daily living, part II the motor-experiences of daily living and part IV the treatment related complications of PD. Predicted progression in the first 5 years from diagnosis are estimated to be an increase in part I of 0.25 points per year and for Part II 1.0 points per year.<sup>212</sup> Part III It is the most widely used clinical scale to assess the motor symptoms of PD as assessed by the examiner and covers the cardinal features of PD namely rigidity, bradykinesia, tremor and gait impairment, although gait assessment is comparatively a smaller proportion of the scale compared to the other features. The MDS-UPDRS III is expected to change by 2.4 points per year in the first five years following diagnosis.<sup>212</sup> This is a key secondary endpoint to assess for differences in motor progression between groups. Part III is performed in both the ‘ON’ and ‘OFF’ states. The ‘OFF’ state assessment is the measure used in the secondary outcomes described above and aims to quantify PD motor impairment without the influence of dopaminergic medication.

**Modified Hoehn & Yahr (mH&Y):** The original Hoehn & Yahr staging was developed in 1967 and described relatively broad categories of PD that provide an overview of an individual’s functional status and the severity of their PD.<sup>213</sup> This proved useful for the more advanced stages of PD but did not fully capture early progression and underwent revision by the Movement disorders Society in 2004 that added new stages to try and improve the characterisation of early PD as shown in **Table 2.1**.<sup>214</sup>

<b>Modified Hoehn &amp;Yahr Scale<sup>214</sup></b>	
1.0	Unilateral involvement only
1.5	Unilateral and axial involvement
2.0	Bilateral involvement without impairment of balance
2.5	Mild bilateral disease with recovery on pull test
3.0	Mild to moderate bilateral disease; some postural instability; physically independent
4.0	Severe disability; still able to walk or stand unassisted
5.0	Wheelchair bound or bedridden unless aided

**Table 2.1: Modified Hoehn and Yahr Scale**

### Genetic Analysis

All participants supplied an EDTA blood sample for genetic analysis using the NeuroChip rapid genotyping array that assesses for 179,467 genetic variants associated with a diverse range of neurological diseases including PD but also ranging to amyotrophic lateral sclerosis and multiple system atrophy.<sup>215</sup> The purpose of this analysis was primarily to identify monogenic familial forms of PD within the cohort or *GBA1* variants associated with increased risk of PD.

### <sup>31</sup>P-MRS Acquisition

<sup>31</sup>P-MRS was undertaken in all participants using protocols developed locally at 3 Tesla in a clinical-research dedicated multinuclear scanner and adapted from a similar study assessing <sup>31</sup>P-MRS in MND.<sup>180</sup> Spectroscopic acquisition parameters (flip angle, sampling bandwidth, proton-decoupling parameters etc.) were optimised and implemented locally prior to the commencement of the study (Prof I. Wilkinson). All spectra were visually inspected at time of acquisition on the MRI scanner to ensure acceptable signal to noise, prior to any analysis.

All <sup>31</sup>P-MRS scans were obtained using a Philips Ingenia 3 Tesla system (Philips Healthcare, Best, Netherlands) and a transmit-receive dual-tuned <sup>1</sup>H/<sup>31</sup>P birdcage quadrature head-coil (Rapid Biomedical, Würzburg, Germany).

Two-dimensional chemical shift imaging (CSI) with image-selected *in vivo* spectroscopy was used for spectral spatial localisation (ISIS). Two separate CSI sequences were obtained focused on the midbrain and the putamen. Acquisition parameters for the midbrain CSI were: repetition time (TR)=4000ms, echo time (TE)=0.22ms, number of signal averages (NSA)=8, sampling points=2048, spectral

bandwidth=3000Hz, flip angle (FA)=90°, slice thickness=20mm, field of view (FOV)=210mm<sup>2</sup>, acquired voxel sizes of 40x40x20mm<sup>3</sup> and, following k-space filtering and zero filling using a reconstruction matrix of 14x14, reconstructed voxel size=15x15x20mm<sup>3</sup>, acquisition time=10:16min. The putamen CSI acquisition parameters differed from the midbrain acquisition only in NSA=10, reconstructed voxel size=17.5x17.5x20mm<sup>3</sup>, reconstruction matrix of 14x14 and acquisition time=12:48. All CSI sequences used adiabatic pulses, with a second order pencil-beam shim and WALTZ-4 broadband heteronuclear decoupling with NOE.

Alignment of CSI sequences was guided by a T2-weighted spin-echo image: TR=3000ms, TE=80ms, FA=90°, slice thickness=4mm, FOV=230mm<sup>2</sup>, acquisition voxel 0.55x0.65x4.0 mm<sup>3</sup>, reconstruction matrix=432x432mm<sup>2</sup>, reconstructed voxel size=0.53x0.53x4.0mm<sup>3</sup>, acquisition time=3:48 minutes. Details of spectral localisation and voxels of interest are shown in **Figure 2.1**. Midbrain CSI grid placement was kept consistent using the superior border of the pons and the inferior border of the splenium of the corpus callosum to guide the placement of the inferior and superior borders of the acquisition respectively. The anterior border was placed to align with the cerebral peduncles to ensure substantia nigra was captured within the acquisition. Putaminal CSI acquisition was placed to capture the entirety of the putamen across two voxels (one for anterior putamen and one for posterior) for each side, with the anterior border of the putamen aligned the anterior edge of the anterior voxel. The acquisition was angled to capture the superior and inferior borders of the putamen within the two voxels.

A whole-brain 3D T1 inversion recovery volumetric image was also obtained of the whole brain to allow group-wide morphometric analysis and guide CSI grid placement in the coronal and sagittal planes with the following parameters: TR = 6.8ms, TE = 3.2ms, FOV = 240x267mm, FA=8°, inversion time=1000ms, slice thickness=1.5mm, acquired voxel size=1.2x1.2x1.5mm<sup>3</sup>, reconstruction matrix= 352x 352mm<sup>2</sup>, reconstructed voxel size=0.76x0.76x1.5mm<sup>3</sup>, acquisition time=11:19 minutes.

A limited 3D T1 inversion-recovery volumetric image was obtained corresponding to each of the midbrain and putamen CSI acquisitions. These were acquired exactly co-registered to the acquisition of the CSI sequences to allow precise co-localisation of anatomical imaging to enable the calculation and correction for partial volume effects:

TR=8.3ms, TE=3.8ms, FOV=240mm<sup>2</sup>, FA=8°, inversion time=1000ms, slice thickness=1mm, acquired voxel size=1.00x1.08x1.00mm<sup>3</sup>, reconstruction matrix=256x256mm<sup>2</sup>, reconstructed voxel size=0.94x0.94x1mm<sup>3</sup>, acquisition time=4:01 minutes. Given the length of the whole MRI protocol it is possible participants may have moved small amounts during acquisition, hence why a shorter limited 3D T1 image was acquired immediately following CSI acquisition to obtain as representative anatomical data for the calculation of partial volume effects as possible.

All structural MR imaging assessed for incidental abnormalities by a Consultant Neuroradiologist. Any clinically relevant abnormalities were communicated to the participant and their General Practitioner and appropriate clinical action taken. The presence of any incidental abnormalities considered to have potential to bias results (for example, incidental tumour) was an exclusion criterion for further analysis of that <sup>31</sup>P-MRS data.

For follow-up scans, placement of the CSI voxel grid was compared to those acquired at baseline and placed using identical methodology. This was performed by the same radiographers who performed all baseline scans and confirmed by myself. This attempts to keep tissue composition of each voxel consistent across multiple scans.

The total duration of the scan protocol was 1 hour and 6 minutes.

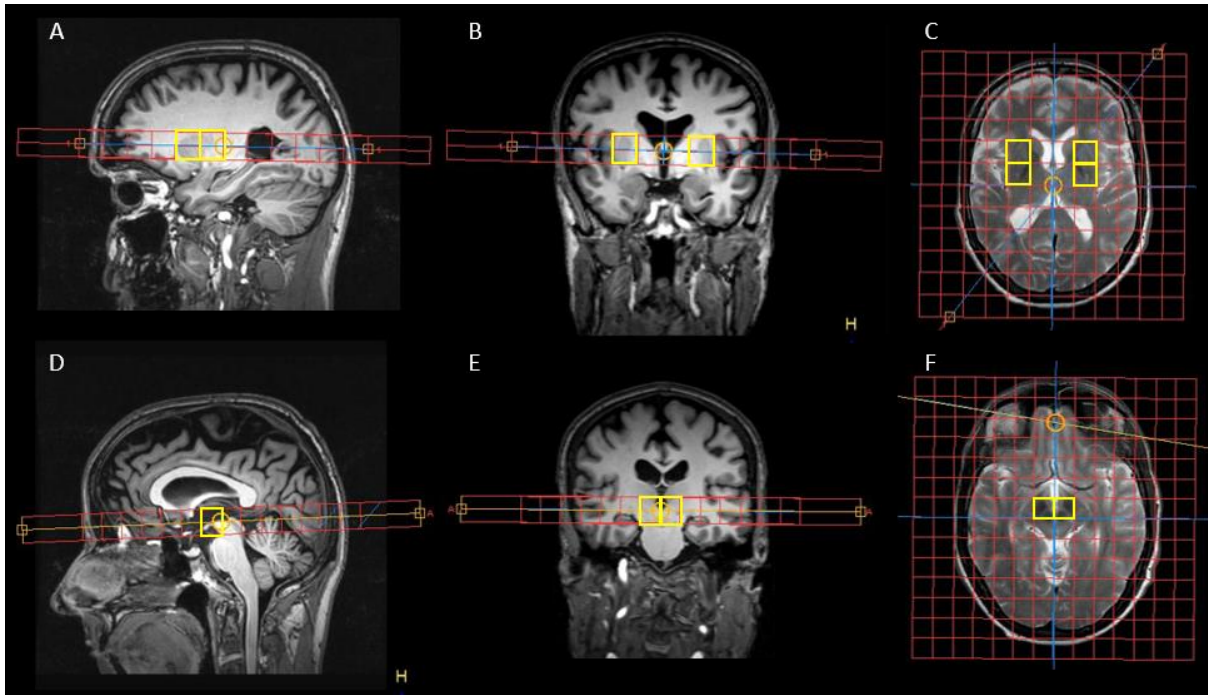


**Figure 2.1: Localisation of  $^{31}\text{P}$ -MRS 2D CSI acquisition sequences**

(A) T1 sagittal, (B) T1 coronal and (C) T2 axial alignment of the putaminal CSI acquisition, here the CSI grid is placed and angled to capture as much of the putamen as possible with one voxel aligning with the anterior boundary of the putamen. Given the size of the putamen it is captured within two CSI voxels for both the anterior and posterior putamen. (D) T1 sagittal, (E) T1 coronal and (F) T2 axial alignment of the midbrain CSI acquisition using the anatomical landmarks of the superior border of the pons and the posterior inferior border of the corpus callosum to guide appropriate placement and angulation across all participants. Additionally, for the midbrain acquisition the CSI grid was adjusted to place the border between the two voxels aligned with midline of the brain and the anterior border was placed aligned with the cerebral peduncle. Although the substantia nigra is not readily visualised on standard T1 and T2 imaging at 3T the placement of the CSI acquisition ensures the structure is captured within the relevant voxel of interest. All voxels of interest for data analysis are highlighted with a yellow border.

### <sup>31</sup>Phosphorous Magnetic Resonance Spectroscopy Analysis

Six voxels of interest were defined a priori and analysed: the left and right midbrain, and the left and right of each of the anterior and posterior putamen.

All spectroscopic data was anonymised at acquisition and analysed blinded to participant status. Spectra were imported into jMRUI (Version 5.2, available at <http://www.mrui.uab.es>) for analysis of free induction decay (FID) signals in the time domain. Spectra were manually phased using both zero- and first-order phasing for each of the spectra of interest (4 spectra in the basal ganglia acquisition and 2 spectra in the substantia nigra acquisition) to ensure all resonances of interest are in the absorptive phase in each spectrum prior to quantitative analysis. To aid phasing, the spectra were visually apodised using a Lorentzian line shape (an optical filtering technique). However, during spectral peak quantification, the FID was not apodized thus ensuring the raw FID signal was unchanged. Prior to quantification the spectra were frequency shifted such that the PCr peak was located to 0 parts per million (ppm), according to standard convention.

The AMARES protocol (advanced method for accurate, robust, and efficient spectral fitting) is a technique that employs a least squares fitting method to determine the relative amplitude of each spectral resonance.<sup>183</sup> The software allows the input of specific prior knowledge prior to analysis to improve accuracy of spectral fitting based on the known physical properties of the nuclei and tissue of interest.

Using the AMARES protocol, a total of 13 resonances were fitted with assumed Lorentzian line shapes, with  $\gamma$ -ATP and  $\alpha$ -ATP having doublet peaks with amplitudes and linewidths constrained to a 1:1 ratio to each other, and  $\beta$ -ATP having triplet peaks with amplitudes constrained in a ratio of 0.5:1:0.5 and linewidths constrained to a ratio of 1:1:1. The remaining resonances quantified were phosphoethanolamine (PE), phosphocholine (PC), inorganic phosphate (Pi), glycerophosphoethanolamine (GPE), glycerophosphocholine (GPC) and phosphocreatine (PCr). PE and PC comprise the phosphomonoesters (PME), GPE and GPC the phosphodiester (PDE). J-coupling constants for ATP multiplets were set at 18Hz as used in previous literature and soft constraints limited ATP linewidths to 5-35Hz.<sup>179,189</sup> Additional soft constraints were used to control linewidths for phosphocreatine (5-20Hz), and all other remaining resonances to 5-30Hz.<sup>180,216</sup> All amplitudes were normalised to the total phosphorus

signal detected prior to any statistical analyses. The three multiplets of ATP were summed to calculate total ATP. The AMARES protocol was set to weight the first 20 points of the FID. This operation is useful in the quantitation of a signal with a large background signal, or if the baseline is particularly prominent as is the case in many  $^{31}\text{P}$ -MRS spectra. All spectra were visually inspected for quality of fit and spurious signals were excluded, according to recently published consensus criteria.<sup>217</sup> Example spectra pre- and post-analysis are shown in **Figure 2.2**.

The prior knowledge used for the AMARES protocol was guided by previously published work using similar techniques, optimised for this dataset using the healthy control data, and was applied identically to analyses of both midbrain and putaminal spectra.<sup>180</sup> This optimised prior knowledge was generated through multiple manual analyses using 10 healthy control scans. All peaks were manually assigned by a single operator using visual inspection with the only prior knowledge being the above coupling constants. The mean values for the peak frequencies and line widths were then used to optimise this prior knowledge developed previously in the literature. Final prior knowledge used for all analyses is shown in **Table 2.2**. The data used to guide these choices are shown in **Appendix 1**.

For comparisons between participants, relative amplitudes for each resonance were normalised to the total phosphorous signal measured in the spectra within each voxel, by expressing each metabolite amplitude as a ratio with total phosphorus signal always the denominator. This avoids the issues with absolute quantification of  $^{31}\text{P}$ -MRS using external references discussed earlier.

A total of six voxels were used for data analysis: left midbrain, right midbrain, left posterior putamen, right posterior putamen, left anterior putamen and right anterior putamen. Following normalisation of amplitudes within each voxel, mean values of voxels were created for the mean midbrain, mean posterior putamen and mean anterior putamen.

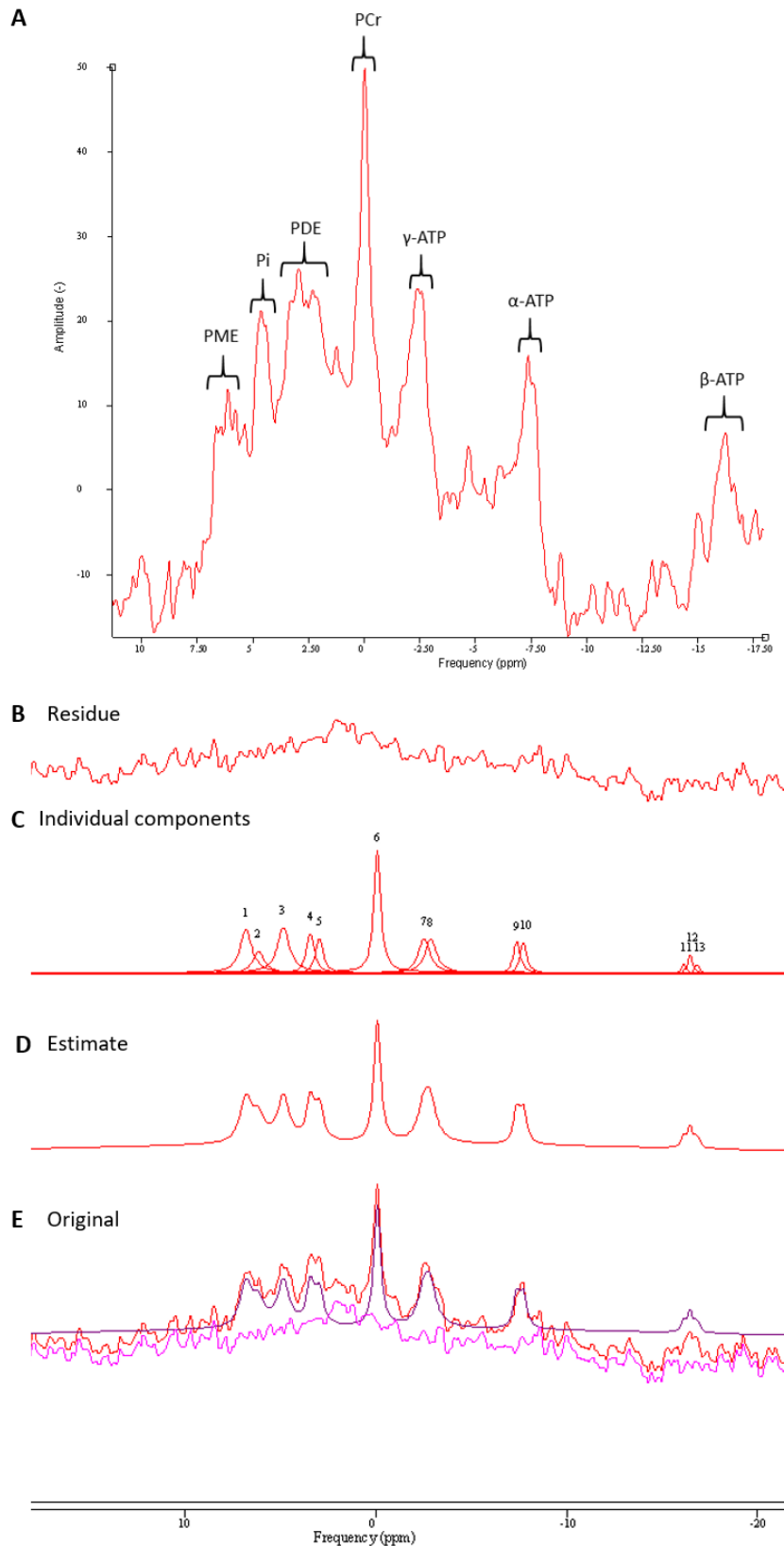


**Figure 2.2: AMARES quantification of  $^{31}\text{P}$ -MRS**

(A) An example spectrum obtained from the midbrain of a healthy volunteer. This spectrum has been phased and apodised to aid visualisation with phosphocreatine frequency shifted to

0ppm. (B) Residual baseline of the spectra following analysis. This is the remaining FID signal once the frequency components of all spectral resonances have been quantified. (C) Peak fitting of each individual frequency component analysis following AMARES using the prior knowledge supplied to guide peak selection. Thirteen resonances are fitted: 1=phosphocholine, 2=phosphoethanolamine, 3=inorganic phosphate, 4=glycerophosphorylcholine, 5=glycerophosphorylethanolamine, 6=phosphocreatine, 7,8=gamma adenosine triphosphate, 9,10=  $\alpha$ -ATP=gamma adenosine triphosphate, 11-13=  $\beta$ -ATP=gamma adenosine triphosphate. PME=phosphomonoesters, PDE=phosphodiester, Pi=inorganic phosphate, PCr=phosphocreatine,  $\gamma$ -ATP=gamma adenosine triphosphate,  $\alpha$ -ATP=gamma adenosine triphosphate,  $\beta$ -ATP=gamma adenosine triphosphate. (D) Overall estimate of the quantified spectra (E) Combined depiction of the original spectra pre-analysis with the residual and estimated spectra superimposed, allowing visualisation of all components contributing the quantification of the raw data.

Spectral resonance	Starting frequency (ppm)	Frequency range (ppm)	Line width (Hz)
PE	6.69	6.60 - 7.50	5.0 - 30.0
PC	6.06	6.00 - 6.55	Fixed ratio 1:1 PE
Pi	4.88	4.50 - 5.70	5.0 - 30.0
GPE	3.54	3.20 - 3.80	Fixed ratio 1:1 GPC
GPC	2.93	2.80 - 3.20	5.0 - 30.0
PCr	0.02	-0.50 - 0.50	5.0 - 20.0
$\gamma$ -ATP <sup>1</sup>	-2.43	$\gamma$ -ATP <sup>2</sup> +18Hz	5.0-35.0
$\gamma$ -ATP <sup>2</sup>	-2.73	<sup>a</sup> estimated	Fixed ratio 1:1 $\gamma$ -ATP <sup>1</sup>
$\alpha$ -ATP <sup>1</sup>	-7.38	$\alpha$ -ATP <sup>2</sup> +18Hz	5.0 - 35.0
$\alpha$ -ATP <sup>2</sup>	-7.74	<sup>a</sup> estimated	Fixed ratio 1:1 $\alpha$ -ATP <sup>1</sup>
$\beta$ -ATP <sup>1</sup>	-15.76	$\beta$ -ATP <sup>3</sup> +36Hz	Fixed ratio 0.5:1 $\beta$ -ATP <sup>2</sup>
$\beta$ -ATP <sup>2</sup>	-16.21	$\beta$ -ATP <sup>3</sup> +18Hz	5.0 - 35.0
$\beta$ -ATP <sup>3</sup>	-16.66	<sup>a</sup> estimated	Fixed ratio 0.5:1 $\beta$ -ATP <sup>2</sup>

**Table 2.2: Prior knowledge used for the AMARES method of spectral quantification for both midbrain and putamen**

<sup>a</sup>Note 'estimated' frequencies are determined by the AMARES algorithm. This is used to quantify one peak for all multiplet ATP resonances as they are proportionately large components of the <sup>31</sup>P spectra without surrounding spectral resonances and are easily identified by the AMARES algorithm without needing constraints on peak identification. The remaining peaks for each of the three main ATP groups are then expressed to the estimated peak according to their J-coupling constants. ppm=parts per million

The tissue pH from the sampled voxel can then be determined indirectly using the chemical shift of Pi relative to PCr and applying a formula derived from a modified Henderson-Hasselbach equation shown in **Equation 2.2**.<sup>218</sup>

$$pH = 6.75 + \log_{10} \frac{\delta_{Pi} - 3.27}{5.63 - \delta_{Pi}}$$

**Equation 2.2: Calculation of <sup>31</sup>P-MRS pH**

*δ<sub>Pi</sub> is the chemical shift of inorganic phosphate relative to phosphocreatine.*

The concentration of magnesium can also be calculated indirectly from the chemical shift of β-ATP relative to PCr and has been utilised widely in the field using, shown in **Equation 2.3**.<sup>219</sup>

$$Mg = \log_{10} \left[ \frac{(\delta_{\beta ATP} + 18.58)^{0.420}}{(-15.74 - \delta_{\beta ATP})^{0.640}} \right]$$

**Equation 2.3: Calculation of the concentration of magnesium in <sup>31</sup>P-MRS**

*δ<sub>βATP</sub> is the chemical shift of β-ATP relative to phosphocreatine*

In addition to the above parameters, it was also possible to calculate both ΔG<sub>ATP</sub> and the concentration of ADP from the data acquired above according to previously published methods.<sup>220</sup> For these calculations, the values of ATP, phosphocreatine and inorganic phosphate in millimoles were required for each participant. In line with previous literature, the ATP concentration in the brain in healthy individuals was assumed to be 3 millimoles and the mean healthy control values of γ-ATP (obtained from the observational study described in the second part of this chapter ‘Mechanistic stratification of Parkinson’s disease using <sup>31</sup>Phosphorus Magnetic Resonance Spectroscopy and patient derived tissue fibroblasts’) was used as an external reference to derive the millimolar values of γ-ATP in all participants.<sup>221</sup> The equation for the calculation of ΔG<sub>ATP</sub> is shown in **Equation 2.4**.

$$\Delta G_{MgATP^2} = c_1 + c_2z + c_3x^2 + c_4z^2 + c_5x^3 + c_6z^3 + c_7x^2y$$

**Equation 2.4: Calculation Gibbs free energy of ATP hydrolysis.**

*Where x = pH, y = -log<sub>10</sub> [Mg(in M)] and z = [PCr]<sub>tot</sub>. Constants c<sub>1</sub> through to c<sub>7</sub> are coefficient values that vary depending on tissue and conditions the ΔG<sub>ATP</sub> is being calculated in. The set*

of coefficients used were those for the assumed conditions of  $[Na]_{tot}=10$  mM and  $[K]_{tot}=150$  mM in the brain as reported by Iotti et al, 2005.<sup>220</sup>

Calculation of the creatine kinase equilibrium constant subsequently allows indirect quantification of the concentration of ADP using the equations shown in equation 2.5 and 2.6. To calculate ADP, a concentration for creatine (Cr) is also required, which is not possible to calculate directly from <sup>31</sup>P-MRS and therefore values from previous literature are imputed. A concentration of 11 millimoles was assumed for creatine based upon previously published estimates.<sup>222,223</sup>

$$(A) \text{Log}K_{CK} = a + bx + cy + dx^2 + exy + fy^2 + gx^3 + hx^2y + ixy^2 + jy^3$$

$$(B) [ADP] = \frac{[ATP][Cr]}{[PCr] \times K_{CK}}$$

**Equation 2.5: Calculation of the creatine kinase equilibrium constant and ADP concentration.**

(A) Calculation of the creatine kinase equilibrium constant where  $x = pH$ ,  $y = -\log_{10} [Mg(\text{in } M)]$ . Constants  $a, b, c, d, e, f, g$  are a set of coefficients used were those for the assumed conditions of  $[Na]_{tot}=10$  mM and  $[K]_{tot}=150$  mM in the brain as reported by Iotti et al, 2005.<sup>220</sup> (B) Using the creatine kinase equilibrium constant the concentration of ADP can be calculated if the concentrations of ATP, PCR and creatine (Cr) are known.

Further calculated parameters have been used in <sup>31</sup>P-MRS to compare between participants, many of these use ratios between metabolites in each individual to infer bioenergetic dysfunction. The Pi/ATP ratio has been used previously and an increase in this value is felt to reflect a relative increase in Pi due to impaired oxidative phosphorylation to maintain phosphorylation of ADP with a third phosphate group.<sup>181</sup> The main focus of data analysis will be on the normalised amplitudes of each resonance, although these ratios were used in exploratory analyses detailed in the relevant results chapters.

**Quantification of partial volume effects**

Spectroscopic voxels contain various proportions of white matter (WM), grey matter (GM) and cerebrospinal fluid (CSF) at individual level. This is an important confound which requires adjustment as larger proportions of CSF in particular would potentially impact results, an issue particularly important for the midbrain voxel. The proportion of GM and WM within voxels has previously been shown to be important in proton spectroscopy, estimated to affect metabolite quantitation by 5-10%.<sup>224</sup> This guidance

is incorporated into consensus guidelines on the analysis of proton spectroscopy, and should also be taken into account for  $^{31}\text{P}$ -MRS.<sup>217</sup>

To calculate partial volume measures for each voxel, the 3D T1 inversion-recovery images that were acquired with each CSI acquisition were first co-registered to the voxel of interest using a voxel mask generated using Gannett software (<http://www.gabamrs.com/>) and subsequently segmented using Statistical Parametric Mapping software (SPM12, <https://www.fil.ion.ucl.ac.uk/spm/software/spm12/>) in MATLAB and Statistics Toolbox Release R2020a (The MathWorks, Inc., Natick, Massachusetts, United States). SPM segments each voxel of interest into proportions of grey matter, white matter and cerebrospinal fluid.<sup>225</sup>

For each midbrain voxel, brain proportion (grey plus white matter divided by total voxel volume) was calculated for use as a partial volume measure. GM proportion was used as the partial volume measure for analysis of the data from putaminal voxels, given the extremely small CSF fraction that would be found in these voxels.

#### Serum bile acid profiling

Exogenous administration of UDCA has been shown to have a range of effects on the bile acid pool as discussed earlier and is therefore of key interest to quantify throughout the duration of the trial. Aside from the expected rise in UDCA, it could be of relevance if exogenous UDCA were to suppress certain bile acids which are considered pro-inflammatory.<sup>109</sup> Serum bile acid profiling was performed using ultra-performance liquid chromatography linked to mass spectrometry (UPLC-MS) using ACQUITY UPLC (Waters Ltd, Elstree, UK) coupled to a Xevo G2 Q-ToF mass spectrometer equipped with an electrospray ionisation source operating in negative ion mode as previously described.<sup>226</sup> This was performed by collaborators and not by myself.

#### Statistical Analysis

During the course of the study the COVID-19 pandemic occurred which prevented several visits being conducted face-to-face. The impact of this is covered in greater detail in the results of The UP Study in Chapter 5.

Statistical analyses include all randomised participants (an intention-to-treat analysis population). Additionally, due to several assessments being delayed due to COVID-19 a sensitivity analysis was performed for each analysis excluding data collected

outside of the planned assessment window to assess if the inclusion of delayed assessments (e.g.  $^{31}\text{P}$ -MRS parameters being performed after the washout period rather than at the end of treatment) had a significant impact upon secondary and exploratory outcomes. All results presented are using the full analysis dataset unless stated otherwise.

The primary outcome of interest for this study was the safety and tolerability of UDCA. This trial was a pilot study and therefore was not powered to compare the SAE rate between the groups statistically. All SAEs and adverse treatment reactions are presented descriptively with the placebo group providing a baseline against which to view any SAEs in the UDCA group.

Demographic and clinical assessment data were summarised using relevant summary statistics depending on data distribution (e.g. mean, standard deviation, range). Differences in demographic and clinical features at baseline were tested using a t-test with Welch's correction for continuous data and the chi-squared test for categorical data. To assess for treatment effect in clinical rating scales and gait analysis t-tests with Welch's correction were performed to assess for group differences in the total change in the parameter of interest from either baseline to week 48, baseline to week 56 or week 48 to week 56. QQ plots were examined for each demographic, clinical and gait parameter to assess for normality prior to statistical testing. In the event of non-normality, a Mann Whitney U test was performed to assess for differences in change between treatment groups.

For the analysis of  $^{31}\text{P}$ -MRS parameters the generalised linear model with a gaussian distribution was used to assess for differences between groups in the change of the  $^{31}\text{P}$ -MRS parameter of interest with respect to baseline value, sex and age using the model in **Equation 2.6**. Choice of covariates is based on previous work which showed differences between sexes in PD with respect to ATP and PCr measurements.<sup>193</sup> There is also evidence that mitochondria undergo functional and morphological changes as part of the aging process.<sup>227</sup> A  $^{31}\text{P}$ -MRS study utilising a 3D CSI acquisition over the whole brain in healthy volunteers aged 21-84 found that per decade brain pH decreased by 0.53%, PCr increased by 1.1% and PME increased by 1.7%.<sup>228</sup>

$$(31P_{week48} - 31P_{baseline}) \sim 31P_{baseline} + Treatment + Age_{baseline} + Sex$$

**Equation 2.6: Generalised linear model to assess differences in 31P-MRS between treatment groups.**

*Beta coefficients and error term not included for ease of visualisation. In the event that partial volume effects showed a clear relationship to <sup>31</sup>P-MRS parameters then this was also included as a relevant parameter. <sup>31</sup>P-MRS parameters denoted by '31P'. Sex and treatment were both binary coded. Sex differences have previously been noted in spectroscopic studies in PD and partial volume correction is key in any spectroscopic study.<sup>193,217</sup>*

Partial volume effects should be accounted for in any spectroscopic study as advised by international experts consensus guidelines.<sup>217</sup> Partial volume effects were assessed separately in a correlation analysis between the <sup>31</sup>P-MRS parameters and the partial volume measure relevant to the voxel examined (brain proportion for midbrain voxels and GM proportion for putaminal voxels). If a significant correlation was identified with a <sup>31</sup>P-MRS parameter then the relevant partial volume effect was added as a further covariate to the generalised linear model for analysis.

## Mechanistic stratification of Parkinson's disease using <sup>31</sup>P Phosphorus Magnetic Resonance Spectroscopy and patient derived tissue fibroblasts

A clinically characterised cohort of 35 early and non-demented PD patients and 25 controls underwent <sup>31</sup>P-MRS, skin biopsy, genetic analysis and comprehensive clinical assessment at a baseline visit. A further follow-up visit was offered to those eligible at a duration of  $\geq 2$  years for further clinical assessment and a repeat <sup>31</sup>P-MRS.

The baseline data was analysed to characterise <sup>31</sup>P-MRS in PD vs healthy controls and to characterise relationships between <sup>31</sup>P-MRS and measures of mitochondrial dysfunction in the patient-derived tissue fibroblasts. This is a completely novel approach as mitochondrial function in peripheral tissue in PD has never previously been correlated with in vivo imaging measures of bioenergetics within the central nervous system. Additionally, <sup>31</sup>P-MRS was assessed for any relationships with clinical features to determine if bioenergetic measures were related to key clinical parameters of interest and whether those with clear bioenergetic dysfunction display clinical differences compared to those without.

The longitudinal data provided the opportunity to assess the changes in <sup>31</sup>P-MRS over time in PD and to correlate this with both observed and predicted progression. Again, this is a novel study, with no previous longitudinal studies of <sup>31</sup>P-MRS in PD.

### Participants, Recruitment, Consent and schedule of activities

This study is sponsored by Sheffield Teaching Hospitals (Reference number STH 20087) and has Research Ethics Committee approval (reference number 18/NW/0328).

35 patients with recently diagnosed PD (less than 3 years since diagnosis) and 25 age and sex-matched controls were recruited from the movement disorders out-patient clinics of the Royal Hallamshire Hospital, satellite clinics and through the Parkinson's UK Research Network. All participants with PD were diagnosed by a movement disorder specialist according to the Queen Square Brain Bank Criteria.<sup>12</sup> Each participant was provided with full verbal and written information about the study prior to recruitment in the form of a patient information sheet (PIS), given time to consider whether they wish to take part, made aware that they would be free to withdraw at any time, and provided with contact details to register interest. If they decided to proceed, informed written consent was obtained prior to any study activities.

Following an amendment to the study protocol to allow further study visits to assess longitudinal changes in <sup>31</sup>P-MRS all participants eligible for a further follow-up visit at an interval of ≥2years were invited to attend for a repeat <sup>31</sup>P-MRS scan and repeat clinical assessments. At this visit all participants were supplied with the updated PIS and re-consented prior to any research activities at the follow-up visit.

Detailed inclusion and exclusion criteria are shown in **Table 2.3**. A full schedule of assessments can be seen in **Table 2.4**.

<b>Inclusion Criteria</b>
For all research participants:
<ul style="list-style-type: none"> <li>• Age 18 years or older</li> <li>• Mini-mental state examination score &gt;24<sup>229</sup></li> <li>• Adequate command of English language to understand patient information sheet, consent form and verbal explanations</li> </ul>
For patients only:
<ul style="list-style-type: none"> <li>• Clinical diagnosis of PD</li> <li>• Response to dopaminergic medication</li> <li>• Diagnosis of PD was made up to three years ago by Clinician with expertise in movement disorders according to the Queen Square Brain Bank Criteria.<sup>12</sup></li> <li>• No current or previous history of other neurological diseases</li> </ul>
For healthy controls only:
<ul style="list-style-type: none"> <li>• No current or previous history of any neurological disease</li> </ul>
<b>Exclusion criteria</b>
<ul style="list-style-type: none"> <li>• Age &lt; 18 yr</li> <li>• Significant cognitive impairment (MMSE &lt; 23) since this would limit the ability of any potential research participants to give informed consent</li> <li>• Claustrophobia</li> <li>• Bleeding disorder</li> <li>• Treatment with therapeutic anticoagulation</li> <li>• Severe general on-going general medical problems (i.e. cancer)</li> <li>• Evidence of respiratory failure (since this would make it difficult for research participants to lie flat in the MRI scanner)</li> <li>• Significant back pain (which would make it too uncomfortable for the patient/control to lie flat in the MRI scanner)</li> <li>• Presence of a pacemaker or other non-MR-compatible device</li> <li>• Pregnancy.</li> </ul>

**Table 2.3: Inclusion and Exclusion Criteria**

	Visit 1		Visit 2 (≥2 years)	
Assessments	Participants with Parkinson's Disease	Healthy Volunteers	Participants with Parkinson's Disease	Healthy Volunteers
<b>Cognitive</b>	<ul style="list-style-type: none"> <li>• Mini-mental state examination</li> </ul>	<ul style="list-style-type: none"> <li>• Mini-mental state examination</li> </ul>	<ul style="list-style-type: none"> <li>• MMSE</li> <li>• Montreal cognitive assessment</li> </ul>	
<b>Clinical Examination</b>	<ul style="list-style-type: none"> <li>• Full neurological</li> <li>• Lying/Standing BP</li> <li>• MDS-UPDRS III 'ON'</li> <li>• NMSS</li> <li>• Predicted Risk of Disease Progression</li> </ul>	<ul style="list-style-type: none"> <li>• Full neurological</li> </ul>	<ul style="list-style-type: none"> <li>• Full neurological</li> <li>• Lying/Standing BP</li> <li>• MDS-UPDRS I-IV 'ON'</li> <li>• NMSS</li> <li>• Predicted Risk of Disease Progression</li> </ul>	<ul style="list-style-type: none"> <li>• Full neurological</li> </ul>
<b>Procedures</b>	<ul style="list-style-type: none"> <li>• <sup>31</sup>P-MRS</li> <li>• 3mm punch skin biopsy</li> <li>• EDTA sample for genetics</li> </ul>	<ul style="list-style-type: none"> <li>• <sup>31</sup>P-MRS</li> <li>• 3mm punch skin biopsy</li> <li>• EDTA sample for genetics</li> </ul>	<ul style="list-style-type: none"> <li>• <sup>31</sup>P-MRS</li> <li>• Serum sample for storage</li> </ul>	<ul style="list-style-type: none"> <li>• <sup>31</sup>P-MRS</li> <li>• Serum sample for storage</li> </ul>

**Table 2.4: Schedule of Assessments.**

*Note that for the MMSE at Visit 1 this was only used to assess with respect to inclusion/exclusion criteria and not used for formal data analysis*

### <sup>31</sup>Phosphorus Magnetic Resonance Spectroscopy and morphometric analysis

Acquisition and analysis of <sup>31</sup>P-MRS was identical to that described in The UP Study, using the same AMARES protocol and parameters.

### Clinical Assessment

Participants with PD underwent a detailed clinical history and neurological examination, a recording of their medication, lying and standing blood pressure, recorded at three minutes after the change in posture to assess for orthostatic hypotension and the following clinical assessments in addition to the MoCA, LED and MDS-UPDRS (parts 1-4) and Modified Hoehn & Yahr as described in The UP Study.

Healthy controls had their past medical history taken, their current medications, social history and family history recorded before undergoing a neurological examination to ensure there was no evidence of undiagnosed neurological conditions that may confound the study.

Further assessments performed not previously described are discussed below.

***Mini-mental state examination (MMSE):*** The mini-mental state examination (MMSE) is a 30-point scale and a long-established screening tool for dementia using a cut-off score of >24 which results in a sensitivity for detecting dementia of 0.87 and specificity of 0.82.<sup>230</sup> This is purely used for the detection of significant cognitive impairment as part of the inclusion and exclusion criteria and is not used for any formal data analysis.

***Movement Disorders Society Non-motor symptom scale (NMSS):*** As described above this scale assess a wide variety of non-motor symptoms and scores them in a multiplicative fashion between the severity (scored as none (0), mild (1), moderate (2) or severe (3)) and the frequency (rarely (1), often (2), frequent (3) or very frequent (4)). This groups symptoms into a total of nine domains: cardiovascular including falls, sleep/fatigue, mood/cognition, perceptual problems/hallucinations, attention/memory, gastrointestinal tract, urinary, sexual function and a final miscellaneous domain that assesses unexplained pain, change in smell/taste, weight change and excessive sweating. This provides a comprehensive assessment of the non-motor state of an individual's PD and has been used extensively across many clinical studies.<sup>124</sup>

**Semantic fluency:** This was performed as part of the baseline assessment to calculate the predicted risk of clinical progression. For the analysis of longitudinal

clinical data it is not of utility to repeat a calculation of the predicted risk of disease progression to compare with the baseline data. However semantic fluency is a key component of this and was already performed at baseline. Therefore, it was also assessed at follow-up to assess for any changes reflective of cognitive change reflecting a poor prognosis as reflected in the original calculation. This was performed by asking the patient to name as many different animals as possible in one minute.

#### Skin biopsy and establishment of fibroblast cell lines

The skin biopsy was performed as an out-patient procedure. Informed consent was obtained following which 1-2ml of 2% lignocaine was infiltrated to the skin either just above or below the antecubital fossa. Using a 3mm punch skin biopsy needle a slither of skin 3mm in diameter was removed and placed in culture media. The skin was dressed with a light dressing. The participant was given post-procedural skin care advice and a supply of dressings, detailing how to look after the biopsy site over the following week.

Eagles Minimum Essential Media (EMEM) (1000 mg/L glucose, Corning) supplemented with 10% foetal bovine serum (FBS, Biosera), 100 IU/ml penicillin (Lonza), 100 µg/ml streptomycin (Lonza), 50 µg/ml uridine (Sigma-Aldrich) and 1 mM sodium pyruvate (Sigma-Aldrich), 0.1 mM non-essential amino acids (Lonza), and 0.1 × MEM vitamins (Lonza) was used for continuous fibroblast culture.

Biopsies were cut into 6 pieces and mounted in a T25cm<sup>2</sup> cell culture flask using a composition of 50% culture media described above and 50% FBS within 24 hours of the biopsy being taken. Once the biopsy pieces were established culture media was changed to full EMEM and volumes of feed were gradually increased over 2 weeks until they reached 5mls of EMEM. Feeding frequency was every 48-72 hours.

Once populations of fibroblasts had become established and confluent the T25cm<sup>2</sup> flask was washed in potassium buffered saline (PBS) and trypsinised using 1xTrypsin (Lonza) solution mixed in PBS to generate the first cell passage. The solution containing trypsinised cells was then be quenched in EMEM and centrifuged at 550RCF for 4 minutes to generate a pellet of cells. This pellet was re-suspended in EMEM and transferred to another T25cm<sup>2</sup> flask.

Once the fibroblasts have become confluent again and are ready for a second passage, the flask is trypsinised using the same technique as above and transferred

to a T75cm<sup>2</sup> flask in 10mls EMEM media. At this stage all further passages are transferred to T75cm<sup>2</sup> flask using the same technique.

From passage 4 onwards cells were frozen down to maintain stock prior to assay. The same process for typsinisation was followed however the cell pellet was resuspended in 2mls of a solution containing 80% EMEM, 10%FBS and 10% dimethylsulfoxide (DMSO). This suspension was then split into 2 cryovials containing 1ml of suspension and placed in a Corning® CoolCell® Container and placed in -80°C freezer. Cells were fully frozen after 2 hours at -80°C. Cells are subsequently transferred into liquid nitrogen for long term storage. The establishment of fibroblast cell lines was consistent with previously reported protocols.<sup>231</sup>

#### Assessment of mitochondrial function in fibroblast cell lines

Fibroblast cell lines were assayed from passage 6 onwards up to a maximum of passage 15. Assays were performed in age, sex and passage matched groups of 6-10 fibroblast lines. All assays were performed in 96 well plates with triplicate wells per cell line and media condition. For all assays, 24 hours after plating, the media was exchanged to incubate the fibroblasts for 72 hours prior to analysis under the following two conditions; glucose containing (using the EMEM media described above for culture) or galactose containing media which was composed of Glucose-free DMEM supplemented with 10% FBS (Biosera), 100 IU/ml penicillin (Lonza), 100 µg/ml streptomycin (Lonza), 50 µg/ml uridine (Sigma-Aldrich), 1 mM sodium pyruvate (Sigma-Aldrich) and 5mM galactose (Sigma-Aldrich).

#### *Mitochondrial Membrane Potential, mitochondrial morphology and lysosomal morphology*

MMP and mitochondrial morphology was assessed using tetramethylrhodamine (TMRM, ThermoFischer Scientific), a potentiometric dye that binds to the most negatively charged areas of a cell, usually the mitochondria. Therefore, the amount of TMRM fluorescence is directly related to the MMP and can be used as functional assessment of the MMP. Additionally, given that TMRM binds the mitochondrial membrane it can be used to assess various parameters reflecting mitochondrial morphology. This was assessed in accordance with previously published methodology.<sup>159</sup>

Lysosomal morphology was assessed as previously described using LysoTracker® (Life Technologies), a fluorescent acidotropic probe that dye acidic organelles such as lysosomes in cells. This allows the morphological assessment of lysosomes but does not provide any functional assessment of lysosomes.<sup>161</sup>

Hoescht (Sigma Aldrich) stains the nuclei of cells to allow the quantification of cell count and the localisation of other organelles relative to the perinuclear region.

For these assays' fibroblasts were plated at a density of 1000 cells per well. Staining with a solution of phenol-red free media containing 80nM TMRM, 1µM LysoTracker® and 1 µM Hoescht was added to each well 1 hour prior to imaging. Live fibroblasts were imaged using either the InCell Analyzer 2000 high-content imager (GE Healthcare) or Opera Phenix (Perkin Elmer) imaging systems as previously described.<sup>73,159</sup>

Raw images were analysed and parameters obtained using the InCell Developer software (GE Healthcare) or Harmony software (Perkin Elmer). A custom imaging protocol was used where the DAPI channel allowed for the segmentation of nuclei, which was utilised to count cell numbers and identify the perinuclear region. The cy3 channel was used to segment mitochondria to calculate mitochondria count, mitochondrial form factor and mitochondrial perinuclear localisation, and associated intensity was used to calculate MMP. The mitochondria population was further divided into long and small mitochondria; mitochondrial form factor was calculated using **Equation 2.7**.

$$FF = \frac{Pm^2}{4\pi Am}$$

**Equation 2.7: Calculation of mitochondrial form factor**

*Where Pm is the length of the mitochondrion perimeter and Am is the area of the mitochondrion.*

Cut-off values for small mitochondria based upon form factor were >2.08 for groups assayed using the InCell Analyzer 2000 and >0.878 with a spot area greater than 45px<sup>2</sup> for groups assayed using the Opera Phenix. These cut off values were calculated by measuring the control population and selecting cut offs that defined 45% of mitochondria as long and 55% as small to ensure consistency across the different software.

The FITC channel was used to segment the lysosomes to quantify lysosome count, individual lysosome area and lysosome form factor. Analysis outputs were consistent across imagers and software, enabling combination of groups in the final analysis.

### *Intracellular ATP*

Total intracellular ATP was assessed in fibroblasts using the ATPlite kit (Perkin Elmer) which is a luminescence assay for ATP. Cells were plated at a density of 4000 cells per well for both media conditions. After 72 hours of exposure to the two media conditions, and as per manufacturer's instructions, media was aspirated, then 50µl of mammalian cell lysis and 100µl of PBS was added to each well and placed in an orbital shaker for five minutes at 700rpm. This lyses the cells and stabilises ATP prior to quantification. Then 50µl of substrate solution is added to each well and placed in an orbital shaker for five minutes at 700rpm. Following this the plate was dark adapted for 10 minutes and then quantified for luminescence. Luminescence is generated by the substrate solution which contains d-Luciferin and reacts with ATP to generate luminescence. ATP was then quantified using the luminescence mode of a PHERAstar plate reader (BMG Labtech). Following acquisition of this data it is necessary to also measure the quantity of cells in each well. This was done using the average nuclei count obtained from the corresponding matching media condition wells from the mitochondrial and lysosomal morphology plate which was ran simultaneously.

Raw luminescence data for each well was manually inspected for spurious results for the removal of gross outliers prior to statistical analysis.

### *Cross-sectional statistical Analysis*

Differences in demographic between groups were tested using a t-test with Welch's correction for continuous data and chi-squared test for categorical data.

### *<sup>31</sup>P magnetic resonance spectroscopy statistical analysis*

All resonances will be tested for normality. Each individual resonance will be presented for both control and patient groups as a mean and standard deviation if normally distributed and median and interquartile range if not.

Primary <sup>31</sup>P-MRS parameters of interest were determined *a priori* as total levels of ATP, inorganic phosphate and phosphocreatine in the mean midbrain, mean posterior putamen and mean anterior putamen, normalised to total phosphorus signal. Secondary <sup>31</sup>P-MRS parameters include PE, PC, GPE and GPC, the

phosphomonoesters (PME, the sum of PE and PC) and the phosphodiester (PDE, the sum of GPE and GPC).

Pearson's correlation coefficient was used to assess relationships between each  $^{31}\text{P}$ -MRS parameter and the following continuous clinical variables of interest: MDS-UPDRS III, NMSS and the predicted risk of rapid disease progression.

The F-test of equality of variances was used to assess for differences in variance between groups.

To assess for differences between PD and healthy controls at baseline individual  $^{31}\text{P}$ -MRS parameters were each entered into separate general linear models (assuming a gaussian distribution) as the response variable, with the predictor variables specified as disease group, age and sex for same reasons specified in The UP Study analysis earlier. This model is shown in **Equation 2.8**.

$$^{31}\text{P} \sim \text{disease group} + \text{age} + \text{sex}$$

**Equation 2.8: General linear model for the assessment of group differences in  $^{31}\text{P}$ -MRS parameters**

*Beta coefficients and error term not included for ease of visualisation. In the event that partial volume effects showed a clear relationship to  $^{31}\text{P}$ -MRS parameters then this was also included as a relevant parameter.  $^{31}\text{P}$ -MRS parameters denoted by ' $^{31}\text{P}$ '. Sex and treatment were both binary coded.*

Partial volume effects were analysed separately for any relationship with  $^{31}\text{P}$ -MRS parameters using correlation analysis as described in The UP Study and included in the generalised linear model if found to be significant.

*Patient-derived fibroblast cell assay statistical analysis*

All data for each fibroblast line were normalised to the controls on each plate. Due to the differences in sample size between PD and controls, several lines were assayed across multiple groups. Participants that had been assayed in multiple groups had their data averaged across all plates to derive a single value per participant.

Raw intracellular ATP fluorescence was first divided by the average nuclei count obtained from the corresponding matching media condition wells from the mitochondrial and lysosomal morphology plate that was ran simultaneously. This controls for differences in growth rates between cell lines once plated.

MMP values from live cell imaging are given for overall MMP, MMP in small mitochondria and MMP in large mitochondria. These are then corrected for the area of all cells detected in the image, again correcting for differences in growth rates and imaging fields with varying numbers of cells captured.

Key primary fibroblast parameters of interest specified *a priori* were intracellular ATP, MMP (in all mitochondria, long mitochondria only and short mitochondria only), mitochondrial count per cell, ratio of long:short mitochondria, percentage of perinuclear mitochondria, and lysosome count.

For all fibroblast assay parameters of interest differences in variances between groups were analysed using the F-test. For fibroblast parameters group differences in each media condition were tested using t-test for normally distributed data or the Mann-Whitney U test for non-normally distributed data. Pearson's correlation coefficient was used to assess relationships each other fibroblast parameters and each other, these were corrected for multiple comparisons using the Benjamini-Hochberg method.<sup>232</sup>

#### *Assessing relationships between <sup>31</sup>P magnetic resonance spectroscopy and fibroblast cell assays*

To assess associations between <sup>31</sup>P-MRS and fibroblast data in a common domain, all relevant <sup>31</sup>P-MRS parameters and each individual biological fibroblast assay repeat were first transformed to Z-scores. In brief, prior to conversion to z-scores, each parameter of interest was first assessed for normality with the visual inspection of Q-Q plots in the healthy control data. If the data was normally distributed, the values of each healthy control parameter were transformed to a z-score with mean 0 and standard deviation of 1. Z-scores for patients were then calculated with reference to healthy control distribution.

Using previously published methodology, each biological repeat for the fibroblast data was combined into a composite z-score with equal weighting given to each individual repeat, and one z-score for each media condition. This methodology is shown in **equation 2.10**.<sup>233</sup>

$$z_{xc} = \frac{\sum_{i=0}^n z_x}{\sqrt{n + 2r_{sum}}}$$

#### **Equation 2.9: The calculation of composite z-scores**

Where  $z_{xc}$  is the composite score,  $z_x$  is the z-scored component and  $r_{sum}$  is the sum of the Pearson correlation coefficients between each and every individual  $n$  components.

This resulted in a composite z-score for each fibroblast assay parameter for both glucose-containing and galactose-containing media. These two individual composite z-scores were then combined into a single composite z-score using the same method to generate a single composite z-score for each fibroblast assay parameter that summarises data from both media conditions.

Composite Z-scores were also generated using the same above method to reflect  $^{31}\text{P}$ -MRS parameters in combinations of voxels, these combinations were the composite of all 4 putaminal voxels and a composite of both midbrain voxels.

Pearson's correlation coefficient was used to assess relationships between composite z-scores derived from  $^{31}\text{P}$ -MRS and fibroblast assay parameters within each disease group. Any significant correlations were then assessed and corrected with generalised linear models with the additional covariates of age and sex entered.

All statistical analyses were completed in R version 4.1.0.

#### Cross-sectional sample size sample size calculations

Due to the exploratory nature of the analysis and the lack of prior data for  $^{31}\text{P}$ -MRS methodology, a formal power calculation cannot be performed. However, to illustrate that this sample size is appropriate, a power calculation for a simple comparison of case vs control based on data from a previous  $^{31}\text{P}$ -MRS study has been used.<sup>189</sup> The planned initial sample size for this study (35 patients and 15 controls) has 99% power to detect the difference of 0.38 (around 20% lower) in ATP levels between early PD and controls reported in the referenced cross-sectional study.<sup>189</sup> Further, it still has 80% power to detect a smaller difference of 0.21 (around 11% lower). These calculations assume a 5% 2-sided significance level and standard deviations of 0.23. It should be noted that the referenced study quantified ATP in mmol and not using the amplitude of ATP normalised to total phosphorus signal however the calculations are still useful as the equivalent proportion of reduction would likely be similar.

#### Longitudinal $^{31}\text{P}$ Phosphorus Magnetic Resonance Spectroscopy statistical analysis

All  $^{31}\text{P}$ -MRS parameters were assessed for normality using QQ plots.  $^{31}\text{P}$ -MRS parameters of interest were ATP, inorganic phosphate, phosphocreatine, PME and PDE. These were analysed using mean midbrain, mean posterior putamen and mean

anterior putamen values described earlier. A mixed effects two-way ANOVA was performed assessing differences in these values across timepoints and between disease groups as fixed effects with participant change modelled as random effects. The Greenhouse-Geisser sphericity correction was applied to any models not meeting the assumption of sphericity.

Post-hoc comparisons were only performed if the ANOVA test statistic was significant. Post-hoc comparisons used t-tests with p-values corrected using the false discovery rate method with alpha set at 0.05. For post-hoc comparisons assessing between group differences an unpaired t-test was performed and for comparisons within groups comparing timepoints a paired t-test was performed. Variances were not assumed to be equal for the t-tests.

For any significant post-hoc tests identifying differences in a  $^{31}\text{P}$ -MRS parameter that parameter was then analysed further for any relationships with clinical measures of progression in PD only. This was performed using a mixed effects linear model detailed in **Equation 2.11**.

$$\text{Clinical parameter} \sim \text{Timepoint} + 31P + \text{Age} + (1|\text{Participant})$$

**Equation 2.10: Mixed effects linear model to assess relationships between  $^{31}\text{P}$ -MRS parameters and clinical markers of disease progression.**

*Each individual is modelled as having random intercept as the random effect in the model.*

If the clinical parameter being assessed was an MDS-UPDRS score LED was an added to the mixed effects linear model as a further fixed effect predictor. For significant results, estimated effect sizes, confidence intervals and associated p-values are reported for predictor variables.

All statistical analyses were completed in R version 4.1.0. Packages used in analysis are found in the **Appendix 2**.

## Chapter 3: The UP study confirms the neuroprotective potential of ursodeoxycholic acid in Parkinson's disease

### Introduction to chapter

This chapter discusses the results of 'The UP Study', a Phase II double-blind randomised-controlled trial of UDCA in PD. This trial employs a novel design to address some of the issues highlighted earlier in previous neuroprotective trials in PD. The primary outcome is safety and tolerability in PD. UDCA has not been trialled in PD and the chosen dose of 30mg/kg daily is double the usual clinical dose used in hepatobiliary diseases. The increased dose of 30 mg/kg was chosen to ensure sufficient CSF levels.<sup>209</sup> Alongside classical clinical rating scales to assess motor impairment in PD, The UP Study has employed an objective sensor-based approach to quantify motor impairment. Target engagement was assessed using <sup>31</sup>P-MRS to detect changes in bioenergetic parameters that could reflect an improvement in mitochondrial function. These results are reported in a manuscript in preparation for submission entitled "The UP study confirms the neuroprotective potential of ursodeoxycholic acid in Parkinson's disease".

### Contributions to published paper

I was responsible for the recruitment, consenting and all blinded clinical assessments of all Sheffield recruited participants during the length of the study. I was responsible for the analysis of all <sup>31</sup>P-MRS data throughout the whole study and assisted in the statistical analysis of clinical data in conjunction with the statistician associated with the trial (Miss Rosie Taylor). The acquisition and analysis of the sensor-based gait analysis was performed by co-authors in the Institute for In-silico Medicine (Dr Ellen Buckley, Dr Linda van Gelder, Prof Claudia Mazza), The University of Sheffield. I was not involved in active AE or safety review during the course of the trial. Serum bile acid analysis was performed by collaborators and co-authors Dr Benjamin H Mullish and Professor Julian Marchesi.

I drafted the manuscript with the exception of the methods and results for the sensor-based gait analysis which was done by a co-author (Dr Linda van Gelder) and sections pertaining to methodology of serum bile acid analysis which was done by Dr Benjamin H Mullish and Professor Julian Marchesi. The manuscript was drafted under the guidance of my primary supervisor (and co-author Professor Oliver Bandmann).

### Manuscript in preparation for submission

The following manuscript is intended for submission to *The Journal of Clinical Investigation* and as such has been prepared to meet their formatting requirements for submitted manuscripts.

# The UP study confirms the neuroprotective potential of ursodeoxycholic acid in Parkinson's disease

Thomas Payne,<sup>1</sup> Matthew Appleby,<sup>2</sup> Ellen Buckley,<sup>3</sup> Linda M.A. van Gelder,<sup>3</sup> Benjamin H. Mullish,<sup>4</sup> Matilde Sassani,<sup>1,5</sup> Mark J Dunning,<sup>6</sup> Dena Hernandez,<sup>7</sup> Sonja Scholz,<sup>8,9</sup> Alisdair McNeil,<sup>1</sup> Sarah Moll,<sup>10</sup> Julian R Marchesi,<sup>4</sup> Rosie Taylor,<sup>11</sup> Li Su,<sup>1,12</sup> Claudia Mazzà,<sup>3</sup> Tom Jenkins,<sup>1,13</sup> Thomas Foltynie,<sup>2</sup> Oliver Bandmann<sup>1</sup>

## Author affiliations:

<sup>1</sup>Sheffield Institute for Translational Neuroscience, University of Sheffield, Sheffield, S10 2HQ, United Kingdom

<sup>2</sup>Department of Clinical and Movement Neurosciences, Institute of Neurology, University College London, London, WC1N 3BG, United Kingdom

<sup>3</sup>Department of Mechanical Engineering and Insigneo Institute for In Silico Medicine, The University of Sheffield, Sheffield, S1 3JD, United Kingdom

<sup>4</sup>Division of Digestive Diseases, Department of Metabolism, Digestion and Reproduction, St Mary's Hospital Campus, Imperial College London, London, W2 1NY, United Kingdom

<sup>5</sup>Institute of Metabolism and Systems Research, College of Medical and Dental Sciences, The University of Birmingham, Edgbaston, Birmingham B15 2TT, United Kingdom

<sup>6</sup>The Bioinformatics Core, Sheffield Institute of Translational Neuroscience, University of Sheffield, Sheffield, S10 2HQ, United Kingdom

<sup>7</sup>Molecular Genetics Section, Laboratory of Neurogenetics, NIA, NIH, Bethesda, Maryland, USA

<sup>8</sup>Neurodegenerative Diseases Research Unit, Laboratory of Neurogenetics, National Institute of Neurological Disorders and Stroke, National Institutes of Health, Bethesda, Maryland, USA

<sup>9</sup>Department of Neurology, Johns Hopkins University Medical Center, Baltimore, Maryland, USA

<sup>10</sup>NIHR Sheffield Biomedical Research Centre, Royal Hallamshire Hospital, Sheffield, S10 2JF, United Kingdom

<sup>11</sup>Statistical Services Unit, The University of Sheffield, Sheffield, S3 7RH, United Kingdom

<sup>12</sup>Department of Psychiatry, University of Cambridge CB2 0SP, United Kingdom

<sup>13</sup>Royal Perth Hospital, Victoria Square, Perth, WA6000, Australia

## Abstract

**Background:** Mitochondrial dysfunction is a key pathogenic mechanism for Parkinson's disease (PD). We previously undertook the first screen of an entire compound library in PD patient tissue and identified ursodeoxycholic acid (UDCA) as a powerful mitochondrial rescue compound. We have now undertaken a "proof of concept" clinical trial to determine safety and tolerability of UDCA in PD and explore its neuroprotective potential.

**Methods:** The UP (UDCA in PD) study is a phase II, randomised, double-blind, placebo-controlled trial of high dose UDCA (30mg/kg) in 31 participants with early PD for 48 weeks followed by an 8-week washout period. Randomisation was 2:1 drug to placebo. Primary outcome was safety and tolerability. Secondary outcomes combined subjective clinical rating scales with objective, motion sensor-based quantification of gait impairment. Target engagement was explored using <sup>31</sup>phosphorus magnetic resonance spectroscopy (<sup>31</sup>P-MRS).

**Results:** UDCA was safe and extremely well tolerated. Both groups improved in the Movement Disorders Society Unified Parkinson's Disease Rating Scale, part III with no significant differences between groups. Objective quantification of motor impairment demonstrated improvement of several gait parameters such as cadence, stride time and stance time in the UDCA treatment group compared to placebo. Midbrain <sup>31</sup>P-MRS revealed an increase in Gibb's free energy, indicating improved ATP hydrolysis in the UDCA treatment group compared to placebo.

**Conclusion:** The results of our UP study establish safety and tolerability of UDCA in early PD, confirm its neuroprotective potential and provide strong justification for a definitive Phase III trial to establish the disease-modifying effect of UDCA in PD.

**Trial Registration:** EudraCT 2018-001887-46, ClinicalTrials.gov: NCT03840005

## Introduction

Parkinson's disease (PD) remains incurable and relentlessly progressive. The prevalence of PD worldwide more than doubled from 1990 to 2015, its annual economic burden exceeds \$50 Billion Dollars in the US alone.<sup>9,234</sup> Mitochondrial dysfunction was first identified in sporadic PD brains and has also been implicated in all forms of familial PD.<sup>5,235</sup> Rescue of mitochondrial function has therefore long been proposed as a promising neuroprotective strategy.<sup>7,236</sup> However, previous clinical trials assessing putative mitochondrial rescue compounds yielded disappointing results.<sup>112-115,237</sup>

The selected compounds for these previous negative trials were typically chosen for their promising beneficial effect in toxin-induced model systems of PD, only some of these trials assessed the selected compounds for target engagement and efficacy was solely judged on the outcome of clinical rating scales, in particular the motor examination (part III) of the Movement Disorders Society (MDS) Unified Parkinson's Disease Rating scale (MDS-UDPRS). Our group undertook the first screen of an entire compound library in genetically stratified PD patient tissue which led to the identification of ursodeoxycholic acid (UDCA), as a promising mitochondrial rescue compound for PD.<sup>200,201</sup> We subsequently confirmed the mitochondrial rescue effect of UDCA in mechanistically stratified sporadic PD patient tissue.<sup>161</sup> Other groups had independently reported a beneficial effect of UDCA or its taurine conjugate tauroursodeoxycholic acid (TUDCA) in classical MPTP- or rotenone-induced rodent models of PD.<sup>203,204,238-240</sup> UDCA has been licensed to treat primary biliary cholangitis (PBC) at the dose of 15mg/kg for > 30 years. Its excellent safety and tolerability profile makes it ideally suited for the drug repurposing strategy.<sup>207,241</sup>

Pharmacokinetic (PK) studies in patients with amyotrophic lateral sclerosis (ALS) confirmed blood-brain-barrier penetrance of UDCA, especially at higher doses.<sup>209</sup> In 2015 the international Linked Clinical Trials Initiative (iLCT) named UDCA as its most highly prioritized neuroprotective compound for investigation in clinical trials to further validate its neuroprotective potential in PD.

Here we present the results of a phase II, double-blind, randomised, placebo-controlled trial of 30 mg/kg of UDCA in early PD, the UP study. The primary outcome of our study was safety and tolerability of this comparatively high dose of UDCA in PD,

chosen to balance CNS penetration and side-effect profile.<sup>209</sup> . A key part of this “proof of concept” study was also the evaluation of novel secondary outcome measures to address key limitations of traditional PD neuroprotection trial designs. Clinical assessment with validated, “gold standard” clinical rating scales, widely used in previous neuroprotective trials, was complemented by the in-depth objective quantification of motor impairment, utilising sensor-based supervised gait analysis before and after treatment.<sup>242,243</sup> In addition, we applied <sup>31</sup>P-phosphorus magnetic resonance spectroscopy (<sup>31</sup>P-MRS) to confirm mechanistic target engagement of UDCA in the midbrain. <sup>31</sup>P-MRS is an MRI-based technique which allows non-invasive spectroscopic quantification of key energy metabolites such as ATP, or phosphocreatine (PCr) before and after treatment with an investigative medicinal compound (IMP) such as UDCA.<sup>180</sup>

## **Methods**

### **Design**

A comprehensive protocol for this trial has previously been published.<sup>244</sup> In brief, this was a phase II, two-centre, double-blind, randomised, placebo-controlled trial of 30 mg/kg of UDCA in recent onset Parkinson's disease ( $\leq 3$  years since diagnosis) who demonstrated a clear subjective, sustained ( $>3$  months) motor response to dopaminergic medication which was confirmed by the treating physician. UDCA was administered orally for 48 weeks with a subsequent 8-week washout phase to 31 participants with a 2:1 randomisation of drug vs placebo. The trial was conducted at two sites, STH and University College London Hospitals NHS Foundation Trust (UCLH). Trial recruitment was advertised online by the Parkinson's UK Research Network, the Cure Parkinson's Trust, the Sheffield National Institute for Health-Related Research (NIHR)-Biomedical Research Centre website and the NIHR Clinical Research Network websites.

Following a screening visit to confirm eligibility, participants attended 6 further visits: baseline (start of treatment period), week 12, week 24, week 36, week 48 (end of treatment period) and week 56 (end of washout period). Treatment with either UDCA or placebo was commenced at a dose of 250mg per day and increased by 250mg every 3 days until the target weight-dependant dose of 30mg/kg was achieved. All patients were advised to completely stop taking the Investigational Medicinal Product (IMP) the evening prior to the week 48 visit.

Placebo and UDCA were provided by PRO.MED.CS Praha a.s. and completely matched with no identifiable differences in taste, appearance, or smell. Each capsule was provided as a hard, clear, gelatine capsule containing white powder and capsules of the active drug contained 250mg of UDCA.

### **Outcome Measures**

#### **Primary Outcome**

The primary outcome was to compare the safety and tolerability of UDCA at 30 mg/kg in PD compared to placebo as indicated by the following: number of serious adverse events (SAEs), number of adverse treatment-reactions and number of patients who completed the study.

## Secondary and Exploratory Outcomes

Secondary outcomes included the change from baseline to week 48 of treatment in the UDCA versus placebo group with respect to: MDS-UPDRS Part III in the practically defined “OFF” medication state (defined as >8 hours off levodopa medication and >36 hours off dopamine agonists and drugs such as monoamine oxidase B inhibitors); *in vivo* parameter estimates of high and low energy metabolite levels derived from <sup>31</sup>P-MRS (ATP, PCr and inorganic phosphate) in the midbrain; sensor-based objective quantification of motor impairment in both supervised instrumented clinical gait assessment (consisting of triaxial OPAL sensors, APDM Inc., Portland, OR, USA and OPTOGait 5m system, Microgate Corporation, Bolzano, Italy) and unsupervised continuous 7-day real world physical activity monitoring (using the McRoberts Dynaport Movemonitor+, Netherlands sensor).<sup>122</sup>

Exploratory clinical outcomes focused on the changes between baseline and week 48 of: MDS-UPDRS I-IV in the ‘ON’ state; Levodopa equivalent dose (LED); Montreal Cognitive assessment (MoCA); Montgomery-Ashberg Depression Rating Scale (MADRS); Non-Motor Symptoms Scale (NMS-QUEST); Parkinson’s Disease 39 item quality of life questionnaire (PDQ-39); calculated <sup>31</sup>P-MRS Gibbs free energy of ATP hydrolysis ( $\Delta$ GATP) and ADP concentration in the midbrain.<sup>122,125,211,245-247</sup> If performed at week 56 all measures listed were also assessed for the change between week 48 and week 56 over the washout period.

## Assessment Procedures

### Safety and clinical assessment

At each visit, adverse events (AEs) were reviewed and assessed for severity and likely relationship to UDCA. Safety monitoring was performed at each visit to capture any adverse events including ECG and blood monitoring (full blood count, urea & electrolytes, liver function tests, blood glucose, HbA1c, lipid profile). Compliance was assessed by counting the number of IMP tablets returned by the participant and was expressed as the following percentage: (IMP dispensed - IMP returned)/IMP prescribed. A simplified summary of the safety and clinical assessment study procedures is reported (**Figure 3.1**). At baseline, the predicted risk of rapid disease progression was calculated according to a validated prognostic model, estimating the



## **Genetic analysis**

All participants supplied an EDTA blood sample for genetic analysis using the NeuroChip platform.<sup>215</sup> Results were assessed for any known pathogenic mutations in monogenic PD genes (e.g., PINK1, PARK2, LRRK2 etc.) and any variants of GBA1 associated with increased risk of PD. All detected variants were searched in dbSNP (<https://www.ncbi.nlm.nih.gov/snp/>) and classified according to published guidelines.<sup>248</sup>

## **Serum bile acid analysis**

Serum samples were collected from all participants at each face-to-face visit and stored at -80°C. Serum samples were available for all 30 participants (UDCA n=19, placebo n=11) at both baseline and week 12. One sample from the placebo group at week 24 was removed due to being a gross outlier likely due to technical error (around 75x greater value than all other placebo values across all visits). COVID-19 restrictions reduced the number of face-to-face study visits; therefore a reduced number of serum samples were available for week 24 (UDCA n=17, placebo n=8), week 36 (UDCA n=13, placebo n=4), week 48 (UDCA n=11, placebo n=6) and week 56 (UDCA n=15, placebo n=7). Serum bile acid profiling was performed using ultra-performance liquid chromatography linked to mass spectrometry (UPLC-MS) using a previously-described technique.<sup>226</sup> Quality control (QC) samples were prepared using equal parts of each sample (with some QC samples spiked with known bile acid standards), and were run alongside them. LC-MS was performed using ACQUITY UPLC (Waters Ltd, Elstree, UK) coupled to a Xevo G2 Q-ToF mass spectrometer equipped with an electrospray ionisation source operating in negative ion mode (ESI-), as previously-described.<sup>226</sup> peakPanther was used to facilitate identification and relative quantification of bile acids.<sup>249</sup>

## **Sensor Based Quantification of motor impairment**

Sensor-based gait analysis was undertaken at the Clinical Research Facility (CRF) of the Sheffield study site only. All 19 Sheffield participants were fitted with three tri-axial inertial sensors (OPAL, APDM Inc., Portland, OR, USA) firmly attached to their pelvis and shanks, which measured acceleration and angular velocity signals. Gait outcomes including temporal metrics and gait quality measures related to intensity and regularity

were then extracted from these signals.<sup>250-252</sup> The experimental design is shown in **Figure 3.2**.

Acceleration and angular velocity signals were recorded along the anatomical vertical, medio-lateral, and anteroposterior axes at a sampling frequency of 128 Hz. The accelerometer range was set at  $\pm 6$  g. Participants were asked to walk at their comfortable speed back and forth in a hospital corridor at least six times along a walkway of approximately 10m in length. This setting was intended to capture around 30 steps per trial without causing fatigue. For trials where a low number of steps were captured, an additional two passes were recorded. The walkway used also included an OPTOGait 5m system. This system was configured in a two-dimensional layout to provide a coverage of approximately 10m x 2m with a 4m x 1m two-dimensional assessment area. The systems' built-in software captured and recorded LED activations and triangulated each footfall that occurred within the assessment area. From this, several spatial gait parameters were computed with a spatial resolution of 1cm.

Temporal measures were computed based on the timings of the foot striking (initial contact) and leaving (final contact) the floor as identified from the angular velocity data. These parameters included: gait speed (meter per second), cadence (steps per minute), stride (timing between initial contacts of same foot), step (timing between initial contacts of contralateral foot), stance (time each foot spent in contact with the floor), swing (time each foot spent of the floor), double support durations (time both feet were on the floor), and stance percentage (percentage of the stride where the foot was on the floor). Spatial measures such as step and stride length and step width were measured by the OPTOGait system. The variability in stride, step, stance, and swing durations and step width were calculated using data from at least 50 steps.<sup>253</sup> Intensity, step regularity, and stride regularity were computed from the lumbar sensor acceleration signals.

## **Processing**

The tri-axial accelerations were reoriented to a horizontal-vertical coordinate system and filtered with a 10 Hz cut-off, zero phase, low-pass Butterworth filter.<sup>254</sup> Accelerations and angular velocities were segmented into walking passes (i.e., straight-line walking), with turning and resting times detected from the lumbar angular

velocities and discarded from subsequent analysis in order to compute the gait measures of interest from steady-state walking passes only.<sup>255</sup> Finally, initial contacts (when the foot strikes the floor) and final contacts (when the foot leaves the floor), gait events were identified for each walking pass by searching for local maxima in medio-lateral angular velocity of both legs.<sup>256</sup>

The sensor data were processed into 32 gait measures, grouped into six domains: rhythm, pace, variability, intensity, and regularity. Gait speed, cadence, stride, step, stance, swing, double support durations, and stance percentage were computed based on the gait events.

The variability in stride, step, stance, and swing durations and step width were calculated including at least 50 steps as described by Galna and co-workers<sup>253</sup>. Intensity, step regularity, and stride regularity were computed from the lumbar acceleration signals for each walking pass with a minimum of three consecutive strides for each of the three axial directions (AP, ML, V) (see Payne *et al*<sup>244</sup> for more details and definitions about all gait metrics).

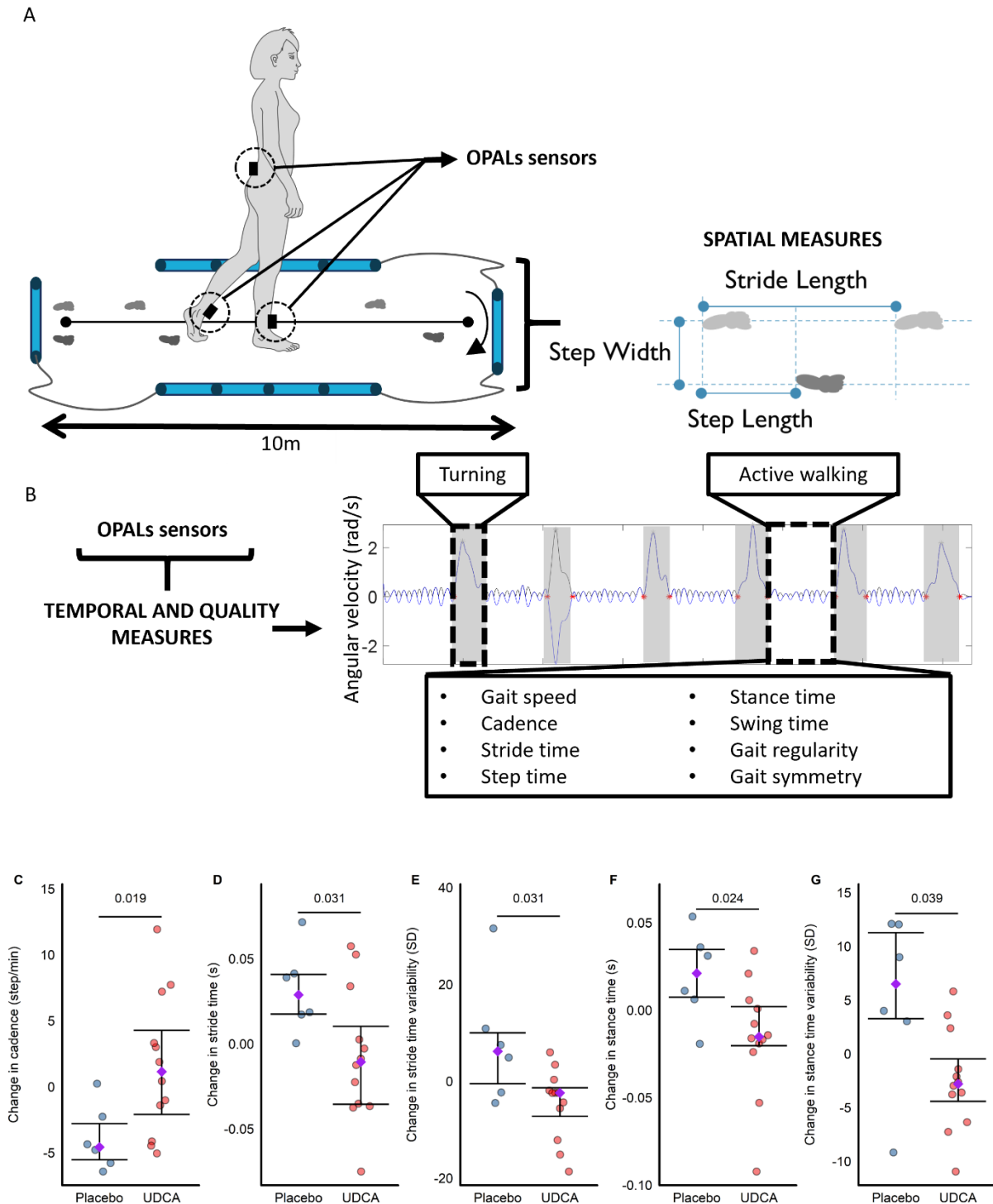


**Figure 3.2: Gait analysis equipment and data processing.**

(A) Schematic of testing procedure with the OPTOgait system in a two-dimensional configuration with a participant wearing OPALs sensors on the lower shins, as well as their lower back (denoted by black boxes). (B) Angular velocity signals recorded using the lumbar sensor during the walking test used to define the turns within the data. Acceleration and angular velocity are then used during active walking to generate temporal, intensity, and

*regularity quality measures of gait. Comparison of gait parameters from baseline to week 48 in the two treatment groups (12 on UDCA 30 mg/kg vs 6 on placebo) demonstrated that PD patients on UDCA took more steps per minute (increased cadence) (C), with reduced amount of time between each heel strike of the same foot (stride time) (D) and reduced stride time variability (E) as well as reduced stance time (F) and stance time variability (G). For C-G purple diamond and error bars signify median and interquartile range as gait analysis data was not normally distributed, p values show significance for group differences as assessed by the Wilcoxon signed rank test.*

### **Physical Activity Monitoring**

A single lumbar physical activity monitor (PAM) was used to assess unsupervised home-based physical activity (McRoberts, Dynaport Movemonitor+, Netherlands) for seven consecutive days prior to commencing treatment and treatment cessation. This is a small and compact PAM that is worn in the centre of the lower back as shown in **Figure 3.3**.

PAM data was processed using the device proprietary algorithms, which provided the following parameters: the total average movement intensity, movement intensity in the active period, active period as a percentage of total time worn, and moving time as a percentage of total time worn. Active periods are defined as any activity that is moving and not static in posture (e.g. lying, sitting, standing). Movement intensity is the average body acceleration (measured in G, the gravitational constant) during a period of activity, greater intensity reflects the ability of the participant to generate greater force during a period of activity. Moving time is the time spent performing activities such as walking, running and cycling but excludes smaller active movements such as changes in posture and shuffling.



**Figure 3.3: The Dynaport MoveMonitor+**

*The Dynaport Movemonitor+ contains an accelerometer and tri-axial gyroscope, weighs only 55 grams and easily fits in the small of the back. Battery capacity allows continuous recording for up to 7 days. Data is uploaded directly to McRoberts and analysed using proprietary algorithms to give measures of physical activity and movement intensity.*

### **<sup>31</sup>Phosphorus Magnetic Resonance Spectroscopy**

#### **Acquisition**

All participants were invited for <sup>31</sup>P-MRS scans both at baseline and week 48 at the Sheffield site, using a Philips Ingenia 3 Tesla system (Philips Healthcare, Best, Netherlands) and a transmit-receive dual-tuned <sup>1</sup>H/<sup>31</sup>P birdcage quadrature head-coil (Rapid Biomedical, Würzburg, Germany). Follow-up scans were delayed in 5 participants from week 48 to 56 due to COVID-19 and a further participant was unable to attend for a second <sup>31</sup>P-MRS scan at all. One participant had their <sup>31</sup>P-MRS follow-up scan repeated at week 56 due to poor technical acquisition at week 48. One data point from one follow-up scan quantifying magnesium had to be removed from the analysis for technical issues prior to unblinding.

All <sup>31</sup>P-MRS scans were obtained using a Philips Ingenia 3 Tesla system (Philips Healthcare, Best, Netherlands) and a transmit-receive dual-tuned <sup>1</sup>H/<sup>31</sup>P birdcage quadrature head-coil (Rapid Biomedical, Würzburg, Germany). Two-dimensional chemical shift imaging (CSI) with image-selected in vivo spectroscopy was used for spectral spatial localisation<sup>257,258</sup>. Alignment of CSI sequences was guided by a T2-

weighted spin-echo image: TR=3000ms, TE=80ms, FA=90°, slice thickness=4mm, FOV=230mm<sup>2</sup>, acquisition voxel 0.55x0.65x4.0mm<sup>3</sup>, reconstruction matrix=432x432mm<sup>2</sup>, reconstructed voxel size=0.53x0.53x4.0mm<sup>3</sup>. To ensure consistency between each visit, CSI grid placement was guided by the same experienced radiographers and researcher using the superior border of the pons and the inferior border of the splenium of the corpus callosum to guide the placement of the inferior and superior borders of the acquisition respectively.

Two separate CSI sequences were obtained focused on the midbrain and the putamen. Acquisition parameters for the midbrain CSI were repetition time (TR)=4000ms, echo time (TE)=0.22ms, number of signal averages (NSA) =8, sampling points=2048, spectral bandwidth=3000Hz, flip angle (FA)=90°, slice thickness=20mm, field of view (FOV)=210mm<sup>2</sup>, acquired voxel sizes of 40x40x20mm<sup>3</sup> and, following k-space filtering and zero filling using a reconstruction matrix of 14x14, a reconstructed voxel size=15x15x20mm<sup>3</sup>. The putamen CSI acquisition parameters differed only in NSA=10 and reconstructed voxel size=17.5x17.5x20mm<sup>3</sup>. All CSI sequences used adiabatic pulses, with a second order pencil-beam shim and WALTZ-4 broadband heteronuclear decoupling with nuclear Overhauser enhancement.

To allow quantification of partial volume effects, a 3D T1 inversion-recovery volumetric image was obtained, co-registered to each voxel within the CSI acquisition, and segmented into grey matter, white matter and cerebrospinal fluid (CSF).

### **Spectroscopic Data Processing**

All spectroscopic data was analysed blinded to participant status. Spectra were processed in the time domain using jMRUI software V5.2 (<http://www.jmrui.eu>) and manually pre-processed using zero and first-order phasing for purely absorptive line shapes. No apodization was performed. All spectra were frequency shifted to 0 parts per million for phosphocreatine prior to quantification.

Signal fitting was performed using the Advanced Method for Accurate, Robust and Efficient Spectral fitting (AMARES) algorithm to determine the relative area under each peak<sup>183,259</sup>. A total of 13 resonances were fitted with assumed Lorentzian line shapes, with  $\gamma$ -ATP and  $\alpha$ -ATP having doublet peaks with amplitudes and linewidths constrained to a 1:1 ratio to each other and  $\beta$ -ATP having triplet peaks with amplitudes constrained in a ratio of 0.5:1:0.5 and linewidths constrained to a ratio of 1:1:1.

Coupling constants for ATP multiplets were set at 18Hz as used in previous literature and soft constraints limited ATP linewidths to 5-35Hz<sup>189,260</sup>. Additional soft constraints were used to control linewidths for phosphocreatine (5-20Hz), and all other remaining resonances to 5-30Hz<sup>216</sup>. All spectra were visually inspected for quality of fit and spurious signals were excluded, according to recently published consensus criteria<sup>217</sup>.

To allow correction for partial volume effects T1 weighted images were segmented using Statistical Parametric Mapping software (SPM12, <https://www.fil.ion.ucl.ac.uk/spm/software/spm12/>) and co-registered to the voxel of interest using Gannett software (<http://www.gabamrs.com/>) and MATLAB and Statistics Toolbox Release R2020a (The MathWorks, Inc., Natick, Massachusetts, United States) to segment each voxel of interest into grey matter, white matter and cerebrospinal fluid.

Intracellular pH, Gibbs free energy of ATP hydrolysis ( $\Delta G_{ATP}$ ) and ADP were calculated according to previously published methods.<sup>219,220,261</sup> All amplitudes of compounds of interest (eg ATP, Pi, PCr) were normalised to the total phosphorus signal detected in each voxel prior to any statistical analyses. The three multiplets of ATP were summed to calculate the total ATP within each spectrum. For the assessment of ratio values (Pi/ATP, PCr/ATP, Pi/PCr) the raw (i.e. non-normalised) amplitudes were used for calculation. Again for these ratio values, the raw amplitudes of all ATP resonances were used to calculate the Pi/ATP and PCr/ATP ratios.

For the calculation of Gibbs free energy of ATP hydrolysis ( $\Delta G_{ATP}$ ) and ADP the expression of ATP, PCr and Pi in millimoles was required for each participant the, mean healthy control values of  $\gamma$ ATP from another study using identical <sup>31</sup>P-MRS acquisition and analysis methodology was used as an external reference of 3 millimoles (as assumed and reported previously) to then derive the millimolar values in all participants.<sup>221</sup> Brain creatine was assumed to be equal to 10 millimoles in health as reported in previous literature.<sup>262</sup>

Voxel localisation and exemplar spectra are shown in **Figure 3.4**.

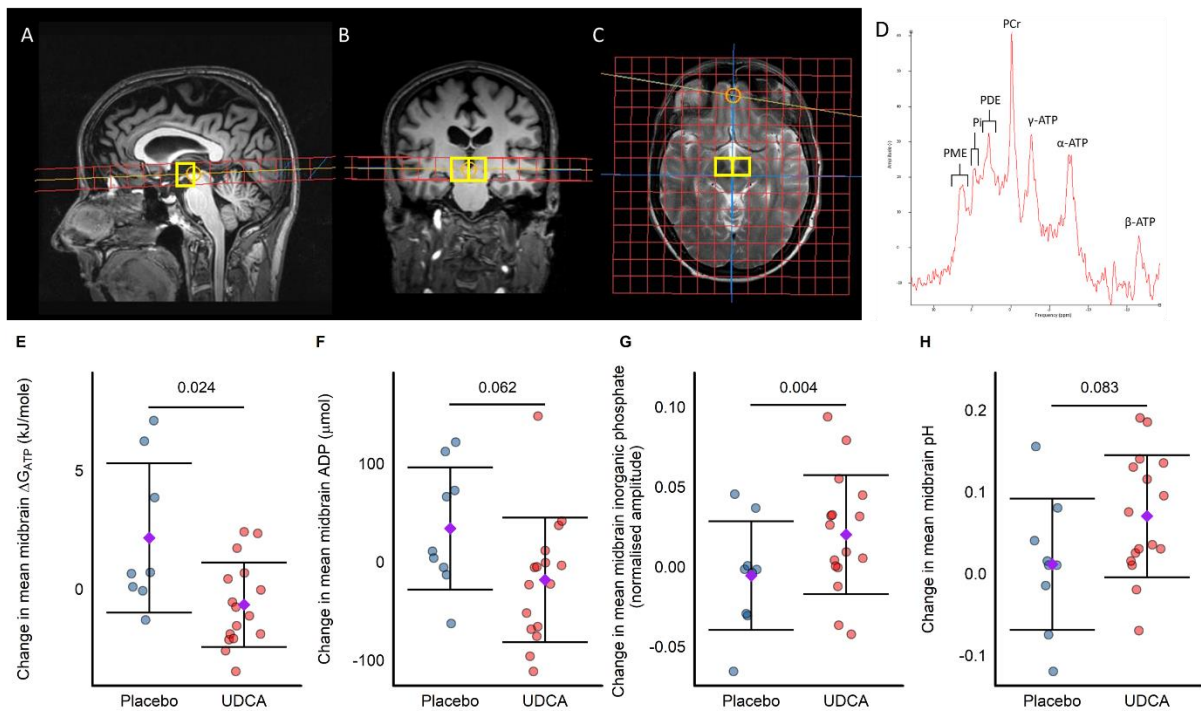


**Figure 3.4:**  $^{31}\text{P}$ Phosphorus Magnetic Resonance voxel localisation, example spectra and results.

Sagittal (A), coronal (B) and axial (C) images demonstrating 14x14 CSI spectroscopic grid positioning for the midbrain voxels. Voxel placement ensures the substantia nigra will be included within the voxel of interest. Voxels of interest from each acquisition are highlighted in yellow. (D) Example spectrum obtained from the midbrain of a participant in the placebo group. This spectrum has been phased and apodised to aid visualisation with phosphocreatine frequency shifted to 0ppm. Change from baseline to week 48 in key  $^{31}\text{P}$ -MRS parameters from the midbrain for; (E)  $\Delta G_{\text{ATP}}$ , (F) ADP concentration, (G) inorganic phosphate and pH (H). For E-H purple diamond and error bars signify mean  $\pm$  standard deviation and p values are for the significance of the estimated treatment coefficient with UDCA as assessed by linear regression. UDCA n=16, placebo n=9 except panel (E) where placebo n=8 due to excluded magnesium value prior to unblinding required for calculation of  $\Delta G_{\text{ATP}}$ . PME=phosphomonoesters, PDE= phosphodiester, Pi= inorganic phosphate, PCr= phosphocreatine,  $\gamma$ -ATP= gamma adenosine triphosphate,  $\alpha$ -ATP= gamma adenosine triphosphate,  $\beta$ -ATP= gamma adenosine triphosphate,  $\Delta G_{\text{ATP}}$  = Gibbs free energy of ATP hydrolysis.

## Statistical Analysis

Statistical analyses was by intention-to-treat. Due to several assessments being unavoidably delayed (see below), sensitivity analyses were performed for each analysis excluding data collected outside of the planned assessment window. All results presented are using the full analysis dataset unless stated otherwise. SAEs

and adverse treatment reactions are presented descriptively, in summaries individual AEs (by preferred term) are counted once per participant at the worst severity. We considered the rate of SAEs reported in the exenatide trial in Parkinson's disease to be tolerable and acceptable (i.e., 20%). If no SAEs were found in the group receiving UDCA (n=20) then the likelihood that the true SAE rate is less than 20% is 0.9908 (i.e., there is a less than 1% chance that the true SAE rate is  $\geq 20\%$ ).<sup>263</sup> The study was not powered to detect differences in the secondary or exploratory endpoints and therefore, the interpretation of observed differences and confidence intervals will take priority over statistical significance conferred by *p*-values and no adjustment was made for multiple testing.

Demographic and clinical assessment data were assessed for normality using QQ plots and summarised using relevant summary statistics. Between-group differences in demographics, clinical parameters at baseline, and changes in both clinical parameters from baseline to week 48, baseline to week 56, or week 48 to week 56 were assessed using t-tests for continuous data and chi-squared tests for categorical data. Between-group differences in supervised gait analysis parameters from baseline to week 48 were compared using Mann-Whitney U tests as data were not normally distributed.

<sup>31</sup>P-MRS was analysed using linear regression with the change from baseline to week 48 as the response variable and the baseline value of the parameter, treatment group, age and sex as predictors. Sex differences in PD have been previously observed in <sup>31</sup>P-MRS and changes in pH and PCr have been observed with age in the healthy brain<sup>193,228</sup> To ensure the number of covariates in linear regression was appropriate to sample size and prevent over-fitting of linear regression models partial volume effects were analysed separately. The correlations between midbrain voxel total brain (grey and white matter) content and <sup>31</sup>P-MRS parameters were assessed using Pearson's correlation coefficient. In the event of a significant correlations, the relevant partial volume measure was added to the model for that <sup>31</sup>P-MRS parameter.

Multi-variate statistical analysis of serum bile acid profiling data was performed using SIMCA 17.0 (MKS Umetrics AB). Both unsupervised and supervised models (OPLS-DA) were performed using Pareto-scaled, log-transformed data.

## **Study Approval**

The trial was approved by the East of England – Cambridgeshire and Hertford Shire Research Ethics committee in the United Kingdom (Protocol ID: 18/EE0280). Sheffield Teaching Hospitals Foundation Trust (STH) acted as the sponsor of the study (local sponsor study number STH18493). The trial was registered on European Union Drug Regulating Authorities Clinical Trials Database (EudraCT no. 2018-001887-46). All participants provided written informed consent prior to any study related activities being performed in accordance with the Declaration of Helsinki.

## Results

*Patient characteristics.* A comprehensive protocol for this trial has previously been published.<sup>244</sup> A total of 33 participants were assessed for eligibility from January 2019 to October 2019, two participants were excluded due to a Montreal Cognitive Assessment (MoCA) score < 25. Full details of the cohort enrollment are shown in **Figure 3.5**. Demographic and clinical characteristics are summarized in **Table 3.1**. Treatment groups were well matched for age, sex, disease duration, family history of PD and predicted risk of rapid disease progression. None of the trial participants carried pathogenic mutations in monogenic PD genes (e.g., *LRRK2*, *SNCA* etc.) or pathogenic risk variants of *GBA*. In total 31 patients were randomised, 11 to placebo and 20 to 30mg/kg of UDCA daily, titrated to target dose over approximately 8 weeks.

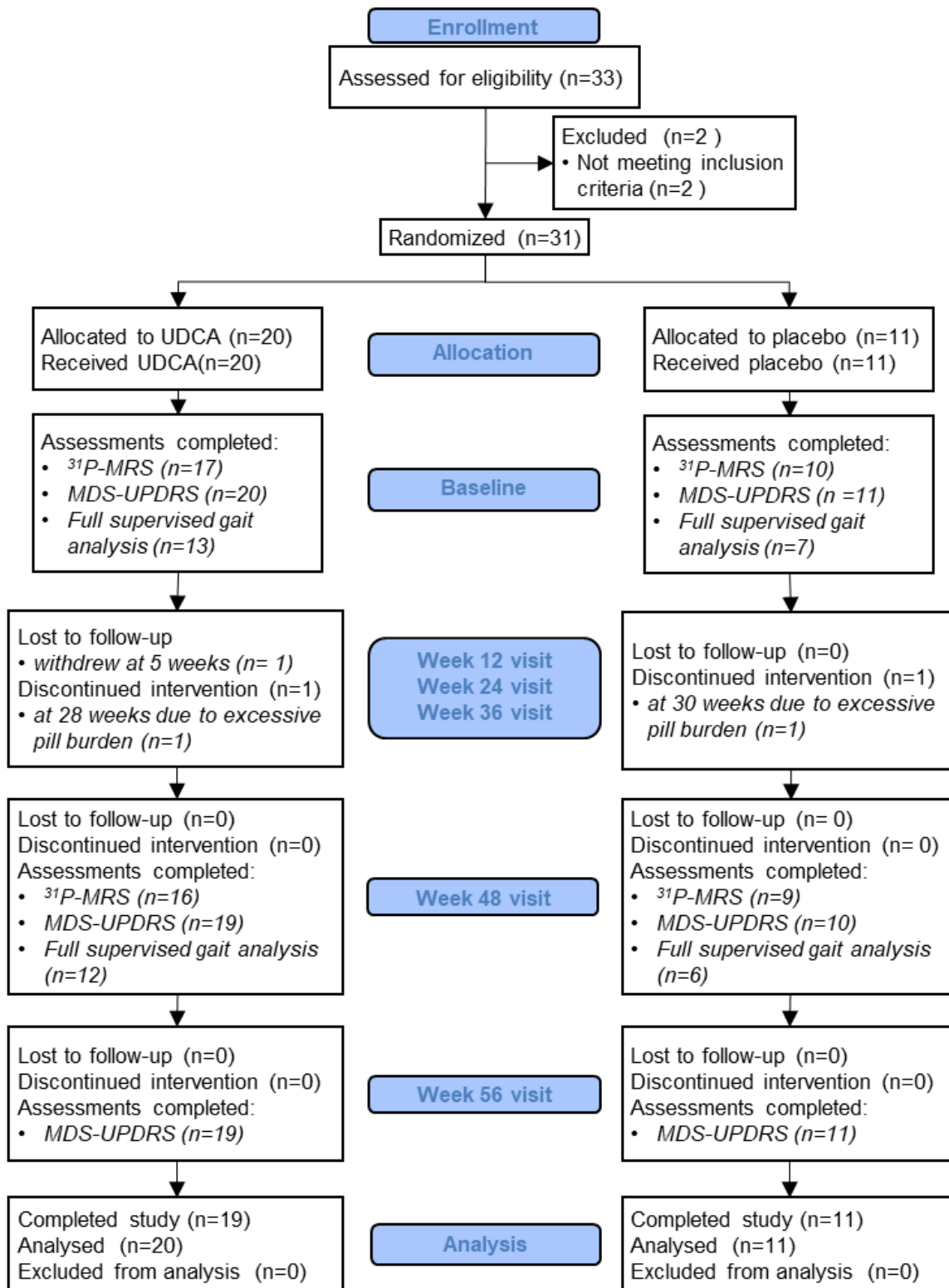


**Figure 3.5: Consort flowchart of enrollment, allocation and follow-up assessments performed.**

*Analysis used an intention-to-treat population therefore all patients randomised were included in the analysis dataset. Details of key secondary outcome assessments are included to demonstrate data completeness.*

		<b>UDCA (n=20)</b>	<b>Placebo (n=11)</b>
Age (years)	Mean $\pm$ SD	56.3 $\pm$ 7.6	61.9 $\pm$ 8.28
	Range	40-74	53-73
Sex	Male (%)	14 (70)	5 (45.5)
	Female (%)	6 (30)	6 (54.5)
Disease Duration (months)	Mean $\pm$ SD	16.3 $\pm$ 11.7	22.1 $\pm$ 7.2
	Range	2.3 - 41.5	10.7 – 32.7
Family History of PD in a first degree relative (n, %)	Present	1 (5)	2 (18.2)
	Absent	19 (95)	9 (81.8)
Modified Hoehn &Yahr (n, %)	Stage 1	5 (25)	2 (18.2)
	Stage 1.5	2 (10)	2 (18.2)
	Stage 2	13 (65)	7 (63.6)
Predicted Risk of Rapid Disease Progression	Mean $\pm$ SD	0.31 $\pm$ 0.16	0.28 $\pm$ 0.21
	Range	0.09 – 0.77	0.10 – 0.69

**Table 3.1. The UP Study: Demographic and clinical features**

*Serum bile acid analysis.* Serum samples were collected from study participants at baseline and at each subsequent visit until the end of study; results of serum bile acid analysis from these samples are summarised in **Figure 3.6**. Following the commencement of treatment with UDCA, changes in the overall serum bile acid profile compared to baseline were found at all visits during the treatment period (weeks 12, 24, 36 and 48, **Fig. 3.6A**). Bile acid profiles returned to levels comparable to baseline values at week 56 following the 8 week washout. No changes compared to baseline were seen at any time point in placebo-treated patients. Supervised multivariate modelling of serum bile acid profiles of UDCA- vs placebo-treated patients at week 12 (chosen for data completeness, using an orthogonal projections to latent structures discriminant analysis; OPLS-DA, **Fig. 3.6B**) revealed a robust model for group separation ( $R^2X=0.721$ ,  $R^2Y=0.964$ ,  $Q^2=0.929$ , CV-ANOVA:  $p=4.68 \times 10^{-12}$ ). Discriminatory feature analysis derived from this model confirmed a marked enrichment in serum UDCA and its conjugates glyoursodeoxycholic acid (GUDCA) and tauroursodeoxycholic acid (TUDCA) in the serum of UDCA-treated patients compared to controls (**Fig. 3.6C**). OPLS-DA did not demonstrate any statistical differences in serum bile acid profiles between UDCA- and placebo-treated groups at baseline or week 56. Relative abundance of UDCA and related conjugates across all time points between groups is shown in **Figure 3.2D**, with further data detailing OPLS-DA modelling of all bile acids in **Fig 3.6E**.

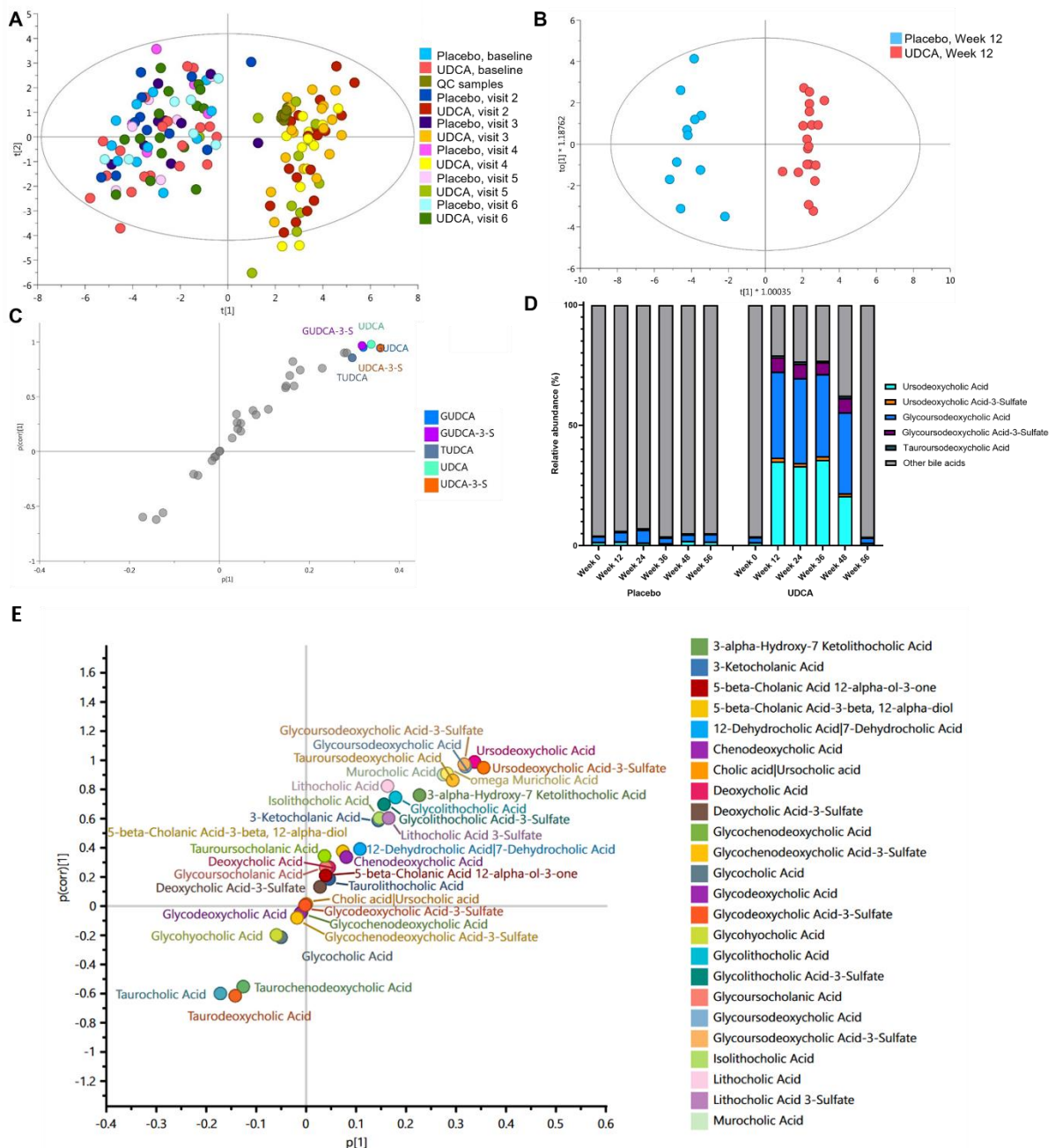


**Figure 3.6: Impact of UDCA upon serum bile acid profiles.**

As assessed using analysis of ultra-performance liquid chromatography linked to mass spectrometry serum bile acid profiling data. **(A)** PCA scores plot, all participants at all time points. **(B)** OPLS-DA scores plot, placebo vs UDCA-treated patients at week 12. **(C)** Discriminatory metabolomic analysis via S-plot, placebo vs UDCA-treated patients at week 12; metabolites at top right of plot are those enriched in UDCA vs placebo week 12 serum samples. Other detected bile acids are in grey with further detail on these bile acids shown in the supplementary information **(D)** Relative abundance plot of key bile acids of interest. Features in top right of S-plot are bile acids elevated in serum of UDCA vs placebo participants at week 12; features in bottom left of S-plot are bile acids elevated in serum of placebo vs UDCA participants at week 12. **(E)** Discriminatory metabolomic analysis via S-plot, placebo vs UDCA-treated patients at week 12 (i.e., derived from **B**). Features in top right of S-plot are

*bile acids enriched in serum of UDCA vs placebo participants at week 12; features in bottom left of S-plot are bile acids enriched in serum of placebo vs UDCA participants at week 12. For (B) and (C), placebo, n=11; UDCA, n=19. Abbreviations: GUDCA= glyoursodeoxycholic acid; GUDCA-3-S= glyoursodeoxycholic acid-3-sulfate; OPLS-DA= orthogonal projections to latent structures discriminant analysis; PCA= principal component analysis; TUDCA= tauroursodeoxycholic acid; UDCA= ursodeoxycholic acid; UDCA-3-S= ursodeoxycholic acid-3-sulfate; QC= Quality control.*

**Safety and tolerability.** One patient withdrew from the trial after 5 weeks of treatment due to significant difficulties with swallowing the number of investigational medicinal product (IMP) capsules in addition to their regular medication, but not side effects of the IMP as such. This participant was replaced with a new patient. The remaining 30 participants all completed the trial, resulting in a total intention-to-treat analysis cohort of 31 trial participants. One participant in the UDCA group and one participant in the placebo group stopped taking the medication early (28 weeks and 30 weeks); both cited the burden of taking an additional 9-10 tablets in addition to their usual medications. All other trial participants (18/20 in the UDCA group and 10/11 in the placebo group) completed the full treatment period. Compliance was excellent in participants completing the 48-week treatment period (mean  $\pm$  SD; 97.6 $\pm$ 5.4% in UDCA vs 95.2 $\pm$ 8.4% in placebo).

Two serious adverse events (SAEs) occurred, both in the same participant, namely retroperitoneal haemorrhage leading to hospital admission and subsequent hospital acquired pneumonia. Administration of the study drug was withheld during the inpatient admission. The independent data monitoring committee (IDMC) advised that this event was unlikely to be related to study medication, unblinding was not indicated and the trial medication was restarted after discharge. Unblinding after completion of the trial revealed that this participant was randomised to the placebo group.

Twenty-four adverse reactions (ARs) were observed in 14/31 participants (10 UDCA and 4 placebo, **Table 3.2**). The most frequent ARs were gastrointestinal symptoms: 5/20 (25.0%) participants on UDCA developed mild diarrhoea (i.e., not requiring any treatment) with most episodes resolving within 48 hours or less (two patients had episodes which resolved within 72 hours). In the placebo group, 1/11 (9.1%) developed diarrhoea that resolved within 24 hours. Mild nausea (i.e., not requiring any treatment) occurred in 2/20 (10%) of participants taking UDCA; in one participant this

episode resolved within 24 hours and, in the second, was of unspecified duration due to missing data. No other ARs occurred in the UDCA treatment group at a frequency of more than 1 of the 20 participants. An SAE rate of 20% was deemed to be tolerable and acceptable in the recent Exenatide-2 trial, the only clinical trial to date with a favourable outcome suggestive of a neuroprotective effect in PD.<sup>263</sup> Since we found no SAEs in the UDCA group in the full intention-to-treat population (n=20), the likelihood that the true SAE rate for UDCA was less than 20% is 0.9908. Blood monitoring performed at all face-to-face visits revealed no clinically significant changes in any blood tests performed other than one incidental finding of hyperkalaemia (5.6mmol/L) in the UDCA group and one isolated increase in alkaline phosphatase (194 IU/L) in the placebo group. The hyperkalaemia was already present at baseline prior to commencement of treatment and therefore unrelated to UDCA. The raised ALP in the placebo group was only observed in the participant who had suffered the retroperitoneal haemorrhage at the visit following the associated hospital admission and normalized for all subsequent visits.

System Organ Class	Adverse Treatment Reaction	UDCA (n=20)	Placebo (n=11)
Gastrointestinal disorders	Abdominal distension	1 (5.0%)	1 (9.1%)
	Abdominal pain	1 (5.0%)	1 (9.1%)
	Constipation	1 (5.0%)	1 (9.1%)
	Diarrhoea	5 (25.0%)	1 (9.1%)
	Dry mouth	0 (0.0%)	1 (9.1%)
	Gastroesophageal reflux disease	0 (0.0%)	1 (9.1%)
	Nausea	2 (10.0%)	0 (0.0%)
	Salivary hypersecretion	1 (5.0%)	0 (0.0%)
Metabolism and nutrition disorders	Abnormal loss of weight	1 (5.0%)	0 (0.0%)
Musculoskeletal disorders	Arthralgia	1 (5.0%)	0 (0.0%)
Nervous system disorders	Parkinson's Disease progression	0 (0.0%)	1 (9.1%)
	Restless legs syndrome	1 (5.0%)	0 (0.0%)
Skin and subcutaneous tissue disorders	Pruritis	1 (5.0%)	0 (0.0%)
	Rash	1 (5.0%)	0 (0.0%)

**Table 3.2. The UP Study: Details of Adverse Treatment Reactions**

*All patients with at least 28 days exposure to study treatment or an occurrence of a SAE prior to 28 days exposure are included in this analysis. Only Adverse Reactions recorded as having a definite, probable or possible relationship to trial medication which started on or after first dose are included. Patients are counted once per row but may appear in more than one row.*

*Clinical assessment.* All secondary and exploratory outcome results are summarised in **Table 3.3**. All treatment differences are reported as the difference between UDCA and placebo groups. We assessed for the clinical response in PD to treatment using the MDS-UPDRS in both the 'OFF' state (where dopaminergic medication was withheld prior to assessment) and the 'ON' state (at least 60 minutes following the administration of a participant's usual dopaminergic medication). Whenever COVID-19 restrictions prevented face-to-face review of participants, clinical assessments were conducted remotely over video. These video reviews occurred for 5/30 week 48

visits and 5/30 week 56 visits. For visits when the MDS-UPDRS III was performed remotely we were unable to obtain rigidity and postural instability scores; missing data were handled according to previously published guidance.<sup>264</sup>

MDS-UPDRS III scores in the 'OFF' state changed from baseline to week 48 by a mean of -1.68 points (95% CI -4.90, 1.53) in the UDCA group and by -5.2 points in the placebo group (95% CI -9.82, -0.58) with a mean difference between UDCA and placebo of 3.52 (95% CI -1.83, 8.86,  $p=0.1844$ ); from week 48 to week 56 (end of treatment to end of washout period) scores changed by -3.42 points (95% CI -6.48, 0.36) in the UDCA group and by -0.9 points (95% CI -2.96, 1.16) in the placebo group with a mean difference between UDCA and placebo of -2.52 (95% CI -6.05, 1.01  $p=0.1543$ ); from baseline to week 56 the MDS-UPDRS scores changed by -5.11 points (95% CI -9.33, -0.89) in the UDCA group and by -5.55 points (95% CI -9.36, -1.73) in the placebo group with a mean difference between UDCA and placebo of 0.44 (95% CI -4.97, 5.85  $p=0.8688$ ). There was therefore no significant treatment effect at any time point between the two treatment groups.

The mean MDS-UPDRS III scores in the 'ON' state showed similar trends from baseline to week 48, week 48 to week 56 and baseline to week 56 to those seen in the 'OFF' state, again with no significant treatment effect between groups seen at any timepoint (see **Table 3.3**). There were no significant differences between groups in the changes in MDS-UPDRS part I or II scores in the 'ON' state from baseline to week 48. MDS-UPDRS part IV scores reduced from baseline to week 48 in in the UDCA group by -1.26 (95% CI -2.74, 0.22) compared to a mild increase in the placebo group (0.55, 95% CI -0.21, 1.3) with a mean difference between UDCA and placebo of -1.81 (95% CI 0.20 3.42,  $p=0.0293$ ). However, scores at each visit remained low overall (see **Table 3.3**).

		Baseline (mean ± SD)	Week 48 (mean ± SD)	Week 56 (mean ± SD)	Change from baseline to week 48 (mean ± SD)	Change from week 48 to week 56 (mean ± SD)	Change from baseline to Week 56 (mean ± SD)
<b>Clinical Rating Scales</b>							
MDS-UPDRS I	UDCA	6.6 ± 5.1	6.8 ± 6.1	7.4 ± 5.6	0.5 ± 2.9	0.6 ± 3.6	1.3 ± 3.8
	Placebo	6.0 ± 2.8	6.5 ± 2.7	6.1 ± 3.5	0.7 ± 4.4	-0.7 ± 2.0	-0.1 ± 3.6
MDS-UPDRS II	UDCA	5.6 ± 5.5	5.1 ± 5.3	5.5 ± 5.0	-0.4 ± 4.0	0.5 ± 3.7	0.1 ± 4.1
	Placebo	5.1 ± 5.2	5.0 ± 3.1	4.4 ± 3.3	-0.1 ± 2.8	-0.7 ± 3.1	-1.0 ± 3.9
MDS-UPDRS III ("OFF" state)	UDCA	32.5 ± 11.5	29.5 ± 10.8	26.1 ± 10.3	-1.7 ± 6.7	-3.4 ± 6.4	-5.1 ± 8.8
	Placebo	31.2 ± 7.88	26.4 ± 11.1	25.6 ± 9.5	-5.2 ± 6.5	-0.9 ± 2.88	-5.5 ± 5.7
MDS-UPDRS III ("ON" state)	UDCA	24.0 ± 11.2	20.3 ± 9.2	20.3 ± 9.2	-1.7 ± 5.4	-0.9 ± 5.0	-2.8 ± 6.8
	Placebo	22.5 ± 8.0	19.3 ± 9.3	19.5 ± 9.0	-3.3 ± 8.3	0.2 ± 8.2	-3.1 ± 6.2
MDS-UPDRS IV	UDCA	3.1 ± 2.8	1.9 ± 2.3	2.4 ± 3.1	-1.3 ± 3.1 <sup>b*</sup>	0.5 ± 2.3	-0.7 ± 3.4
	Placebo	1.2 ± 1.8	1.7 ± 1.7	2.1 ± 2.1	0.5 ± 1.1 <sup>b*</sup>	0.4 ± 1.3	0.9 ± 1.14
Levodopa Equivalent Daily Dosage (mg)	UDCA	438 ± 198	510 ± 241	512 ± 237	79 ± 124	2 ± 39	81 ± 116
	Placebo	464 ± 123	516 ± 157	541 ± 155	52 ± 82	25 ± 49	77 ± 86
Montreal Cognitive Assessment <sup>a</sup>	UDCA	27.4 ± 1.9	28.3 ± 1.3	28.4 ± 1.6	1.1 ± 1.6	0.1 ± 1.1	1.2 ± 1.7
	Placebo	28.3 ± 1.2	28.6 ± 1.4	29.2 ± 0.8	0.4 ± 1.1	0.6 ± 1.3	0.9 ± 1.2
MADRS <sup>a</sup>	UDCA	2.5 ± 2.8	4.1 ± 4.7	4.6 ± 5.3	1.7 ± 3.4 <sup>b*</sup>	0.5 ± 3.0	2.2 ± 4.9 <sup>b**</sup>
	Placebo	2.9 ± 2.8	2.6 ± 2.6	1.2 ± 1.6	-0.4 ± 1.7 <sup>b*</sup>	-1.4 ± 2.1	-1.7 ± 2.6 <sup>b**</sup>
NMS-QUEST	UDCA	5.6 ± 3.5	6.3 ± 4.1	6.5 ± 4.3	0.9 ± 2.3	0.2 ± 2.4	1.1 ± 2.5 <sup>b**</sup>
	Placebo	5.4 ± 3.9	5.2 ± 3.2	4.4 ± 2.7	-0.2 ± 1.6	-0.8 ± 1.5	-1.0 ± 1.9 <sup>b**</sup>
<b>Sensor-based objective quantification of motor impairment (NB. Data shown here is median and interquartile range)</b>							
Cadence (step/min)	UDCA	117.80 (110.23; 122.65)	115.82 (107.90; 126.52)	NA	1.14 (-2.10; 4.28) <sup>c*</sup>	NA	NA
	Placebo	114.75 (111.85; 119.15)	111.43 (107.69-124.74)	NA	-4.58 (-5.54; 2.58) <sup>c*</sup>	NA	NA
Stride time (s)	UDCA	1.04 (0.99; 1.10)	1.04 (0.95, 1.11)	NA	-0.01 (-0.04; 0.01) <sup>c*</sup>	NA	NA
	Placebo	1.05 (1.02; 1.07)	1.08 (1.04, 1.12)	NA	0.03 (0.02; 0.04) <sup>c*</sup>	NA	NA
	UDCA	26.29 (24.70, 38.32)	22.19 (20.62, 31.95)	NA	-2.43 (-7.27; -1.38) <sup>c*</sup>	NA	NA

Stride time variability (SD)	Placebo	23.04 (19.81, 27.98)	27.90 (25.17, 31.74)	NA	6.16 (-0.54; -9.99) <sup>c*</sup>	NA	NA
Stance time (s)	UDCA	0.62 (0.58, 0.66)	0.62 (0.54, 0.66)	NA	-0.02 (-0.02; 0) <sup>c*</sup>	NA	NA
	Placebo	0.62 (0.59, 0.65)	0.64 (0.62, 0.65)	NA	0.02 (0.01; 0.03) <sup>c*</sup>	NA	NA
Stance time variability (SD)	UDCA	24.90 (18.57; 30.95)	22.33 (17.16; 26.38)	NA	-2.81 (-4.43; -0.48) <sup>c*</sup>	NA	NA
	Placebo	18.49 (15.60; 21.29)	26.44 (19.81, 28.32)	NA	6.48 (3.26; 11.26) <sup>c*</sup>	NA	NA
<b>Midbrain <sup>31</sup>Phosphorus Magnetic Resonance Spectroscopy</b>							
Total ATP	UDCA	0.449 ± 0.058	0.418 ± 0.076	NA	-0.028 ± 0.089	NA	NA
	Placebo	0.429 ± 0.050	0.453 ± 0.061	NA	0.0268 ± 0.077	NA	NA
Total Phosphocreatine	UDCA	0.184 ± 0.023	0.192 ± 0.022	NA	0.0072 ± 0.031	NA	NA
	Placebo	0.194 ± 0.033	0.181 ± 0.025	NA	-0.0135 ± 0.040	NA	NA
Total Inorganic Phosphate	UDCA	0.080 ± 0.025	0.101 ± 0.018	NA	0.020 ± 0.037 <sup>d***</sup>	NA	NA
	Placebo	0.08 ± 0.023	0.071 ± 0.028	NA	-0.006 ± 0.034 <sup>d***</sup>	NA	NA
$\Delta G_{ATP}$ (kilojoule/mole)	UDCA	-64.0 ± 2.39	-64.4 ± 2.13	NA	-0.672 ± 1.780 <sup>d*</sup>	NA	NA
	Placebo	-65.5 ± 3.35	-63.2 ± 1.42	NA	2.145 ± 3.153 <sup>d*</sup>	NA	NA
ADP (micromolar)	UDCA	104.4 ± 55.0	88.7 ± 43.5	NA	-1.86 ± 63.3	NA	NA
	Placebo	77.7 ± 68.7	116.0 ± 36.6	NA	3.37 ± 62.2	NA	NA
Inorganic phosphate/ATP ratio	UDCA	0.184 ± 0.069	0.252 ± 0.080	NA	0.065 ± 0.127 <sup>d*</sup>	NA	NA
	Placebo	0.191 ± 0.061	0.164 ± 0.078	NA	-0.021 ± 0.090 <sup>d*</sup>	NA	NA
Inorganic phosphate/phosphocreatine ratio	UDCA	0.438 ± 0.129	0.535 ± 0.121	NA	0.093 ± 0.211 <sup>d*</sup>	NA	NA
	Placebo	0.435 ± 0.158	0.405 ± 0.167	NA	-0.010 ± 0.219 <sup>d*</sup>	NA	NA
Phosphocreatine/ATP ratio	UDCA	0.419 ± 0.088	0.482 ± 0.150	NA	0.058 ± 0.155	NA	NA
	Placebo	0.459 ± 0.096	0.408 ± 0.089	NA	-0.056 ± 0.137	NA	NA
<b>Mean Posterior Putamen <sup>31</sup>Phosphorus Magnetic Resonance Spectroscopy</b>							
Total ATP	UDCA	0.454 ± 0.045	0.464 ± 0.053	NA	0.012 ± 0.068	NA	NA
	Placebo	0.450 ± 0.037	0.459 ± 0.035	NA	0.011 ± 0.055	NA	NA
Total Phosphocreatine	UDCA	0.206 ± 0.022	0.191 ± 0.026	NA	-0.016 ± 0.031	NA	NA
	Placebo	0.187 ± 0.015	0.185 ± 0.014	NA	-0.002 ± 0.018	NA	NA
Total Inorganic Phosphate	UDCA	0.084 ± 0.017	0.080 ± 0.021	NA	-0.005 ± 0.030	NA	NA
	Placebo	0.088 ± 0.018	0.075 ± 0.010	NA	-0.016 ± 0.015	NA	NA

$\Delta G_{ATP}$ (kilojoule/mole)	UDCA	-65.0 ± 1.77	-63.9 ± 1.56	NA	1.025 ± 1.843	NA	NA
	Placebo	-64.4 ± 2.00	-63.7 ± 1.51	NA	0.418 ± 2.13	NA	NA
ADP (micromolar)	UDCA	78.89 ± 26.68	105.96 ± 34.4	NA	25.58 ± 47.31	NA	NA
	Placebo	92.26 ± 40.86	99.20 ± 34.77	NA	4.95 ± 46.94	NA	NA
Inorganic phosphate/ATP ratio	UDCA	0.189 ± 0.049	0.178 ± 0.058	NA	-0.014 ± 0.080	NA	NA
	Placebo	0.198 ± 0.043	0.163 ± 0.023	NA	-0.042 ± 0.047	NA	NA
Inorganic phosphate/ phosphocreatine ratio	UDCA	0.414 ± 0.097	0.432 ± 0.131	NA	0.015 ± 0.179	NA	NA
	Placebo	0.473 ± 0.103	0.412 ± 0.070	NA	-0.078 ± 0.081	NA	NA
Phosphocreatine/ ATP ratio	UDCA	0.462 ± 0.078	0.418 ± 0.078	NA	-0.048 ± 0.100	NA	NA
	Placebo	0.420 ± 0.046	0.408 ± 0.055	NA	-0.014 ± 0.072	NA	NA

**Table 3.3. Results of secondary outcomes**

<sup>a</sup>performed at screening rather than baseline, <sup>b</sup>tested with two-sample t-test with Welch's correction, <sup>c</sup>tested with Mann Whitney U test, <sup>d</sup>significant treatment effect assessed using linear regression, \*indicates significance at the 0.05 level comparing treatment groups, \*\*indicates significance at the 0.01 level comparing treatment groups, \*\*\* indicates significance at the <0.001 level comparing treatment groups

Dopaminergic medication regimes were expressed as total levodopa equivalent daily dosage (LED). LED increased in 9/19 (47%) in the UDCA group and in 4/11 (36%) in the placebo group. LED reduced in 1/19 participants in the UDCA group. The range of change was -100mg – 264mg in UDCA group and 0 mg – 240 mg in the placebo group. The remaining 16/30 participants completed the study at the same LED as they started.

Depressive symptoms were assessed using the Montgomery-Asberg Depression Rating Scale (MADRS). Mean MADRS scores increased slightly in the UDCA group from baseline to week 48 by 1.7 (95% CI 0.1, 3.3), but decreased in the placebo group (-0.4, 95% CI -1.5, 0.8), with a mean difference between UDCA and placebo of 2.05 (95% CI 0.15, 3.94,  $p=0.0353$ ). Overall, MADRS scores remained relatively low across groups throughout the study (**Table 3.3**).

There were no differences between UDCA and placebo in the mean change from baseline to week 48 for cognitive function as assessed by MoCA, (treatment difference 0.7, 95% CI -0.3, 1.7,  $p=0.1758$ ), autonomic function as assessed by Non-motor Symptom Questionnaire (NMS-QUEST, treatment difference 1.1, 95% CI -0.4, 2.6,  $p=0.1479$ ) or quality of life as assessed by Parkinson's Disease 39 item quality of life questionnaire (PDQ-39, treatment difference -0.9, 95% CI -5.5, 3.7,  $p=0.6983$ ).

*Sensor Based Quantification of Motor Impairment.* To complement clinical assessment applying subjective clinical rating scales we also assessed changes in motor impairment using an objective, supervised, sensor-based gait analysis approach. Data before and after treatment was available for 12/19 in the UDCA group and 6/11 in the placebo group (**Table 3.3** and **Figure 3.2**). All  $p$  values reported in this section are for group differences tested by the Mann-Whitney U method. Between baseline and 48 weeks, cadence (steps per minute) increased in the UDCA group (median change +1.14 step/min) but decreased in the placebo group (median change -4.58 step/min, group-difference  $p=0.019$ , **Fig. 3.2C**). Stride time was slightly reduced in the UDCA group (median change -0.01s) but increased in the placebo group (median change +0.03s, group-difference  $p=0.031$ , **Fig. 3.2D**). Stride time became less variable in the UDCA group (median change -2.43 standard deviations, SDs), but more variable in the placebo group (median change +6.16SDs, group-difference  $p=0.031$ , **Fig. 3.2E**). Similarly, stance time decreased in the UDCA group (median

change -0.02s) and increased in the placebo group (median change +0.02s, group-difference  $p=0.024$ , **Fig. 3.2F**). A similar difference was observed for stance time variability with a decrease in the UDCA group (median change -2.81SDs), but an increase in the placebo group (median change +6.48SDs,  $p=0.039$ , **Fig. 3.2G**). Taken together, these results indicate less deterioration in core bradykinetic gait features such as overall speed and time taken standing on each lower limb and stride time in the UDCA treated group compared to the placebo. Of note there was no clear relationship between the change in gait parameters and the change in MDS-UPDRS III scores. No significant differences were found between groups for gait speed, any of the spatial parameters (step length, stride length or step width) or the intensity or regularity measures. Further individualised results are detailed in **Figure 3.7** and in **Figure 3.8A-E** and demonstrate that the statistical results are driven by a wider group change (with approximately 60% or more of the UDCA responding) rather than by a small subset of marked responders.



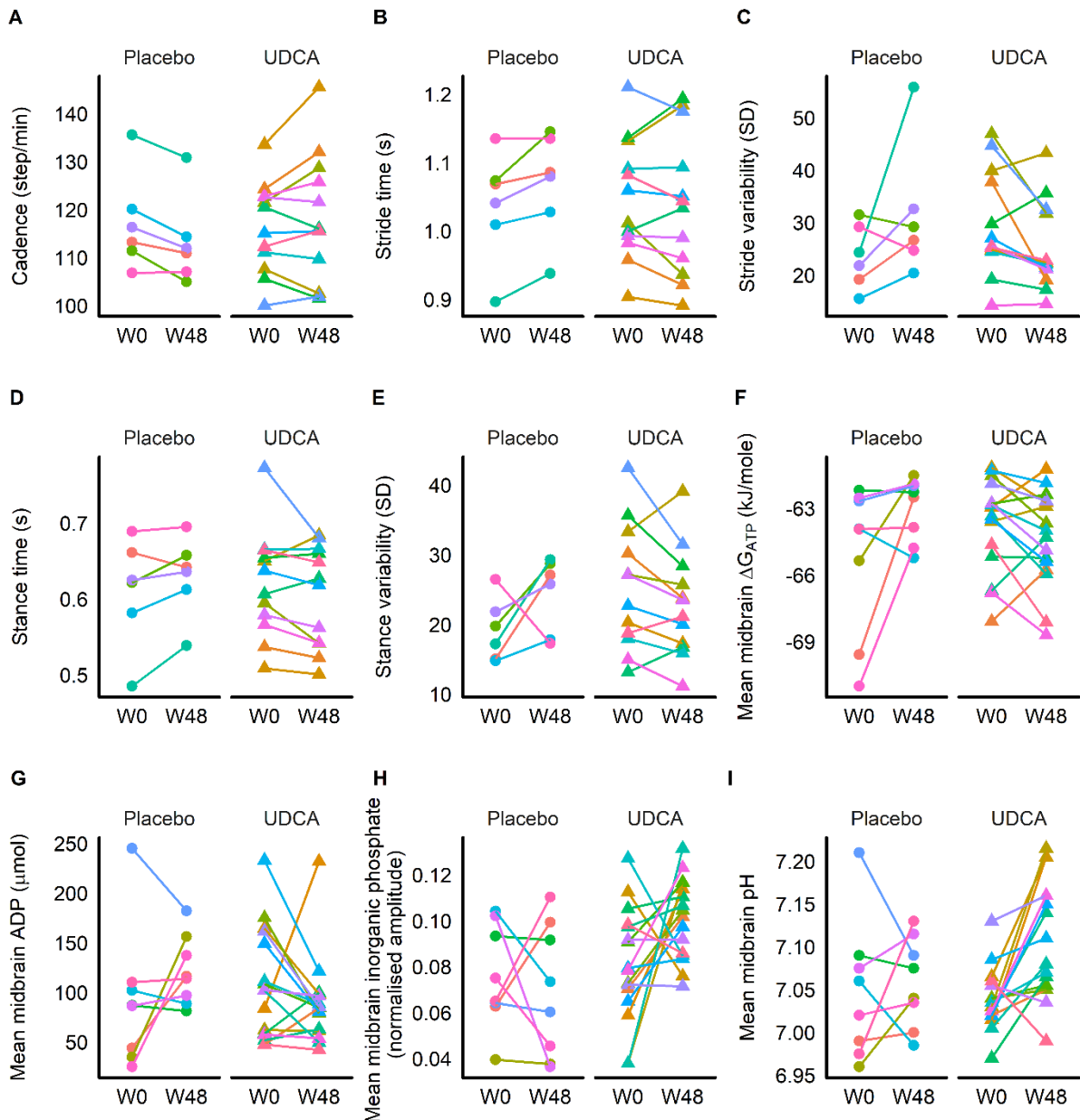


**Figure 3.8: Individual changes in key gait and spectroscopic parameters**

Individual changes for each of (A) cadence where 7/12 on UDCA demonstrated improvement (increase in number of steps), (B) stride time where 8/12 on UDCA demonstrated improvement (reduction in time), (C) variability in stride time which improved (reduced in value) in 9/12 on UDCA, (D) stance time where 8/12 on UDCA demonstrated improvement (reduction in time), (E) variability in stance time which improved (reduced in value) in 9/12 on UDCA, (F)  $^{31}\text{P}$ -MRS mean midbrain  $\Delta G_{\text{ATP}}$  which improved (became more negative) in 11/16 taking UDCA, (G)  $^{31}\text{P}$ -MRS mean midbrain ADP which improved in 12/16 taking UDCA, (H)  $^{31}\text{P}$ -MRS mean midbrain inorganic phosphate and (I)  $^{31}\text{P}$ -MRS mean midbrain pH. Values shown for baseline (W0, prior to commencement of treatment) and for week 48 (W48, end of treatment period). For panels A-E, UDCA  $n=12$ , placebo  $n=6$ . For panels F-I, UDCA  $n=16$ , placebo  $n=9$  except panel (F) where placebo  $n=8$  due to excluded magnesium value prior to unblinding required for calculation of  $\Delta G_{\text{ATP}}$ .

*Physical Activity Monitoring.* Home-based physical activity monitoring data at both visits was available for 18 participants in the UDCA group and 10 participants in the placebo group. Parameters were calculated from 5 of the 7 days where the Dynaport MoveMonitor+ was worn for  $\geq 60\%$  of the day. There were no differences between groups with respect to total average movement intensity, movement intensity in the active period, active period as a percentage of total time worn or moving time as a percentage of total time worn. These results are summarised in **Table 3.4**.

		Baseline	Week 48	Change from baseline to week 48	95% CI, p-value
Total average movement intensity (G)	Placebo	0.038 $\pm$ 0.0117	0.035 $\pm$ 0.013	-0.001 $\pm$ 0.006	-0.008, 0.007 p=0.943
	UDCA	0.050 $\pm$ 0.020	0.048 $\pm$ 0.017	-0.002 $\pm$ 0.012	
Movement intensity in the active period (G)	Placebo	0.111 $\pm$ 0.025	0.099 $\pm$ 0.020	-0.012 $\pm$ 0.018 $\pm$	-0.011, 0.021 p=0.530
	UDCA	0.120 $\pm$ 0.031	0.115 $\pm$ 0.026	-0.007 $\pm$ 0.021	
Active period of total time worn (%)	Placebo	23.8 $\pm$ 7.2	23.8 $\pm$ 7.5	0.6 $\pm$ 3.3	-4.3, 5.2 p=0.767
	UDCA	28.7 $\pm$ 7.2	29.7 $\pm$ 7.8	1.3 $\pm$ 8.8	
Total moving time of total time worn (%)	Placebo	7.3 $\pm$ 2.6	6.3 $\pm$ 2.0	-0.9 $\pm$ 1.9	-1.6, 2.5 p=0.657
	UDCA	9.8 $\pm$ 3.8	9.5 $\pm$ 4.1	-0.4 $\pm$ 3.2	

**Table 3.4: Summary results of 7-day physical activity monitoring.**

95% confidence intervals and p-values presented are from a t-test comparing the differences in mean change from baseline to week 48 between UDCA and placebo. Baseline data was available for 19 participants in the UDCA group and 10 participants in the placebo group. Week 48 and the change from baseline to week 48 was available for 17 participants in the UDCA group and 9 participants in the placebo group. Data presented is mean  $\pm$  SD.

*<sup>31</sup>Phosphorus Magnetic Resonance Spectroscopy:* Evidence of target engagement was assessed using <sup>31</sup>P-MRS to determine the effect of the IMP on the bioenergetic profile in the midbrain (including the substantia nigra). Twenty-six of the 30 participants completing the study had <sup>31</sup>P-MRS at the baseline visit, and twenty-five (96%) had follow-up scans after completion of treatment. There was no correlation between total brain volume in each midbrain voxel and any <sup>31</sup>P-MRS parameter (data not shown), therefore the reported linear regression did not include these measures as additional

covariates to prevent overfitting. Reported  $p$  values and confidence intervals are for treatment estimates of UDCA as assessed by linear regression.

Gibbs free energy of ATP hydrolysis ( $\Delta G_{ATP}$ ) expresses the amount of energy released from the hydrolysis of ATP to ADP and Pi. As this reaction is exergonic the value is negative, with more negative values representing greater amounts of energy released to the tissue examined. Mean midbrain  $\Delta G_{ATP}$  reduced by -0.672 kJ/mole (95% CI, -1.62, 0.277) in the UDCA group, but increased by +2.145 kJ/mole (95% CI -0.491, 4.781) in the placebo group from baseline to week 48 (treatment estimate -1.929, 95% CI -3.472, -0.385,  $p=0.024$ ; **Fig. 3.4D**). This reduction was accompanied by a non-significant trend towards decreased calculated ADP in the UDCA group (-18.6  $\mu$ mol, 95% CI -52.3, 15.17) and an increase of calculated ADP by 33.7  $\mu$ mol (95% CI -14.1, 81.5) in the placebo group (treatment estimate -36.3, 95% CI -72.3, -0.3  $p=0.062$ ; **Fig. 3.4E**). Mean midbrain Pi increased by +0.02 (95% CI 0.00, 0.04) in the UDCA group and reduced by -0.006 (95% CI -0.032, 0.02) in the placebo group (treatment estimate 0.032, 95% CI 0.013, 0.051,  $p=0.004$ , **Fig. 3.4G**).

There were no significant differences between groups with respect to any changes between the initial  $^{31}\text{P}$ -MRS scan at baseline visit and the subsequent follow-up scan (typically week 48) for pH (**Fig. 3.4H**), ATP or PCr (**Table 3.3**).

In the midbrain, Pi/ATP ratios increased by +0.065 (95% CI -0.003, 0.132) in the UDCA group but reduced by -0.0207 (95% CI -0.090, 0.048) in the placebo group from baseline to week 48 (treatment estimate 0.090, 95% CI 0.018, 0.163,  $p=0.017$ ). Pi/PCr ratios also increased in the midbrain by +0.093 (95% CI -0.020, 0.205) in the UDCA and reduced by -0.010 (95% CI -0.179, 0.158) in the placebo group from baseline to week 48 (treatment estimate 0.139, 95% CI 0.005, 0.273,  $p=0.043$ ). However, the marked increase in mean midbrain Pi (**Fig. 3.4G**) appeared to be driven predominantly by a small number of participants with large increases in Pi (**Fig. 3.8H**) and this was further reflected in both of these ratio measures with particularly marked increase in two participants. Although elevated Pi/ATP ratios are likely to closely reflect oxidative phosphorylation these ratio measures should be interpreted with caution in this dataset as it likely does not reflect a clear group-wide change. The Pi/PCr ratio is used more widely in dynamic muscle  $^{31}\text{P}$ -MRS testing protocols as elevated Pi/PCr ratios reflects the reliance of the tissue on PCr to maintain ATP levels as a buffer system during

activity, its role in the central nervous system in resting protocols is less clear. The same is true for the PCr/ATP ratio which did not show any treatment differences throughout the trial. As the Pi/PCr and Pi/ATP data appears to be driven by a smaller proportion of participants it is in contrast to the data regarding  $\Delta G_{ATP}$  and ADP where the changes observed were reflected in the majority of those taking UDCA (**Fig. 3.8F, G**).

There were no significant differences between placebo and UDCA treatment groups with respect to any  $^{31}\text{P}$ -MRS parameters in the mean posterior putamen (**Table 3.3, Figure 3.9**).

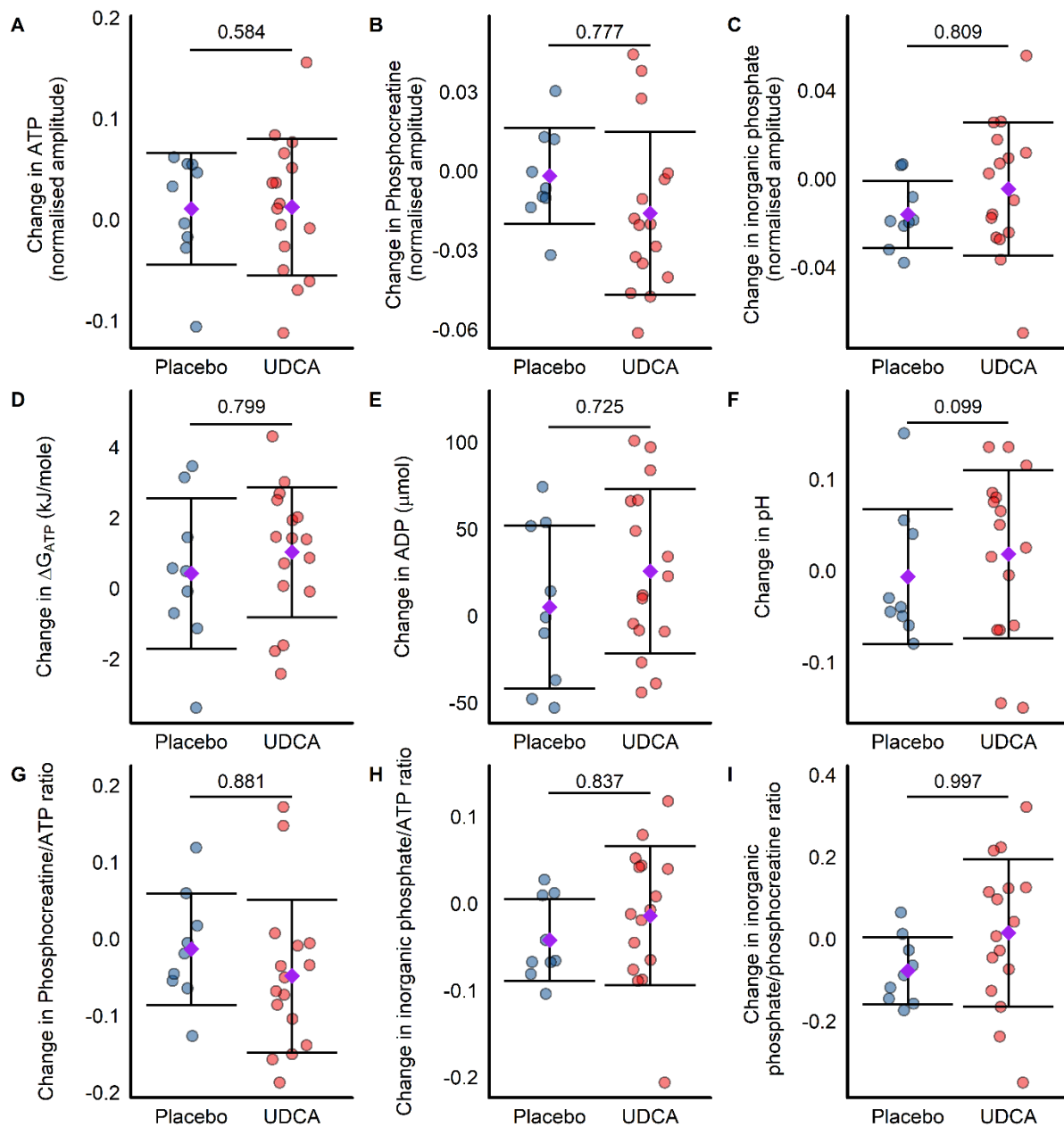


**Figure 3.9: Changes in  $^{31}\text{P}$ -MRS derived measures acquired from the mean posterior putamen baseline to week 48 between treatment groups.**

(A) change in ATP; (B) change in Phosphocreatine; (C) change in inorganic phosphate; (D) change in Gibbs free energy of ATP hydrolysis ( $\Delta G_{\text{ATP}}$ ), (E) change in ADP; (F) change in pH; (G) change in phosphocreatine/ATP ratio; (H) change in inorganic phosphate/ATP ratio; (I) change in inorganic phosphate/phosphocreatine ratio. For all data placebo  $n=9$ , UDCA=16. P-values presented represented the estimated treatment effect of UDCA as assessed by linear regression.

## Discussion

The UP study has confirmed that UDCA at a dose of 30mg/kg is safe and extremely well tolerated in Parkinson's with no SAE's and only mild, transient side effects reported in the UDCA treatment group (primary outcome). Additionally, we demonstrated a beneficial effect of UDCA on the progression of motor impairment (as assessed by objective sensor-based gait analysis, secondary outcome) and provide additional tentative, <sup>31</sup>P-MRS based evidence of mechanistic target engagement (exploratory outcome). The latter part of our UP study was compromised by the COVID-19 pandemic and required change to remote study visits and/or delayed assessments such as repeat <sup>31</sup>P-MRS imaging. However, our sensitivity analysis of data only collected at the originally intended time points suggests that this did not have a significant effect on the overall outcome of the trial.

We only recruited patients with recent onset PD (arbitrarily defined as  $\leq 3$  yr. since diagnosis) to increase the homogeneity of the study cohort which may be of particular importance in a small proof of concept study. In our view, it is also plausible to assume that the likelihood of any compound exerting a neuroprotective effect on the remaining dopaminergic neurons is considerably greater in PD patients with comparatively short disease duration.<sup>39</sup> Further, we only included participants diagnosed by movement disorder specialists and demonstrating a clear response to dopaminergic medication, to reduce the risk of including patients with atypical parkinsonian syndromes.<sup>13</sup>

Both the frequency and the observation that UDCA-specific AR's were limited to transient, typically mild gastrointestinal symptoms is similar to previous studies which investigated high-dose UDCA for the treatment of primary biliary cirrhosis and related disorders.<sup>265</sup> The excellent safety and tolerability of UDCA is reflected by an extremely high compliance rate (mean of 97.6%) of those in the UDCA treated group completing the full treatment duration. Early treatment cessation was due to high pill burden in combination with regularly prescribed medications or, in the case of one participant who withdrew after 5 weeks, difficulties in swallowing the IMP and not due to the presence of side-effects. The lack of clinically significant changes in blood monitoring throughout the trial related to UDCA is also extremely reassuring. This safety profile contrasts with the side effect profile of other recently explored putative neuroprotective compounds.<sup>266,267</sup> The increase in MADRS scores in the UDCA treatment group

continued throughout the washout period following cessation of UDCA and may therefore not be related to the administration of UDCA.

The relative abundance of serum bile acids following treatment with UDCA showed a marked enrichment of detectable UDCA (increasing from ~1% of the serum bile acid profile at baseline to ~30% of this across the period of treatment) as expected but also of UDCA-related conjugates; including TUDCA, which has also separately been linked with neuroprotection in rodent models of PD.<sup>204</sup> Although not specifically studied in PD, GUDCA has also shown protective effects in *in vitro* models of oxidative stress which is an intrinsically linked mechanism to mitochondrial dysfunction.<sup>268,269</sup> UDCA administration resulted in marked changes in bile acids after only 12 weeks treatment (which also included a titration period to target dose). These changes were persistent and extremely similar at week 24 and 36. The fall in UDCA and related conjugates at week 48 compared to other visits in the treatment period can be explained by participants taking their last UDCA dose the evening prior to their week 48 visit (rather than on the morning of the study visit day itself) together with all other PD medication to enable repeat clinical examination in the practically defined OFF. Serum peak concentrations for 30 mg/kg UDCA are achieved at 1h.<sup>209</sup>

Changes in the PD gut microbiome are associated with changes in the bile acid pool.<sup>109</sup> Intriguingly, a marked reduction of UDCA and its taurine conjugate TUDCA has been reported in an experimental model of prodromal PD and UDCA treatment partially restores the gut microbial profile in other conditions.<sup>111,270,271</sup> A beneficial effect of UDCA in PD may therefore not be limited to a restoration of mitochondrial function but also exert an additional, but as yet entirely speculative beneficial effect on the PD microbiome and the gut-brain axis.

Non-significant improvement of MDS-UPDRS III “OFF” scores between baseline visit and after treatment (week 48) was observed in both the UDCA and placebo groups, but was more marked in the placebo group (approximately 18% mean improvement). The improvement was similar for ‘ON’ state assessments although less marked. This is unlikely to be due to changes in dopaminergic medication as the increases in LED over the course of the trial were small in both treatment arms. It is unclear why this would be the case although it should be noted that prominent placebo effects have been noted in other PD neuroprotection treatment trials.<sup>272</sup> Additionally, it may reflect

the benefits to PD care when participants are receiving more frequent nursing and neurologist input when participating in a clinical trial.

Previous clinical trials investigating putative neuroprotective compounds for their beneficial effect in PD frequently relied on clinical outcomes only, in particular, favourable changes on the MDS-UPDRS III and whether this represents the optimum primary outcome remains debated.<sup>112-114,116,273</sup> To address the inherent shortcomings of this approach, we included sensor-based, objective quantification of motor impairment as a secondary trial outcome. The supervised, motion-sensor based gait analysis showed a change suggestive of a degenerative pattern for several gait variables in the placebo treatment group. In contrast, we observed either an improvement in the UDCA treatment group or comparatively less worsening in gait over the treatment period. The longitudinal deterioration in the placebo group is comparable with previous studies of similar PD cohorts that identified stride time variability, irregularity and increased step time variability as potential progression markers.<sup>126,274</sup> Decreases in gait speed have also been identified to closely correlate with disease progression.<sup>275,276</sup> A greater burden of axial features has consistently been associated with poorer adverse clinical phenotypes and increased risk of rapid progression PD.<sup>17,277</sup> Therefore, the changes observed appear consistent with a disease modifying effect of UDCA, reflected in a reduction of the natural progression of gait impairment in PD, but this awaits confirmation in a subsequent, larger trial. Changes in MDS-UPDRS III scores did not correlate with any gait parameters, which is not unexpected as only a small proportion of MDS-UPDRS III is comprised of gait related assessments. Supervised clinic gait analysis therefore offers promise as an alternative or complementary endpoint in future neuroprotective trials in PD and may be more sensitive to detecting disease progression, in particular over comparatively short periods of time than the MDS-UPDRS. Physical activity monitoring failed to identify any clear differences between treatment groups. There was a general trend to reduced activity over time in both groups, this may have been related to a substantial number of participants performing their physical activity monitoring during national lockdown restrictions due to COVID-19 which has been recognised to reduce activity.<sup>278</sup>

Conceptually, the proof of target engagement is a key aspect of early, proof of concept studies for any IMP, but has been lacking for many PD neuroprotection studies.

Elevated (e.g. less negative)  $^{31}\text{P}$ -MRS measured  $\Delta\text{G}_{\text{ATP}}$  has previously been observed in mitochondrial cytopathies and is therefore consistent with mitochondrial dysfunction.<sup>221</sup> More recently, using a similar  $^{31}\text{P}$ -MRS protocol, our group has demonstrated differences in  $\Delta\text{G}_{\text{ATP}}$  in the midbrain of patients with amyotrophic lateral sclerosis, a further neurodegenerative disorder with growing evidence of mitochondrial dysfunction.<sup>180</sup> In the context of otherwise stable ATP levels, a more negative value in  $\Delta\text{G}_{\text{ATP}}$  (as observed in the UDCA treatment arm) implies that a relatively greater amount of energy was released by ATP hydrolysis. In mitochondrial cytopathies the administration of coenzyme Q10 resulted in a lowering of both  $\Delta\text{G}_{\text{ATP}}$  and ADP, approaching the values found in healthy controls and providing evidence of possible target engagement.<sup>184</sup> Similarly, the observed lowering of  $\Delta\text{G}_{\text{ATP}}$  in the UDCA treatment arm of our study is in keeping with the assumption of mechanistic target engagement for UDCA, resulting in improved mitochondrial function. Sathe and co-workers also reported  $^{31}\text{P}$ -MRS based evidence of target engagement for UDCA in PD in a small open label pilot-study.<sup>196</sup> However, a different imaging protocol was applied and only three PD patients had  $^{31}\text{P}$ -MRS imaging before and after a 6-week course of UDCA at a dose of 50 mg/kg. We also note the use of  $^{31}\text{P}$ -MRS in other completed or on-going proof-of-concept studies for mitochondrial rescue compounds in PD.<sup>132,195</sup> The lack of a beneficial effect of UDCA on putaminal  $^{31}\text{P}$ -MRS parameters may reflect the difference in anatomical disease burden between the substantia nigra/midbrain and the putamen in PD. Further, dopaminergic neurons in the substantia nigra are particularly metabolically active and have a large unmyelinated axonal arbor necessitating high ATP production to meet metabolic demands.<sup>279</sup> UDCA may have a greater effect on the midbrain, and specifically the substantia nigra as there may be more marked mitochondrial dysfunction in this tissue to exert a treatment effect upon. Although we observed changes in Pi/ATP and Pi/PCr ratios which would not typically imply an improvement in bioenergetics this data was driven by a small proportion of participants and should be interpreted with caution with respect to the overall size of our cohort. It cannot be excluded that the changes in Pi may be due to a noisy  $^{31}\text{P}$ -MRS baseline affecting quantification of this particular resonance. Even if this were the case it should not affect the results regarding ADP and Gibb's and therefore the data is still promising regarding evidence of target engagement.

<sup>31</sup>P-MRS has been used previously to identify bioenergetic deficits in Parkinson's disease, with deficits of PCr and ATP in the midbrain compared to healthy controls.<sup>189</sup> We did not observe any increases in ATP or PCr, this may be due to methodological differences as we have not attempted absolute quantification of the concentration of <sup>31</sup>P-MRS metabolites. Alternatively, rather than directly increasing the overall amount of ATP, UDCA may be reducing the reliance upon alternative pathways to ATP production such as glycolysis by improving the efficiency of oxidative phosphorylation. Our trial excluded those of more advanced age (<75) to limit the impact of additional co-morbidities on clinical assessments, such as the gait analysis, to reduce the impact of confounding factors on secondary outcome measures. This does result in an overall younger cohort than the general PD population and therefore the results should be interpreted with caution.

Conceptually, the trial design of our UP study is in keeping with other recent early clinical trials such as the AiM-PD trial, an open label trial of ambroxol, and a recent randomised controlled-trial assessing niacin (a vitamin B3 derivative) which both focused on determining the mechanistic effect of the respective trial compound in human PD patients.<sup>280,281</sup> As stated above, the UP study was not formally powered to confirm or refute a neuroprotective effect of UDCA. Subsequent, considerably larger and therefore more costly phase IIb/III studies will be required to firmly confirm or refute such a neuroprotective effect for UDCA. However, the excellent safety profile of UDCA at 30 mg/kg, combined with the tentative <sup>31</sup>P-MRS-based evidence of target engagement and the promising results from the gait analysis provide a strong rationale for such future phase IIb/III trials which will also help to calculate appropriate effect sizes and formally power any future trials of UDCA in PD.

**END OF CHAPTER MANUSCRIPT**

## Chapter 4: Combining <sup>31</sup>P Phosphorus magnetic resonance spectroscopy and patient derived peripheral tissue to mechanistically stratify Parkinson's disease

### Introduction to chapter

In this chapter *in vivo* measures of bioenergetic dysfunction obtained from <sup>31</sup>P-MRS of the brain and *in vitro* measures of mitochondrial function and morphology obtained from patient derived peripheral tissue are used as complementary approaches to mechanistically stratify PD. This is the first study ever to combine these two approaches to correlate measures of *in vivo* bioenergetic dysfunction in the brain with *in vitro* measures of mitochondrial dysfunction in patient derived peripheral tissue.

The manuscript, in preparation for submission, that forms the focus of this chapter identifies a clinically relevant relationship between midbrain PCr and the predictive risk of rapid disease progression (as defined by the presence of dementia or postural instability at five years). Several biologically plausible relationships are identified between <sup>31</sup>P-MRS metabolites in the putamen and both functional and morphological measures of mitochondria in patient derived peripheral tissue.

### Phospholipids in <sup>31</sup>P-MRS

Although not the primary focus of <sup>31</sup>P-MRS in this thesis, the assessment of phospholipids still offers some utility in the context of PD and is directly relevant to the longitudinal data presented in Chapter 5. The key MR-visible phospholipids are PE, PC, GPE and GPC. PE and PC are the phosphomonoesters (PME) whereas GPE and GPC are the phosphodiester (PDE). These are integral components of phospholipid membranes. PME comprises the phospholipid membrane precursors where PC is converted into phosphatidylcholine (PtdCho) and PE is converted into phosphatidylethanolamine (PtdEth). Both PtdCho and PtdEth are key components of all phospholipid membranes with PtdEth being the second most abundant phospholipid in mammalian tissue and is particularly abundant on inner phospholipid membranes and the inner mitochondrial membrane. Outside of synthesis in the endoplasmic reticulum via the Kennedy Pathway, mitochondria are the second major source of PtdEth via phosphatidylserine decarboxylase.<sup>282</sup>

PtdCho is converted from PtdEth in the ER or synthesised directly by the Kennedy pathway.<sup>283</sup> Both PtdCho and PtdEth are reduced in the substantia nigra of untreated PD at post-mortem, despite overall lipid content between PD and controls being similar.<sup>284</sup> In serum PtdCho and PtdEth have been found to be reduced in the serum of PD compared to controls, with the greatest reductions being seen in more advanced PD.<sup>285</sup> PE has also been observed to be reduced in the CSF of untreated PD, although this normalised following treatment with levodopa.<sup>286</sup>

Previous <sup>31</sup>P-MRS work has identified reduced PE in the midbrain of early, but not advanced PD compared to controls.<sup>189</sup> The same group utilising the same <sup>31</sup>P-MRS protocol identified increased GPE in the putamen of GBA-PD.<sup>287</sup>

PDE is comprised of GPE and GPC and represent phospholipid membrane breakdown products. In health these can be recycled back into PE and PE. In <sup>31</sup>P-MRS studies the PME/PDE ratio has been used to reflect membrane turnover and the balance between degradation and synthesis. There is a lack of previous literature assessing the PME/PDE ratio in PD. This has been much more widely assessed in Alzheimer's disease and mild cognitive impairment, in which mitochondrial dysfunction has also been implicated as a potential pathogenic process.<sup>288</sup> Outside of neurodegeneration the PME/PDE ratio has been widely used in psychiatric disorders. Reduced PME/PDE in bipolar depression, reduced PME in frontal brain regions in schizophrenia and elevated PDE in temporal brain regions in schizophrenia have all previously been observed.<sup>289,290</sup>

### Contributions to published paper

I was responsible for the recruitment, consenting, clinical assessments and skin biopsy of almost all participants during the length of the study, around 8 participants were recruited and assessed by a Clinical Fellow and co-author (Dr Emily Reed). I was responsible for the establishment and growth of all skin biopsies into fibroblast lines. I was responsible for the spectroscopic analysis of all <sup>31</sup>P-MRS data.

Fibroblast cell assays (cellular ATP, mitochondrial membrane potential and live cell imaging of mitochondrial and lysosomal morphology) were performed by three separate research technicians during the course of the project (co-authors Sarah Roscoe, Stephen Bradley and Toby Burgess).

I performed all statistical analyses on  $^{31}\text{P}$ -MRS and clinical data. Statistical analysis of fibroblast assay data was performed by myself in conjunction with a co-author (Toby Burgess) and under the guidance of a statistician associated with the project (co-author Miss Rosie Taylor).

I drafted all sections of the manuscript under the guidance of my supervisory team. Methods sections detailing cell culture and assay methods were written in conjunction with a co-author (Toby Burgess).

### Manuscript in preparation for submission

This manuscript is currently intended to be submitted to *Molecular Neurodegeneration*, as such it is formatted and written to fulfil the submission requirements.

# **<sup>31</sup>P Phosphorus magnetic resonance spectroscopy in Parkinson's disease demonstrates relationships with predicted disease progression and mitochondrial dysfunction in the peripheral tissue**

Thomas Payne,<sup>1</sup> Toby Burgess,<sup>1</sup> Stephen Bradley,<sup>1</sup> Sarah Roscoe,<sup>1</sup> Matilde Sassani,<sup>1,2</sup> Mark J Dunning,<sup>3</sup> Alisdair McNeil,<sup>1</sup> Rosie Taylor,<sup>4</sup> Li Su,<sup>1,5</sup> Iain Wilkinson,<sup>6†</sup> Thomas Jenkins,<sup>1,7</sup> Heather Mortiboys,<sup>1</sup> Oliver Bandmann<sup>1</sup>

## **Author affiliations:**

<sup>1</sup>Sheffield Institute for Translational Neuroscience, University of Sheffield, S10 2HQ, United Kingdom

<sup>2</sup>Institute of Metabolism and Systems Research, College of Medical and Dental Sciences, The University of Birmingham, B15 2TT, United Kingdom

<sup>3</sup>The Bioinformatics Core, Sheffield Institute of Translational Neuroscience, University of Sheffield, S10 2HQ, United Kingdom

<sup>4</sup>Statistical Services Unit, The University of Sheffield, S3 7RH, United Kingdom

<sup>5</sup>Department of Psychiatry, University of Cambridge CB2 0SP, United Kingdom

<sup>6</sup>Academic Unit of Radiology, University of Sheffield, S10 2JF

<sup>7</sup>Royal Perth Hospital, Victoria Square, Perth, WA6000, Australia

## Abstract

**Objective:** The aim of this study was to characterise bioenergetic dysfunction in Parkinson's disease (PD) by applying a multimodal approach, combining standardized clinical assessment with midbrain and putaminal  $^{31}\text{P}$  phosphorus magnetic resonance spectroscopy ( $^{31}\text{P}$ -MRS) as well as deep mechanistic phenotyping of mitochondrial and lysosomal function in peripheral tissue.

**Methods:** 60 participants (35 PD patients and 25 healthy controls) underwent  $^{31}\text{P}$ -MRS for quantification of ATP, phosphocreatine and inorganic phosphate (Pi) in the putamen and midbrain. A skin biopsy was obtained to establish fibroblast cell lines for assessment of intracellular ATP, mitochondrial membrane potential (MMP) and mitochondrial/lysosomal morphology, using high content live cell imaging.

**Results:** We observed considerably broader variance of  $^{31}\text{P}$ -MRS midbrain ATP in PD compared to controls (F-test,  $p=0.0030$ ). Similarly, there was a marked increase in variance in the Pi/ATP ratio in the posterior putamen in PD (F-test  $p=0.0036$ ). Higher midbrain phosphocreatine correlated with a higher risk of rapid disease progression ( $r=0.47$ ,  $p=0.0384$ ). In fibroblasts, lower MMP correlated with higher intracellular ATP ( $r=-0.55$ ,  $p=0.0016$ ), higher mitochondrial counts ( $r=-0.72$ ,  $p<0.0001$ ) and higher lysosomal counts ( $r=-0.62$ ,  $p=0.0002$ ) in PD only. Correlation of  $^{31}\text{P}$ -MRS and fibroblast assays revealed that higher putaminal ATP was associated with higher mitochondria counts in control fibroblasts as expected ( $r=0.416$ ,  $p=0.0484$ ). In contrast, an inverse trend between putaminal ATP and mitochondrial count was observed in PD ( $r=0.298$ ,  $p=0.0865$ ). In PD, lower  $^{31}\text{P}$ -MRS-derived putaminal ATP correlated with lower MMP in both long and short mitochondria MMP. This correlation was weaker in long mitochondria ( $r=0.359$ ,  $p=0.0372$ ) and strongest in short mitochondria ( $r=0.442$ ,  $p=0.0084$ ). Lower putaminal ATP also correlated with greater numbers of lysosomes in PD, but not controls ( $r=0.433$ ,  $p=0.0105$ ).

**Interpretation:**  $^{31}\text{P}$ -MRS may help to enrich future neuroprotection trials for PD patients with aggressive disease course. The observed fibroblast and  $^{31}\text{P}$ -MRS correlations provide further evidence of impaired mitophagy in PD and demonstrate the potential utility of combined  $^{31}\text{P}$ -MRS and deep phenotyping in peripheral tissue to mechanistically stratify PD for future neuroprotective trials.

## Introduction

Parkinson's disease (PD) is the second most common neurodegenerative disorder and increasing in global prevalence<sup>1</sup>. A key challenge in developing disease-modifying therapies is the clinical and pathogenic heterogeneity in PD. There is therefore a great need to develop tools for the mechanistic stratification of PD in individual patients to develop precision medicine approaches for future clinical trials.<sup>291</sup>

There is strong evidence for mitochondrial and lysosomal dysfunction in PD.<sup>5,52,292,293</sup> Abnormal mitochondrial and lysosomal function and morphology have been demonstrated in peripheral tissue of both genetic and sporadic PD.<sup>64,159,294</sup> Impaired mitophagy has also been implicated in both genetic and sporadic PD.<sup>62,74</sup> Previously, we mechanistically stratified a large cohort of sporadic PD and identified distinct subgroups with mitochondrial or lysosomal dysfunction. Mitochondrial dysfunction was rescued in a mechanistically stratified subgroup, using the putative neuroprotective compound ursodeoxycholic acid (UDCA).<sup>161</sup> This demonstrates the potential of mechanistic stratification and compound testing in peripheral tissue of individual patients, to facilitate precision medicine approaches. However, translation to clinical practice is challenging since obtaining tissue fibroblasts is an invasive procedure, labour-intensive and has conceptual limitations.

<sup>31</sup>Phosphorus magnetic resonance spectroscopy (<sup>31</sup>P-MRS) allows the non-invasive *in vivo* quantification of key bioenergetic metabolites such as adenosine triphosphate (ATP) and phosphocreatine (PCr), enabling the indirect assessment of oxidative phosphorylation.<sup>295</sup> <sup>31</sup>P-MRS may therefore be a suitable non-invasive tool to identify those PD patients most likely to benefit from putative mitochondrial rescue compounds.

In this study, we undertook the largest <sup>31</sup>P-MRS study in PD to date, combined with deep mechanistic phenotyping in peripheral tissue to comprehensively assess cellular bioenergetics in PD. Our aims were: (1) to compare <sup>31</sup>P-MRS bioenergetic profiles in PD and healthy controls; (2) to assess whether distinct <sup>31</sup>P-MRS bioenergetic parameters correlate with trial-relevant clinical aspects of PD; (3) to correlate <sup>31</sup>P-MRS and fibroblast-derived mitochondrial and lysosomal functional measures.

We identified an inverse correlation between midbrain PCr levels and predicted rapid disease progression in PD. Additionally, we identified correlations between low <sup>31</sup>P-

MRS putaminal ATP and multiple indices of impaired cellular function in peripheral tissue in keeping with the assumption of impaired mitophagy in PD.

## Methods

### Recruitment

35 participants with recent onset PD (arbitrarily defined as  $\leq 3$  yr since diagnosis) and 25 age and sex matched healthy controls were recruited from movement disorder clinics at Sheffield Teaching Hospitals NHS Foundation Trust and through the Parkinson's UK Research Network. The clinical diagnosis was made by a movement disorders specialist according to the Queen Square Brain Bank Criteria.<sup>12</sup> Exclusion criteria were contraindications to either MRI or skin biopsy (e.g., through ferromagnetic implants or therapeutic anticoagulation) or evidence of significant cognitive impairment (Mini Mental State Examination score  $<25$ ).<sup>229</sup> All participants provided written informed consent. The study received Research Ethics Committee approval (REC 18/NW/0328).

### Clinical assessment

A detailed clinical history, neurological examination, and assessment with the following clinical rating scales were undertaken: Modified Hoehn & Yahr Staging, Movement Disorders Society-Unified Parkinson's Disease Rating Scale Part 3 (MDS-UPDRS-III), and Movement Disorders Society Non-Motor Symptom Scale (MDS-NMSS).<sup>117,122,124,211</sup>

A predictive disease progression score was calculated in all PD patients based on a validated prognostic model, which estimates the risk of an unfavourable outcome in PD, as defined by the presence of either postural instability or dementia at 5 years.<sup>17</sup>

### Genetic Analysis

All participants supplied an EDTA blood sample for genetic analysis to known pathogenic mutations in monogenic PD genes (eg. *PINK1*, *PARK2*, *LRRK2*) and any variants of *GBA1* associated with increased risk of PD using the NeuroChip platform.<sup>215</sup> All detected variants were searched in dbSNP (<https://www.ncbi.nlm.nih.gov/snp/>) and then classified according to published guidelines.<sup>248</sup>

### <sup>31</sup>Phosphorus Magnetic Resonance Spectroscopy

#### Acquisition

<sup>31</sup>P-MRS scans were obtained using a Philips Ingenia 3 Tesla system (Philips Healthcare, Best, Netherlands) and a transmit-receive dual-tuned <sup>1</sup>H/<sup>31</sup>P birdcage quadrature head-coil (Rapid Biomedical, Würzburg, Germany). Two-dimensional chemical shift imaging (CSI) with image-selected *in vivo* spectroscopy was used for spectral spatial localisation. Two separate CSI sequences were obtained focused on the midbrain and the putamen. Acquisition parameters for the midbrain CSI were: repetition time (TR)=4000ms, echo time (TE)=0.22ms, number of signal averages (NSA)=8, sampling points=2048, spectral bandwidth=3000Hz, flip angle (FA)=90°, slice thickness=20mm, field of view (FOV)=210mm<sup>2</sup>, acquired voxel sizes of 40x40x20mm<sup>3</sup> and, following k-space filtering and zero filling using a reconstruction matrix of 14x14, reconstructed voxel size=15x15x20mm<sup>3</sup>. The putamen CSI acquisition parameters differed only in NSA=10 and reconstructed voxel size=17.5x17.5x20mm<sup>3</sup> using a reconstruction matrix of 12x12. All CSI sequences used adiabatic pulses, with a second order pencil-beam shim and WALTZ-4 broadband heteronuclear decoupling with nuclear Overhauser effect.

Alignment of CSI sequences was guided by a T2-weighted spin-echo image: TR=3000ms, TE=80ms, FA=90°, slice thickness=4mm, FOV=230mm<sup>2</sup>, acquisition voxel 0.55x0.65x4.0 mm<sup>3</sup>, reconstruction matrix=432x432mm<sup>2</sup>, reconstructed voxel size=0.53x0.53x4.0mm<sup>3</sup>. A 3D T1 inversion-recovery volumetric image was obtained and aligned to each CSI acquisition to allow co-localisation and correction for partial volume effects: TR=8.3ms, TE=3.8ms, FOV=240mm<sup>2</sup>, FA=8°, inversion time=1000ms, slice thickness=1mm, acquired voxel size=1.2x1.2x1.5mm, reconstruction matrix=256x256mm<sup>2</sup>, reconstructed voxel size=0.94x0.94x1mm<sup>3</sup>. Details of spectral localisation and voxels of interest are shown in **Figure 4.1**.

### **Spectroscopic Data Processing**

All spectroscopic data was anonymised at acquisition and analysed blinded to participant status. Spectra were processed in the time domain using jMRUI software V5.2 (<http://www.jmrui.eu>) and signal fitting was performed using the Advanced Method for Accurate, Robust and Efficient Spectral fitting (AMARES) algorithm to determine the relative area under each peak.<sup>183,259</sup> In total, six voxels were analysed representing left midbrain, right midbrain, left posterior putamen, right posterior putamen, left anterior putamen and right anterior putamen.

Manual pre-processing included zero and first-order phasing for purely absorptive line shapes with no apodisation performed. All spectra were frequency shifted to 0 parts per million for PCr.

A total of 13 resonances were fitted with assumed Lorentzian line shapes, with  $\gamma$ -ATP and  $\alpha$ -ATP having doublet peaks with amplitudes and linewidths constrained to a 1:1 ratio to each other and  $\beta$ -ATP having triplet peaks with amplitudes constrained in a ratio of 0.5:1:0.5 and linewidths constrained to a ratio of 1:1:1. Coupling constants for ATP multiplets were set at 18Hz as used in previous literature and soft constraints limited ATP linewidths to 5-35Hz.<sup>179,189</sup> Additional soft constraints were used to control linewidths for PCr (5-20Hz), and all other remaining resonances to 5-30Hz.<sup>180,216</sup> For ratio measures, the raw amplitudes were used to calculate the ratio on interest. For the assessment of total levels of metabolites, amplitudes were normalised to the total phosphorus signal detected within the respective voxel prior to any statistical analyses. The three multiplets of ATP were summed to calculate total ATP. All spectra were visually inspected for quality of fit and spurious signals were excluded, according to recently published consensus criteria.<sup>217</sup> Example spectra pre- and post-analysis are shown in **Figure 4.1**.

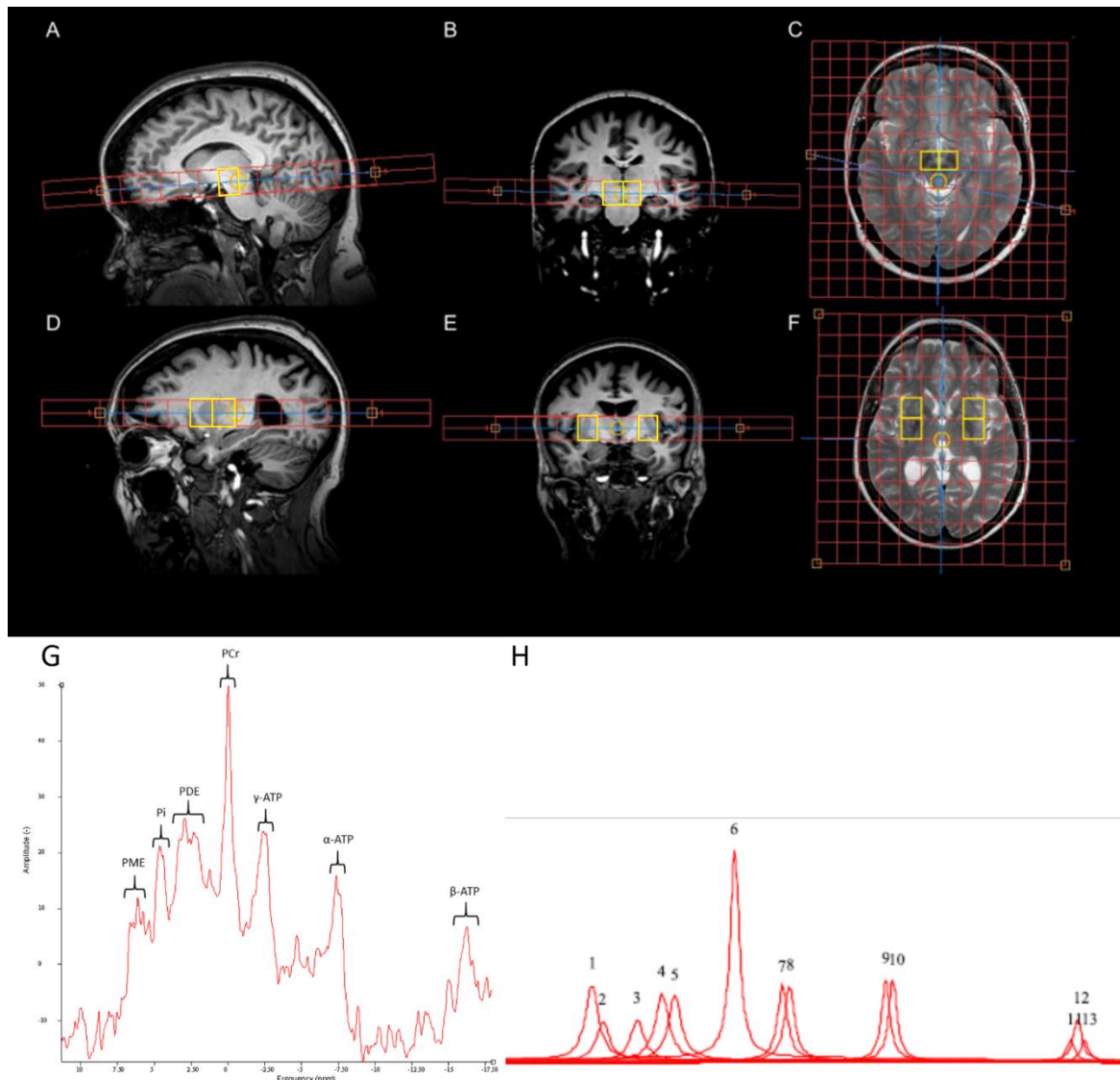


**Figure 4.1:  $^{31}\text{P}$ Phosphorus magnetic resonance spectroscopy methodology.**

Analysed voxels are highlighted in yellow. Sagittal (A), coronal (B) and axial (C) images demonstrating spectroscopic grid (14x14) positioning for the midbrain voxels, placement is performed to capture a voxel from the right and left side. Voxel placement ensures the substantia nigra will be included within the voxel of interest. Sagittal (D), coronal (E) and axial (F) images demonstrating spectroscopic grid (12x12) positioning for the putaminal voxels, placement is performed to capture a voxel from the right and left side for both the anterior and posterior putamen. (G) An example spectrum obtained from the midbrain of a healthy control. This spectrum has been phased and apodised to aid visualisation with phosphocreatine frequency shifted to 0ppm. (H) An example output of peak fitting following AMARES analysis. Thirteen resonances are fitted: 1=phosphocholine, 2=phosphoethanolamine, 3=Pi, 4=glycerophosphocholine, 5=glycerophosphoethanolamine, 6=PCr, 7,8= $\gamma$ -ATP, 9,10=  $\alpha$ -ATP, 11-13=  $\beta$ -ATP. Phosphocholine and phosphoethanolamine form the phosphomonoesters (PME). Glycerophosphocholine and glycerophosphoethanolamine form the phosphodiester's (PDE). Pi=inorganic phosphate, PCr=phosphocreatine.

T1 weighted images were segmented using Statistical Parametric Mapping software (SPM12, <https://www.fil.ion.ucl.ac.uk/spm/software/spm12/>) and co-registered to the voxel of interest using Gannett (<http://www.gabamrs.com/>) and MATLAB and Statistics Toolbox Release R2020a (The MathWorks, Inc., Natick, Massachusetts, United States). Each voxel was segmented into grey matter, white matter and cerebrospinal fluid. To represent partial volume effects the brain proportion (grey plus white matter divided by total voxel volume) was calculated for midbrain voxels and grey matter proportion was calculated for putaminal voxels.

### **Fibroblast cell line assessment**

Skin biopsies were obtained using a 3mm punch biopsy needle from the upper forearm and fibroblast lines were established according to previously reported protocols.<sup>231</sup> Assays were performed under two conditions; glucose containing media (1000mg/L) or glucose-free media containing 5mM galactose.

Mitochondrial membrane potential (MMP) and total intracellular ATP levels were assessed as previously described.<sup>159</sup> Mitochondrial and lysosomal morphology was quantified by staining live fibroblasts with 80nM tetramethylrhodamine (TMRM), 1 $\mu$ M LysoTracker® (Life Technologies) and 1  $\mu$ M Hoescht for 1 hour prior to imaging, using either the InCell Analyzer 2000 high-content imager (GE Healthcare) or Opera Phenix (Perkin Elmer) imaging systems as previously described.<sup>73</sup>

Raw images were analysed and parameters obtained using the InCell Developer software (GE Healthcare) or Harmony software (Perkin Elmer). A custom imaging protocol was used for the segmentation of nuclei, lysosomes, and mitochondria to generate total counts for each. The mitochondrial population was further subdivided into long and short mitochondria for the assessment of MMP in these subpopulations. Short mitochondria are more likely to be destined for mitophagy, this is particularly true in shorter mitochondria with low MMP.<sup>59</sup> Analysis outputs were consistent across imagers and software, enabling combination of groups in the final analysis.

### **Statistical Analysis**

Primary <sup>31</sup>P-MRS parameters of interest were determined *a priori* as total levels of ATP, Pi and PCr in the mean midbrain, mean posterior putamen and mean anterior putamen. Individual <sup>31</sup>P-MRS parameters of interest were entered as the response

variable into a linear regression model, with the predictor variables specified as disease group, age and sex. This choice was based on previous work which showed differences between sexes in PD with respect to ATP and PCr measurements and changes in pH and PCr with age in the healthy brain.<sup>193,228</sup> <sup>31</sup>P-MRS parameters of interest and partial volume measures were assessed separately in a correlation analysis, only in the event of a significant correlation was partial volume added as a further covariate to the linear regression models. This was done to limit the number of covariates with respect to sample size.

The <sup>31</sup>P-MRS Pi/ATP, Pi/PCr, PCr/ATP ratios were also investigated in an exploratory analysis for differences between groups. Elevated Pi/ATP ratios have previously been associated with impaired oxidative phosphorylation and have been found to be elevated in PD.<sup>181,295</sup> Both PCr/ATP and Pi/PCr have been used widely in the assessment of muscle bioenergetics, particularly in dynamic testing protocols where reduced PCr/ATP ratios and elevated Pi/PCr ratios infer an over-reliance of the creatine-phosphocreatine buffer to maintain ATP levels.<sup>296</sup> As these are ratios it avoids the need for normalising to the total phosphorus signal within the voxel.

Phospholipid analysis used the same regression model to assess the normalised amplitudes of PME, PDE and the PME/PDE ratio for differences between groups using the same regression model. The PME/PDE ratio has been used to reflect membrane turnover and the balance between phospholipid degradation (PDE) and synthesis (PME). Phospholipid parameters were not assessed for their relationship with fibroblast parameters as they don't directly represent bioenergetics, the primary focus of the fibroblast assays performed.

All data for each fibroblast line were normalised to the controls on each plate. Key primary fibroblast parameters of interest specified *a priori* were intracellular ATP, MMP (in all mitochondria, long mitochondria only and short mitochondria only), mitochondrial count per cell and lysosome count. Group differences were assessed using t-tests.

Differences in variances for all <sup>31</sup>P-MRS and fibroblast assay parameters between groups were analysed using the F-test of equality of variances. Pearson's correlation coefficient was used to assess relationships between each <sup>31</sup>P-MRS parameter and continuous clinical variables of interest, and the relationships between each fibroblast

parameters and each other. For these analyses, all p-values were adjusted for multiple comparisons using the Benjamini-Hochberg method.<sup>232</sup>

To assess associations between <sup>31</sup>P-MRS and fibroblast data in a common domain, all relevant bioenergetic <sup>31</sup>P-MRS parameters (ATP, Pi, PCr) and each individual biological fibroblast assay repeat were first transformed to Z-scores. Prior to this each parameter was confirmed to be normally distributed with the visual inspection of Q-Q plots in the healthy control data only and subsequently transformed to a z-score with mean of 0 and standard deviation of 1. Z-scores for patients were then calculated with reference to healthy control population distribution.

For fibroblast data, and for each media condition, each biological repeat was combined into a composite z-score with equal weighting given to each individual repeat using the below equation.<sup>233</sup>

$$z_{xc} = \frac{\sum_{i=0}^n z_x}{\sqrt{n + 2r_{sum}}}$$

Where  $z_{xc}$  is the composite score,  $z_x$  is the z-scored component and  $r_{sum}$  is the sum of the Pearson correlation coefficients between each and every individual  $n$  components.

Each media condition z-score was then combined using the same method to generate a single composite z-score for each fibroblast assay parameter that summarises data from both media conditions. Composite Z-scores were also generated using the same above method to reflect <sup>31</sup>P-MRS parameters as either the composite of all 4 putaminal voxels or a composite of both midbrain voxels. The further exploratory analysis of composite z-scored putaminal Pi/ATP, Pi/PCr and PCr/ATP ratio was also calculated using this method.

Pearson's correlation coefficient was used to assess relationships between composite z-scores derived from <sup>31</sup>P-MRS and fibroblast assay parameters within each disease group. To determine if any correlations seen in PD and healthy controls were significantly different to each other, the correlation coefficients from each group were compared using Fishers z-test. Any significant correlations between <sup>31</sup>P-MRS and fibroblast assay parameters were further assessed in a sensitivity analysis with linear regression with the additional covariates of age and sex entered to confirm if the relationship remained significant, these sensitivity analyses are not reported unless

the observed relationship lost significance. Given the exploratory nature of these relationships, this analysis was not corrected for multiple comparisons.

All statistical analyses were completed in R version 4.1.0.

## Results

Demographic characteristics are summarised in **Table 4.1**. PD and healthy controls were well-matched for age and sex, with no significant differences between groups. There were two cases of familial PD, a 50-year-old female homozygous for a *parkin* mutation (c.337-376del) and a 28-year-old female heterozygous for the G51D *SNCA* mutation.<sup>297,298</sup> No other *PARK* gene mutations or *GBA* PD risk variants were detected.

Sixty <sup>31</sup>P-MRS datasets were obtained from the putamen and 59 from the midbrain. Midbrain <sup>31</sup>P-MRS values from one control were excluded from further analysis for technical reasons.

The fibroblast dataset included 57 cell lines. Two participants were unable to have fibroblast cell lines established due to COVID-19 restrictions impacting research practice at the time of recruitment. One further control fibroblast cell line was excluded from analysis due to recurrent cell line infections.

All primary <sup>31</sup>P-MRS metabolite concentrations and fibroblast-derived parameters were normally distributed in healthy controls. In both PD and healthy controls, there were no significant correlations between either age or sex with <sup>31</sup>P-MRS metabolite levels or fibroblast assay parameters of interest (data not shown). There were no significant correlations between <sup>31</sup>P-MRS parameters and partial volume measures (data not shown) and therefore partial volume was not included in the linear regression models presented.

	Control (n=25)	Parkinson's (n=35)	p-value
<b>Sex</b>			
Male (n, %)	12 (48)	19 (54)	
Female (n, %)	13 (52)	16 (46)	0.8272 <sup>a</sup>
<b>Age</b>			
Minimum	28	28	
Maximum	81	82	0.839 <sup>b</sup>
Mean ± SD	60.64 ± 10.96	60.06 ± 10.74	
<b>Family history of PD in a first-degree relative</b>			
Yes (n, %)	6 (24)	4 (11)	
No (n, %)	19 (76)	31 (89)	0.535 <sup>a</sup>
<b>Disease Duration (months)</b>			
Minimum	NA	2	
Maximum	NA	32	
Mean ± SD	NA	13.71 ± 7.50	
<b>Modified Hoehn &amp; Yahr</b>			
Minimum	NA	1	
Maximum	NA	3	
Mean ± SD	NA	2.01 ± 0.39	
<b>MDS-UPDRS Part III scores</b>			
Minimum	NA	14	
Maximum	NA	54	
Mean ± SD	NA	32.60 ± 9.89	
<b>Non-Motor Symptom Scale</b>			
Minimum	NA	3	
Maximum	NA	119	
Mean ± SD	NA	40.09 ± 31.99	
<b>Total Levodopa Equivalent Daily Dosage (mg)</b>			
Minimum	NA	0	
Maximum	NA	1000	
Mean ± SD	NA	370.43 ± 218.44	
<b>Predictive Risk Score</b>			
Minimum	NA	0.03	
Maximum	NA	0.91	
Mean ± SD	NA	0.40 ± 0.25	

**Table 4.1: Demographic and clinical features of the study cohort.**

There are no significant differences between age, sex or family history of PD between patients and controls. <sup>a</sup>Chi-squared test, <sup>b</sup>Independent samples t-test with Welch's correction. MDS-UPDRS=Movement Disorders Society – Unified Parkinson's Disease Rating Scale.

### **<sup>31</sup>P Phosphorus Magnetic Resonance Spectroscopy**

Key <sup>31</sup>P-MRS results are shown in **Figure 4.2** and summarised in **Table 4.2**. 10/34 PD patients had ATP midbrain values outside two standard deviations from the healthy control mean (**Fig. 4.2A**, F-test  $p=0.0030$ ). In the posterior putamen 9/35 with PD had levels of Pi that fell outside two standard deviations, (**Fig. 4.2B**, F-test  $p=0.0041$ ). Similarly, there was a marked increase in variance in the Pi/ATP ratio in the posterior putamen (**Fig. 4.2C**, F-test  $p=0.0036$ ) with 7/35 PD patients having Pi/ATP ratios outside two standard deviations. There were no differences between groups with respect to either the Pi/PCr or PCr/ATP ratio. The values of all energy-rich metabolites were similar in both anterior and posterior putamen (**Table 4.2**).

Higher <sup>31</sup>P-MRS-derived midbrain PCr was correlated with a higher predicted risk of adverse outcome in disease progression, defined as the presence of either postural instability or dementia at five years (**Fig. 4.2D**,  $r=0.47$ , 95% confidence interval= $0.164 - 0.695$ , adjusted  $p= 0.0384$ ,). There were no other correlations of <sup>31</sup>P-MRS data with other clinical characteristics (MDS-UPDRS III, MDS-NMSS,).

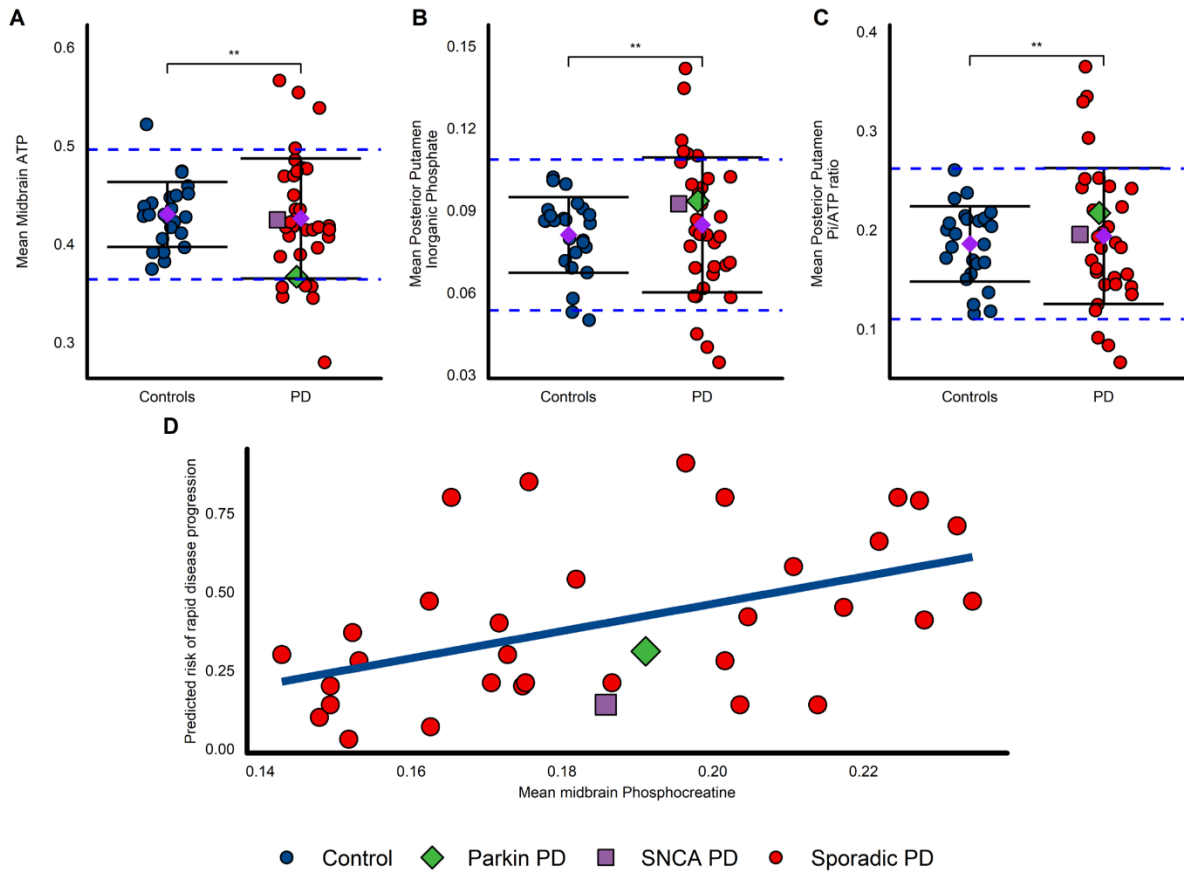


**Figure 4.2: <sup>31</sup>P-MRS in PD compared to controls.**

All <sup>31</sup>P-MRS values are normalised to total phosphorus signal detected in the spectra. A) mean midbrain ATP, B) mean posterior putamen inorganic phosphate, C) mean posterior putamen inorganic phosphate (Pi)/ATP ratio D) Correlation of mean midbrain phosphocreatine and predicted risk of rapid disease progression in PD which predicts risk of adverse outcome (postural instability or dementia) at 5 years. Mean (purple diamond)  $\pm$  standard deviation (SD) presented for panels A-C. Variances between groups were tested with the f-test of equality of variances and statistical significance is displayed on panels A-C. Blue dashed lines denote 2 SDs from the control mean values. Midbrain data, control  $n = 24$ , PD  $n = 35$ . Putamen data, control  $n = 25$ , PD  $n = 35$ .

<sup>31</sup> P-MRS Parameters	Control (n = 24)	Parkinson's (n = 35)		
<b>Total ATP</b>	<b>Amplitude</b>	<b>Amplitude</b>	<b>F-test</b>	<b>β<sub>group</sub></b>
Mean midbrain	0.430 ± 0.033	0.426 ± 0.061	**	ns
Mean posterior putamen	0.446 ± 0.038	0.452 ± 0.043	ns	ns
Mean anterior putamen	0.430 ± 0.043	0.439 ± 0.040	ns	ns
<b>Total inorganic phosphate</b>				
Mean midbrain	0.080 ± 0.025	0.089 ± 0.030	ns	ns
Mean posterior putamen	0.081 ± 0.014	0.085 ± 0.025	**	ns
Mean anterior putamen	0.082 ± 0.016	0.088 ± 0.026	*	ns
<b>Inorganic phosphate/ATP ratio</b>				
Mean midbrain	0.190 ± 0.068	0.217 ± 0.089	ns	ns
Mean posterior putamen	0.186 ± 0.038	0.194 ± 0.069	**	ns
Mean anterior putamen	0.197 ± 0.049	0.206 ± 0.073	ns	ns
<b>Total phosphocreatine</b>				
Mean Midbrain	0.192 ± 0.021	0.186 ± 0.028	ns	ns
Mean posterior putamen	0.195 ± 0.018	0.197 ± 0.021	ns	ns
Mean anterior putamen	0.202 ± 0.017	0.203 ± 0.022	ns	ns
<b>Total phosphomonoesters</b>				
Mean Midbrain	0.150 ± 0.026	0.150 ± 0.043	*	ns
Mean posterior putamen	0.128 ± 0.025	0.135 ± 0.026	ns	ns
Mean anterior putamen	0.129 ± 0.027	0.128 ± 0.031	ns	ns
<b>Total phosphodiester</b>				
Mean Midbrain	0.137 ± 0.038	0.137 ± 0.041	ns	ns
Mean posterior putamen	0.138 ± 0.028	0.124 ± 0.029	ns	ns
Mean anterior putamen	0.142 ± 0.033	0.133 ± 0.029	ns	ns
<b>Phosphomonoester/phosphodiester ratio</b>				

Mean Midbrain	1.226 ± 0.613	1.200 ± 0.587	ns	ns
Mean posterior putamen	0.940 ± 0.257	1.133 ± 0.378	ns	*
Mean anterior putamen	0.94 ± 0.292	1.007 ± 0.388		

**Table 4.2: <sup>31</sup>P-MRS summary results.**

*Mean and standard deviation and f-test shown for all data. Group differences in <sup>31</sup>P-MRS parameters were tested with linear regression controlling for age and sex, the significance of the  $\beta$  coefficient for group effect is reported ( $\beta_{group}$ ). All <sup>31</sup>P-MRS amplitudes are normalised to the total phosphorus signal detected within the respective voxel. ns=not significant, \* $<0.05$ , \*\* $<0.01$ , \*\*\* $<0.001$ .*

Summary statistics for the exploratory analysis of <sup>31</sup>P-MRS phospholipids are shown in **Table 4.3** and data is also shown in **Figure 4.3**. Participants with PD demonstrated higher PME/PDE ratio than controls in the mean posterior putamen as assessed with linear regression (**Fig. 4.3F**, PD effect estimate= 0.186, 95% CI 0.0136, 0.358,  $p=0.0337$ ). There were no other differences in group means or variances with respect to PME, PDE or the PME/PDE ratio in either the midbrain, mean posterior putamen or mean anterior putamen.

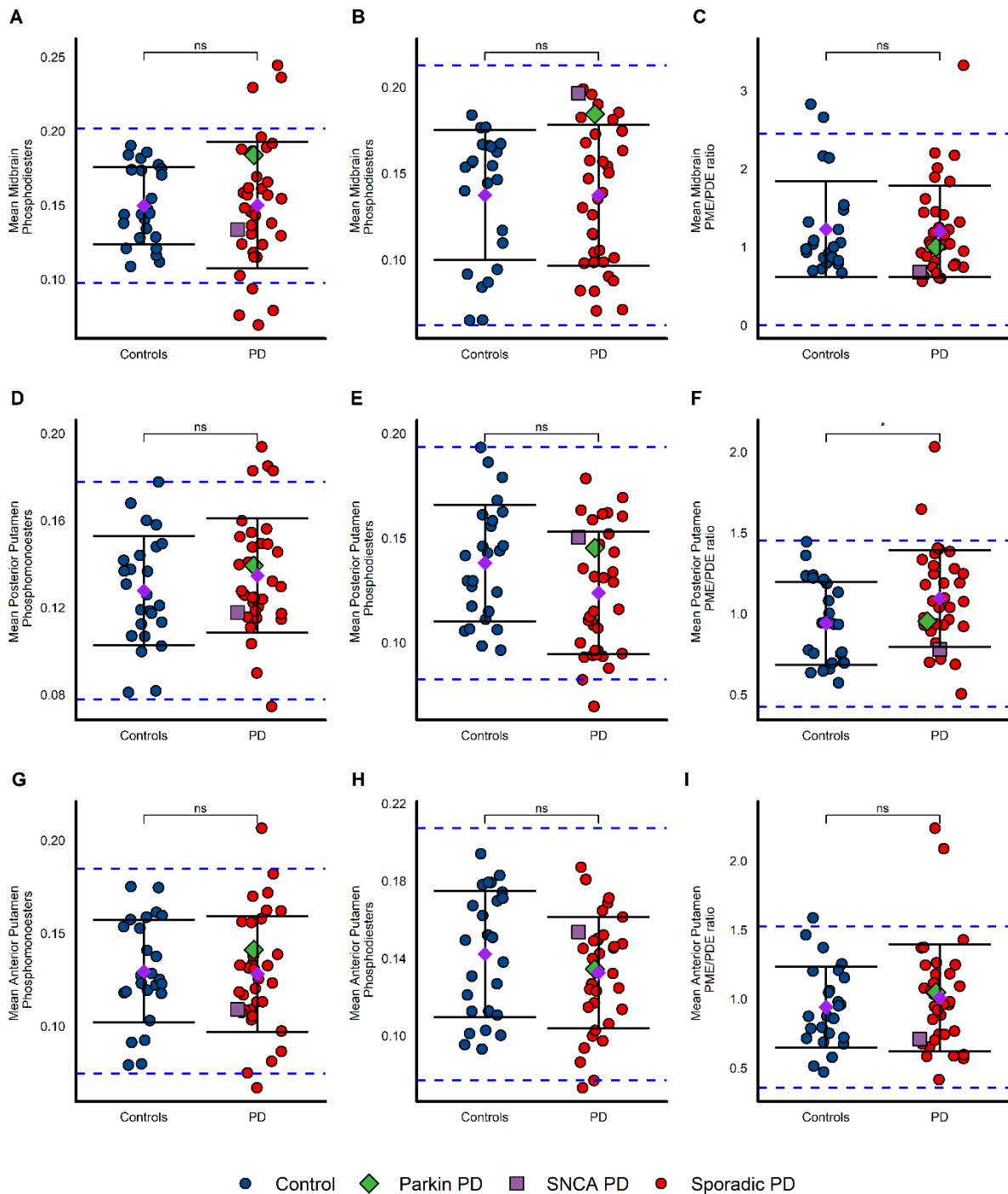


**Figure 4.3:  $^{31}\text{P}$ -MRS measured phospholipids acquired from the mean midbrain, mean posterior putamen and mean anterior putamen.**

(A), (D) and (G) show phosphomonoesters (PME, combination of phosphocholine and phosphoethanolamine) in each anatomical area. (B), (E) and (H) show the phosphodiester (PDE, combination of glycerophosphocholine and glycerophosphoethanolamine) in each anatomical site. (C), (F) and (I) show the PME/PDE ratio in each anatomical site. Mean (purple diamond) and standard deviation (error bars) shown. Group differences tested using linear regression. Significance: ns=non-significant, \* $p < 0.05$

## Fibroblast Cell Line Assessment

Key fibroblasts assay results from experiments undertaken in both glucose-containing and galactose media are shown in **Figure 4.4** (glucose-containing results) and summarised in **Table 4.3**. Results from experiments undertaken in galactose-containing media were highly similar to those in glucose-containing media (**Table 4.3** and **Supplementary Figure 4.1**). For simplicity the glucose containing media is discussed here. There was a much wider variance in PD data compared to controls across all fibroblast assay parameters in glucose-containing media. 7/34 PD patients had intracellular ATP values outside two standard deviations from the healthy control mean (F-test  $p=0.0056$ , **Fig. 4.4A**). 14/34 PD patients had MMP values outside two standard deviations of the healthy control mean (F-test  $p<0.0001$ , **Fig. 4.4B**), this was also the case for long mitochondrial MMP (8/34 PD patients, F-test  $p=0.0007$ , **Fig. 4.4C**) and short mitochondria MMP (9/34 PD patients, F-test  $p=0.0003$ , **Fig. 4.5D**). 15/34 PD patients had mitochondria counts per cell outside two standard deviations (F-test  $p<0.0001$ , **Fig. 4.4E**) and 6/34 PD patients had lysosomal counts outside two standard deviations (F-test  $p<0.0001$ , **Fig. 4.4F**).

Within this section all p-values are adjusted for multiple comparisons. Within the fibroblasts, higher intracellular ATP correlated with higher mitochondrial counts in both PD ( $p<0.0001$ ) and healthy controls ( $r=0.55$ ,  $p=0.0107$ , **Fig. 4.5A**,). However, lower MMP correlated with higher intracellular ATP, ( $r=-0.55$ ,  $p=0.0016$ , **Fig. 4.5B**) and higher mitochondrial counts ( $r=-0.72$ ,  $p<0.0001$ , **Fig. 4.5C**,) in PD only, but not in controls ( $r=-0.04$ ,  $p=0.8660$  and  $r=-0.38$ ,  $p=0.1074$  respectively). Lysosomal counts correlated inversely with lower MMP ( $r=-0.62$ ,  $p=0.0002$ , **Fig. 4.5D**) and higher mitochondrial counts in PD only ( $r=0.7$ ,  $p<0.0001$ , **Fig. 4.5E**), but not in controls ( $r=-0.21$ ,  $p=0.432$  and  $r=0.43$ ,  $p=0.0602$  respectively).

In PD the association of lower MMP with both higher mitochondria and lysosome counts would be in keeping with the induction of mitophagy.<sup>299,300</sup> This assumption is further supported by the observation that the correlation between lower MMP and higher lysosomal counts was strongest in short mitochondria ( $r=-0.73$ ,  $p<0.0001$ , **Fig. 4.6F**), which are most likely to undergo mitophagy.<sup>59</sup>

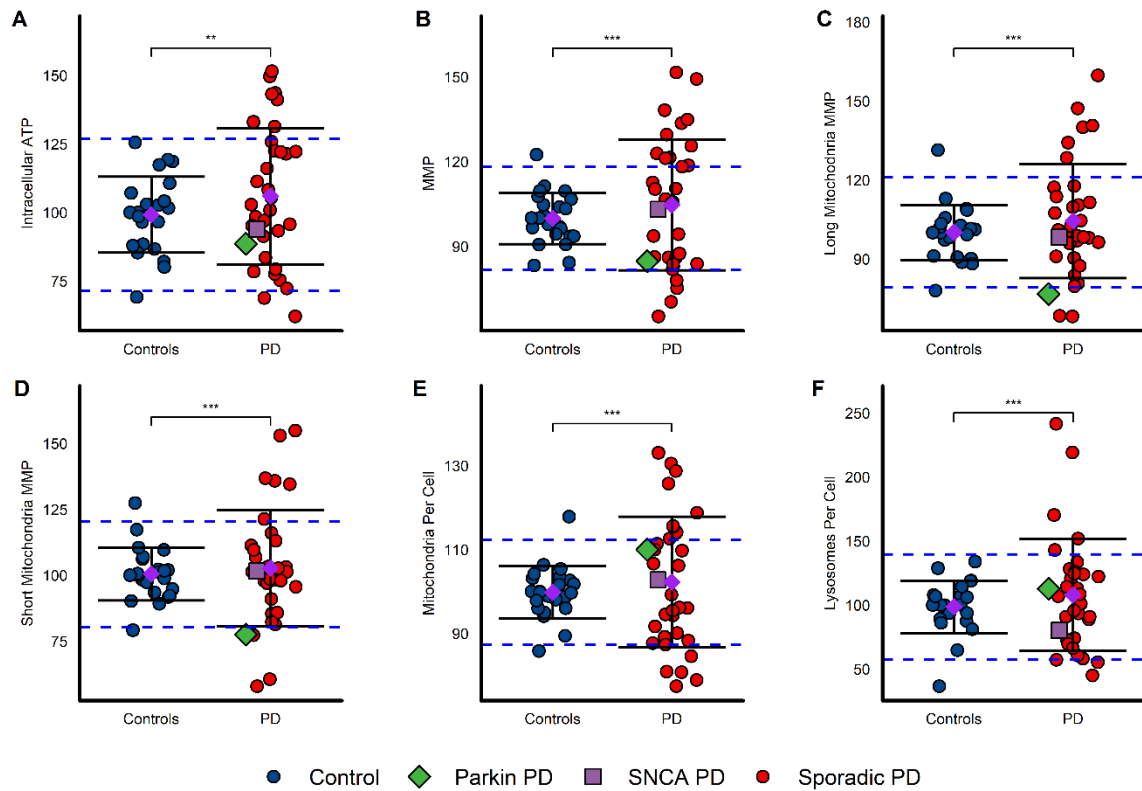


**Figure 4.4: Fibroblast assay results in PD compared to controls**

A) Intracellular ATP, B) MMP, C) mitochondria count per cell, D) lysosomal count per cell, E) long mitochondria MMP only, F) short mitochondria MMP. Mean (purple diamond)  $\pm$  standard deviation (SD) presented. All data presented is from experiments performed in glucose-containing media. Variances between groups were tested with the f-test of equality of variances and statistical significance is displayed on panels A-C. Blue dashed lines denote 2 SD's from the control mean values. Control  $n = 23$ , PD  $n = 34$ . All fibroblast assays repeated in triplicate.

	Control (n = 23)	Parkinson's (n = 34)		
<b>Intracellular ATP</b>	<b>Normalised values</b>	<b>Normalised values</b>	<b>F-test</b>	<b>T-test</b>
Glucose containing media	99.164 ± 13.864	105.928 ± 24.845	**	ns <sup>a</sup>
Galactose containing media	99.317 ± 13.649	104.386 ± 21.872	*	ns <sup>a</sup>
<b>Overall Mitochondrial Membrane Potential</b>				
Glucose containing media	99.902 ± 9.114	104.64 ± 23.127	***	ns <sup>a</sup>
Galactose containing media	100.096 ± 7.420	99.858 ± 16.621	***	ns <sup>a</sup>
<b>Short Mitochondria Mitochondrial Membrane Potential</b>				
Glucose containing media	100.458 ± 10.019	102.678 ± 22.102	***	ns <sup>b</sup>
Galactose containing media	100.420 ± 8.984	98.896 ± 18.679	***	ns <sup>b</sup>
<b>Long Mitochondria Mitochondrial Membrane Potential</b>				
Glucose containing media	100.108 ± 10.438	104.444 ± 21.702	***	ns <sup>b</sup>
Galactose containing media	99.989 ± 9.317	99.955 ± 16.724	**	ns <sup>b</sup>
<b>Mitochondria Per Cell</b>				
Glucose containing media	99.810 ± 6.236	102.268 ± 15.571	***	ns <sup>a</sup>
Galactose containing media	99.471 ± 6.287	102.954 ± 14.934	***	ns <sup>a</sup>
<b>Lysosomes per cell</b>				
Glucose containing media	98.505 ± 20.522	112.592 ± 51.366	***	ns <sup>b</sup>
Galactose containing media	98.109 ± 18.427	94.895 ± 32.303	**	ns <sup>b</sup>
<b>Percentage of Perinuclear Mitochondria</b>				
Glucose containing media	100.298 ± 5.52	102.121 ± 12.779	***	ns
Galactose containing media	102.372 ± 5.642	100.448 ± 11.46	***	ns

**Table 4.3 Fibroblast assay summary statistics for the entire study cohort in both media conditions.**

Mean, standard deviation, F-test and t-test results for primary <sup>31</sup>P-MRS and fibroblast parameters are shown. <sup>a</sup>Independent samples t-test with Welch's correction. <sup>b</sup>Group differences tested with Mann-Whitney U test as data was non-normally distributed \*<0.05, \*\*<0.01, \*\*\*<0.001

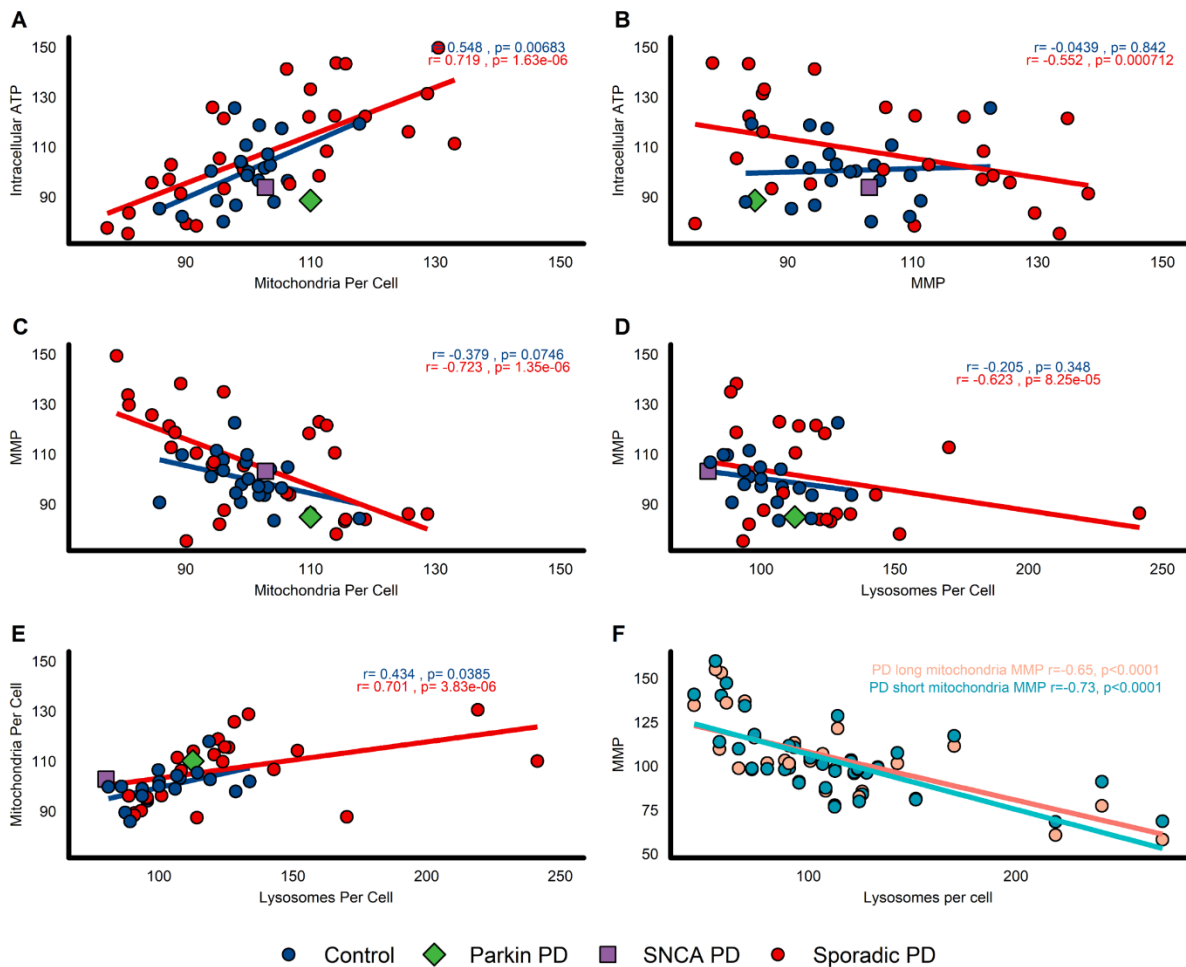


**Figure 4.5: Fibroblast measures of mitochondrial and lysosome function/morphology; correlations between measures for both PD and controls.**

Data from each participant is normalised to mean control values. Data presented is from glucose-containing media experiments. The following correlations are plotted: A) intracellular ATP and mitochondria per cell, B) intracellular ATP and MMP, C) MMP and mitochondria per cell, D) MMP and lysosomes per cell, E) mitochondria per cell and lysosomes per cell, F) Long mitochondria MMP (peach) and short mitochondria MMP (turquoise) and lysosomes per cell in patients only. Pearson's correlation coefficient is displayed for all correlations. Displayed *p*-values are reported unadjusted for multiple comparisons. Following multiple comparisons correction, all relationships remained significant other than the relationship between MMP and mitochondria per cell and mitochondria per cell and lysosomes per cell in healthy controls. Control *n* = 23, PD *n* = 34.

## Correlations of <sup>31</sup>P Phosphorus Magnetic Resonance Spectroscopy and mechanistic phenotyping of peripheral tissue

In healthy controls, higher putaminal ATP was associated with higher mitochondria counts in fibroblasts as expected ( $r=0.416$ ,  $p=0.0484$ , **Fig. 4.6A**). In contrast, an inverse trend between putaminal ATP and mitochondrial count was observed in PD ( $r=0.298$ ,  $p=0.0865$ , **Fig. 4.6A**). Fishers Z-test demonstrated a significant difference in the correlation coefficients observed between PD and healthy controls ( $p=0.0089$ ).

In PD, lower <sup>31</sup>P-MRS-derived putaminal ATP correlated with lower MMP in both long and short mitochondria MMP. This correlation was weaker in long mitochondria ( $r=0.359$ ,  $p=0.0372$ , **Fig. 4.6B**) and strongest in short mitochondria ( $r=0.442$ ,  $p=0.0084$ , **Fig. 4.6C**). In PD lower putaminal ATP correlated with greater numbers of lysosomes ( $r=0.433$ ,  $p=0.0105$ , **Fig. 4.6D**). These correlations were not present in healthy controls.

The correlation of lower putaminal ATP with lower MMP, greater lysosomal counts and greater mitochondrial counts in PD only may be suggestive of impaired mitophagy, reflecting the accumulation of defective mitochondria. This interpretation is again supported by the observation that the correlation was strongest in short mitochondria. Following fission events short mitochondria are more likely to be destined for mitophagy, rather than undergoing subsequent fusion and/or fission events.<sup>59</sup>

Similarly, in our exploratory analysis, an elevated putaminal Pi/ATP ratio (reflecting greater ATP hydrolysis or reduced ATP synthesis) was associated with higher mitochondrial counts ( $r=0.369$ ,  $p=0.0319$ , **Fig. 4.6E**), reduced MMP in both long ( $r=-0.469$ ,  $p=0.0052$ , **Fig. 4.6F**) and short mitochondria ( $r=-0.522$ ,  $p=0.0016$ , **Fig. 4.6G**) and greater lysosome counts ( $r=0.476$ ,  $p=0.0044$ , **Fig. 4.6H**) in PD only, but not in controls. Putaminal Pi changes were consistent with these observations (**Figure 4.7**).

There were no significant relationships between putaminal PCr and fibroblast results. There were no significant between midbrain ATP, PCr and Pi with any fibroblast parameters (**Figure 4.8**). There were no correlations between the exploratory analysis of Pi/PCr and PCr/ATP ratios and any fibroblast parameters (data not shown).

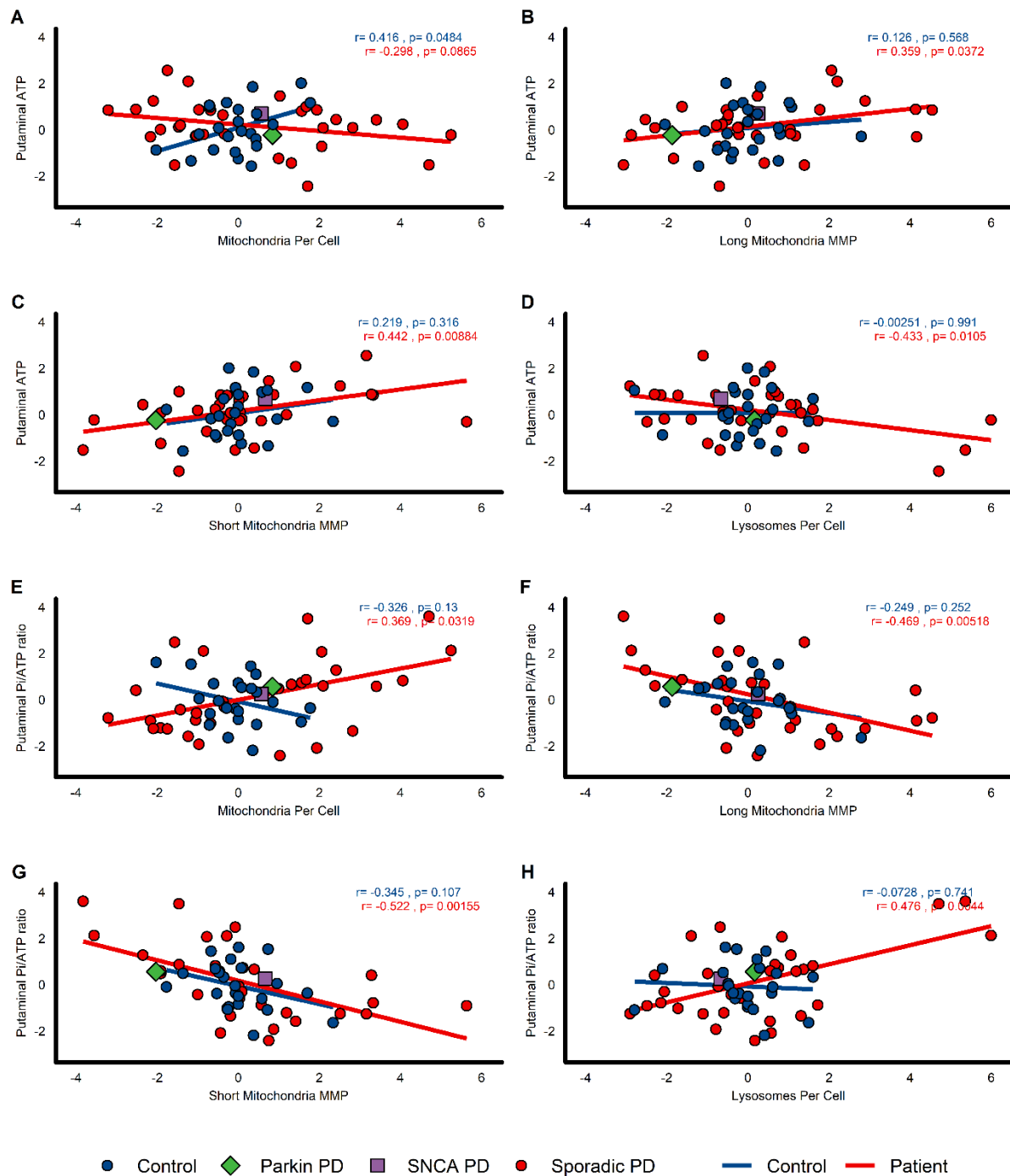


**Figure 4.6: Correlations between <sup>31</sup>P-MRS measures and fibroblast assay data.**

All <sup>31</sup>P-MRS data is expressed as composite z-scored data of all putaminal voxels. Pearson's correlation coefficient is displayed for all correlations. The following plots show: A) putaminal ATP and mitochondria per cell, B) putaminal ATP and MMP in long mitochondria only, C) putaminal ATP and MMP in short mitochondria only, D) putaminal ATP and lysosomes per cell, E) putaminal Pi/ATP ratio and mitochondria per cell, F) putaminal Pi/ATP ratio and MMP in long mitochondria only, G) putaminal Pi/ATP ratio and MMP in short mitochondria only, H) putaminal Pi/ATP ratio and lysosomes per cell. Control n = 23, PD n = 34.

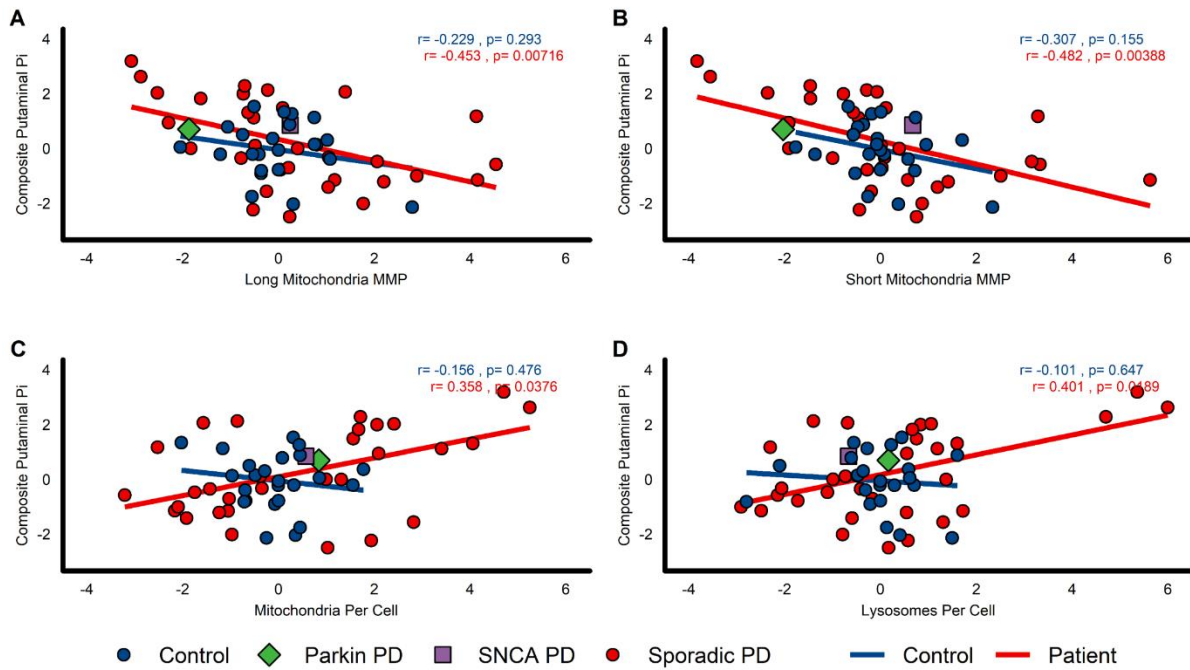


**Figure 4.7:  $^{31}\text{P}$ -MRS measured putaminal inorganic phosphate and relationships to fibroblast assay results.**

All  $^{31}\text{P}$ -MRS data is expressed as composite z-scored data of all midbrain voxels. All fibroblast data is expressed as composite z-scores of the named parameter in both experimental conditions (glucose-containing media and galactose-containing media). Pearson's correlation coefficient is displayed for all correlations. The following plots show: A) putaminal inorganic phosphate (Pi) and mitochondrial membrane potential (MMP) in long mitochondria, B) putaminal Pi MMP in short mitochondria, C) putaminal Pi and mitochondrial count per cell, D) putaminal Pi and lysosomes per cell. Fisher's Z test was used to assess differences in correlation between groups. Control  $n = 22$ , PD  $n = 34$ .

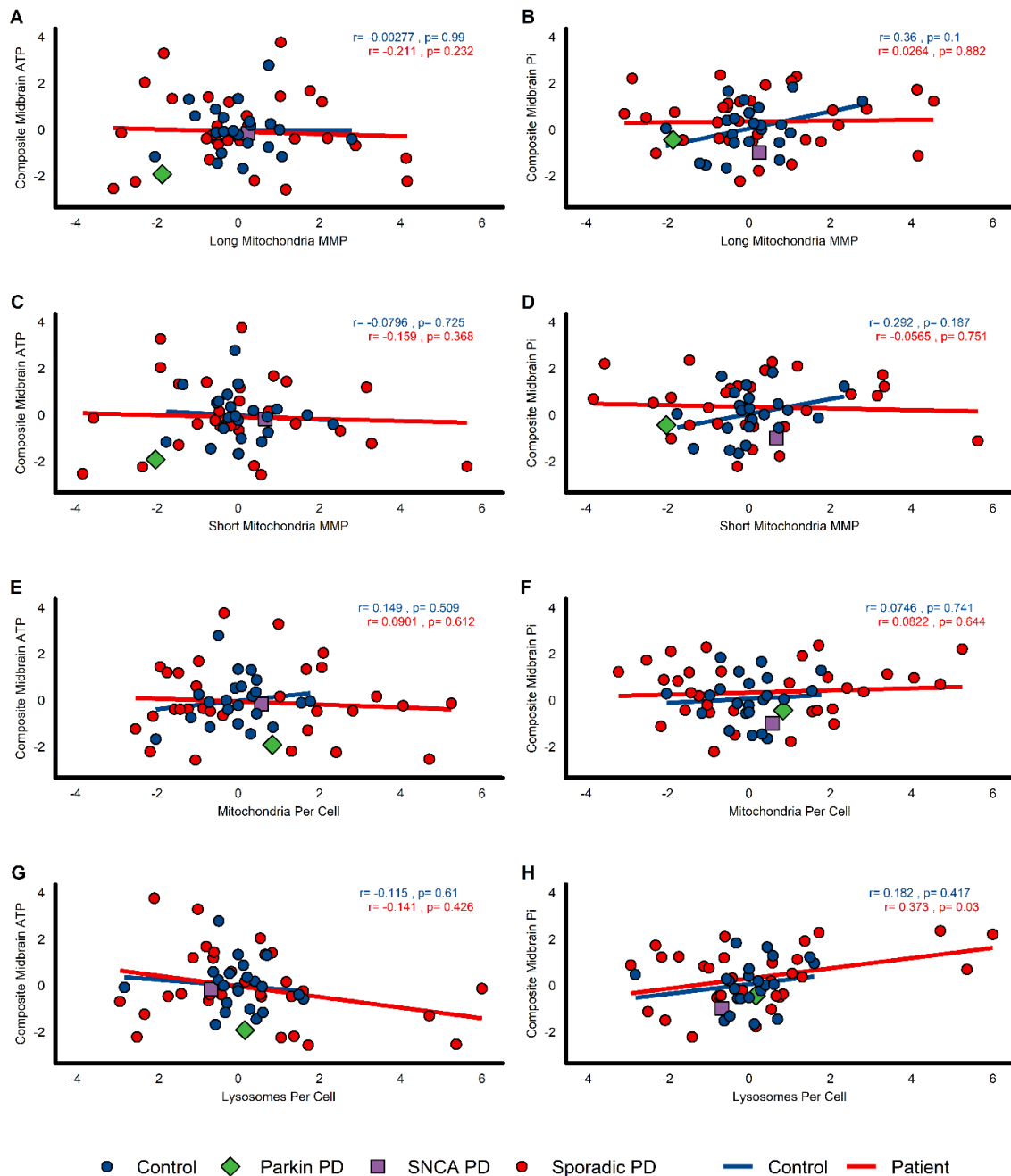


**Figure 4.8:  $^{31}\text{P}$ -MRS measured midbrain ATP and inorganic phosphate and relationships to fibroblast assay results.**

All  $^{31}\text{P}$ -MRS data is expressed as composite z-scored data of all midbrain voxels. All fibroblast data is expressed as composite z-scores of the named parameter in both experimental conditions (glucose-containing media and galactose-containing media). Pearson's correlation coefficient is displayed for all correlations. The following plots show: A) midbrain ATP and mitochondrial membrane potential (MMP) in long mitochondria, B) midbrain inorganic phosphate (Pi) and MMP in long mitochondria, C) midbrain ATP and MMP in short mitochondria, D) midbrain Pi and MMP in short mitochondria, E) midbrain ATP and mitochondria per cell, F) midbrain Pi and mitochondria per cell, G) midbrain ATP and lysosomes per cell, H) midbrain Pi and lysosomes per cell. Fisher's Z test was used to assess differences in correlation between groups. Control  $n = 22$ , PD  $n = 34$ .

## Discussion

Previous  $^{31}\text{P}$ -MRS studies in PD have provided conflicting results. Hattingen *et al*<sup>189</sup> reported reduced concentrations of ATP in the midbrain and reduced concentrations of both ATP and PCr in the putamen. Hu *et al*<sup>181</sup> identified elevated ratios of Pi/ATP in the temporoparietal region of PD. In contrast Weiduschat *et al*<sup>192</sup> reported no differences compared to healthy controls in either the striatum or temporoparietal cortex but did identify higher ATP in female compared to male PD patients.<sup>193</sup> Of note, there were significant differences in  $^{31}\text{P}$ -MRS acquisition and sample size as well as considerable variability in the severity and heterogeneity of PD patients included in these different studies.

In this study, we present the largest cross-sectional PD cohort investigated with  $^{31}\text{P}$ -MRS to date. We focussed on recent onset PD to increase the homogeneity of the patient cohort. Furthermore,  $^{31}\text{P}$ -MRS based mechanistic disease stratification is most likely to be relevant for future PD neuroprotection trials if a relevant  $^{31}\text{P}$ -MRS signature can be detected whilst the patients are still in the early stages of the disease.<sup>39</sup>

The markedly increased variance in the PD patient cohort for both  $^{31}\text{P}$ -MRS metabolites and key measures of cellular function in peripheral tissue is likely to reflect the heterogenous aetiology of PD and is in keeping with our previous work.<sup>161</sup> The observation of comparatively low  $^{31}\text{P}$ -MRS ATP levels in the midbrain and posterior putamen of our single *Parkin*-PD patient is in keeping with the assumption that mitochondrial dysfunction is a particularly important mechanism in *Parkin*-PD. In contrast,  $^{31}\text{P}$ -MRS ATP levels in midbrain and putamen of our G51D *SNCA*-PD patient were similar to the healthy control mean and in keeping with the assumption that mitochondrial dysfunction may not be the main pathogenic mechanism in *SNCA*-related PD. However, these data should be interpreted with caution since they are based on single patients only.<sup>80,297</sup>

The clinically relevant correlation between  $^{31}\text{P}$ -MRS derived PCr in midbrain and the predicted risk of rapid disease progression (as defined by the presence of postural instability or dementia at 5 years) suggests that  $^{31}\text{P}$ -MRS may be a useful tool to enrich future PD neuroprotection trials for patients with a more aggressive disease course. The creatine-phosphocreatine system is a key high-energy buffer in the central nervous and ensures that during periods of high activity (such as generating action

potentials) there is a sufficient supply of ATP from the breakdown of PCr to creatine and Pi by creatine kinase (CK).<sup>301</sup> Elevated PCr conferring a greater risk of rapid progression may reflect an excessive synthesis of PCr, or an inability to utilise it correctly. There are multiple isoforms of CK, ubiquitous mitochondrial CK (found in all tissues) is closely coupled to oxidative phosphorylation, but brain-specific cytoplasmic CK is closely coupled to glycolysis.<sup>301</sup> The observation of greater risk of rapid progression in PD could therefore be related to changes in either mitochondrial function or glucose homeostasis.

There were no clear differences in variance for any of the phospholipid parameters (PME, PDE, PME/PDE ratio) in any anatomical location. However, in PD, there was an increased PME/PDE ratio in the mean posterior putamen. The PME/PDE ratio is reflective of membrane turnover, with reduced PME/PDE ratios identified previously in neurodegenerative disease such as Alzheimer's.<sup>302</sup> Elevated ratios may be reflective of a shift towards phospholipid membrane synthesis. There were no clear differences at a group level in either PME and PDE and therefore it is unclear whether this is being driven by an increase in synthesis of phospholipid membrane precursors or a reduction in membrane break down and therefore interpretation should be cautious. It may also be that the source of increased phospholipid synthesis is non-neuronal.

Midbrain <sup>31</sup>P-MRS failed to demonstrate any meaningful relationships between composite <sup>31</sup>P-MRS bioenergetics parameters and composite fibroblast assay results. It is unclear why this was the case when several relationships were identified between the putamen and fibroblast suggested impaired mitophagy in a subgroup of PD. The midbrain has a much higher proportion of glial cell types to neurons compared to the striatum.<sup>303</sup> Therefore oxidative phosphorylation specific changes may be more readily seen in the striatum where there are a greater proportion of metabolically active neurons.

We undertook the first comparison of *in vivo* measures of bioenergetic dysfunction in the central nervous system with *in vitro* assessment of mitochondrial function and morphology in peripheral tissue of PD patients and controls. We consistently observed correlations between <sup>31</sup>P-MRS metabolites and key aspects of mitochondrial function or morphology (as well as respective changes in the number of lysosomes) highly suggestive of impaired mitophagy in PD.

There is strong evidence of impaired mitophagy in PD patient tissue, including post-mortem studies but also previous work undertaken in sporadic PD fibroblasts.<sup>74,304</sup> Impaired mitophagy may be due to the impairment of signalling mitochondria for degradation as seen in *PINK1/parkin* related PD.<sup>305</sup> Alternatively, it may be further downstream where impaired lysosomal function could reduce the clearance of damaged mitochondria. Lysosomal dysfunction is well recognised in both sporadic PD and GBA-PD.<sup>52,76,293</sup> PINK1/Parkin mediated mitophagy increases the transcription factors Nrf2 and TFEB and promotes both mitochondrial and lysosomal biogenesis, further supporting our observation of increased lysosomes and mitochondria being related to the induction of mitophagy.<sup>300</sup>

The correlation of higher ATP with lower MMP in the PD peripheral tissue may reflect mitochondrial uncoupling. Mitochondrial uncoupling can paradoxically lead to greater concentrations of ATP and increased mitochondrial biogenesis.<sup>46</sup> Mitochondrial uncoupling also induces mitophagy.<sup>299,306</sup>

Our study has several limitations. The <sup>31</sup>P-MRS signal captured from a voxel is reflective of the underlying tissue composition and therefore a degree of spectroscopic signal derived will be from non-neuronal cell types, such as astrocytes and microglia rather than specific for neuronal tissue. Similarly, changes in <sup>31</sup>P-MRS bioenergetic parameters such as ATP and Pi are not specific to oxidative phosphorylation in <sup>31</sup>P-MRS as glycolysis may contribute to ATP production, particularly in resting protocols. Furthermore, the patient-derived tissue assessed in this study is non-neuronal which limits direct correlations with <sup>31</sup>P-MRS imaging-based results. Nonetheless, our results suggest that the two techniques provide complementary perspectives on bioenergetic pathways and related mechanisms in PD.

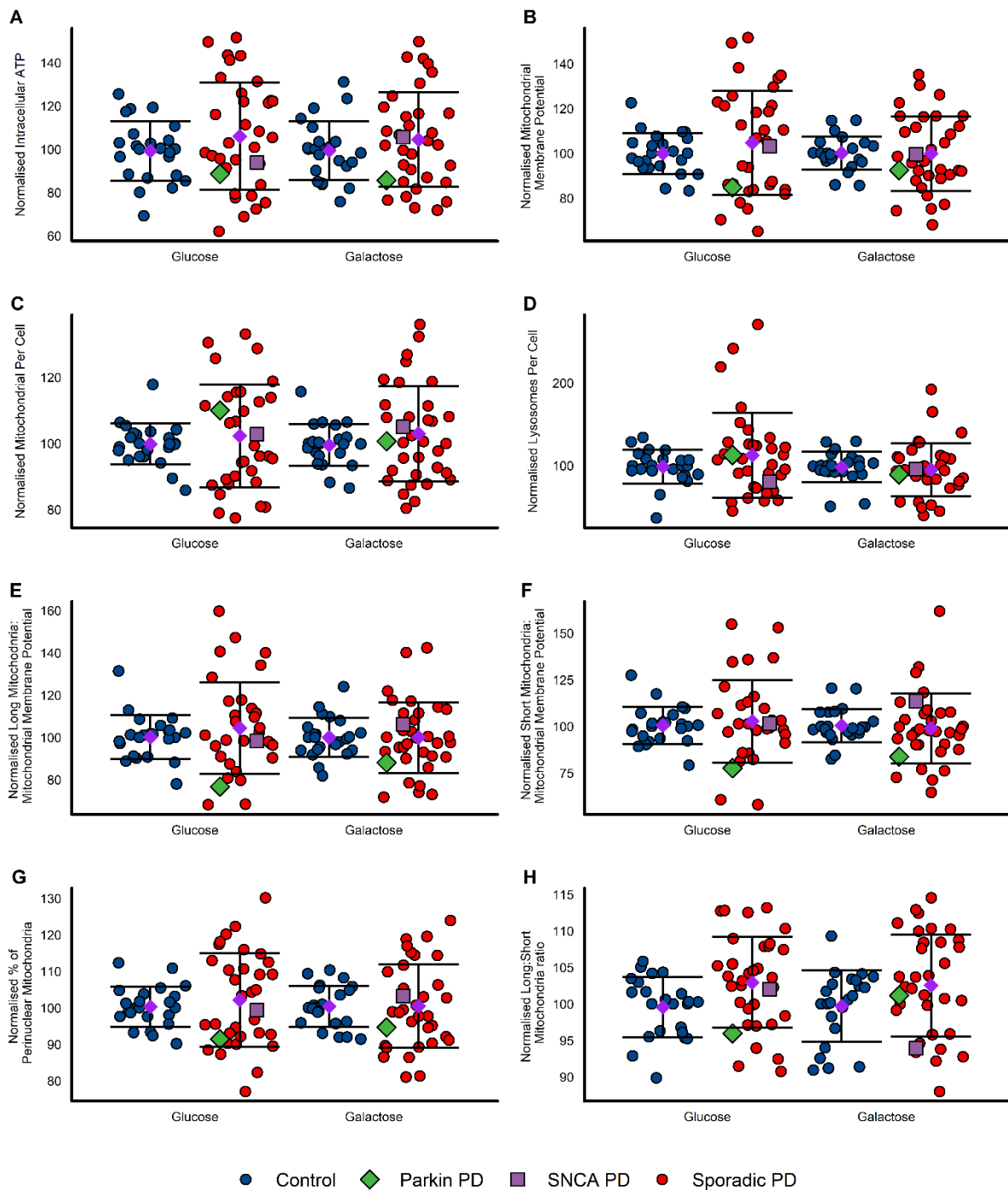
Of note, there was no clear change in the data when assessed in galactose (glucose-free) media. This is somewhat unexpected as galactose media forces fibroblasts to rely on oxidative phosphorylation as their primary source of ATP production by limiting ATP production through glycolysis. It would therefore be expected that any mitochondrial deficits in PD would be worsened in galactose media. This was not what we observed and may reflect the low bioenergetic demands of fibroblasts. Alternatively, the establishment of these fibroblast lines from skin biopsies in relatively

low glucose conditions may contribute to them already predominantly relying upon oxidative phosphorylation for ATP production.

In conclusion, our study provides early support that combined  $^{31}\text{P}$ -MRS and fibroblast analysis may facilitate mechanistic stratification for future disease modifying trials assessing compounds with a putative rescue effect on mitophagy and enrich future trials for PD patients with more aggressive disease progression.

Future work is required to elucidate longitudinal changes of  $^{31}\text{P}$ -MRS measures in PD and their possible correlation with clinical progression over time and explore the underlying mechanisms of impaired mitophagy in sporadic PD.

## Supplementary Figures



### Supplementary Figure 4.1: Fibroblast assay results in each media type.

Results of fibroblast assays between groups and media types. All values are normalised to the control mean in glucose. Mean (purple diamond) and standard deviation (error bars) shown. All data points are the mean of triplicate assay repeats for a single participant. A) Intracellular ATP, B) mitochondrial membrane potential, C) mitochondrial count per cell, D) lysosomal count per cell, E) mitochondrial membrane potential in long mitochondria only, F) mitochondrial membrane potential in short mitochondria only, G) percentage of mitochondria

*localised to the perinuclear region (an area associated with autophagy), H) Ratio of long:short mitochondria count. All fibroblast assays repeated in triplicate.*

**END OF CHAPTER MANUSCRIPT**

## Chapter 5: Longitudinal assessment of <sup>31</sup>P magnetic resonance spectroscopy and relationships to clinical progression

### Introduction to chapter

In this chapter the characterisation of <sup>31</sup>P-MRS in PD discussed in Chapter 4 is now examined in a longitudinal study using the same study cohort and acquisition protocol. This is the first ever longitudinal study of <sup>31</sup>P-MRS in PD and has an average follow-up time of around 2.5 years, which is substantial when compared to longitudinal <sup>31</sup>P-MRS studies across other diseases.

This study utilises a two-step approach towards characterising the longitudinal changes of <sup>31</sup>P-MRS in PD. First, a mixed-effect two-way ANOVA is used to identify changes in <sup>31</sup>P-MRS metabolites across groups and/or visits, with appropriate post-hoc tests comparing groups. Subsequently, only those metabolites identified in this analysis were taken forward to assess for clinically relevant relationships with common clinical scales. This approach identifies abnormalities within the putamen regarding phospholipid metabolism. In addition, the relationship between midbrain PCr and increased risk of rapid disease progression identified earlier is explored further and a clear relationship between longitudinal changes in midbrain PCr and semantic fluency is identified.

The manuscript that forms the focus of this chapter is currently in preparation for submission.

### Contributions to paper

I was responsible for the recruitment, consenting and clinical assessment of all participants. I was responsible for the spectroscopic analysis of all <sup>31</sup>P-MRS data. I performed all statistical analyses on <sup>31</sup>P-MRS and clinical data under the guidance of a statistician associated with the project (co-author Miss Rosie Taylor). I drafted all sections of the manuscript under the guidance of my primary supervisor (and co-author Professor Oliver Bandmann).

### Paper in preparation for submission

This manuscript is currently intended to be submitted to *Movement Disorders*, as such it is formatted and written to fulfil the submission requirements.

# **Longitudinal <sup>31</sup>P Phosphorus Magnetic Resonance Spectroscopy in Parkinson's Disease reveals altered phospholipid metabolism and a relationship between midbrain bioenergetics and semantic fluency**

Thomas Payne,<sup>1</sup> Rosie Taylor,<sup>2</sup> Li Su,<sup>1,3</sup> Thomas Jenkins,<sup>1,4</sup> Oliver Bandmann<sup>1</sup>

## **Author affiliations:**

<sup>1</sup>Sheffield Institute for Translational Neuroscience, University of Sheffield, Sheffield, S10 2HQ, United Kingdom

<sup>2</sup>Statistical Services Unit, The University of Sheffield, Sheffield, S3 7RH, United Kingdom

<sup>3</sup>Department of Psychiatry, University of Cambridge CB2 0SP, United Kingdom

<sup>4</sup>Royal Perth Hospital, Victoria Square, Perth, WA6000, Australia

## Abstract

**Background:** Parkinson's Disease (PD) is a pathogenically heterogeneous disorder with strong evidence for mitochondrial dysfunction as one such key mechanism. <sup>31</sup>P Magnetic Resonance Spectroscopy (<sup>31</sup>P-MRS) allows the assessment of key bioenergetic metabolites such as ATP and metabolites associated with both phospholipid synthesis (phosphomonoesters, PME) and breakdown (phosphodiesteres, PDE). The PME/PDE ratio reflects overall phospholipid membrane turnover.

**Objectives:** The key aims of our study were to undertake the first <sup>31</sup>P-MRS longitudinal study in PD and assess the temporal relationship between <sup>31</sup>P-MRS and clinical progression.

**Methods:** 19 participants with PD and 11 healthy controls underwent two <sup>31</sup>P-MRS scans approximately 30 months apart. <sup>31</sup>P-MRS used 2D chemical shift imaging to assess ATP, phosphocreatine (PCr), inorganic phosphate (Pi), PME and PDE in both the putamen and midbrain. Clinical assessments included the Movement Disorders Society Unified Parkinson's Disease Rating Scale Part III (MDS-UPDRS III), semantic fluency and non-motor symptom scale (NMSS).

**Results:** In the posterior putamen contralateral to the worst clinically affected side the PME/PDE ratio was elevated at baseline in PD compared to controls and significantly reduced at follow-up compared to both baseline PD values and follow-up healthy control values. In PD, there was a significant deterioration from baseline to follow-up in semantic fluency. Deteriorating semantic fluency in PD correlated with higher PCr values in the midbrain.

**Conclusions:** The observed changes in phospholipid metabolism may represent underlying neurodegenerative cell loss but requires further investigation given the limitations of our study. Relationships between PCr and semantic fluency warrant further investigation to determine if <sup>31</sup>P-MRS can predict cognitive impairment in PD.

## Introduction

Parkinson's disease (PD) is an incurable neurodegenerative disease for which there are no disease modifying therapies.<sup>307</sup> It continues to increase in global prevalence, with 6.1million people globally affected in 2016 compared to 2.5million in 1990, with age-standardised rates increasing by 21.7% during this interval.<sup>9</sup>

PD demonstrates both clinical and pathogenic heterogeneity which has likely contributed to the failure of many neuroprotective trials in PD. Mitochondrial dysfunction is well recognised in both sporadic and genetic PD.<sup>308</sup>

<sup>31</sup>P-MRS allows the *in vivo* quantification of brain bioenergetics in pathologically relevant areas of the brain by assessing relevant metabolites such as adenosine triphosphate (ATP), inorganic phosphate (Pi) and phosphocreatine (PCr).<sup>295</sup> It also allows the measurement of phosphomonoesters (PME) and phosphodiesteres (PDE) which reflect phospholipid membrane metabolism with PME representing phospholipid membrane precursors (i.e., synthesis) and PDE representing metabolites of phospholipid membrane breakdown.

Our previous work demonstrated a much broader variance of <sup>31</sup>P-MRS parameters such as ATP in the midbrain of PD patients compared to controls. Further, midbrain PCr demonstrated a positive correlation with predicted risk of rapid disease progression.<sup>309</sup> The predicted risk of disease progression is a validated score that uses semantic fluency, age and the Unified Parkinson's Disease Rating Scale (UPDRS) Axial sub-score to calculate the risk of either dementia or postural instability at 5 years.<sup>17</sup>

Currently, there is no observational longitudinal data on <sup>31</sup>P-MRS in PD. Assessing the longitudinal changes of <sup>31</sup>P-MRS within the natural history of PD and their relationship to clinical progression will facilitate the adaptation of <sup>31</sup>P-MRS into future neuroprotective trials. This could be particularly relevant to any trials assessing putative neuroprotective compounds targeting bioenergetic dysfunction and/or wishing to identify PD patients with a poor prognosis.

Here we present the first longitudinal study of <sup>31</sup>P-MRS in PD. Our aims were: (1) to determine if longitudinal changes in <sup>31</sup>P-MRS parameters differ between PD and

healthy controls; (2) to assess if longitudinal changes in  $^{31}\text{P}$ -MRS are associated with changes in clinical disease progression.

## Methods

### Recruitment

19 participants with recent onset PD ( $\leq 3$  years from a diagnosis made by a movement disorders specialist according to the Queen Square Brain Bank Criteria) and 11 healthy volunteers who had previously participated in the aforementioned cross-sectional study were invited to return for a further clinical assessment and follow-up  $^{31}\text{P}$ -MRS scan at  $> 2$  years following their baseline assessment.<sup>12</sup> All participants provided written informed consent. The study was reviewed by the regional Research Ethics Committee (REC 18/NW/0328). Genetic analysis has previously been undertaken in this cohort.<sup>309</sup>

### Clinical Assessment

The following clinical rating scales were performed on all participants with PD at both baseline and follow-up whilst on dopaminergic medication: Modified Hoehn & Yahr Staging, Movement Disorders Society-Unified Parkinson's Disease Rating Scale Part 3 (MDS-UPDRS-III), quantification of daily total levodopa equivalent dose (LED) and Movement Disorders Society Non-Motor Symptom Scale (MDS-NMSS).<sup>117,122,124,211</sup> At baseline all participants had undergone the calculation of the predictive risk of rapid disease progression described above. Semantic fluency (number of animals named in one minute) and the UPDRS axial sub-score are key components for this score and assessed at both visits.<sup>17</sup>

Healthy volunteers underwent a neurological history and examination to exclude the development of any neurological disease between visits.

### $^{31}\text{P}$ Phosphorus Magnetic Resonance Spectroscopy

All participants underwent a further  $^{31}\text{P}$ -MRS scan as previously reported, using the identical acquisition protocol.<sup>309</sup> In brief, 2D chemical shift imaging (CSI) was obtained using in-vivo selected *in vivo* spectroscopy (ISIS) in two separate acquisitions. All CSI sequences had acquired voxel sizes of  $40 \times 40 \times 20 \text{mm}^3$ , used adiabatic pulses, a second order pencil-beam shim and WALTZ-4 broadband heteronuclear decoupling with nuclear Overhauser effect. One acquisition was aligned to capture both putamen with one voxel for each of the anterior and posterior putamen using a  $12 \times 12$  reconstruction matrix for a reconstructed voxel size of  $17.5 \times 17.5 \times 20 \text{mm}^3$ . The second

acquisition aligned to the midbrain was placed to ensure that the substantia nigra was contained within the voxel of interest. This used a reconstruction matrix of 14x14 for a voxel size of 15x15x20mm<sup>3</sup>. Repetition time (TR) was 4000ms and echo time (TE) was 0.22ms. In total there were six voxels analysed left midbrain, right midbrain, left posterior putamen, left anterior putamen, right posterior putamen and right anterior putamen.

Consistent voxel placement across visits was guided by a T2-weighted spin-echo image to align voxels along the same anatomical landmarks as used in the baseline acquisition. Partial volume effects were quantified T1 weighted imaging as previously described.<sup>309</sup>

Spectra were processed as previously described and signal fitting was performed in the time domain using jMRUI software V5.2 (<http://www.jmrui.eu>) and the Advanced Method for Accurate, Robust and Efficient Spectral fitting (AMARES) algorithm to determine the relative area under each peak.<sup>183,259,309</sup> This fit thirteen total resonances, seven represented by the multiplets of  $\gamma$ -ATP,  $\alpha$ -ATP and  $\beta$ -ATP and a further six representing phosphoethanolamine (PE), phosphocholine (PC), glycerophosphoethanolamine (GPE), glycerophosphocholine (GPC), inorganic phosphate (Pi) and phosphocreatine (PCr). All amplitudes were normalised to the total phosphorus signal detected prior to any statistical analyses. PME were defined as the sum of the amplitudes of PE and PC. PDE were defined as the sum of the amplitudes of GPE and GPC. Total ATP was defined as the sum of all ATP resonances. PME/PDE, PCr/ATP, Pi/PCr and Pi/ATP ratios were calculated using the raw amplitudes (i.e. non-normalised) within each voxel prior to any statistical analysis. All spectra were visually inspected for fit and any clearly spurious data excluded according to previously published quality control consensus criteria.<sup>217</sup>

### **Statistical analyses**

Differences in demographics between groups were tested using a t-test with Welch's correction for continuous data and chi-squared test for categorical or non-normally distributed data. Longitudinal changes in continuous clinical measures (MDS-UPDRS III, LED, MDS-NMSS and semantic fluency) were analysed using paired t-tests.

<sup>31</sup>P-MRS parameters of interest for longitudinal analysis were determined *a priori* as total levels of ATP, Pi, PCr, PME, PDE and the ratios of PME/PDE, PCr/ATP, Pi/PCr

and Pi/ATP. Voxels were combined to derive mean values of the midbrain, posterior putamen and anterior putamen. The ratio measures were chosen to infer further bioenergetic relationships. A raised Pi/ATP ratio reflects impaired oxidative phosphorylation.<sup>295</sup> Both PCr/ATP and Pi/PCr have been used widely in the assessment of muscle bioenergetics, particularly in dynamic testing protocols where reduced PCr/ATP ratios and elevated Pi/PCr ratios infer an over-reliance of the creatine-phosphocreatine buffer to maintain ATP levels.<sup>296</sup>

A mixed effects two-way ANOVA was used to assess for differences in each <sup>31</sup>P-MRS parameter in each anatomical location between groups and timepoints (baseline and follow-up) with the individual participant as a random effect. For any models not meeting the assumption of sphericity a Greenhouse-Geisser sphericity correction was applied. For any statistically significant ANOVA results post-hoc pairwise t-tests were performed with *p*-values controlled using a false discovery rate and alpha of 0.05. This assessed for differences between groups at each timepoint (unpaired t-test) and for differences within groups between timepoints (paired t-test).

Any significant <sup>31</sup>P-MRS parameters emerging from the above analysis were then further explored for clinical relevance, by entering into a mixed effects linear model. Clinical parameters (MDS-UPDRS III score, UPDRS axial sub-score, semantic fluency and MDS-NMSS) were specified as the response variable and timepoint, age, sex and the <sup>31</sup>P-MRS parameter of interest entered as fixed effect predictor variables. Differences in <sup>31</sup>P-MRS ATP between sexes has been observed in PD and PCr has been observed to increase with age in the healthy brain<sup>193,228</sup> For random effects, an intercept was modelled for each participant. For the assessment of MDS-UPDRS scores, LED was an additional fixed effect predictor as the symptomatic effect of dopaminergic medication may influence MDS-UPDRS scores. Estimated effect sizes, confidence intervals and associated *p* values were reported; *p*<0.05 was considered significant.

We previously reported that increased mean midbrain PCr correlated with a higher predicted risk of more aggressive PD progression.<sup>309</sup> Longitudinal measurements of midbrain PCr were therefore assessed for their relationship to the UPDRS axial sub-score and semantic fluency, given their use in the predicted model detailed previously. Greater axial involvement has consistently been linked with both a poorer prognosis

and postural instability in PD.<sup>121,310</sup> Poorer semantic fluency has consistently been linked with the development of cognitive impairment in PD.<sup>311,312</sup> This was done using the same mixed effects linear model described above. If either clinical component demonstrated a significant relationship a further post-hoc analysis was performed to determine if both baseline and longitudinal change in the <sup>31</sup>P-MRS measure correlated with the respective change in the clinical component.

Effects of partial volume were assessed using Pearson's correlation coefficient of the <sup>31</sup>P-MRS parameters of interest with the proportion of grey-matter in the putaminal voxels and with the proportion of brain (grey and white matter combined) in the midbrain voxels. Partial volume effects were assessed separately to limit the number of covariates and complexity of the mixed-effects models with respect to sample size. Any significant relationships identified were incorporated into these models.

All statistical analyses were completed in R version 4.1.0.

## Results

Demographic features of the cohort are summarised in **Table 5.1**. The  $^{31}\text{P}$ -MRS data for one participant with PD was excluded from analysis due to particularly poor signal-to-noise ratio and poor-quality baseline which was attributed to movement artefact confirmed on T2 and T1 weighted imaging. This left a full dataset of 18 participants with PD and 11 healthy volunteers. Summary descriptive statistics for clinical assessments are shown in **Table 5.2**. No participants had any pathogenic mutations in any *PARK* genes or pathogenic *GBA* variants.

There were no significant correlations between partial volume measures and any  $^{31}\text{P}$ -MRS parameters of interest in any voxels (data not shown), partial volume effects were not included as a covariate in any models.

			PD (n=19)	Controls (n=11)	p-value
Age (years) at enrolment	Mean $\pm$ SD		62.3 $\pm$ 9.7	66.7 $\pm$ 9.2	0.2281 <sup>a</sup>
	Range		50 – 82	52 - 81	
Sex	Male (%)		10 (53%)	3/11 (27%)	0.3328 <sup>b</sup>
	Female (%)		9 (47%)	8/11 (73%)	
Follow-up (months) interval	Mean $\pm$ SD		26.0 $\pm$ 2.2	28.6 $\pm$ 2.1	0.2234 <sup>b</sup>
	Range		22 – 30	24 - 31	
Predicted risk of rapid disease progression	Mean $\pm$ SD		0.46 $\pm$ 0.27	NA	NA
	Range		0.07 – 0.91	NA	

**Table 5.1: Demographic features of the study cohort.**

*There were no significant differences between age, sex or follow-up interval between patients and controls. <sup>a</sup>differences between groups assessed with t-test <sup>b</sup>differences between groups assessed with chi-squared test*

		<b>Baseline</b>	<b>Follow-up</b>	<b>Change</b>	<b>p-value</b>
Disease duration (months)	Mean $\pm$ SD	13.4 $\pm$ 8.5	42.6 $\pm$ 9.6	29.1 $\pm$ 2.7	NA
	Range	2 - 32	32 - 63	23 - 33	
NMSS	Mean $\pm$ SD	42.1 $\pm$ 35.1	37.6 $\pm$ 27.5	-6.4 $\pm$ 23.8	ns
	Range	10 - 119	0-118	-79 - 26	
Semantic fluency	Mean $\pm$ SD	20.8 $\pm$ 7.1	18.2 $\pm$ 5.5	-3.0 $\pm$ 3.4	p=0.0017
	Range	6 - 32	8 - 29	-8 - 3	
MDS-UPDRS III	Mean $\pm$ SD	35.7 $\pm$ 10.3	33.2 $\pm$ 10.9	-2.8 $\pm$ 9.7	ns
	Range	15 - 54	12 - 53	-22 - 14	
MDS-UPDRS Axial	Mean $\pm$ SD	2.9 $\pm$ 1.5	3.2 $\pm$ 1.5	0.1 $\pm$ 1.6	NA
	Range	1 - 6	1 - 6	-2 - 4	
LED (mg)	Mean $\pm$ SD	347 $\pm$ 277	610 $\pm$ 235	255 $\pm$ 188	p<0.0001
	Range	0 - 1000	299 - 1100	100 - 800	
mH&Y	Median	2	2	0	NA
	Range	1.5 - 2.5	1.5 - 2.5	-0.5 - 0.5	

**Table 5.2: Clinical features of participants with PD.**

mH&Y = modified Hoehn & Yahr stage, LED = levodopa equivalent daily dosage, NMSS = Non-motor symptoms scale, MDS-UPDRS = Movement Disorders society Unified Parkinson's Disease Rating Scale. Changes from baseline to follow-up in continuous clinical measures were tested with a paired t-test.

<sup>31</sup>P-MRS results at each visit are summarised in **Table 5.3**. Graphs of key metabolites of the primary <sup>31</sup>P-MRS parameters of interest in the mean posterior putamen at baseline and follow-up are shown in **Figure 5.1**. Individual changes in participants across all <sup>31</sup>P-MRS parameters in the mean posterior putamen are shown in **Figure 5.2**. There were no differences in posterior putamen ATP, Pi, PCr (**Fig. 5.1A-C, Fig. 5.2A-C**) or the ratios of PCr/ATP, Pi/PCr or Pi/ATP (**Fig. 5.2G-I**).

<b>Mean Midbrain</b>		<b>Baseline</b>	<b>Follow-up</b>	<b>Change</b>
Total ATP	Controls	0.419 ± 0.020	0.413 ± 0.049	-0.006 ± 0.058
	PD	0.429 ± 0.066	0.436 ± 0.069	0.007 ± 0.101
PCr	Controls	0.194 ± 0.021	0.185 ± 0.026	-0.010 ± 0.032
	PD	0.194 ± 0.026	0.193 ± 0.021	0.000 ± 0.036
Pi	Controls	0.092 ± 0.022	0.093 ± 0.026	0.001 ± 0.029
	PD	0.092 ± 0.026	0.076 ± 0.029	-0.015 ± 0.035
PME	Controls	0.139 ± 0.022	0.160 ± 0.043	0.020 ± 0.051
	PD	0.146 ± 0.039	0.142 ± 0.032	-0.004 ± 0.060
PDE	Controls	0.146 ± 0.037	0.138 ± 0.029	-0.008 ± 0.045
	PD	0.129 ± 0.036	0.142 ± 0.033	0.013 ± 0.043
PME/PDE ratio	Controls	1.100 ± 0.664	1.186 ± 0.303	0.085 ± 0.791
	PD	1.203 ± 0.449	1.040 ± 0.324	-0.162 ± 0.591
PCr/ATP ratio	Controls	0.465 ± 0.051	0.453 ± 0.083	-0.012 ± 0.080
	PD	0.463 ± 0.098	0.460 ± 0.125	-0.003 ± 0.172
Pi/PCr ratio	Controls	0.481 ± 0.137	0.512 ± 0.171	0.031 ± 0.209
	PD	0.486 ± 0.173	0.395 ± 0.135	-0.091 ± 0.213
Pi/ATP ratio	Controls	0.222 ± 0.061	0.231 ± 0.079	0.009 ± 0.097
	PD	0.224 ± 0.085	0.187 ± 0.093	-0.037 ± 0.120
<b>Mean posterior putamen</b>				
Total ATP	Controls	0.460 ± 0.039	0.438 ± 0.049	-0.021 ± 0.075
	PD	0.429 ± 0.037	0.451 ± 0.038	0.022 ± 0.057
PCr	Controls	0.194 ± 0.020	0.194 ± 0.020	0.001 ± 0.027
	PD	0.199 ± 0.016	0.198 ± 0.018	-0.001 ± 0.024
Pi	Controls	0.083 ± 0.012	0.088 ± 0.024	0.005 ± 0.030
	PD	0.094 ± 0.023	0.085 ± 0.019	-0.009 ± 0.023
PME	Controls	0.122 ± 0.022	0.145 ± 0.022	0.023 ± 0.033
	PD	0.142 ± 0.020	0.127 ± 0.03	-0.015 ± 0.036
PDE	Controls	0.133 ± 0.030	0.123 ± 0.027	-0.010 ± 0.049
	PD	0.128 ± 0.029	0.129 ± 0.024	0.001 ± 0.038
PME/PDE ratio	Controls	0.939 ± 0.243	1.189 ± 0.279	0.250 ± 0.442
	PD	1.131 ± 0.242	0.981 ± 0.277	-0.150 ± 0.363
PCr/ATP ratio	Controls	0.425 ± 0.057	0.451 ± 0.063	0.026 ± 0.087
	PD	0.469 ± 0.051	0.444 ± 0.052	-0.025 ± 0.074
Pi/PCr ratio	Controls	0.439 ± 0.085	0.469 ± 0.172	0.030 ± 0.188
	PD	0.477 ± 0.120	0.435 ± 0.109	-0.041 ± 0.138
Pi/ATP ratio	Controls	0.184 ± 0.034	0.211 ± 0.074	0.027 ± 0.099
	PD	0.225 ± 0.068	0.191 ± 0.044	-0.035 ± 0.067
<b>Mean anterior putamen</b>				
Total ATP	Controls	0.437 ± 0.044	0.414 ± 0.065	-0.023 ± 0.087
	PD	0.424 ± 0.041	0.428 ± 0.047	0.004 ± 0.061
PCr	Controls	0.202 ± 0.018	0.210 ± 0.017	0.008 ± 0.020
	PD	0.206 ± 0.021	0.211 ± 0.029	0.005 ± 0.036
Pi	Controls	0.085 ± 0.014	0.085 ± 0.029	0.000 ± 0.032
	PD	0.093 ± 0.028	0.085 ± 0.028	-0.009 ± 0.039
PME	Controls	0.127 ± 0.027	0.143 ± 0.045	0.017 ± 0.047
	PD	0.130 ± 0.027	0.126 ± 0.042	-0.004 ± 0.056
PDE	Controls	0.138 ± 0.037	0.135 ± 0.031	-0.003 ± 0.061
	PD	0.138 ± 0.073	0.139 ± 0.036	0.001 ± 0.043
PME/PDE ratio	Controls	0.973 ± 0.327	1.123 ± 0.528	0.150 ± 0.675
	PD	0.966 ± 0.256	0.986 ± 0.465	-0.162 ± 0.591
PCr/ATP ratio	Controls	0.467 ± 0.051	0.518 ± 0.090	0.052 ± 0.106
	PD	0.494 ± 0.072	0.498 ± 0.071	0.004 ± 0.096
Pi/PCr ratio	Controls	0.432 ± 0.103	0.410 ± 0.148	-0.022 ± 0.165
	PD	0.458 ± 0.146	0.409 ± 0.140	-0.049 ± 0.198
Pi/ATP ratio	Controls	0.199 ± 0.047	0.218 ± 0.097	0.019 ± 0.113
	PD	0.227 ± 0.082	0.200 ± 0.068	-0.027 ± 0.097

**Table 5.3: Summary of key <sup>31</sup>P-MRS parameters in the mean midbrain, mean posterior putamen and mean anterior putamen.**

*Mean ± standard deviation presented. Controls n = 11, PD n=18 unless otherwise specified. ATP= Adenosine triphosphate, PCr=phosphocreatine, Pi=inorganic phosphate, PME=phosphomonoesters, PDE = phosphosphodiester*

A mixed two-way ANOVA revealed a significant interaction between disease group and time point in the mean posterior putamen for both PME (**Fig. 5.1D**,  $F = 7.981$ ,  $p=0.009$ ) and the PME/PDE ratio. PME was increased at baseline in participants with PD compared to controls (mean difference = 0.020, 95%CI 0.002 - 0.037,  $p=0.022$ ). There was an unexpected increase in PME in controls from baseline to follow-up (mean change = 0.023, 95% CI 0.01 – 0.05,  $p=0.044$ ) but no change in PD patients from baseline to follow-up. This rise in controls was consistent across the control group with 10/11 showing a clear rise in PME (**Fig. 5.2D**).

PME/PDE ratio was increased at baseline in PD compared to controls (mean difference=0.192, 95%CI 0.002 – 0.385,  $p=0.0486$ ). There were non-significant trends for PME/PDE to reduce in PD ( $p=0.098$ ) and increase in controls ( $p=0.09$ ) from baseline to follow-up. At follow-up there was a trend for PD to have lower PME/PDE ratios compared to controls ( $p=0.061$ ). Again these changes appeared relatively consistent across the groups with 8/11 controls demonstrating an increase in PME/PDE ratio and 11/18 PD participants showing a reduction in PME/PDE ratio (**Fig. 5.2F**). There were no changes in mean posterior putamen PDE seen between groups or time points (**Fig. 5.1E**).

Mean posterior putamen PME and PME/PDE ratio were therefore assessed for their relationship to clinical progression. Linear mixed effects models revealed no relationship between these measures and any of the clinical parameters assessed (MDS-UPDRS III score, UPDRS axial sub-score, semantic fluency and MDS-NMSS).

PD is an asymmetrical disorder and as a further post-hoc exploratory analysis it was assessed if the trends seen in PME/PDE ratio in PD were more prominent in the putaminal voxel contralateral to the worst clinically affected side. These values were compared to mean posterior putamen values in healthy controls. Mixed two-way ANOVA revealed a significant interaction between disease group and timepoint for the contralateral putaminal PME/PDE ratio (**Fig. 5.1F**,  $F = 11.27$ ,  $p=0.002$ ). Pairwise

comparisons revealed higher PME/PDE ratio in PD at baseline (mean difference=0.292, 95% CI 0.048, 0.537,  $p=0.038$ ) but lower PME/PDE ratio at follow-up compared to controls (mean difference= -0.273, 95%CI -0.496, -0.051,  $p=0.017$ ). PME/PDE ratios reduced from baseline to follow-up in PD only (mean-difference=-0.315, 95%CI -0.534, -0.097,  $p=0.007$ ).

In PD patients there was a significant reduction in semantic fluency from baseline to follow-up (mean change= -3.0, 95%CI -1.3, -4.7,  $p=0.0017$ ). There was also a significant increase in LED from baseline to follow-up, as expected in the natural history of PD (mean change=254mg, 95%CI 158mg, 351mg,  $p<0.0001$ ). There were no other changes in clinical assessments.

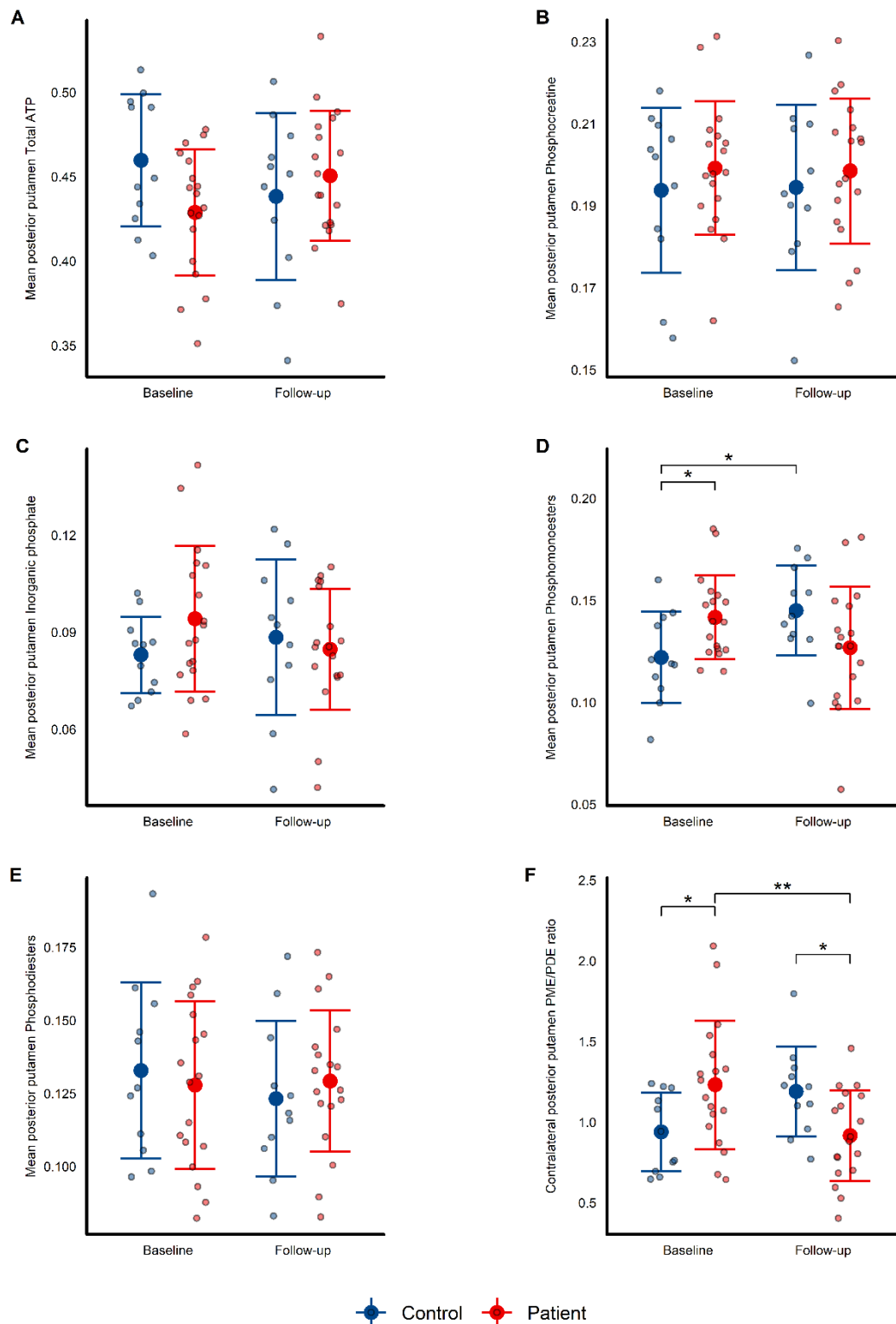


**Figure 5.1: Key <sup>31</sup>P-MRS spectroscopy at each time point and by disease group.**

A) mean posterior putamen ATP, B) mean posterior putamen phosphocreatine, C) mean posterior putamen inorganic phosphate, D) mean posterior putamen phosphomonoesters (PME), E) mean posterior putamen phosphodiester (PDE), F) ratio of PME to PDE in the contralateral putamen to the worst clinically affected side in PD compared to mean posterior putamen values in healthy controls. Between group differences tested with unpaired t-test,

between timepoint differences tested with paired *t*-test. *P*-values adjusted for false discovery rate. PME=phosphomonoesters, PDE=phosphodiesters. Statistical significance: \* $<0.05$ , \*\* $<0.01$

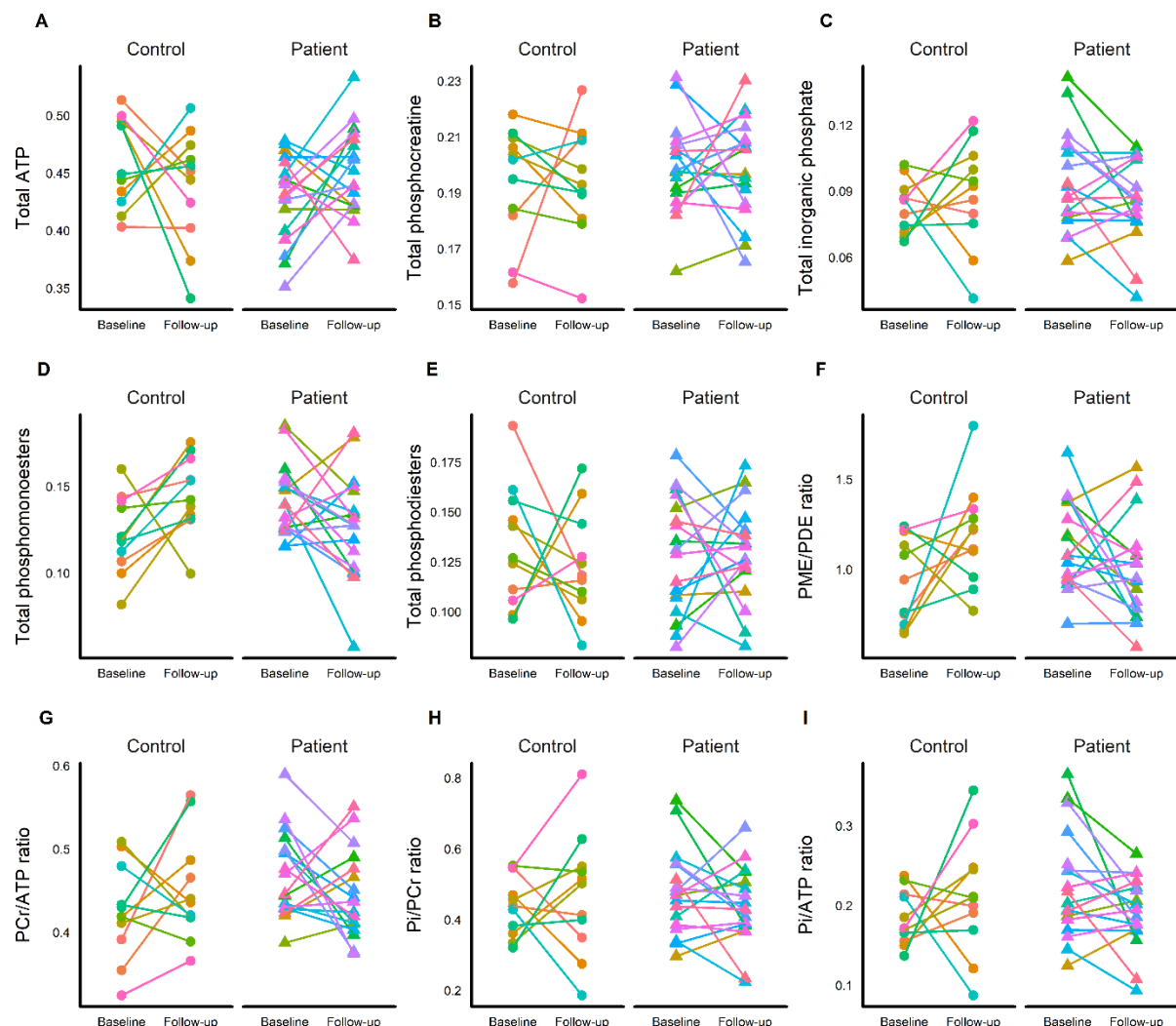


**Figure 5.2: Change in each individual across all key  $^{31}\text{P}$ -MRS parameters in the mean posterior putamen.**

Each participant is denoted by a different colour. A) Total ATP, B) total phosphocreatine, C) total inorganic phosphate, D) total phosphomonoesters, E) total phosphodiesters, F) phosphomonoester (PME)/phosphodiester (PDE) ratio, G) phosphocreatine (PCr)/ATP ratio, H) inorganic phosphate (Pi)/PCr ratio and I) Pi/ATP ratio.

There were no differences between PD patients and controls for ATP, Pi, PCr, PME, PDE or the PME/PDE, PCr/ATP, Pi/PCr and Pi/ATP ratios in either the midbrain (**Figure 5.3**) or anterior putamen as analysed using two-way ANOVA. This is in contrast to the mean posterior putamen. The distribution of the bioenergetics parameters in the midbrain remains similar between groups and appears stable across time points.

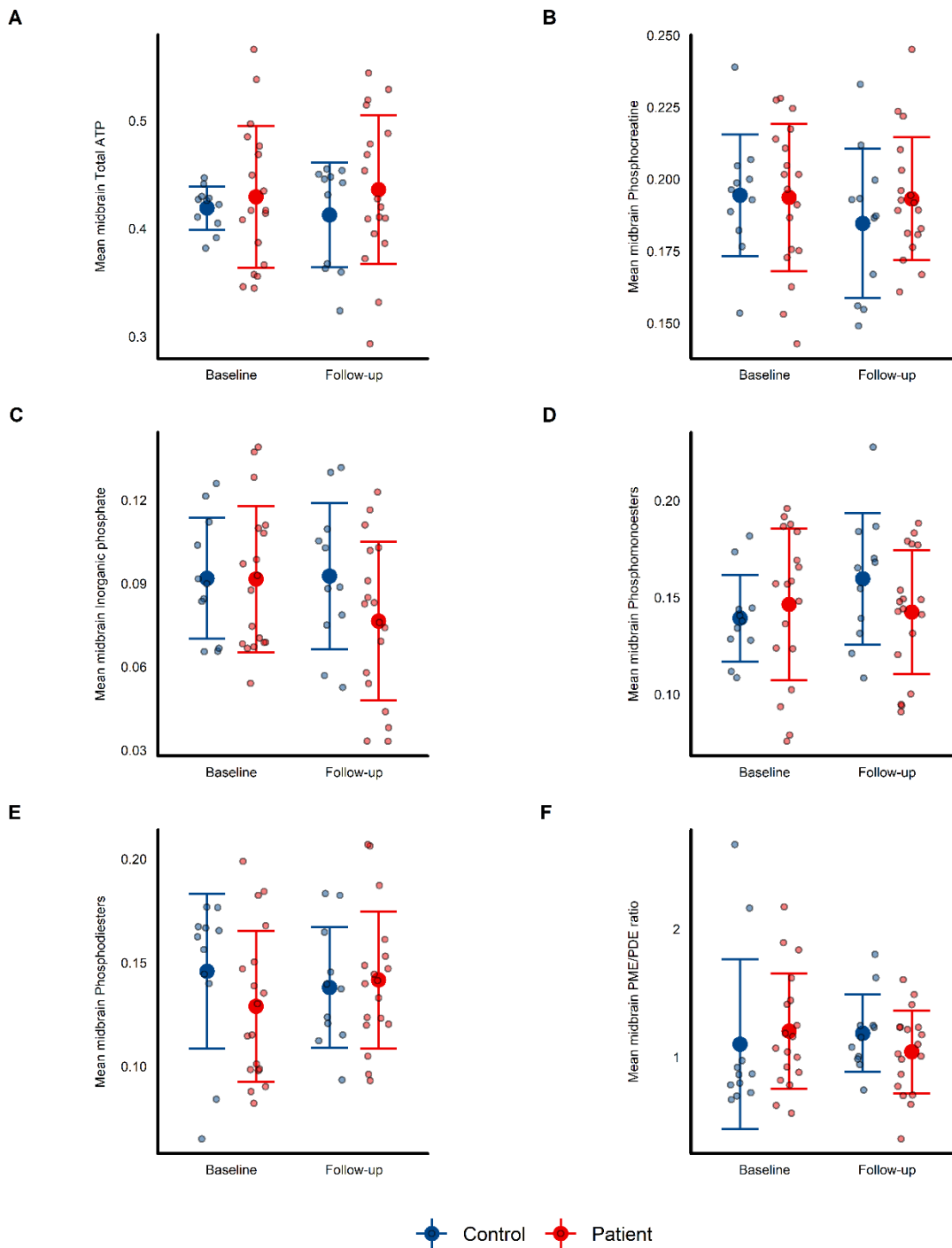


**Figure 5.3: <sup>31</sup>P-MRS midbrain bioenergetics and phospholipid measures at baseline and follow-up.**

Mean (large, coloured circle) and standard deviation (error bars) shown. All values are normalised to the total phosphorus signal within the voxel with the exception of the PME/PDE ratio. (A) Mean midbrain ATP; (B) mean midbrain phosphocreatine; (C) mean midbrain inorganic phosphate; (D) mean midbrain phosphomonoesters (PME); (E) mean midbrain phosphodiesteres (PDE); (F) mean midbrain PME/PDE ratio. Differences between groups

assessed using a two-way mixed effect ANOVA, pairwise comparisons only shown if this was significant.

The mixed effects linear model assessing semantic fluency and mean midbrain PCr across visits revealed that midbrain PCr was associated with semantic fluency (estimated effect = -62.70, 95%CI -98.59, -28.01,  $p=0.003$ ). To determine these relationships further a post-hoc assessment with Pearson's correlation coefficient was performed and unexpectedly revealed that higher baseline midbrain PCr correlated with less deterioration in semantic fluency (**Fig. 5.4A**,  $r=0.48$ ,  $p=0.0434$ ). However, as would be expected with our previous findings increases in midbrain PCr demonstrated a much stronger correlation with a greater deterioration in semantic fluency (**Fig. 5.4B**,  $r=-0.64$ ,  $p=0.0043$ ). There was no relationship between either age or sex and semantic fluency. There was no relationship between mean midbrain PCr and UPDRS axial sub-score.

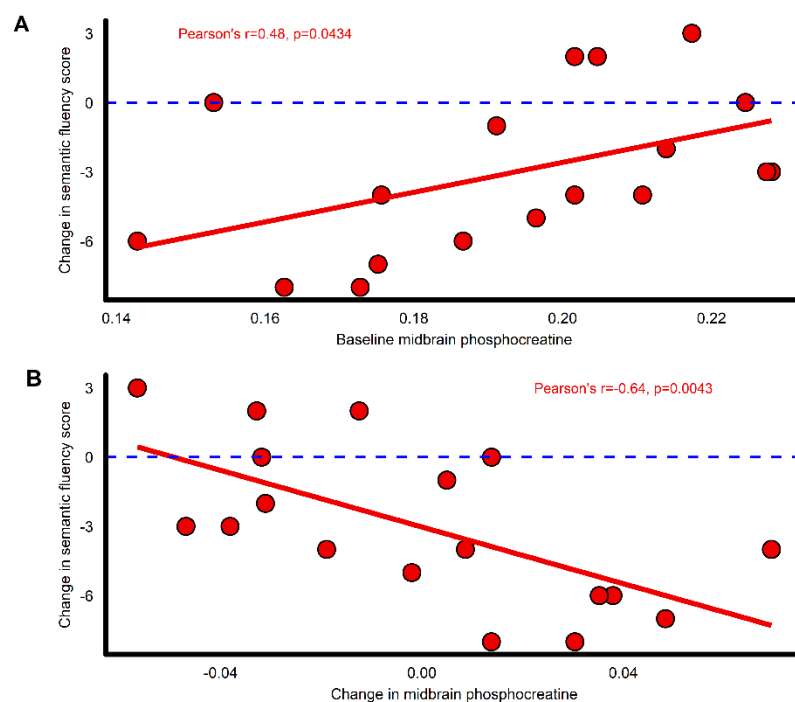


**Figure 5.4: Correlation of  $^{31}\text{P}$ -MRS midbrain phosphocreatine and semantic fluency score.**

A) correlation of baseline mean midbrain phosphocreatine and changes in semantic fluency score from baseline to follow-up, B) correlation of changes in both midbrain phosphocreatine and semantic fluency score from baseline to follow-up. Dashed blue line denotes no change in semantic fluency score.

## Discussion

Previous cross-sectional studies of  $^{31}\text{P}$ -MRS in PD identified reduced PCr and ATP in the putamen, reduced ATP in the midbrain and elevated Pi/ $\beta$ -ATP ratios (reflective of bioenergetic dysfunction) in the temporoparietal region.<sup>181,189</sup> However, other groups have failed to demonstrate any changes in PD, or only sex-specific changes in PD with greater ATP in female patients with PD.<sup>192,193</sup> Phospholipid abnormalities have been seen in GBA-PD with elevated levels of GPE, a component of PDE.<sup>287</sup> There is significant methodological variance across all previous  $^{31}\text{P}$ -MRS studies in PD.

We did not see any changes between groups or timepoints in bioenergetic parameters such as PCr, Pi or ATP in either the midbrain or putamen. We also did not observe any differences in ratio measures such as Pi/ATP, Pi/PCr and PCr/ATP. We observed similar patterns in midbrain ATP variance as in our previous cross-sectional work, with a much greater variation in mean midbrain ATP in PD compared to controls, reflecting the pathogenic heterogeneity of PD (data not shown).<sup>309</sup> This inherent heterogeneity may therefore limit the detection of such changes at a group level.

Further, stability across timepoints in the midbrain may simply reflect the slow nature of disease progression in PD. Alternatively, the fact that abnormalities in early PD were more marked in the putamen may reflect the comparatively sharp increase in degeneration in the dorsal striatum in the years following diagnosis compared to the substantia nigra.<sup>39</sup>

We found higher PME in PD at baseline compared to controls. However, on follow-up, whereas the control values of PME had increased, there were no changes for PD. Our observation of PME increasing in healthy controls at follow-up contradicts previous literature assessing longitudinal  $^{31}\text{P}$ -MRS changes in health, where it is expected to fall with increasing age.<sup>228,262</sup> Our results regarding phospholipid changes should be interpreted with caution. PME is more prone to quantification issues due to a poorly estimated baseline signal in the  $^{31}\text{P}$ -MRS spectra. Despite all spectra being visually inspected for quality of fit it is difficult to exclude the effects of poor baseline estimation completely. Poor baseline estimation is also more likely to affect the overall detected phosphorus signal and therefore normalised amplitude measures for PME and PDE may be less reliable in these circumstances. The PME/PDE ratio is more resistant to

this error as it does not rely on the overall phosphorus signal acquired and only measures the relative amplitude of the peaks to each other.

We observed that the ratio of PME/PDE in the contralateral putamen to the worst clinically affected side, whilst higher at baseline in PD, fell significantly compared to controls at follow-up. The ratio of PME/PDE is generally considered to reflect membrane turnover with reduced ratios demonstrating a reduction in phospholipid synthesis. This observation may suggest a shift from membrane synthesis to membrane breakdown in PD over time. This could be reflective of reduced synaptic plasticity as hypothesised in other disorders such as schizophrenia which demonstrates consistently reduced PME in the frontal lobe and increased PDE in the temporal lobe.<sup>313</sup> Lower PME/PDE ratio is also associated with reduced performance on attention testing using selective auditory tasks in amnesic mild cognitive impairment, possibly reflecting synaptic dysfunction.<sup>302</sup> Alternatively, given changes in <sup>31</sup>P-MRS phospholipids have been identified in GBA-PD, our observations may reflect lysosomal dysfunction as is heavily implicated in both sporadic and *GBA* related PD.<sup>52,77,287</sup> Given our findings in PME in healthy controls and the fact that assessment of PME/PDE in the contralateral putamen was an additional post-hoc analysis, these results should be interpreted with caution.

We saw no clear progression in MDS-UPDRS scores from baseline to follow-up, although we did observe an expected increase in LED, consistent with the natural history of PD. As we tested participants on their dopaminergic medication these increases in LED may have somewhat masked the expected clinical progression in MDS-UPDRS scores. We also observed an overall mean decrease by 3 words in semantic fluency testing from baseline to follow-up in PD, this is of interest as this clinical assessment should not be affected by dopaminergic medication.

We identified no clinical relationships with <sup>31</sup>P-MRS phospholipids. This is not unexpected, as we previously failed to find correlations between <sup>31</sup>P-MRS and clinical rating scales such as MDS-UPDRS and NMSS in our previous cross-sectional analysis of a larger cohort.<sup>309</sup>

In contrast to the putaminal data we did see a clinically relevant relationship between midbrain PCr and semantic fluency, that further supports our previous cross-sectional observation that higher PCr may be an indicator of rapid disease progression with

respect to either dementia or postural instability. Reduced semantic fluency is predictive of the development of Parkinson's disease dementia (PDD). Up to 17% of patients with PD may develop PDD within 5 years from and this was associated with reduced semantic fluency.<sup>312</sup> Naming less than 21 animals in 90s had a hazard ratio of 2.9 in a large UK-based ICICLE-PD incident cohort study.<sup>311</sup> Our semantic fluency testing results of animals named in one minute (baseline mean  $\pm$  SD = 20.8 $\pm$ 7.1) are consistent with those previously reported in large cohorts such as the Parkinson's Progression Marker's Initiative (baseline mean  $\pm$  SD = 20.81 $\pm$ 5.9,  $n=503$  PD).<sup>314</sup>

There was a strong correlation between increases in midbrain PCr from baseline to follow-up and deteriorations in semantic fluency, although higher baseline midbrain PCr seemed to correlate with somewhat less deterioration. Regardless of baseline midbrain PCr we still observed a significant reduction semantic fluency in the PD group as whole and therefore this weaker correlation between baseline PCr and change in semantic fluency may be less relevant. It is unclear why increasing midbrain PCr would have this relationship with semantic fluency. PCr has been noted to increase slightly with age although the mechanism as to why is unclear.<sup>228</sup> Increased PCr has also been seen in anatomically relevant areas of the brain affected in early Alzheimer's such as the hippocampi and retrosplenial cortex.<sup>179</sup> Given that age is a significant risk factor for the development of both PD and dementia this relationship between PCr and semantic fluency may be reflective of an accelerated aging process in PD. This has been observed in previous morphometric imaging studies predicting brain age, although the effect in PD is milder than in other neurodegenerative disorders such as Alzheimer's disease.<sup>315</sup>

We did not assess <sup>31</sup>P-MRS in anatomical areas that would typically be associated with semantic fluency as our focus was upon the nigrostriatal pathways which are affected early in the neurodegenerative process of PD. Additionally, we did no further neuropsychological testing to quantify cognitive impairment in other domains, again limiting our interpretation.

There are further limitations to our study, <sup>31</sup>P-MRS signal is derived from all cell types found within the examined tissue and therefore will include non-neuronal cell populations such as astrocytes and microglia. Additionally, our cohort is still comprised of predominantly early PD with a mean disease duration of around 3.5 years. This may

simply be too early in the disease process and too short an interval of follow-up to observe a large magnitude of change in  $^{31}\text{P}$ -MRS. Further, our sample size was reduced compared to our initial cross-sectional study. There were two main reasons for this cohort attrition. Firstly, a number of participants in PD subsequently took part in other interventional studies at our centre that excluded them from taking part in follow-up for this observational study. Secondly, in an effort to create as homogenous a follow-up period as possible several controls could not be scanned due to their baseline scan occurring significantly later than other participants, in a small number of participants this was due to reduced research capacity during the COVID-19 pandemic.

Our observations in this study present intriguing data regarding longitudinal  $^{31}\text{P}$ -MRS changes in PD and their relationship to pertinent clinical markers of disease progression. This data should be seen as hypothesis generating, to facilitate the design of future studies interrogating brain bioenergetics and phospholipid metabolism in PD and their relationship to both clinical progression and neurodegeneration. The relationships observed between midbrain PCr and semantic fluency warrant further study of brain bioenergetics in anatomical sites relevant to semantic fluency to determine if changes in  $^{31}\text{P}$ -MRS could be used to predict future cognitive decline in PD which would be of great interest to future neuroprotective trials.

**END OF CHAPTER MANUSCRIPT**

## Chapter 6: Discussion

The aims of this thesis were to assess the safety and tolerability of UDCA in a phase II randomised, double-blind, placebo-controlled trial with a key secondary aim being the evaluation of novel secondary outcome measures, in particular, assessing target engagement with  $^{31}\text{P}$ -MRS. In tandem, and to complement the trial work, a further study was performed to mechanistically stratify PD according to both *in vivo* measures of mitochondrial function obtained by  $^{31}\text{P}$ -MRS and *in vitro* measures of mitochondrial function and mitochondrial and lysosomal morphology in patient derived fibroblasts and to study the longitudinal changes of  $^{31}\text{P}$ -MRS in PD in relation to clinical progression. This discussion will focus on the key findings of the data presented and the implications for current research and future work.

### The UP Study and early phase neuroprotective trial design

The UP Study has provided a 'proof-of-concept' approach to assess novel outcome measures for future neuroprotective trials. Sensor-based gait analysis and  $^{31}\text{P}$ -MRS offer new approaches to quantify motor impairment and assess target engagement. The UP Study presents a trial design that could be adapted to other phase II study assessing neuroprotective compounds, in particular mitochondrial rescue agents.

### Previous neuroprotective trials targeting mitochondrial dysfunction

Given the strong evidence of mitochondrial dysfunction in the pathogenesis of PD it is unsurprising that there have been a multitude of clinical trials targeting mitochondrial dysfunction. With the exception of exenatide all have failed to demonstrate a clear neuroprotective effect.

The first such trial targeting mitochondrial dysfunction was the DATATOP study investigating both selegiline (an MAO-B) and tocopherol (Vitamin E, which has antioxidant properties) in 800 drug-naïve patients with PD. It contained four equal randomised study arms consisting of; selegiline, tocopherol, selegiline and tocopherol or placebo. The primary endpoint was the time until levodopa treatment commencement based upon level of disability measured using scales such as Hoehn & Yahr Staging, Schwab and England Activities of Daily Living scale (SEADL) and the UPDRS.<sup>112</sup> There was no clear benefit for tocopherol and although selegiline did appear to have an initial benefit during the first 12 months this was likely reflective of the symptomatic benefit of MAO-B agents rather than any true neuroprotective

effect.<sup>316</sup> Selegiline treated arms demonstrated a reduction in homovallinic acid consistent with MAO-B inhibition, however there was no assessment of target engagement by measuring oxidative stress or mitochondrial dysfunction.<sup>317</sup>

Coenzyme Q10 has been assessed in two separate studies. Coenzyme Q10 (also known as ubiquinone) is an endogenous antioxidant and electron transporter in the respiratory chain in the mitochondrial membrane. The first study was a randomised double-blind placebo-controlled trial assessing MitoQ (coenzyme Q10 combined with triphenylphosphonium to facilitate transport into the mitochondria) in 128 newly diagnosed PD patients. This trial had negative results with no difference in the Unified Parkinson's Disease Rating Scale (UPDRS) at 12 months between groups.<sup>113</sup> Coenzyme Q10 alone was subsequently assessed in a much larger cohort of 600 drug naïve PD cases in the double-blind randomised placebo controlled QE3 study assessing coenzyme Q10 administered with tocopherol (Vitamin E). Again, this trial showed no difference between treatment and placebo in the primary outcomes of either total UPDRS parts I-III scores or time to commencement of dopaminergic medication.<sup>114</sup> Neither of these studies attempted to assess target engagement.

Pioglitazone is a peroxisome proliferator-activated receptor- $\gamma$  (PPAR- $\gamma$ ) and used in the treatment of type 2 diabetes mellitus. The cofactor Peroxisome proliferator-activated receptor-gamma coactivator-1 $\alpha$  (PGC-1 $\alpha$ ) is a transcriptional mitochondrial master regulator and there is previous evidence of PGC-1 $\alpha$  regulated pathways being disrupted in PD. This led to a phase 2 multicentre, randomised, double blind, placebo-controlled trial using two different doses of pioglitazone and a placebo treatment arm. The trial included a total of 210 patients diagnosis of early Parkinson's disease on a stable regimen of either rasagiline or selegiline and showed no evidence of any effect upon the MDS-UPDRS score from baseline to 44 week follow-up.<sup>237</sup> Target engagement was assessed using quantitative real-time PCR but failed to demonstrate any changes in the expression profile of leucocyte PGC-1 $\alpha$ , or changes in urine 8-hydroxydeoxyguanosine to demonstrate antioxidant effect.<sup>318</sup>

Uric acid is an antioxidant found in abundance in the peripheral circulation and decreased levels of urate have been associated with an increased risk of PD, presumably due to higher levels of oxidative stress.<sup>319</sup> This led to SURE-PD3, a phase III randomised double-blind placebo-controlled trial of inosine (a uric acid precursor)

in 587 people with early PD, 298 of which were drug naïve. The primary outcome was the MDS-UPDRS parts I-III scores. The trial was terminated early due to a planned interim futility analysis, with no difference in either primary several secondary outcomes between treatment groups. Although inosine demonstrated a clear rise in serum uric acid (as expected through pharmacological mechanism) there was no attempt to assess target engagement in the brain.<sup>116</sup>

A randomised double blind controlled trial assessing 10g per day of creatine supplementation (a molecule that acts as an alternative energy reservoir after conversion to phosphocreatine by creatine kinase) compared to placebo in 1741 patients over a minimum of 5 years was unfortunately terminated early due to futility based upon the interim analysis of 995 enrolled participants at 5-year follow-up showing no benefit upon disease progression between groups as measured by 5 outcome measures: Modified Rankin Scale, Symbol Digit Modalities Test, PDQ-39 Summary Index, SEADL and ambulatory capacity.<sup>115</sup> There was no attempt to assess the target engagement of creatine.

Only exenatide, a glucagon-like peptide-1 agonist used in the treatment of type 2 diabetes mellitus has demonstrated an improvement in MDS-UPDRS scores in response to treatment. Exenatide appears to have a neuroprotective effect in the MPTP-mouse model. A single centre, randomised, double blind, placebo controlled trial of exenatide 2mg weekly, for an active treatment period of 48 weeks in 62 patients with moderate PD and a 12 week washout found that the Movement Disorders Society-Unified Parkinson's Disease Rating Scale (MDS-UPDRS, discussed in further detail later) scores had improved by 1 point in the exenatide arm and worsened by 2.1 points in the placebo group.<sup>263</sup> Exenatide has now progressed to a phase III randomised double-blind placebo-controlled trial seeking to recruit 200 participants with mild to moderate PD and a total treatment duration of 96 weeks. The primary outcome is the change in MDS-UPDRS III scores between placebo and exenatide treated groups.<sup>263</sup>

A post-hoc analysis of serum samples from the exenatide trial demonstrated promising results with respect to target engagement. Exenatide was hypothesised to lead to neuroprotection through the increased tyrosine phosphorylation of insulin receptor substrate 1 (IRS-1) and the subsequent downstream phosphorylation of Akt to activate

several downstream targets involved in proliferation, differentiation, survival and metabolism. Participants taking exenatide had increased levels of increased tyrosine phosphorylated IRS-1, Akt and phosphorylated-Akt (p-Akt) at the end of the treatment period (48 weeks) compared to placebo. The changes in p-Akt were still present after the washout phase (60 weeks). This provided strong evidence of target engagement of exenatide and a plausible mechanistic pathway to support the trial findings. This is something lacking from multiple previous neuroprotective trials.<sup>320</sup>

Key common themes underly the possible failure of all of the above trials with the exception of exenatide. Primary outcome measures have all heavily relied upon clinical rating scales to quantify motor impairment, in particular the UPDRS or, following its revision in 2008, the MDS-UPDRS.<sup>122</sup> Cohort stratification has largely focused only on medication status, either only included drug-naïve PD, or in one case, participants controlled on MAO-B only. The need to provide evidence of target engagement has been neglected in many of these trials.

#### Quantification of motor impairment

The UP Study provides evidence to move towards the inclusion of sensor-based objective quantification of motor impairment, such as sensor-based gait analysis, to assess motor impairment in PD neuroprotection trials. This approach is complimentary to clinical rating scales, in particular MDS-UPDRS part III, the 'gold-standard' of quantifying motor impairment in PD.

The minimal clinically important difference in the motor examination (part III) of the MDS-UPDRS is felt to be an improvement of 3.25 points for detecting minimal, but clinically pertinent, improvement and a deterioration of 4.63 points for observing minimal, but clinically pertinent, worsening.<sup>321</sup> Over a period of 5 years MDS-UPDRS Part III scores were observed to increase (deteriorate) by 2.4 points per year, meaning that a 2 year period of follow-up would be required for expected disease progression to be larger than the previously determined clinically important change in a patient.<sup>212</sup>

The potential ability of sensor-based gait analysis to detect changes in motor impairment over a relatively short period of time offers a clear advantage over the MDS-UPDRS III. Objective-sensor based quantification of PD is being utilised in other neuroprotective trials currently in progress or where results are awaited.<sup>263,322</sup>

## Target engagement

The UP Study utilised  $^{31}\text{P}$ -MRS to demonstrate possible target engagement of UDCA in pathologically relevant tissue. This was predominantly demonstrated through an improved (more negative)  $\Delta G_{\text{ATP}}$  in the midbrain. This was accompanied by a non-significant trend for ADP to reduce in the midbrain. Both these findings could suggest an improved efficiency of OXPHOS. Similar findings have been reported in mitochondrial cytopathies utilising  $^{31}\text{P}$ -MRS to demonstrate target engagement of coenzyme Q10.<sup>184</sup>

Of the trials described above, only the trials of pioglitazone and exenatide attempted to determine target engagement and only exenatide was successful. Some trials such as SURE-PD3 and DATATOP demonstrated the expected pharmacological effect (e.g. increased serum uric acid and decreased homovallinic acid respectively). Other than pioglitazone all other trials failed to provide any assessment of target engagement through the demonstration of reduced oxidative stress or improved mitochondrial function as hypothesised.

There are a growing number of trials utilising  $^{31}\text{P}$ -MRS to determine target engagement including Sathe et al<sup>196</sup>, who performed a 6 week pilot study of UDCA and used  $^{31}\text{P}$ -MRS in five participants (although only three had data available) to determine the rate of ATP hydrolysis in response to treatment using the magnetisation transfer technique and Schultz et al<sup>195</sup> who used  $^{31}\text{P}$ -MRS to measure whole brain  $\beta$ -ATP/Pi levels to infer improved rates of ATP production due to increased glycolysis. Further, a randomised controlled trial assessing the efficacy of coenzyme Q10 in genetically stratified PD currently using  $^{31}\text{P}$ -MRS is currently in the recruitment phase. This trial will recruit genetically stratified *PINK1/Parkin* related PD and a further two groups of sporadic PD, genetically stratified according to the presence or absence of mitochondrially related single nucleotide polymorphisms (SNPs). The ratio of  $^{31}\text{P}$ -MRS derived PCr/Pi and ATP/Pi are being applied as outcome measures to confirm bioenergetic rescue.<sup>132</sup>

The UP Study is conceptually similar to other early phase trials in PD that have shifted towards the demonstration of target engagement.<sup>280,281</sup> There is clear benefit to this in early phase II trials that are generally under-powered to detect neuroprotective effect using common outcome measures such as the MDS-UPDRS. In these instances, the

absence of a clear neuroprotective effect based upon an underpowered quantification of PD using clinical scales would be less relevant to the progression of that compound through to larger phase III/IV trials compared to the clear demonstration of beneficial physiological effect. Likewise, the demonstration of no target engagement would help eliminate putative agents with a low likelihood to lead to disease modification earlier in the drug development cycle.

### Cohort stratification

PD remains a clinically and pathogenically heterogeneous disorder, presenting a clear challenge to the design of neuroprotective trials, particularly when designing selection criteria and who to target.

Although trials in drug-naïve PD attempt to remove any confounding symptomatic effect of dopaminergic medication that may mask neuroprotective effect there are several limitations to this approach. Many participants do not wish to postpone dopaminergic medication, in DATATOP 44% of investigator determined ineligibility and 39% of participant determined self-exclusion or disinterest prior to screening was due to participants either already using dopaminergic medication or an unwillingness to stop dopaminergic medication to participate in the trial. Of 1004 who proceeded to screening visits, 9.5% declined to participate in the trial and in those 21% declined due to unwillingness to delay dopaminergic medication.<sup>112</sup> Targeting drug-naïve PD introduces a higher risk of including atypical parkinsonian syndromes such as MSA or PSP that typically don't demonstrate as clear a symptomatic response to dopaminergic medication as sporadic PD does. These factors potentially introduce selection bias and may not represent the PD population as a whole.

Targeting early PD is the same approach The UP Study used and has clear benefits in reducing the clinical heterogeneity of PD. Further, the inclusion of participants only diagnosed by movement disorder specialists and displaying a clear response to dopaminergic medication greatly reduces the risk of inclusion of atypical parkinsonian syndromes, something which in small sample sized phase II studies could have a marked impact upon results.<sup>13</sup> There is pathological evidence to suggest that there is a marked and rapid progression in the pathological degeneration in the nigrostriatal pathways in the first few years following diagnosis also supporting the targeting of neuroprotective therapies in early PD.<sup>39</sup> We also targeted predominantly younger PD,

limiting participants to less than 75 years of age. There were a number of reasons for this, the accumulation of age-related and common co-morbidities are likely to have a confounding effect on key secondary outcome measures as they may limit mobility.

The UP Study did not attempt to mechanistically stratify trial participants, although this is a key area of development in moving towards precision medicine approaches in PD and is a key focus of this thesis described in greater detail below.

### Limitations of The UP Study

Although appropriately powered to achieve the primary outcome of determining the safety and tolerability of UDCA in PD the clear limitation of The UP Study are the comparatively under-powered secondary objectives. This is likely true for the MDS-UPDRS but may not be the case for both the sensor-based quantification of motor impairment and the <sup>31</sup>P-MRS assessment of target engagement results for both. These results will inform power calculations for future IIb or III trials of UDCA in PD to more definitively determine any potential neuroprotective properties.

The UP Study was unfortunately affected by COVID-19 with several visits having to be conducted remotely and several delayed assessments with respect to <sup>31</sup>P-MRS acquisition. Our sensitivity analysis using data only collected at the correct timepoints does not suggest that delayed assessments affected our key secondary outcomes, but this effect is difficult to completely exclude. Further, the change in activity due to COVID-19 lockdown measures may have had a negative impact upon several assessments. The observed increase in MADRS, particularly in the UDCA group may have been related to difficulties that people with PD experienced during national lockdown measures and the associated psychological distress. This would not explain the differences between groups.<sup>278</sup> However, the increase in MADRS continued after treatment cessation and therefore may not be a specific effect of UDCA.

The lack of positive results in the physical activity monitoring at home may be related to changes in the types of activity that participants were engaging in due to changes in their behaviour during COVID-19.<sup>278</sup> The physical activity monitoring at home was also largely focused upon the overall measurements of activity and movement intensity.

Basic measures of physical activity may not be sensitive enough to detect meaningful changes in a clinical trial, especially in a small trial such as the UP study. Alternatively,

this approach may be more promising in conditions with more rapid disease progression. The quality of an individual's gait is likely to differ between supervised (clinic-based) and unsupervised (real-life) assessments. Supervised assessments are ideally suited to determine a participant's best gait performance under specific test conditions with standardised tasks and environments across all participants. Unsupervised assessments such as the PAM assesses how an individual's gait performs in their natural environment. Therefore, unsupervised assessments are dictated by the activities that individual actually performs in their usual environment and are susceptible to lifestyle differences between participants such as exercise habits and home environment (e.g. bungalow living). In the context of future neuroprotective trials these two approaches are likely to be complementary to each other.

The McRoberts Dynaport Movemonitor+ is currently being assessed and validated in a large multicentre study across several conditions and is assessing and comparing the ability of continuous 7-day monitoring to detect key digital mobility outcomes that assess gait quality which so far can typically only be obtained with 'gold-standard' supervised gait analysis techniques. This approach requires the development of further raw data processing algorithms from the PAM currently outside the scope of the manufacturer's proprietary software which only focus on overall activity and movement intensity.<sup>323</sup>

The limitations of <sup>31</sup>P-MRS will be discussed in greater detail later.

#### Future directions

The UP Study has demonstrated the potential utility of objective sensor-based analysis as a complementary assessment to standard clinical rating scales to quantify motor impairment in neuroprotective PD trials. Further, <sup>31</sup>P-MRS may have utility as a tool to assess compounds for target engagement. The UP study has also provided confirmation that high-dose UDCA is safe and tolerable in PD. Alongside the potential (but as yet unconfirmed) neuroprotective effect reflected in the outcome of the gait analysis and the tentative evidence of target engagement in the midbrain, UDCA should be considered a potential neuroprotective compound to take forward into further phase IIb/III studies to determine this definitively.

This logical approach in the immediate future would be to design a Phase IIb trial where the primary outcome is disease modification as assessed using further gait analysis and classical motor rating clinical scales such as the MDS-UPDRS.

Such a Phase IIb trial would be required to run over a longer duration than The UP Study and this should ideally be no less than two years to improve the ability of the motor outcome measures to detect a disease modifying effect given that PD is generally a slowly progressive condition.

Future phase IIb studies would likely require a large increase in the numbers of participants and an increased number of study sites to achieve recruitment targets in a timely manner. Although this thesis has not performed any formal power calculations to determine this, the sample size is likely to be similar to other Phase IIb studies in PD, such as the Exenatide trial, and therefore will have at least double the number of participants (60), but may be more (e.g. 80-100).<sup>263</sup> Multi-site studies present specific challenges to some of the endpoints discussed. Measures such as the MDS-UPDRS would be susceptible to an increase in inter-rater variability with increasing numbers of both sites and raters. This can be somewhat ameliorated by instituting strict clinical rating scale training systems against standardised assessments. Further, clinical rating scale assessments could be recorded on video to be assessed by a further common rater to assess for consistent rating across all sites.

Academic led drug development presents its own challenges with respect to the available resources and funding streams in comparison to pharmaceutical led drug development. This is especially true for drug repurposing strategies where the IMP is typically a generic drug off-patent. The UP Study demonstrated excellent safety and tolerability. Throughout the course of the trial there were no UDCA related blood abnormalities or SAE's. It is reasonable based on these results that there would not need to be any interim in-person safety assessments for safety bloods and/or ECG's outside of the visits to assess for disease modification. Therefore, a reduced visit frequency for safety would reduce the associated financial costs.

Although <sup>31</sup>P-MRS can be performed on the vast majority 3T MRI scanners widely used across the UK there may be variations in available acquisition sequences based upon the hardware and software capabilities of each scanner model and across manufacturers. Further, the dual tuned <sup>31</sup>P/<sup>1</sup>H birdcage coil we used for all <sup>31</sup>P-MRS

acquisitions is not routinely available in many centres and only a few academic units in the UK have any significant experience with  $^{31}\text{P}$ -MRS. This would present a significant challenge to acquisition across multiple sites, and therefore assessment of target engagement using  $^{31}\text{P}$ -MRS would need to be limited to a single site to ensure high quality data.

Adapting supervised clinic-based gait analysis across multiple sites would be possible, as the hardware required is more readily distributed and can be used by non-specialists, although data quality may be poorer than those with expertise in the field. Supervised clinic-based gait analysis provides the greatest detail on the gait sequence of PD but is performed in an artificial and supervised environment which is less likely to reflect how an individual mobilises in their typical environment. The UP Study employed an instrumented walkway and body worn motion sensors. Due to the inclusion of an instrumented walkway the distance walked between each turn was inherently limited to the length of the walkway. Future testing protocols may benefit from not using the instrumented walkway and employing testing protocols that utilise greater distances and walking durations to capture a greater number of steps from which to analyse using only body worn motions sensors. This could be supplemented with the inclusion of pressure sensitive insoles as PD demonstrates a significant change in heel-toe foot loading pattern even in mild disease.<sup>324</sup> Future testing protocols may also benefit from dual-task gait analysis, where individuals are given further tasks (e.g. arithmetic, language, memory or motor tasks) as this has a significant detrimental effect on gait performance. This may improve the ability of the testing protocols to detect treatment effects as dual tasking is more likely to 'unmask' greater gait impairment, especially in younger, more active patients with early PD, such as those included in The UP Study.<sup>325</sup>

Physical activity monitoring is the most accessible form of data collection for non-specialists and participants with only a single sensor involved and straightforward data collection, limiting the specialist expertise require to collect high quality-data. Although PAM data did not identify any significant treatment effects, as discussed above this was limited to the proprietary data algorithms that focuses largely on activity and movement intensity across pre-defined periods (e.g. walking, running, posture change) and there remains a wealth of raw data collected that could be further analysed in greater detail to derive more specific and sensitive measures of gait

impairment in PD such as step regularity, variability and symmetry. The key challenges to continuous physical activity monitoring are determining the optimal analysis protocols to identify and analyse specific activities such as walking, running, shuffling or in PD specifically, freezing of gait. The optimal analysis filters used to determine walking periods can be impacted by several patient factors such as disease severity, the type of activities an individual engages in and the environment they perform them in (e.g. outdoor vs indoor) making an optimal algorithm applicable across all participants challenging to determine and ultimately can introduce bias in the extracted values for key measures such as step regularity, variability, symmetry and gait speed.<sup>326</sup>

Given the limited utility and sensitivity in many classical rating scales on their own for detecting neuroprotective effect (e.g. MDS-UPDRS III) it may be of benefit to utilise composite rating scales. Recent studies have utilised composites of the MDS-UPDRS III, timed up and go test (TUG) and Purdue Pegboard test and has been shown to have a lower coefficient of variation, greater correlation with self-reported disease severity and greater longitudinal scoring linearity compared to the MDS-UPDRS III alone.<sup>327</sup>

Cognition in the UP Study was only assessed using the MoCA, which is more effective at detecting both mild cognitive impairment in PD and predicting progression to PDD than similar screening tools such as the Mini Mental State Examination (MMSE).<sup>210</sup> However, the minimal clinically important difference (MCID) for a scale such as the MoCA is poorly defined in PD having previously been established as an approximate improvement of 1.2 points in stroke rehabilitation.<sup>328</sup> However, there is currently no consensus on the clinical rating scale for assessing cognition in PD, PDD or DLB in clinical trials. Currently recommended cognitive assessments for use in PD by the MDS Rating Scales Review Committee are the MoCA, the Mattis Dementia Rating Scale Second Edition (DRS-2) and the Parkinson's Disease-Cognitive Rating Scale (PD-CRS) although there is limited data comparing the utility of these scales against each other and their MCID's in PD.<sup>329</sup>

The Addenbrooke's Cognitive Examination-III (ACE-III) is an alternative cognitive assessment tool, that was not reviewed by the MDS Rating Scales Review Committee that assesses a breadth of cognitive functions in greater detail than assessments such

as the MoCA or MMSE. ACE-III has shown promise in the longitudinal assessment of cognition in PD.<sup>330</sup> It is currently being utilised in a randomised controlled trial of azathioprine in PD as a secondary outcome measure.<sup>96</sup> However, currently all commonly utilised assessments such as the MoCA and ACE-III still demonstrate low sensitivity and specificity for the diagnosis of mild cognitive impairment in PD and highlights the need for the development of more sensitive assessment tools for cognition for use in neuroprotective trials.<sup>331</sup>

Future Phase IIb studies of UDCA could utilise further cognitive assessments outside the MoCA as discussed above or could employ more extensive cognitive assessments such as the ACE-III, and ultimately the optimal choice for cognitive assessment to detect neuroprotective effect is not yet clear.

The UP Study did not include any methods for cohort stratification prior to trial entry, this may be desirable for future Phase IIb/III studies to stratify for those most likely to respond to UDCA. This could either be stratification by pathogenic subtype, for example stratifying for those with PD likely driven by mitochondrial dysfunction or by desirable clinical features, such as rapid predicted disease progression.

Further post-hoc analysis of <sup>31</sup>P-MRS and/or clinical data from The UP Study may help identify common characteristics to identify those most likely to respond to mitochondrial rescue therapies. Although it should be noted that improvements in gait analysis and <sup>31</sup>P-MRS were seen across the majority of participants in the treatment group and therefore the numbers of non-responders may be too small to provide any meaningful data to analyse.

As discussed earlier, mitochondrial specific biomarkers have not shown promise in identifying mitochondrial subtypes of PD . The data from the observational cohort included in this thesis may help provide data on <sup>31</sup>P-MRS signatures that reflect specific patterns of mitochondrial dysfunction in peripheral tissue to target with mitochondrial rescue therapies. As discussed earlier, this requires further work to identify the specific pathogenic mechanisms underlying the abnormalities seen in the peripheral tissue to make any meaningful pathogenic correlate to the <sup>31</sup>P-MRS data to use in future stratification.

Stratification could also utilise the predicted disease progression score to recruit only those predicted to have rapid disease progression and further post-hoc analysis of

The UP study may help guide recommended thresholds as all participants underwent this measurement at baseline.<sup>17</sup> Recently, a combination of blood-based biomarkers (Neurofilament light chain, apolipoprotein E genotype and GBA genotype) combined with clinical assessments have shown a stronger prediction of an unfavourable clinical outcome than clinical assessment alone.<sup>332</sup> Such an approach could be utilised in further Phase IIb/III studies to recruit a homogenous cohort of participants likely to progress rapidly and improve the ability to detect a treatment response.

The UP Study found that the key reason for people finishing treatment early was the high number of IMP capsules to be taken alongside their regularly prescribed medications. Future phase III studies would benefit from a revision to the dosage and size of IMP capsules to reduce the associated burden and improve medication compliance, although it should be noted that compliance overall was excellent in The UP Study.

### [<sup>31</sup>Phosphorus magnetic resonance spectroscopy and the assessment of patient derived peripheral tissue as tools for mechanistic stratification of Parkinson's Disease](#)

The inherent clinical and pathogenic heterogeneity in PD necessitates a paradigm shift in how we currently investigate neuroprotective compounds in early clinical trials.<sup>333</sup> Under such an approach, neuroprotective trials would target homogenous, biomarker-defined phenotypes in participants likely to respond to specific therapies targeting those pathways.<sup>334</sup>

This thesis has focused on the assessment of bioenergetic dysfunction using different, but complementing approaches, targeting both the central nervous system and patient derived peripheral tissue.

### [Relationships between <sup>31</sup>P-MRS measured brain bioenergetics and the \*in vitro\* assessment of mitochondria in patient derived peripheral tissue](#)

Mechanistic stratification in peripheral tissue in a much larger cohort (100 PD participants and 50 controls) identified clear subgroups of PD with significant mitochondrial or lysosomal dysfunction, these phenotypes remained consistent within subgroups once fibroblasts were differentiated into TH-positive neurons.<sup>161</sup> Reassuringly, the differences in variance between PD and controls in many fibroblast measures in our data closely mirrors this study. However, establishing fibroblast lines from skin biopsies is a time-consuming and labour-intensive process. Although this

approach offers *ex vivo* testing of putative neuroprotective compounds in patient derived tissue, and importantly neuronal cell types through the direct reprogramming of fibroblasts to neurons, this approach would be difficult to scale to large numbers of participants to enable mechanistic stratification for entry into neuroprotective trials.

The key advantage of  $^{31}\text{P}$ -MRS is that it can measure bioenergetic dysfunction *in vivo* in pathologically relevant areas of the brain. Previous work has demonstrated certain relationships between  $^{31}\text{P}$ -MRS measures and broad biological mechanisms, such as elevated Pi/ATP ratios being more reflective of dysfunctional oxidative phosphorylation in rodent livers.<sup>295</sup> This is the first study in PD aiming to correlate  $^{31}\text{P}$ -MRS measures with relevant and specific pathogenic mechanisms in peripheral tissue.

The identified relationships with fibroblast MMP, mitochondrial and lysosomal count are consistent with well recognised possible pathogenic mechanisms in PD such as impaired mitophagy.

This requires further investigation to confirm if the suspected pathogenic mechanisms are in fact impaired in these participants, as they were not interrogated directly. Regardless, the possibility of detecting distinct pathogenic subgroups in PD could have implications for future neuroprotective trial design. Therapies still in pre-clinical testing that could benefit from this approach would include inhibitors of Ubiquitin-specific protease-30 (USP-30), a deubiquitinating enzyme (DUB) that regulates the ubiquitination of various targets by E3-ubiquitin ligases such as Parkin. Inhibiting USP-30 would therefore lead to an increase in ubiquitination and increase mitophagy. So far, inhibition of DUBs have focused on rescue effects in *Parkin* or *PINK1* models of PD but DUB inhibition may be beneficial in a carefully stratified population of PD with impaired mitophagy.<sup>335</sup>

#### Longitudinal changes in $^{31}\text{P}$ -MRS and the relationship to clinical progression

This thesis also presents the first ever observational longitudinal study of  $^{31}\text{P}$ -MRS in PD. Longitudinal data is of crucial importance for any imaging technique assessing neurodegenerative diseases. The longitudinal data presented suggests progressive changes in membrane turnover in the posterior putamen, where over a period of 2.5 years participants with PD switched from slightly favouring membrane synthesis to demonstrating a reduction in membrane synthesis and increase in membrane

breakdown. The exact pathogenic link here is unclear but may represent progressive neurodegeneration within the posterior putamen. This abnormality has previously been observed in Alzheimer's disease (AD) and was associated with attention deficits in cognitive testing.<sup>302</sup> Of interest a previous longitudinal study in AD assessing phospholipids in the prefrontal cortex found that early mild AD had elevated PME that then seemed to normalise to control values in moderate AD as the disease progressed, possibly mirroring the changes we observed in PD with an increase in PME early in disease course and subsequently falling as neurodegeneration progresses.<sup>336</sup> There are suggestions that PME and PDE are related to membrane integrity. Where membrane integrity is not maintained (as suggested by a lower PME/PDE ratio), there is disrupted synaptic transmission.<sup>337</sup> It is also important to acknowledge that in the first 5 years of PD dramatic and rapid nigrostriatal degeneration has been reported, particularly in the posterior putamen, our observations would be in keeping with this.<sup>39</sup> This offers an intriguing prospect where <sup>31</sup>P-MRS may be able to monitor disease progression and neurodegeneration in PD within the posterior putamen. The phospholipid data must be interpreted with caution as there was also an unexpected increase in PME in healthy controls, contradicting previous literature.

We also observed a relationship between changes in midbrain PCr and semantic fluency which warrants further investigation to assess if brain bioenergetics are closely related to the development of cognitive impairment in PD.

#### *Limitations of <sup>31</sup>Phosphorus-Magnetic Resonance Spectroscopy*

There are several limitations and methodological considerations of <sup>31</sup>P-MRS. In all <sup>31</sup>P-MRS studies the abnormalities cannot be attributed to a single cell type. The composition of any <sup>31</sup>P-MRS voxel acquired from the brain will contain both neuronal and non-neuronal populations (astrocytes and microglia). Further, it is not possible in the midbrain acquisition presented to state that these abnormalities are specifically due to dopaminergic neurons and their degeneration. Although this is a key limitation, it also possibly explains the difference in findings between midbrain and putamen. The relationships between bioenergetic measures in the putamen and fibroblast assay results may be due to differences in the proportion of neurons and glial cell types in the tissue examined. The midbrain has a higher proportion of glial cell types to neurons compared to the striatum.<sup>303</sup> Neurons rely on oxidative phosphorylation for ATP

production whereas astrocytes and microglia are generally glycolytic.<sup>186</sup> Therefore mitochondrial dysfunction is more likely to be detected in tissue with higher proportions of neurons. Our acquisition time in total (both anatomical and spectroscopic imaging) was around 1 hour, including the planning time for the localisation of the <sup>31</sup>P-MRS acquisitions. The long acquisition times introduce several concerns, particularly from the participant perspective. It is unreasonable to expect participants to remain comfortable and still for long periods of time and this may introduce a greater risk of movement artifact. Although this is readily appreciable on anatomical imaging, movement artefact on spectroscopic results is harder to determine other than gross movement artefact which will result in a clearly poor SNR as was the case in one participant in the longitudinal study. The length of the <sup>31</sup>P-MRS acquisition protocol also limits the ability to perform other complementary sequences within the acquisition. One such sequence would be high-resolution susceptibility weighted imaging focused upon identifying the substantia nigra. Nigrosomal structure which has recently become an area of interest has it has demonstrated promising diagnostic utility although longitudinal data remains somewhat lacking.<sup>338</sup>

There are two broad approaches to <sup>31</sup>P-MRS quantification using either relative or absolute quantitation. This thesis has used relative quantification techniques which have either expressed metabolites relative to the total phosphorus signal detected (normalised amplitudes), to allow comparisons between subjects, or using ratio measure such as the PME/PDE ratio, where each raw peak amplitude is expressed as ratio of another raw peak. The advantages and disadvantages of these approaches are discussed in greater detail in Chapter 1.

Although, much of the previous <sup>31</sup>P-MRS literature has been obtained at 3T, there are clear advantages to performing <sup>31</sup>P-MRS at higher field strengths. Alongside improved SNR, higher field strengths also allow the measurement of additional metabolites such as NADH (a key electron donor in the electron transport chain), which is poorly detected at 3T.<sup>339</sup>

#### *Limitations of tissue fibroblasts*

Fibroblasts have several advantages, in that they are easy to obtain, establish into cell lines and as they tend to grow flat in one plane, they are highly amenable to live-cell imaging techniques. The clear limitation though when trying to mechanistically stratify

an individual with PD is that they are non-neuronal cell lines, somewhat limiting direct comparisons between fibroblast assays to the pathology of PD. However, previous studies have repeatedly demonstrated abnormalities even in the peripheral tissue of PD, supporting the view that metabolic abnormalities in PD are not just limited to the central nervous system.<sup>161,340</sup> Fibroblasts also demonstrate quite differing bioenergetic demands compared to the highly metabolically active dopaminergic neurons affected early in PD, tend to be quite resilient to most stressors and have extremely low expression of  $\alpha$ -synuclein.<sup>160</sup>

The relationships we have identified are based upon morphological measures of mitochondria and lysosomes, with the only specific functional measure of mitochondria being MMP. To confirm whether our identified subgroups truly do exhibit impaired mitophagy or excessive oxidative stress related to impaired oxidative phosphorylation requires further experiments. Mitophagy, can be assessed under both basal conditions and upon induction (by collapsing the MMP) to measure the overall capacity of the cell to process damaged mitochondria through mitophagy. Oxidative stress can be assessed further through the measurement of ROS production and can be complemented by the assessment of specific mitochondrial complex activity assays to determine any defects within the electron transport chain.<sup>73,161</sup>

### Future directions

Ideally, examined patient-derived tissue would be neuronal in nature. This can be achieved now through the direct reprogramming of fibroblasts in iNPCs. iNPCs are tri-potent and can be differentiated into astrocytes, oligodendrocytes and most importantly neurons.<sup>162</sup> Neurons from iNPCs can be further defined into specific neuronal subtypes, such as dopaminergic neurons.<sup>73</sup> This is also achievable by directly reprogramming fibroblasts using induced pluripotent stem cells (iPSCs). However, in comparison, iNPCs are cheaper to generate and retain their aged epigenetic phenotype, which is of huge importance given that age is an important risk factor to the development of PD.<sup>163</sup> iPSCs cannot achieve this as the differentiated neurons are essentially of embryonic origin and therefore lose these potentially important epigenetic features.<sup>341</sup>

iNPC generation although cheaper than iPSC generation remains expensive and is both time-consuming and labour-intensive. It is unrealistic to reprogram and

differentiate all cell lines from the study and therefore future work will focus on deep phenotyping on subgroups of cell lines representing the possibly pathogenic mechanisms identified. This will enable the in-depth phenotyping of these subgroups to identify of the possible pathogenic cellular correlates of  $^{31}\text{P}$ -MRS measures do truly represent impaired mechanisms such as mitophagy or increased oxidative stress.

$^{31}\text{P}$ -MRS could be further developed through the integration of multi-modal imaging techniques. This could include the combination of  $^{31}\text{P}$ -MRS and PET which would offer the opportunity to simultaneously assess glycolysis using a tracer such as  $^{18}\text{F}$ -fluoro-2-deoxy-D-glucose (FDG) and  $^{31}\text{P}$ -MRS measure of bioenergetics and could be used to isolate specific abnormalities to oxidative phosphorylation. This has never been combined previously in neuroimaging but has been explored in the assessment of pancreatic cancer.<sup>342</sup> Our protocol could be further refined to reduce the overall scanning time required for the  $^{31}\text{P}$ -MRS parameters, this could be done by reducing the number of spectroscopic acquisitions or combining our two current acquisitions into a single 3D CSI acquisition. This could allow the inclusion of other sequences such as imaging of the nigrosome to use in the analysis of the spectroscopic data.<sup>338</sup>

## Conclusions

The UP Study has clearly demonstrated both the safety and tolerability of UDCA in PD, a key achievement given the dose of 30mg/kg trialled is double that routinely used in clinical practice for liver disorders.<sup>206</sup>

The UP Study has also developed new outcome measures that can aid the development of future neuroprotective trials. Sensor-based quantification of gait can complement existing clinical rating scales with an objective measure of gait as a key early clinical feature in PD that closely correlates with disease progression, and therefore represents a promising outcome measure. We have also provided further evidence that  $^{31}\text{P}$ -MRS may be a useful tool to assess target engagement *in vivo* in pathologically relevant tissue.

Additionally,  $^{31}\text{P}$ -MRS may assist with the identification of individuals with impaired brain bioenergetics in anatomically relevant regions in PD. These bioenergetic parameters demonstrate relationships with mitochondrial and lysosomal assessments in peripheral tissue that further supports this approach.  $^{31}\text{P}$ -MRS also demonstrates changes in phospholipids membrane components over time which may reflect the

progressive neurodegenerative cell loss in PD and relationships between midbrain bioenergetics and semantic fluency that may be relevant to future disease progression and the development of cognitive impairment.

## References

1. Dorsey, E.R., *et al.* Projected number of people with Parkinson disease in the most populous nations, 2005 through 2030. *Neurology* **68**, 384-386 (2007).
2. Kalia, L.V. & Lang, A.E. Parkinson's disease. *The Lancet* **386**, 896-912 (2015).
3. Findley, L.J., *et al.* The economic burden of advanced Parkinson's disease: an analysis of a UK patient dataset. *J Med Econ* **14**, 130-139 (2011).
4. Lees, A. An essay on the shaking palsy. *Brain* **140**, 843-848 (2017).
5. Schapira, A.H., *et al.* Mitochondrial complex I deficiency in Parkinson's disease. *J Neurochem* **54**, 823-827 (1990).
6. van der Brug, M.P., Singleton, A., Gasser, T. & Lewis, P.A. Parkinson's disease: From human genetics to clinical trials. *Sci Transl Med* **7**, 205ps220 (2015).
7. Schapira, A.H., Olanow, C.W., Greenamyre, J.T. & Bezdard, E. Slowing of neurodegeneration in Parkinson's disease and Huntington's disease: future therapeutic perspectives. *Lancet* **384**, 545-555 (2014).
8. Pringsheim, T., Jette, N., Frolkis, A. & Steeves, T.D. The prevalence of Parkinson's disease: a systematic review and meta-analysis. *Mov Disord* **29**, 1583-1590 (2014).
9. Collaborators, G.B.D.P.s.D. Global, regional, and national burden of Parkinson's disease, 1990-2016: a systematic analysis for the Global Burden of Disease Study 2016. *Lancet Neurol* **17**, 939-953 (2018).
10. Heinzl, S., *et al.* Update of the MDS research criteria for prodromal Parkinson's disease. *Mov Disord* **34**, 1464-1470 (2019).
11. Berg, D., *et al.* MDS research criteria for prodromal Parkinson's disease. *Mov Disord* **30**, 1600-1611 (2015).
12. Gibb, W.R. & Lees, A.J. The relevance of the Lewy body to the pathogenesis of idiopathic Parkinson's disease. *J Neurol Neurosurg Psychiatry* **51**, 745-752 (1988).
13. Hughes, A.J., Daniel, S.E., Kilford, L. & Lees, A.J. Accuracy of clinical diagnosis of idiopathic Parkinson's disease: a clinico-pathological study of 100 cases. *J Neurol Neurosurg Psychiatry* **55**, 181-184 (1992).
14. Hughes, A.J., Daniel, S.E., Ben-Shlomo, Y. & Lees, A.J. The accuracy of diagnosis of parkinsonian syndromes in a specialist movement disorder service. *Brain* **125**, 861-870 (2002).
15. Wojtala, J., *et al.* Cognitive decline in Parkinson's disease: the impact of the motor phenotype on cognition. *J Neurol Neurosurg Psychiatry* **90**, 171-179 (2019).
16. Post, B., Merkus, M.P., de Haan, R.J., Speelman, J.D. & Group, C.S. Prognostic factors for the progression of Parkinson's disease: a systematic review. *Mov Disord* **22**, 1839-1851; quiz 1988 (2007).
17. Velseboer, D.C., *et al.* Development and external validation of a prognostic model in newly diagnosed Parkinson disease. *Neurology* **86**, 986-993 (2016).
18. Mancini, M., *et al.* Trunk accelerometry reveals postural instability in untreated Parkinson's disease. *Parkinsonism Relat Disord* **17**, 557-562 (2011).
19. Knudsen, K., Krogh, K., Ostergaard, K. & Borghammer, P. Constipation in parkinson's disease: Subjective symptoms, objective markers, and new perspectives. *Mov Disord* **32**, 94-105 (2017).
20. Adams-Carr, K.L., *et al.* Constipation preceding Parkinson's disease: a systematic review and meta-analysis. *Journal of Neurology, Neurosurgery & Psychiatry* **87**, 710-716 (2016).
21. Zhang, J., Xu, C.Y. & Liu, J. Meta-analysis on the prevalence of REM sleep behavior disorder symptoms in Parkinson's disease. *BMC Neurol* **17**, 23 (2017).
22. Postuma, R.B., *et al.* Risk and predictors of dementia and parkinsonism in idiopathic REM sleep behaviour disorder: a multicentre study. *Brain* **142**, 744-759 (2019).
23. Zis, P., Erro, R., Walton, C.C., Sauerbier, A. & Chaudhuri, K.R. The range and nature of non-motor symptoms in drug-naive Parkinson's disease patients: a state-of-the-art systematic review. *NPJ Parkinsons Dis* **1**, 15013 (2015).

24. Riedel, O., *et al.* Frequency of dementia, depression, and other neuropsychiatric symptoms in 1,449 outpatients with Parkinson's disease. *Journal of Neurology* **257**, 1073-1082 (2010).
25. Wood, R.A., Hopkins, S.A., Moodley, K.K. & Chan, D. Fifty Percent Prevalence of Extracampine Hallucinations in Parkinson's Disease Patients. *Front Neurol* **6**, 263 (2015).
26. Goetz, C.G., Stebbins, G.T. & Ouyang, B. Visual plus nonvisual hallucinations in Parkinson's disease: development and evolution over 10 years. *Mov Disord* **26**, 2196-2200 (2011).
27. Factor, S.A., *et al.* Cognitive correlates of hallucinations and delusions in Parkinson's disease. *Journal of the neurological sciences* **347**, 316-321 (2014).
28. Broeders, M., *et al.* Evolution of mild cognitive impairment in Parkinson disease. *Neurology* **81**, 346-352 (2013).
29. Hobson, P. & Meara, J. Mild cognitive impairment in Parkinson's disease and its progression onto dementia: a 16-year outcome evaluation of the Denbighshire cohort. *International Journal of Geriatric Psychiatry* **30**, 1048-1055 (2015).
30. Aarsland, D., Zaccai, J. & Brayne, C. A systematic review of prevalence studies of dementia in Parkinson's disease. *Movement Disorders* **20**, 1255-1263 (2005).
31. Galtier, I., Nieto, A., Lorenzo, J.N. & Barroso, J. Subjective cognitive decline and progression to dementia in Parkinson's disease: a long-term follow-up study. *J Neurol* **266**, 745-754 (2019).
32. Vossius, C., Larsen, J.P., Janvin, C. & Aarsland, D. The economic impact of cognitive impairment in Parkinson's disease. *Mov Disord* **26**, 1541-1544 (2011).
33. Macleod, A.D., Taylor, K.S. & Counsell, C.E. Mortality in Parkinson's disease: a systematic review and meta-analysis. *Mov Disord* **29**, 1615-1622 (2014).
34. Dommershuijsen, L.J., *et al.* Life expectancy of parkinsonism patients in the general population. *Parkinsonism Relat Disord* **77**, 94-99 (2020).
35. LeWitt, P.A. Levodopa therapy for Parkinson's disease: Pharmacokinetics and pharmacodynamics. *Mov Disord* **30**, 64-72 (2015).
36. Group, T.P.S. Levodopa and the Progression of Parkinson's Disease. *New England Journal of Medicine* **351**, 2498-2508 (2004).
37. Verschuur, C.V.M., *et al.* Randomized Delayed-Start Trial of Levodopa in Parkinson's Disease. *New England Journal of Medicine* **380**, 315-324 (2019).
38. Rossi, C., Del Prete, E. & Bonuccelli, U. A review of adverse events linked to dopamine agonists in the treatment of Parkinson's disease AU - Ceravolo, Roberto. *Expert Opinion on Drug Safety* **15**, 181-198 (2016).
39. Kordower, J.H., *et al.* Disease duration and the integrity of the nigrostriatal system in Parkinson's disease. *Brain* **136**, 2419-2431 (2013).
40. Braak, H., *et al.* Staging of brain pathology related to sporadic Parkinson's disease. *Neurobiol Aging* **24**, 197-211 (2003).
41. Lautenschlager, J., *et al.* C-terminal calcium binding of alpha-synuclein modulates synaptic vesicle interaction. *Nat Commun* **9**, 712 (2018).
42. Diao, J., *et al.* Native alpha-synuclein induces clustering of synaptic-vesicle mimics via binding to phospholipids and synaptobrevin-2/VAMP2. *Elife* **2**, e00592 (2013).
43. Man, W.K., *et al.* The docking of synaptic vesicles on the presynaptic membrane induced by alpha-synuclein is modulated by lipid composition. *Nat Commun* **12**, 927 (2021).
44. Parkkinen, L., Kauppinen, T., Pirttila, T., Autere, J.M. & Alafuzoff, I. Alpha-synuclein pathology does not predict extrapyramidal symptoms or dementia. *Ann Neurol* **57**, 82-91 (2005).
45. Klos, K.J., *et al.*  $\alpha$ -Synuclein pathology in the spinal cords of neurologically asymptomatic aged individuals. *Neurology* **66**, 1100-1102 (2006).
46. Polymeropoulos, M.H., *et al.* Mutation in the  $\alpha$ -Synuclein Gene Identified in Families with Parkinson's Disease. *Science* **276**, 2045-2047 (1997).

47. Book, A., *et al.* A Meta-Analysis of  $\alpha$ -Synuclein Multiplication in Familial Parkinsonism. *Frontiers in Neurology* **9**(2018).
48. Trinh, J., *et al.* Genotype-phenotype relations for the Parkinson's disease genes SNCA, LRRK2, VPS35: MDSGene systematic review. *Mov Disord* **33**, 1857-1870 (2018).
49. Kalia, L.V., *et al.* Clinical correlations with Lewy body pathology in LRRK2-related Parkinson disease. *JAMA Neurol* **72**, 100-105 (2015).
50. Sidransky, E., *et al.* Multicenter analysis of glucocerebrosidase mutations in Parkinson's disease. *N Engl J Med* **361**, 1651-1661 (2009).
51. Winder-Rhodes, S.E., *et al.* Glucocerebrosidase mutations influence the natural history of Parkinson's disease in a community-based incident cohort. *Brain* **136**, 392-399 (2013).
52. Gegg, M.E., *et al.* Glucocerebrosidase deficiency in substantia nigra of parkinson disease brains. *Ann Neurol* **72**, 455-463 (2012).
53. Friedman, J.R. & Nunnari, J. Mitochondrial form and function. *Nature* **505**, 335-343 (2014).
54. Chaban, Y., Boekema, E.J. & Dudkina, N.V. Structures of mitochondrial oxidative phosphorylation supercomplexes and mechanisms for their stabilisation. *Biochim Biophys Acta* **1837**, 418-426 (2014).
55. Kluckova, K., Bezawork-Geleta, A., Rohlena, J., Dong, L. & Neuzil, J. Mitochondrial complex II, a novel target for anti-cancer agents. *Biochim Biophys Acta* **1827**, 552-564 (2013).
56. Kadenbach, B. Complex IV - The regulatory center of mitochondrial oxidative phosphorylation. *Mitochondrion* **58**, 296-302 (2021).
57. Chen, G., Kroemer, G. & Kepp, O. Mitophagy: An Emerging Role in Aging and Age-Associated Diseases. *Front Cell Dev Biol* **8**, 200 (2020).
58. Eisner, V., Picard, M. & Hajnoczky, G. Mitochondrial dynamics in adaptive and maladaptive cellular stress responses. *Nat Cell Biol* **20**, 755-765 (2018).
59. Kleele, T., *et al.* Distinct fission signatures predict mitochondrial degradation or biogenesis. *Nature* **593**, 435-439 (2021).
60. Langston, J., Ballard, P., Tetrud, J. & Irwin, I. Chronic Parkinsonism in humans due to a product of meperidine-analog synthesis. *Science* **219**, 979-980 (1983).
61. Chiueh, C.C., *et al.* Neurochemical and behavioral effects of 1-methyl-4-phenyl-1,2,3,6-tetrahydropyridine (MPTP) in rat, guinea pig, and monkey. *Psychopharmacol Bull* **20**, 548-553 (1984).
62. Nguyen, T.N., Padman, B.S. & Lazarou, M. Deciphering the Molecular Signals of PINK1/Parkin Mitophagy. *Trends in Cell Biology* **26**, 733-744 (2016).
63. Su, Y.C. & Qi, X. Inhibition of excessive mitochondrial fission reduced aberrant autophagy and neuronal damage caused by LRRK2 G2019S mutation. *Hum Mol Genet.* **15**, 4545-4561 (2013).
64. Mortiboys, H., Johansen, K.K., Aasly, J.O. & Bandmann, O. Mitochondrial impairment in patients with Parkinson disease with the G2019S mutation in LRRK2. *Neurology* **75**, 2017-2020 (2010).
65. Giroto, S., *et al.* Dopamine-derived quinones affect the structure of the redox sensor DJ-1 through modifications at Cys-106 and Cys-53. *J Biol Chem* **287**, 18738-18749 (2012).
66. Toulorge, D., Schapira, A.H. & Hajj, R. Molecular changes in the postmortem parkinsonian brain. *J Neurochem* **139 Suppl 1**, 27-58 (2016).
67. Wang, X., *et al.* Pathogenic alpha-synuclein aggregates preferentially bind to mitochondria and affect cellular respiration. *Acta Neuropathologica Communications* **7**, 41 (2019).
68. Shahmoradian, S.H., *et al.* Lewy pathology in Parkinson's disease consists of crowded organelles and lipid membranes. *Nature Neuroscience* **22**, 1099-1109 (2019).
69. Sian, J., *et al.* Alterations in glutathione levels in Parkinson's disease and other neurodegenerative disorders affecting basal ganglia. *Ann Neurol* **36**, 348-355 (1994).

70. Zhang, J., *et al.* Parkinson's disease is associated with oxidative damage to cytoplasmic DNA and RNA in substantia nigra neurons. *The American journal of pathology* **154**, 1423-1429 (1999).
71. Coxhead, J., *et al.* Somatic mtDNA variation is an important component of Parkinson's disease. *Neurobiol Aging* **38**, 217 e211-217 e216 (2016).
72. Pyle, A., *et al.* Reduced mitochondrial DNA copy number is a biomarker of Parkinson's disease. *Neurobiol Aging* **38**, 216 e217-216 e210 (2016).
73. Schwartzenuber, A., *et al.* Oxidative switch drives mitophagy defects in dopaminergic parkin mutant patient neurons. *Sci Rep* **10**, 15485 (2020).
74. Hou, X., *et al.* Age- and disease-dependent increase of the mitophagy marker phospho-ubiquitin in normal aging and Lewy body disease. *Autophagy* **14**, 1404-1418 (2018).
75. Hruska, K.S., LaMarca, M.E., Scott, C.R. & Sidransky, E. Gaucher disease: mutation and polymorphism spectrum in the glucocerebrosidase gene (GBA). *Hum Mutat* **29**, 567-583 (2008).
76. Mazzulli, J.R., *et al.* Gaucher disease glucocerebrosidase and alpha-synuclein form a bidirectional pathogenic loop in synucleinopathies. *Cell* **146**, 37-52 (2011).
77. McNeill, A., *et al.* Ambroxol improves lysosomal biochemistry in glucocerebrosidase mutation-linked Parkinson disease cells. *Brain* **137**, 1481-1495 (2014).
78. Goker-Alpan, O., Stubblefield, B.K., Giasson, B.I. & Sidransky, E. Glucocerebrosidase is present in alpha-synuclein inclusions in Lewy body disorders. *Acta Neuropathol* **120**, 641-649 (2010).
79. Anderson, J.P., *et al.* Phosphorylation of Ser-129 is the dominant pathological modification of alpha-synuclein in familial and sporadic Lewy body disease. *J Biol Chem* **281**, 29739-29752 (2006).
80. Sanjeev, A. & Mattaparthi, V.S.K. Computational investigation on the effects of H50Q and G51D mutations on the  $\alpha$ -Synuclein aggregation propensity. *Journal of Biomolecular Structure and Dynamics* **36**, 2224-2236 (2018).
81. Hayakawa, H., *et al.* Structurally distinct  $\alpha$ -synuclein fibrils induce robust parkinsonian pathology. *Movement disorders : official journal of the Movement Disorder Society* **35**, 256-267 (2020).
82. Lashuel, H.A., *et al.*  $\alpha$ -Synuclein, Especially the Parkinson's Disease-associated Mutants, Forms Pore-like Annular and Tubular Protofibrils. *Journal of Molecular Biology* **322**, 1089-1102 (2002).
83. Li, J.-Y., *et al.* Lewy bodies in grafted neurons in subjects with Parkinson's disease suggest host-to-graft disease propagation. *Nature Medicine* **14**, 501-503 (2008).
84. Kordower, J.H., Chu, Y., Hauser, R.A., Freeman, T.B. & Olanow, C.W. Lewy body-like pathology in long-term embryonic nigral transplants in Parkinson's disease. *Nature Medicine* **14**, 504-506 (2008).
85. Desplats, P., *et al.* Inclusion formation and neuronal cell death through neuron-to-neuron transmission of alpha-synuclein. *Proceedings of the National Academy of Sciences of the United States of America* **106**, 13010-13015 (2009).
86. Masuda-Suzukake, M., *et al.* Prion-like spreading of pathological  $\alpha$ -synuclein in brain. *Brain : a journal of neurology* **136**, 1128-1138 (2013).
87. Hilton, D., *et al.* Accumulation of  $\alpha$ -synuclein in the bowel of patients in the pre-clinical phase of Parkinson's disease. *Acta Neuropathologica* **127**, 235-241 (2014).
88. Stokholm, M.G., Danielsen, E.H., Hamilton-Dutoit, S.J. & Borghammer, P. Pathological  $\alpha$ -synuclein in gastrointestinal tissues from prodromal Parkinson disease patients. *Annals of Neurology* **79**, 940-949 (2016).
89. Van Den Berge, N., *et al.* Evidence for bidirectional and trans-synaptic parasympathetic and sympathetic propagation of alpha-synuclein in rats. *Acta Neuropathol* **138**, 535-550 (2019).
90. Kim, S., *et al.* Transneuronal Propagation of Pathologic alpha-Synuclein from the Gut to the Brain Models Parkinson's Disease. *Neuron* **103**, 627-641 e627 (2019).

91. Gao, X., Chen H Fau - Schwarzschild, M.A., Schwarzschild Ma Fau - Ascherio, A. & Ascherio, A. Use of ibuprofen and risk of Parkinson disease. *Neurology* **76**, 863-869 (2011).
92. Racette, B.A., *et al.* Immunosuppressants and risk of Parkinson disease. *Ann Clin Transl Neurol* **5**, 870-875 (2018).
93. McGeer, P.L., Itagaki, S., Boyes, B.E. & McGeer, E.G. Reactive microglia are positive for HLA-DR in the substantia nigra of Parkinson's and Alzheimer's disease brains. *Neurology* **38**, 1285-1291 (1988).
94. Gerhard, A., *et al.* In vivo imaging of microglial activation with [11C](R)-PK11195 PET in idiopathic Parkinson's disease. *Neurobiology of disease* **21**, 404-412 (2006).
95. Williams-Gray, C.H., *et al.* Serum immune markers and disease progression in an incident Parkinson's disease cohort (ICICLE-PD). *Mov Disord* **31**, 995-1003 (2016).
96. Greenland, J.C., *et al.* Azathioprine immunosuppression and disease modification in Parkinson's disease (AZA-PD): a randomised double-blind placebo-controlled phase II trial protocol. *BMJ Open* **10**, e040527 (2020).
97. Marras, C., Lang, A.E., Austin, P.C., Lau, C. & Urbach, D.R. Appendectomy in mid and later life and risk of Parkinson's disease: A population-based study. *Mov Disord* **31**, 1243-1247 (2016).
98. Kim, R., Lee, J.Y., Park, S., Han, K. & Shin, C.M. Cholecystectomy and subsequent risk of Parkinson's disease: a nationwide retrospective cohort study. *NPJ Parkinsons Dis* **7**, 100 (2021).
99. Malagelada, J.R., Go, V.L.W., Summerskill, W.H.J. & Gamble, W.S. Bile acid secretion and biliary bile acid composition altered by cholecystectomy. *The American Journal of Digestive Diseases* **18**, 455-459 (1973).
100. Hepner, G.W., Hofmann, A.F., Malagelada, J.R., Szczepanik, P.A. & Klein, P.D. Increased Bacterial Degradation of Bile Acids in Cholecystectomized Patients. *Gastroenterology* **66**, 556-564 (1974).
101. Kullak-Ublick, G.-A., Paumgartner, G. & Berr, F. Long-term effects of cholecystectomy on bile acid metabolism. *Hepatology* **21**, 41-45 (1995).
102. Chen, M.L., Takeda, K. & Sundrud, M.S. Emerging roles of bile acids in mucosal immunity and inflammation. *Mucosal Immunology* **12**, 851-861 (2019).
103. Pavlidis, P., *et al.* Systematic review: bile acids and intestinal inflammation-luminal aggressors or regulators of mucosal defence? *Alimentary Pharmacology & Therapeutics* **42**, 802-817 (2015).
104. Grant, S.M. & DeMorrow, S. Bile Acid Signaling in Neurodegenerative and Neurological Disorders. *Int J Mol Sci* **21**, 5982 (2020).
105. Huang, F., *et al.* Deletion of mouse FXR gene disturbs multiple neurotransmitter systems and alters neurobehavior. *Front Behav Neurosci* **9**, 70-70 (2015).
106. McMillin, M., *et al.* TGR5 signaling reduces neuroinflammation during hepatic encephalopathy. *Journal of neurochemistry* **135**, 565-576 (2015).
107. McMillin, M., *et al.* Bile Acid-Mediated Sphingosine-1-Phosphate Receptor 2 Signaling Promotes Neuroinflammation during Hepatic Encephalopathy in Mice. *Frontiers in cellular neuroscience* **11**, 191-191 (2017).
108. Romano, S., *et al.* Meta-analysis of the Parkinson's disease gut microbiome suggests alterations linked to intestinal inflammation. *NPJ Parkinsons Dis* **7**, 27 (2021).
109. Li, P., *et al.* Gut Microbiota Dysbiosis Is Associated with Elevated Bile Acids in Parkinson's Disease. *Metabolites* **11**(2021).
110. Shao, Y., *et al.* Comprehensive metabolic profiling of Parkinson's disease by liquid chromatography-mass spectrometry. *Mol Neurodegener* **16**, 4 (2021).
111. Graham, S.F., *et al.* Metabolomic Profiling of Bile Acids in an Experimental Model of Prodromal Parkinson's Disease. *Metabolites* **8**(2018).
112. Parkinson Study Group. DATATOP: a multicenter controlled clinical trial in early Parkinson's disease. Parkinson Study Group. *Arch Neurol* **46**, 1052-1060 (1989).

113. Snow, B.J., *et al.* A double-blind, placebo-controlled study to assess the mitochondria-targeted antioxidant MitoQ as a disease-modifying therapy in Parkinson's disease. *Mov Disord* **25**, 1670-1674 (2010).
114. The Parkinson Study Group QE3 Investigators, *et al.* A randomized clinical trial of high-dosage coenzyme Q10 in early Parkinson disease: no evidence of benefit. *JAMA Neurol* **71**, 543-552 (2014).
115. Writing Group for the NINDS Exploratory Trials in Parkinson Disease (NET-PD) Investigators, *et al.* Effect of creatine monohydrate on clinical progression in patients with Parkinson disease: a randomized clinical trial. *JAMA* **313**, 584-593 (2015).
116. The Parkinson Study Group SURE-PD3 Investigators, *et al.* Effect of Urate-Elevating Inosine on Early Parkinson Disease Progression: The SURE-PD3 Randomized Clinical Trial. *JAMA* **326**, 926-939 (2021).
117. Jankovic, J., *et al.* Variable expression of Parkinson's disease. *A base-line analysis of the DAT ATOP cohort* **40**, 1529-1529 (1990).
118. Stebbins, G.T., *et al.* How to identify tremor dominant and postural instability/gait difficulty groups with the movement disorder society unified Parkinson's disease rating scale: comparison with the unified Parkinson's disease rating scale. *Mov Disord* **28**, 668-670 (2013).
119. Alves, G., Larsen, J.P., Emre, M., Wentzel-Larsen, T. & Aarsland, D. Changes in motor subtype and risk for incident dementia in Parkinson's disease. *Movement Disorders* **21**, 1123-1130 (2006).
120. Simuni, T., *et al.* How stable are Parkinson's disease subtypes in de novo patients: Analysis of the PPMI cohort? *Parkinsonism Relat Disord* **28**, 62-67 (2016).
121. Aleksovski, D., Miljkovic, D., Bravi, D. & Antonini, A. Disease progression in Parkinson subtypes: the PPMI dataset. *Neurol Sci* **39**, 1971-1976 (2018).
122. Goetz, C.G., *et al.* Movement Disorder Society-sponsored revision of the Unified Parkinson's Disease Rating Scale (MDS-UPDRS): scale presentation and clinimetric testing results. *Mov Disord* **23**, 2129-2170 (2008).
123. Post, B., Merkus, M.P., de Bie, R.M., de Haan, R.J. & Speelman, J.D. Unified Parkinson's disease rating scale motor examination: are ratings of nurses, residents in neurology, and movement disorders specialists interchangeable? *Mov Disord* **20**, 1577-1584 (2005).
124. Chaudhuri, K.R., *et al.* The metric properties of a novel non-motor symptoms scale for Parkinson's disease: Results from an international pilot study. *Mov Disord* **22**, 1901-1911 (2007).
125. Jenkinson, C., Fitzpatrick, R., Peto, V., Greenhall, R. & Hyman, N. The Parkinson's Disease Questionnaire (PDQ-39): development and validation of a Parkinson's disease summary index score. *Age and ageing* **26**, 353-357 (1997).
126. Del Din, S., *et al.* Gait analysis with wearables predicts conversion to parkinson disease. *Ann Neurol* **86**, 357-367 (2019).
127. Buckley, C., Galna, B., Rochester, L. & Mazzà, C. Upper body accelerations as a biomarker of gait impairment in the early stages of Parkinson's disease. *Gait & Posture* **71**, 289-295 (2019).
128. Rehman, R.Z.U., *et al.* Accelerometry-Based Digital Gait Characteristics for Classification of Parkinson's Disease: What Counts? *IEEE Open Journal of Engineering in Medicine and Biology* **1**, 65-73 (2020).
129. Wilson, J., *et al.* Cholinergic Basal Forebrain Volumes Predict Gait Decline in Parkinson's Disease. *Movement disorders : official journal of the Movement Disorder Society* **36**, 611-621 (2021).
130. Wilson, J., *et al.* Gait Progression Over 6 Years in Parkinson's Disease: Effects of Age, Medication, and Pathology. *Frontiers in Aging Neuroscience* **12**(2020).
131. Kluge, A.F., *et al.* Novel highly selective inhibitors of ubiquitin specific protease 30 (USP30) accelerate mitophagy. *Bioorganic & Medicinal Chemistry Letters* **28**, 2655-2659 (2018).

132. Prasuhn, J., *et al.* An omics-based strategy using coenzyme Q10 in patients with Parkinson's disease: concept evaluation in a double-blind randomized placebo-controlled parallel group trial. *Neurol Res Pract* **1**, 31 (2019).
133. Gmitterova, K., *et al.* 8-OHdG in cerebrospinal fluid as a marker of oxidative stress in various neurodegenerative diseases. *Neuro-degenerative diseases* **6**, 263-269 (2009).
134. Abe, T., Isobe, C., Murata, T., Sato, C. & Tohgi, H. Alteration of 8-hydroxyguanosine concentrations in the cerebrospinal fluid and serum from patients with Parkinson's disease. *Neurosci Lett* **336**, 105-108 (2003).
135. Mortiboys, H., *et al.* Translational approaches to restoring mitochondrial function in Parkinson's disease. *FEBS Lett* **592**, 776-792 (2018).
136. Lewitt, P.A., *et al.* 3-hydroxykynurenine and other Parkinson's disease biomarkers discovered by metabolomic analysis. *Mov Disord* **28**, 1653-1660 (2013).
137. Konings, C.H., *et al.* Normal cerebrospinal fluid glutathione concentrations in Parkinson's disease, Alzheimer's disease and multiple system atrophy. *Journal of the neurological sciences* **168**, 112-115 (1999).
138. Waragai, M., *et al.* Increased level of DJ-1 in the cerebrospinal fluids of sporadic Parkinson's disease. *Biochemical and biophysical research communications* **345**, 967-972 (2006).
139. Herbert, M.K., *et al.* CSF levels of DJ-1 and tau distinguish MSA patients from PD patients and controls. *Parkinsonism Relat Disord* **20**, 112-115 (2014).
140. Hong, Z., *et al.* DJ-1 and alpha-synuclein in human cerebrospinal fluid as biomarkers of Parkinson's disease. *Brain* **133**, 713-726 (2010).
141. Shi, M., *et al.* Significance and confounders of peripheral DJ-1 and alpha-synuclein in Parkinson's disease. *Neurosci Lett* **480**, 78-82 (2010).
142. Waragai, M., *et al.* Plasma levels of DJ-1 as a possible marker for progression of sporadic Parkinson's disease. *Neurosci Lett* **425**, 18-22 (2007).
143. Maita, C., *et al.* Secretion of DJ-1 into the serum of patients with Parkinson's disease. *Neurosci Lett* **431**, 86-89 (2008).
144. Chen, C.M., *et al.* Increased oxidative damage in peripheral blood correlates with severity of Parkinson's disease. *Neurobiology of disease* **33**, 429-435 (2009).
145. Shukla, R., Rajani, M., Srivastava, N., Barthwal, M.K. & Dikshit, M. Nitrite and malondialdehyde content in cerebrospinal fluid of patients with Parkinson's disease. *The International journal of neuroscience* **116**, 1391-1402 (2006).
146. Burte, F., *et al.* metabolic profiling of Parkinson's disease and mild cognitive impairment. *Mov Disord* **32**, 927-932 (2017).
147. Pyle, A., *et al.* Reduced cerebrospinal fluid mitochondrial DNA is a biomarker for early-stage Parkinson's disease. *Ann Neurol* **78**, 1000-1004 (2015).
148. Podlesniy, P., *et al.* Low cerebrospinal fluid concentration of mitochondrial DNA in preclinical Alzheimer disease. *Annals of Neurology* **74**, 655-668 (2013).
149. Podlesniy, P., *et al.* Mitochondrial DNA in CSF distinguishes LRRK2 from idiopathic Parkinson's disease. *Neurobiology of disease* **94**, 10-17 (2016).
150. Davis, R.L., *et al.* Fibroblast growth factor 21 is a sensitive biomarker of mitochondrial disease. *Neurology* **81**, 1819-1826 (2013).
151. Davis, R.L., Liang, C. & Sue, C.M. A comparison of current serum biomarkers as diagnostic indicators of mitochondrial diseases. *Neurology* **86**, 2010-2015 (2016).
152. Yao, X., *et al.* Serum Growth Differentiation Factor 15 in Parkinson Disease. *Neuro-degenerative diseases* **17**, 251-260 (2017).
153. Davis, R.L., *et al.* Serum FGF-21, GDF-15, and blood mtDNA copy number are not biomarkers of Parkinson disease. *Neurol Clin Pract* **10**, 40-46 (2020).
154. Shen, C., Guo, Y., Luo, W., Lin, C. & Ding, M. Serum urate and the risk of Parkinson's disease: results from a meta-analysis. *Can J Neurol Sci* **40**, 73-79 (2013).
155. Gao, X., O'Reilly, É.J., Schwarzschild, M.A. & Ascherio, A. Prospective study of plasma urate and risk of Parkinson disease in men and women. *Neurology* **86**, 520-526 (2016).

156. Ascherio, A., *et al.* Urate as a predictor of the rate of clinical decline in Parkinson disease. *Arch Neurol* **66**, 1460-1468 (2009).
157. Koros, C., *et al.* Serum uric acid level as a putative biomarker in Parkinson's disease patients carrying GBA1 mutations: 2-Year data from the PPMI study. *Parkinsonism & Related Disorders* **84**, 1-4 (2021).
158. Koros, C., *et al.* Serum Uric Acid Level as a Biomarker in Idiopathic and Genetic (p.A53T Alpha-Synuclein Carriers) Parkinson's Disease: Data from the PPMI Study. *Journal of Parkinson's Disease* **10**, 481-487 (2020).
159. Mortiboys, H., *et al.* Mitochondrial function and morphology are impaired in parkin-mutant fibroblasts. *Ann Neurol* **64**, 555-565 (2008).
160. Auburger, G., *et al.* Primary skin fibroblasts as a model of Parkinson's disease. *Mol Neurobiol* **46**, 20-27 (2012).
161. Carling, P.J., *et al.* Deep phenotyping of peripheral tissue facilitates mechanistic disease stratification in sporadic Parkinson's disease. *Prog Neurobiol* **187**, 101772 (2020).
162. Meyer, K., *et al.* Direct conversion of patient fibroblasts demonstrates non-cell autonomous toxicity of astrocytes to motor neurons in familial and sporadic ALS. *Proc Natl Acad Sci U S A* **111**, 829-832 (2014).
163. Mertens, J., *et al.* Directly Reprogrammed Human Neurons Retain Aging-Associated Transcriptomic Signatures and Reveal Age-Related Nucleocytoplasmic Defects. *Cell Stem Cell* **17**, 705-718 (2015).
164. Milanese, C., *et al.* Peripheral mitochondrial function correlates with clinical severity in idiopathic Parkinson's disease. *Mov Disord* **34**, 1192-1202 (2019).
165. de Graaf, R.A. Basic Principles. in *In Vivo NMR Spectroscopy* 1-42 (John Wiley & Sons, Ltd., 2019).
166. de Graaf, R.A. In Vivo NMR Spectroscopy – Static Aspects. in *In Vivo NMR Spectroscopy* 43-128 (John Wiley & Sons, Ltd., 2019).
167. de Graaf, R.A. In Vivo NMR Spectroscopy – Dynamic Aspects. in *In Vivo NMR Spectroscopy* 129-210 (John Wiley & Sons, Ltd., 2019).
168. de Graaf, R.A. Magnetic Resonance Imaging. in *In Vivo NMR Spectroscopy* 211-252 (John Wiley & Sons, Ltd., 2019).
169. de Graaf, R.A. Radiofrequency Pulses. in *In Vivo NMR Spectroscopy* 253-291 (John Wiley & Sons, Ltd., 2019).
170. de Graaf, R.A. Spectroscopic Imaging and Multivolume Localization. in *In Vivo NMR Spectroscopy* 335-373 (John Wiley & Sons, Ltd., 2019).
171. Boer, V.O. & Klomp, D.W.J. Chapter 1.3 - Technical Considerations for Multivoxel Approaches and Magnetic Resonance Spectroscopic Imaging. in *Magnetic Resonance Spectroscopy* (eds. Stagg, C. & Rothman, D.) 31-39 (Academic Press, San Diego, 2014).
172. de Graaf, R.A. Chapter 1.4 - Spectral Editing and 2D NMR. in *Magnetic Resonance Spectroscopy* (eds. Stagg, C. & Rothman, D.) 40-48 (Academic Press, San Diego, 2014).
173. Juchem, C. & Rothman, D.L. Chapter 1.1 - Basis of Magnetic Resonance. in *Magnetic Resonance Spectroscopy* (eds. Stagg, C. & Rothman, D.) 3-14 (Academic Press, San Diego, 2014).
174. Lei, H., Xin, L., Gruetter, R. & Mlynárik, V. Chapter 1.2 - Localized Single-Voxel Magnetic Resonance Spectroscopy, Water Suppression, and Novel Approaches for Ultrashort Echo-Time Measurements. in *Magnetic Resonance Spectroscopy* (eds. Stagg, C. & Rothman, D.) 15-30 (Academic Press, San Diego, 2014).
175. Near, J. Chapter 1.5 - Spectral Quantification and Pitfalls in Interpreting Magnetic Resonance Spectroscopic Data: What To Look Out For. in *Magnetic Resonance Spectroscopy* (eds. Stagg, C. & Rothman, D.) 49-67 (Academic Press, San Diego, 2014).
176. Thulborn, K.R. & Atkinson, I.C. Chapter 4.1 - Quantitative Metabolic Magnetic Resonance Imaging of Sodium, Oxygen, Phosphorus and Potassium in the Human

- Brain: A Rationale for Bioscales in Clinical Applications. in *Magnetic Resonance Spectroscopy* (eds. Stagg, C. & Rothman, D.) 291-311 (Academic Press, San Diego, 2014).
177. Blüml, S. Magnetic Resonance Spectroscopy: Basics. in *MR Spectroscopy of Pediatric Brain Disorders* 11-23 (2013).
  178. Weinberg, B.D., Kuruva, M., Shim, H. & Mullins, M.E. Clinical Applications of Magnetic Resonance Spectroscopy in Brain Tumors: From Diagnosis to Treatment. *Radiol Clin North Am* **59**, 349-362 (2021).
  179. Rijma, A., van der Graaf, M., Meulenbroek, O., Olde Rikkert, M.G.M. & Heerschap, A. Altered brain high-energy phosphate metabolism in mild Alzheimer's disease: A 3-dimensional (31)P MR spectroscopic imaging study. *NeuroImage. Clinical* **18**, 254-261 (2018).
  180. Sassani, M., *et al.* Magnetic resonance spectroscopy reveals mitochondrial dysfunction in amyotrophic lateral sclerosis. *Brain* **143**, 3603-3618 (2020).
  181. Hu, M.T.M., *et al.* Cortical dysfunction in non-demented Parkinson's disease patients: A combined 31P-MRS and 18FDG-PET study. *Brain* **123**, 340-352 (2000).
  182. Provencher, S.W. Automatic quantitation of localized in vivo 1H spectra with LCModel. *NMR Biomed* **14**, 260-264 (2001).
  183. Vanhamme, L., van den Boogaart, A. & Van Huffel, S. Improved method for accurate and efficient quantification of MRS data with use of prior knowledge. *J Magn Reson* **129**, 35-43 (1997).
  184. Barbiroli, B., Iotti, S. & Lodi, R. Improved brain and muscle mitochondrial respiration with CoQ. An in vivo study by 31P-MR spectroscopy in patients with mitochondrial cytopathies. *Biofactors* **9**, 253-260 (1999).
  185. Barbiroli, B., *et al.* Phosphorus magnetic resonance spectroscopy in multiple system atrophy and Parkinson's disease. *Mov Disord* **14**, 430-435 (1999).
  186. Belanger, M., Allaman, I. & Magistretti, P.J. Brain energy metabolism: focus on astrocyte-neuron metabolic cooperation. *Cell Metab* **14**, 724-738 (2011).
  187. Rango, M., Bonifati, C. & Bresolin, N. Parkinson's disease and brain mitochondrial dysfunction: a functional phosphorus magnetic resonance spectroscopy study. *J Cereb Blood Flow Metab* **26**, 283-290 (2006).
  188. Rango, M., Dossi, G., Squarcina, L. & Bonifati, C. Brain mitochondrial impairment in early-onset Parkinson's disease with or without PINK1 mutation. *Mov Disord* **35**, 504-507 (2020).
  189. Hattingen, E., *et al.* Phosphorus and proton magnetic resonance spectroscopy demonstrates mitochondrial dysfunction in early and advanced Parkinson's disease. *Brain* **132**, 3285-3297 (2009).
  190. Bottomley, P.A. & Hardy, C.J. Rapid, reliable in vivo assays of human phosphate metabolites by nuclear magnetic resonance. *Clin Chem* **35**, 392-395 (1989).
  191. Hilker, R., *et al.* The bioenergetic status relates to dopamine neuron loss in familial PD with PINK1 mutations. *PLoS One* **7**, e51308 (2012).
  192. Weiduschat, N., *et al.* Usefulness of proton and phosphorus MR spectroscopic imaging for early diagnosis of Parkinson's disease. *J Neuroimaging* **25**, 105-110 (2015).
  193. Weiduschat, N., *et al.* Sex differences in cerebral energy metabolism in Parkinson's disease: a phosphorus magnetic resonance spectroscopic imaging study. *Parkinsonism Relat Disord* **20**, 545-548 (2014).
  194. Cai, R., *et al.* Enhancing glycolysis attenuates Parkinson's disease progression in models and clinical databases. *J Clin Invest* **129**, 4539-4549 (2019).
  195. Schultz, J.L., *et al.* A pilot to assess target engagement of terazosin in Parkinson's disease. *Parkinsonism Relat Disord* **94**, 79-83 (2022).
  196. Sathe, A.G., *et al.* Pharmacokinetics, Safety, and Tolerability of Orally Administered Ursodeoxycholic Acid in Patients With Parkinson's Disease-A Pilot Study. *J Clin Pharmacol* **60**, 744-750 (2020).
  197. Lei, H., Ugurbil, K. & Chen, W. Measurement of unidirectional Pi to ATP flux in human visual cortex at 7 T by using in vivo 31P magnetic resonance spectroscopy.

- Proceedings of the National Academy of Sciences of the United States of America* **100**, 14409-14414 (2003).
198. Nabuurs, C., Huijbregts, B., Wieringa, B., Hilbers, C.W. & Heerschap, A. 31P saturation transfer spectroscopy predicts differential intracellular macromolecular association of ATP and ADP in skeletal muscle. *The Journal of biological chemistry* **285**, 39588-39596 (2010).
  199. Peng, J., Liu, Q., Rao, M.S. & Zeng, X. Using human pluripotent stem cell-derived dopaminergic neurons to evaluate candidate Parkinson's disease therapeutic agents in MPP+ and rotenone models. *J Biomol Screen* **18**, 522-533 (2013).
  200. Mortiboys, H., Aasly, J. & Bandmann, O. Ursocholic acid rescues mitochondrial function in common forms of familial Parkinson's disease. *Brain* **136**, 3038-3050 (2013).
  201. Mortiboys, H., *et al.* UDCA exerts beneficial effect on mitochondrial dysfunction in LRRK2(G2019S) carriers and in vivo. *Neurology* **85**, 846-852 (2015).
  202. Chun, H.S. & Low, W.C. Ursodeoxycholic acid suppresses mitochondria-dependent programmed cell death induced by sodium nitroprusside in SH-SY5Y cells. *Toxicology* **292**, 105-112 (2012).
  203. Abdelkader, N.F., Safar, M.M. & Salem, H.A. Ursodeoxycholic Acid Ameliorates Apoptotic Cascade in the Rotenone Model of Parkinson's Disease: Modulation of Mitochondrial Perturbations. *Mol Neurobiol* **53**, 810-817 (2016).
  204. Castro-Caldas, M., *et al.* Tauroursodeoxycholic acid prevents MPTP-induced dopaminergic cell death in a mouse model of Parkinson's disease. *Mol Neurobiol* **46**, 475-486 (2012).
  205. Greene, L.A., Levy, O. & Malagelada, C. Akt as a victim, villain and potential hero in Parkinson's disease pathophysiology and treatment. *Cell Mol Neurobiol* **31**, 969-978 (2011).
  206. Abbas, G. & Lindor, K.D. Pharmacological treatment of biliary cirrhosis with ursodeoxycholic acid. *Expert opinion on pharmacotherapy* **11**, 387-392 (2010).
  207. Lazaridis, K.N., Gores, G.J. & Lindor, K.D. Ursodeoxycholic acid 'mechanisms of action and clinical use in hepatobiliary disorders'. *J Hepatol* **35**, 134-146 (2001).
  208. Bell, S.M., *et al.* Ursodeoxycholic Acid Improves Mitochondrial Function and Redistributes Drp1 in Fibroblasts from Patients with Either Sporadic or Familial Alzheimer's Disease. *J Mol Biol* **430**, 3942-3953 (2018).
  209. Parry, G.J., *et al.* Safety, tolerability, and cerebrospinal fluid penetration of ursodeoxycholic Acid in patients with amyotrophic lateral sclerosis. *Clinical neuropharmacology* **33**, 17-21 (2010).
  210. Kim, H.M., *et al.* Prediction of cognitive progression in Parkinson's disease using three cognitive screening measures. *Clin Park Relat Disord* **1**, 91-97 (2019).
  211. Tomlinson, C.L., *et al.* Systematic review of levodopa dose equivalency reporting in Parkinson's disease. *Mov Disord* **25**, 2649-2653 (2010).
  212. Holden, S.K., Finseth, T., Sillau, S.H. & Berman, B.D. Progression of MDS-UPDRS Scores Over Five Years in De Novo Parkinson Disease from the Parkinson's Progression Markers Initiative Cohort. *Mov Disord Clin Pract* **5**, 47-53 (2018).
  213. Hoehn, M.M. & Yahr, M.D. Parkinsonism: onset, progression and mortality. *Neurology* **17**, 427-442 (1967).
  214. Goetz, C.G., *et al.* Movement Disorder Society Task Force report on the Hoehn and Yahr staging scale: status and recommendations. *Mov Disord* **19**, 1020-1028 (2004).
  215. Blauwendraat, C., *et al.* NeuroChip, an updated version of the NeuroX genotyping platform to rapidly screen for variants associated with neurological diseases. *Neurobiol Aging* **57**, 247 e249-247 e213 (2017).
  216. RA, d.G. Spectral Quantification. in *In Vivo MR Spectroscopy* 445-477 (John Wiley & Sons, Ltd, 2007).
  217. Wilson, M., *et al.* Methodological consensus on clinical proton MRS of the brain: Review and recommendations. *Magn Reson Med* **82**, 527-550 (2019).

218. Cichocka, M., Kozub, J. & Urbanik, A. PH Measurements of the Brain Using Phosphorus Magnetic Resonance Spectroscopy ((31)PMRS) in Healthy Men - Comparison of Two Analysis Methods. *Polish journal of radiology* **80**, 509-514 (2015).
219. Iotti, S., *et al.* In vivo assessment of free magnesium concentration in human brain by 31P MRS. A new calibration curve based on a mathematical algorithm. *NMR Biomed* **9**, 24-32 (1996).
220. Iotti, S., Frassinetti, C., Sabatini, A., Vacca, A. & Barbiroli, B. Quantitative mathematical expressions for accurate in vivo assessment of cytosolic [ADP] and DeltaG of ATP hydrolysis in the human brain and skeletal muscle. *Biochim Biophys Acta* **1708**, 164-177 (2005).
221. Barbiroli, B., *et al.* Defective brain energy metabolism shown by in vivo 31P MR spectroscopy in 28 patients with mitochondrial cytopathies. *J Cereb Blood Flow Metab* **13**, 469-474 (1993).
222. Minati, L., Aquino, D., Bruzzone, M.G. & Erbetta, A. Quantitation of normal metabolite concentrations in six brain regions by in-vivoH-MR spectroscopy. *J Med Phys* **35**, 154-163 (2010).
223. Hangel, G., *et al.* Inter-subject stability and regional concentration estimates of 3D-FID-MRSI in the human brain at 7 T. *NMR in Biomedicine* **34**, e4596 (2021).
224. Tal, A., Kirov, II, Grossman, R.I. & Gonen, O. The role of gray and white matter segmentation in quantitative proton MR spectroscopic imaging. *NMR Biomed* **25**, 1392-1400 (2012).
225. Wright, I.C., *et al.* A voxel-based method for the statistical analysis of gray and white matter density applied to schizophrenia. *Neuroimage* **2**, 244-252 (1995).
226. Sarafian, M.H., *et al.* Bile acid profiling and quantification in biofluids using ultra-performance liquid chromatography tandem mass spectrometry. *Anal Chem* **87**, 9662-9670 (2015).
227. Bertoni-Freddari, C., *et al.* Role of Mitochondrial Deterioration in Physiological and Pathological Brain Aging. *Gerontology* **50**, 187-192 (2004).
228. Forester, B.P., *et al.* Age-related changes in brain energetics and phospholipid metabolism. *NMR Biomed* **23**, 242-250 (2010).
229. Folstein, M.F., Folstein, S.E. & McHugh, P.R. "Mini-mental state": A practical method for grading the cognitive state of patients for the clinician. *Journal of Psychiatric Research* **12**, 189-198 (1975).
230. Creavin, S.T., *et al.* Mini-Mental State Examination (MMSE) for the detection of dementia in clinically unevaluated people aged 65 and over in community and primary care populations. *Cochrane Database Syst Rev*, CD011145 (2016).
231. Allen, S.P., *et al.* Superoxide dismutase 1 mutation in a cellular model of amyotrophic lateral sclerosis shifts energy generation from oxidative phosphorylation to glycolysis. *Neurobiology of Aging* **35**, 1499-1509 (2014).
232. Benjamini, Y. & Hochberg, Y. Controlling the False Discovery Rate: A Practical and Powerful Approach to Multiple Testing. *Journal of the Royal Statistical Society: Series B (Methodological)* **57**, 289-300 (1995).
233. Evans, L.D. A two-score composite program for combining standard scores. *Behavior Research Methods, Instruments, & Computers* **28**, 209-213 (1996).
234. Yang, W., *et al.* Current and projected future economic burden of Parkinson's disease in the U.S. *NPJ Parkinsons Dis* **6**, 15 (2020).
235. Borsche, M., Pereira, S.L., Klein, C. & Grunewald, A. Mitochondria and Parkinson's Disease: Clinical, Molecular, and Translational Aspects. *J Parkinsons Dis* **11**, 45-60 (2021).
236. Zambrano, K., *et al.* Fighting Parkinson's disease: The return of the mitochondria. *Mitochondrion* **64**, 34-44 (2022).
237. NINDS Exploratory Trials in Parkinson Disease (NET-PD) FS-ZONE Investigators. Pioglitazone in early Parkinson's disease: a phase 2, multicentre, double-blind, randomised trial. *Lancet Neurol* **14**, 795-803 (2015).

238. Cuevas, E., *et al.* Tauroursodeoxycholic acid (TUDCA) is neuroprotective in a chronic mouse model of Parkinson's disease. *Nutr Neurosci*, 1-18 (2020).
239. Rosa, A.I., *et al.* Tauroursodeoxycholic Acid Improves Motor Symptoms in a Mouse Model of Parkinson's Disease. *Mol Neurobiol* **55**, 9139-9155 (2018).
240. Moreira, S., *et al.* Nrf2 activation by tauroursodeoxycholic acid in experimental models of Parkinson's disease. *Exp Neurol* **295**, 77-87 (2017).
241. Goulis, J., Leandro, G. & Burroughs, A.K. Randomised controlled trials of ursodeoxycholic-acid therapy for primary biliary cirrhosis: a meta-analysis. *Lancet* **354**, 1053-1060 (1999).
242. Cole, M.H., Silburn, P.A., Wood, J.M., Worringham, C.J. & Kerr, G.K. Falls in Parkinson's disease: kinematic evidence for impaired head and trunk control. *Mov Disord* **25**, 2369-2378 (2010).
243. Hubble, R.P., Naughton, G.A., Silburn, P.A. & Cole, M.H. Wearable sensor use for assessing standing balance and walking stability in people with Parkinson's disease: a systematic review. *PLoS One* **10**, e0123705 (2015).
244. Payne, T., *et al.* Ursodeoxycholic acid as a novel disease-modifying treatment for Parkinson's disease: protocol for a two-centre, randomised, double-blind, placebo-controlled trial, The 'UP' study. *BMJ Open* **10**, e038911 (2020).
245. Nasreddine, Z.S., *et al.* The Montreal Cognitive Assessment, MoCA: a brief screening tool for mild cognitive impairment. *Journal of the American Geriatrics Society* **53**, 695-699 (2005).
246. Montgomery, S.A. & Asberg, M. A new depression scale designed to be sensitive to change. *Br J Psychiatry* **134**, 382-389 (1979).
247. Chaudhuri, K.R., *et al.* International multicenter pilot study of the first comprehensive self-completed nonmotor symptoms questionnaire for Parkinson's disease: the NMSQuest study. *Mov Disord* **21**, 916-923 (2006).
248. Richards, S., *et al.* Standards and guidelines for the interpretation of sequence variants: a joint consensus recommendation of the American College of Medical Genetics and Genomics and the Association for Molecular Pathology. *Genet Med* **17**, 405-424 (2015).
249. Wolfer, A.M., *et al.* peakPantheR, an R package for large-scale targeted extraction and integration of annotated metabolic features in LC-MS profiling datasets. *Bioinformatics* **37**, 4886-4888 (2021).
250. Trojaniello, D., Ravaschio, A., Hausdorff, J.M. & Cereatti, A. Comparative assessment of different methods for the estimation of gait temporal parameters using a single inertial sensor: application to elderly, post-stroke, Parkinson's disease and Huntington's disease subjects. *Gait Posture* **42**, 310-316 (2015).
251. Spain, R.I., *et al.* Body-worn motion sensors detect balance and gait deficits in people with multiple sclerosis who have normal walking speed. *Gait Posture* **35**, 573-578 (2012).
252. Moe-Nilssen, R. & Helbostad, J.L. Estimation of gait cycle characteristics by trunk accelerometry. *J Biomech* **37**, 121-126 (2004).
253. Galna, B., Lord, S. & Rochester, L. Is gait variability reliable in older adults and Parkinson's disease? Towards an optimal testing protocol. *Gait Posture* **37**, 580-585 (2013).
254. Moe-Nilssen, R. A new method for evaluating motor control in gait under real-life environmental conditions. Part 1: The instrument. *Clin Biomech* **13**, 320-327 (1998).
255. Angelini, L., *et al.* Is a Wearable Sensor-Based Characterisation of Gait Robust Enough to Overcome Differences Between Measurement Protocols? A Multi-Centric Pragmatic Study in Patients with Multiple Sclerosis. *Sensors* **20**, 79 (2019).
256. Salarian, A., *et al.* Gait assessment in Parkinson's disease: toward an ambulatory system for long-term monitoring. *IEEE Trans Biomed Eng* **51**, 1434-1443 (2004).
257. Ordidge, R.J., Connelly, A. & Lohman, J.A.B. Image-selected in Vivo spectroscopy (ISIS). A new technique for spatially selective nmr spectroscopy. *J Magn Reson* **66**, 283-294 (1986).

258. Ordidge, R.J., Bowley, R.M. & McHale, G. A general approach to selection of multiple cubic volume elements using the ISIS technique. *Magn Reson Med* **8**, 323-331 (1988).
259. Stefan, D., *et al.* Quantitation of magnetic resonance spectroscopy signals: the jMRUI software package. *Meas Sci Technol* **20**(2009).
260. de Graaf, R.A. Spectral Quantification. in *In Vivo NMR Spectroscopy* 439-471 (John Wiley & Sons, Ltd., 2019).
261. Iotti, S. & Malucelli, E. In vivo assessment of Mg<sup>2+</sup> in human brain and skeletal muscle by <sup>31</sup>P-MRS. *Magnes Res* **21**, 157-162 (2008).
262. Schmitz, B., *et al.* Effects of Aging on the Human Brain: A Proton and Phosphorus MR Spectroscopy Study at 3T. *J Neuroimaging* **28**, 416-421 (2018).
263. Athauda, D., *et al.* Exenatide once weekly versus placebo in Parkinson's disease: a randomised, double-blind, placebo-controlled trial. *Lancet* **390**, 1664-1675 (2017).
264. Goetz, C.G., *et al.* Handling missing values in the MDS-UPDRS. *Mov Disord* **30**, 1632-1638 (2015).
265. Ward, A., Brogden, R.N., Heel, R.C., Speight, T.M. & Avery, G.S. Ursodeoxycholic acid: a review of its pharmacological properties and therapeutic efficacy. *Drugs* **27**, 95-131 (1984).
266. Simuni, T., *et al.* Efficacy of Nilotinib in Patients With Moderately Advanced Parkinson Disease: A Randomized Clinical Trial. *JAMA Neurol* **78**, 312-320 (2021).
267. Pagan, F.L., *et al.* Nilotinib Effects on Safety, Tolerability, and Potential Biomarkers in Parkinson Disease: A Phase 2 Randomized Clinical Trial. *JAMA Neurol* **77**, 309-317 (2020).
268. Vaz, A.R., *et al.* Bilirubin selectively inhibits cytochrome c oxidase activity and induces apoptosis in immature cortical neurons: assessment of the protective effects of glycooursodeoxycholic acid. *J Neurochem* **112**, 56-65 (2010).
269. Brito, M.A., *et al.* Bilirubin injury to neurons: contribution of oxidative stress and rescue by glycooursodeoxycholic acid. *Neurotoxicology* **29**, 259-269 (2008).
270. Li, H., *et al.* Ursodeoxycholic Acid Treatment Restores Gut Microbiota and Alleviates Liver Inflammation in Non-Alcoholic Steatohepatic Mouse Model. *Front Pharmacol* **12**, 788558 (2021).
271. Tang, R., *et al.* Gut microbial profile is altered in primary biliary cholangitis and partially restored after UDCA therapy. *Gut* **67**, 534-541 (2018).
272. Whone, A., *et al.* Randomized trial of intermittent intraputamenal glial cell line-derived neurotrophic factor in Parkinson's disease. *Brain* **142**, 512-525 (2019).
273. Kieburtz, K., Katz, R., McGarry, A. & Olanow, C.W. A New Approach to the Development of Disease-Modifying Therapies for PD; Fighting Another Pandemic. *Mov Disord* **36**, 59-63 (2021).
274. Mico-Amigo, M.E., *et al.* Potential Markers of Progression in Idiopathic Parkinson's Disease Derived From Assessment of Circular Gait With a Single Body-Fixed-Sensor: A 5 Year Longitudinal Study. *Front Hum Neurosci* **13**, 59 (2019).
275. Hobert, M.A., *et al.* Progressive Gait Deficits in Parkinson's Disease: A Wearable-Based Biannual 5-Year Prospective Study. *Front Aging Neurosci* **11**, 22 (2019).
276. Amboni, M., *et al.* Step length predicts executive dysfunction in Parkinson's disease: a 3-year prospective study. *J Neurol* **265**, 2211-2220 (2018).
277. Galna, B., Lord, S., Burn, D.J. & Rochester, L. Progression of gait dysfunction in incident Parkinson's disease: impact of medication and phenotype. *Mov Disord* **30**, 359-367 (2015).
278. van der Heide, A., Meinders, M.J., Bloem, B.R. & Helmich, R.C. The Impact of the COVID-19 Pandemic on Psychological Distress, Physical Activity, and Symptom Severity in Parkinson's Disease. *J Parkinsons Dis* **10**, 1355-1364 (2020).
279. Pissadaki, E.K. & Bolam, J.P. The energy cost of action potential propagation in dopamine neurons: clues to susceptibility in Parkinson's disease. *Front Comput Neurosci* **7**, 13 (2013).

280. Mullin, S., *et al.* Ambroxol for the Treatment of Patients With Parkinson Disease With and Without Glucocerebrosidase Gene Mutations: A Nonrandomized, Noncontrolled Trial. *JAMA Neurol* **77**, 427-434 (2020).
281. Chong, R., *et al.* Niacin Enhancement for Parkinson's Disease: An Effectiveness Trial. *Front Aging Neurosci* **13**, 667032 (2021).
282. Patel, D. & Witt, S.N. Ethanolamine and Phosphatidylethanolamine: Partners in Health and Disease. *Oxid Med Cell Longev* **2017**, 4829180 (2017).
283. Osman, C., Voelker, D.R. & Langer, T. Making heads or tails of phospholipids in mitochondria. *J Cell Biol* **192**, 7-16 (2011).
284. Riekkinen, P., Rinne, U.K., Pelliniemi, T.-T. & Sonninen, V. Interaction Between Dopamine and Phospholipids: Studies of the Substantia Nigra in Parkinson Disease Patients. *Archives of Neurology* **32**, 25-27 (1975).
285. Chang, K.-H., *et al.* Alterations of Sphingolipid and Phospholipid Pathways and Ornithine Level in the Plasma as Biomarkers of Parkinson's Disease. *Cells* **11**, 395 (2022).
286. Manyam, B.V., Ferraro, T.N. & Hare, T.A. Cerebrospinal Fluid Amino Compounds in Parkinson's Disease: Alterations due to Carbidopa/Levodopa. *Archives of Neurology* **45**, 48-50 (1988).
287. Brockmann, K., *et al.* GBA-associated PD. Neurodegeneration, altered membrane metabolism, and lack of energy failure. *Neurology* **79**, 213-220 (2012).
288. Bell, S.M., *et al.* Mitochondrial Dysfunction in Alzheimer's Disease: A Biomarker of the Future? *Biomedicines* **9**(2021).
289. Shi, X.-F., *et al.* Decreased brain PME/PDE ratio in bipolar disorder: a preliminary 31P magnetic resonance spectroscopy study. *Bipolar Disorders* **17**, 743-752 (2015).
290. Haszto, C.S., Stanley, J.A., Iyengar, S. & Prasad, K.M. Regionally Distinct Alterations in Membrane Phospholipid Metabolism in Schizophrenia: A Meta-analysis of Phosphorus Magnetic Resonance Spectroscopy Studies. *Biol Psychiatry Cogn Neurosci Neuroimaging* **5**, 264-280 (2020).
291. Vijjaratnam, N., Simuni, T., Bandmann, O., Morris, H.R. & Foltynie, T. Progress towards therapies for disease modification in Parkinson's disease. *The Lancet Neurology* **20**, 559-572 (2021).
292. Parker, W.D., Jr., Parks, J.K. & Swerdlow, R.H. Complex I deficiency in Parkinson's disease frontal cortex. *Brain Res* **1189**, 215-218 (2008).
293. Murphy, K.E., *et al.* Reduced glucocerebrosidase is associated with increased alpha-synuclein in sporadic Parkinson's disease. *Brain* **137**, 834-848 (2014).
294. Rakovic, A., *et al.* Mutations in PINK1 and Parkin impair ubiquitination of Mitofusins in human fibroblasts. *PLoS One* **6**, e16746 (2011).
295. Iles, R.A., Stevens, A.N., Griffiths, J.R. & Morris, P.G. Phosphorylation status of liver by 31P-n.m.r. spectroscopy, and its implications for metabolic control. A comparison of 31P-n.m.r. spectroscopy (in vivo and in vitro) with chemical and enzymic determinations of ATP, ADP and Pi. *Biochem J* **229**, 141-151 (1985).
296. Meyerspeer, M., *et al.* 31P magnetic resonance spectroscopy in skeletal muscle: Experts' consensus recommendations. *NMR in Biomedicine* **34**, e4246 (2021).
297. Lesage, S., *et al.* G51D alpha-synuclein mutation causes a novel parkinsonian-pyramidal syndrome. *Ann Neurol* **73**, 459-471 (2013).
298. Pankratz, N., *et al.* Parkin dosage mutations have greater pathogenicity in familial PD than simple sequence mutations. *Neurology* **73**, 279-286 (2009).
299. Lyamzaev, K.G., *et al.* Induction of autophagy by depolarization of mitochondria. *Autophagy* **14**, 921-924 (2018).
300. Ivankovic, D., Chau, K.Y., Schapira, A.H. & Gegg, M.E. Mitochondrial and lysosomal biogenesis are activated following PINK1/parkin-mediated mitophagy. *J Neurochem* **136**, 388-402 (2016).
301. Andres, R.H., Ducray, A.D., Schlattner, U., Wallimann, T. & Widmer, H.R. Functions and effects of creatine in the central nervous system. *Brain Res Bull* **76**, 329-343 (2008).

302. Das, N., Ren, J., Spence, J.S., Rackley, A. & Chapman, S.B. Relationship of Parieto-Occipital Brain Energy Phosphate Metabolism and Cognition Using (31)P MRS at 7-Tesla in Amnesic Mild Cognitive Impairment. *Frontiers in aging neuroscience* **12**, 222-222 (2020).
303. von Bartheld, C.S., Bahney, J. & Herculano-Houzel, S. The search for true numbers of neurons and glial cells in the human brain: A review of 150 years of cell counting. *J Comp Neurol* **524**, 3865-3895 (2016).
304. Yakhine-Diop, S.M.S., *et al.* Impaired Mitophagy and Protein Acetylation Levels in Fibroblasts from Parkinson's Disease Patients. *Mol Neurobiol* **56**, 2466-2481 (2019).
305. Matsuda, N., *et al.* PINK1 stabilized by mitochondrial depolarization recruits Parkin to damaged mitochondria and activates latent Parkin for mitophagy. *J Cell Biol* **189**, 211-221 (2010).
306. Diano, S., *et al.* Uncoupling protein 2 prevents neuronal death including that occurring during seizures: a mechanism for preconditioning. *Endocrinology* **144**, 5014-5021 (2003).
307. Bloem, B.R., Okun, M.S. & Klein, C. Parkinson's disease. *The Lancet* **397**, 2284-2303 (2021).
308. Grunewald, A., Kumar, K.R. & Sue, C.M. New insights into the complex role of mitochondria in Parkinson's disease. *Prog Neurobiol* **177**, 73-93 (2019).
309. Payne, T., *et al.* <sup>31</sup>Phosphorus magnetic resonance spectroscopy in Parkinson's disease demonstrates relationships with predicted disease progression and mitochondrial dysfunction in the peripheral tissue. (Manuscript in preparation for submission to *Annals of Neurology*, 2022).
310. van der Heeden, J.F., *et al.* Postural instability and gait are associated with severity and prognosis of Parkinson disease. *Neurology* **86**, 2243 (2016).
311. Lawson, R.A., *et al.* Which Neuropsychological Tests? Predicting Cognitive Decline and Dementia in Parkinson's Disease in the ICICLE-PD Cohort. *Journal of Parkinson's disease* **11**, 1297-1308 (2021).
312. Williams-Gray, C.H., *et al.* The distinct cognitive syndromes of Parkinson's disease: 5 year follow-up of the CamPaIGN cohort. *Brain* **132**, 2958-2969 (2009).
313. Haszto, C.S., Stanley, J.A., Iyengar, S. & Prasad, K.M. Regionally Distinct Alterations in Membrane Phospholipid Metabolism in Schizophrenia: A Meta-analysis of Phosphorus Magnetic Resonance Spectroscopy Studies. *Biol Psychiatry Cogn Neurosci Neuroimaging* **5**, 264-280 (2020).
314. Combs, H.L., Wyman-Chick, K.A., Erickson, L.O. & York, M.K. Development of standardized regression-based formulas to assess meaningful cognitive change in early Parkinson's disease. *Archives of Clinical Neuropsychology* **36**, 734-745 (2021).
315. Eickhoff, C.R., *et al.* Advanced brain ageing in Parkinson's disease is related to disease duration and individual impairment. *Brain Commun* **3**, fcab191-fcab191 (2021).
316. Ward, C.D. Does selegiline delay progression of Parkinson's disease? A critical re-evaluation of the DATATOP study. *J Neurol Neurosurg Psychiatry* **57**, 217-220 (1994).
317. Group, T.P.S. Cerebrospinal Fluid Homovanillic Acid in the DATATOP Study on Parkinson's Disease. *Archives of Neurology* **52**, 237-245 (1995).
318. Simon, D.K., *et al.* Peripheral Biomarkers of Parkinson's Disease Progression and Pioglitazone Effects. *J Parkinsons Dis* **5**, 731-736 (2015).
319. de Lau, L.M., Koudstaal, P.J., Hofman, A. & Breteler, M.M. Serum uric acid levels and the risk of Parkinson disease. *Ann Neurol* **58**, 797-800 (2005).
320. Athauda, D., *et al.* Utility of Neuronal-Derived Exosomes to Examine Molecular Mechanisms That Affect Motor Function in Patients With Parkinson Disease: A Secondary Analysis of the Exenatide-PD Trial. *JAMA Neurol* **76**, 420-429 (2019).
321. Horvath, K., *et al.* Minimal clinically important difference on the Motor Examination part of MDS-UPDRS. *Parkinsonism Relat Disord* **21**, 1421-1426 (2015).

322. Carroll, C.B., *et al.* Simvastatin as a neuroprotective treatment for Parkinson's disease (PD STAT): protocol for a double-blind, randomised, placebo-controlled futility study. *BMJ Open* **9**, e029740 (2019).
323. Mazzà, C., *et al.* Technical validation of real-world monitoring of gait: a multicentric observational study. *BMJ open* **11**, e050785-e050785 (2021).
324. Kimmeskamp, S. & Hennig, E.M. Heel to toe motion characteristics in Parkinson patients during free walking. *Clinical Biomechanics* **16**, 806-812 (2001).
325. Raffegeau, T.E., *et al.* A meta-analysis: Parkinson's disease and dual-task walking.
326. Del Din, S., Godfrey, A., Mazzà, C., Lord, S. & Rochester, L. Free-living monitoring of Parkinson's disease: Lessons from the field. *Movement Disorders* **31**, 1293-1313 (2016).
327. Lo, C., *et al.* A composite clinical motor score as a comprehensive and sensitive outcome measure for Parkinson's disease. *Journal of Neurology, Neurosurgery & Psychiatry* **93**, 617 (2022).
328. Wu, C.A.-O., *et al.* Responsiveness, Minimal Clinically Important Difference, and Validity of the MoCA in Stroke Rehabilitation.
329. Skorvanek, M., *et al.* Global scales for cognitive screening in Parkinson's disease: Critique and recommendations.
330. Rittman, T., *et al.* The Addenbrooke's Cognitive Examination for the differential diagnosis and longitudinal assessment of patients with parkinsonian disorders.
331. Lucza, T.A.-O.X., *et al.* Comparing Sensitivity and Specificity of Addenbrooke's Cognitive Examination-I, III and Mini-Addenbrooke's Cognitive Examination in Parkinson's Disease.
332. Vijjaratnam, N.A.-O., *et al.* Combining biomarkers for prognostic modelling of Parkinson's disease.
333. Greenland, J.C., Williams-Gray, C.H. & Barker, R.A. The clinical heterogeneity of Parkinson's disease and its therapeutic implications. *Eur J Neurosci* (2018).
334. Espay, A.J., *et al.* Biomarker-driven phenotyping in Parkinson's disease: A translational missing link in disease-modifying clinical trials. *Mov Disord* **32**, 319-324 (2017).
335. Bingol, B., *et al.* The mitochondrial deubiquitinase USP30 opposes parkin-mediated mitophagy. *Nature* **510**, 370-375 (2014).
336. Pettegrew, J.W., Panchalingam, K., Klunk, W.E., McClure, R.J. & Muenz, L.R. Alterations of cerebral metabolism in probable Alzheimer's disease: a preliminary study. *Neurobiol Aging* **15**, 117-132 (1994).
337. Ross, A.J. & Sachdev, P.S. Magnetic resonance spectroscopy in cognitive research. *Brain Research Reviews* **44**, 83-102 (2004).
338. Pavese, N. & Tai, Y.F. Nigrosome Imaging and Neuromelanin Sensitive MRI in Diagnostic Evaluation of Parkinsonism. *Movement disorders clinical practice* **5**, 131-140 (2018).
339. Cuenoud, B., *et al.* Brain NAD Is Associated With ATP Energy Production and Membrane Phospholipid Turnover in Humans. *Frontiers in aging neuroscience* **12**, 609517-609517 (2020).
340. Deus, C.M., *et al.* Mitochondrial remodeling in human skin fibroblasts from sporadic male Parkinson's disease patients uncovers metabolic and mitochondrial bioenergetic defects. *Biochim Biophys Acta Mol Basis Dis* **1866**, 165615 (2020).
341. Lapasset, L., *et al.* Rejuvenating senescent and centenarian human cells by reprogramming through the pluripotent state. *Genes Dev* **25**, 2248-2253 (2011).
342. Chang, C.-K., *et al.* Metabolic Alterations in Pancreatic Cancer Detected by In Vivo (1)H-MR Spectroscopy: Correlation with Normal Pancreas, PET Metabolic Activity, Clinical Stages, and Survival Outcome. *Diagnostics (Basel)* **11**, 1541 (2021).

## Appendices

### Appendix 1: Development of analysis protocol for <sup>31</sup>Phosphorus Magnetic Resonance Spectroscopy

In order to generate appropriate prior knowledge to use in the AMARES analysis, a manual analysis was first performed in 10 scans from healthy volunteers.

In line with previous literature and detailed in the methods section J-coupling constants for ATP multiplets were set at 18Hz as used in previous literature and soft constraints limited ATP linewidths to 5-35Hz.<sup>179,189</sup> Soft constraints were used to control linewidths for phosphocreatine (5-20Hz), and all other remaining resonances to 5-30Hz.<sup>180,216</sup> PCr was shifted to 0ppm prior to analysis.

To develop the soft constraints used to determine the peak of each resonance and the expected range for that resonance to be identified, manual peak assignment was performed in AMARES to assess the resulting peak frequency to then be used in the prior knowledge. The resulting manually identified peaks of each resonance for 10 control scans are displayed in Appendix Table 1. The mean is used as the starting point for the AMARES protocol. The ranges were used to guide the soft constraints on frequency ranges for each peak in conjunction with prior knowledge used in previous literature.<sup>179,180</sup> These ranges were further expanded to ensure that they would be capable of capturing the required resonance without either encroaching upon the expected frequency of the neighbouring resonances or capturing parts of the spectra that did not contain any resonant peaks to quantify.

<b>Resonance</b>	<b>Low</b>	<b>High</b>	<b>Mean</b>
PE	6.54	6.85	6.767
PC	6.18	6.45	6.296667
Pi	4.7	4.93	4.857
GPE	3.36	3.54	3.492
GPC	2.95	3	2.947
PCr	-0.08	0.08	0.006667
$\gamma$ -ATP resonance 1	-2.19	-2.51	-2.332
$\gamma$ -ATP resonance 2	-2.55	-2.77	-2.615
$\alpha$ -ATP resonance 1	-6.81	-7.44	-7.221
$\alpha$ -ATP resonance 2	-7.35	-7.75	-7.582
$\beta$ -ATP resonance 1	-15.33	-16.49	-15.809
$\beta$ -ATP resonance 2	-16.14	-16.99	-16.334
$\beta$ -ATP resonance 3	-16.58	-17.66	-16.955

**Appendix Table 1: means and ranges of manually defined  $^{31}\text{P}$ -MRS peaks in and linewidths in 10 healthy controls**

## Appendix 2: List of R packages used in data analysis

In addition to base R packages used for data handling and statistical analysis the following packages and their dependencies were installed, packages are shown in Appendix Table 2 below but not any further dependencies installed as part of those packages.

Package	Version	Use
corrplot	0.9	Data visualisation, correlation analysis
flextable	0.6.7	Data visualisation
ggpubr	0.4.0	Data visualisation, statistical analysis
ggrepel	0.9.1	Data visualisation
ggsci	2.9	Data visualisation
gridExtra	2.3	Data visualisation
Hmisc	4.5-0	Data handling, data visualisation
huxtable	5.4.0	Data visualisation
lme4	1.1-27.1	Statistical analysis of linear mixed effects models
lmerTest	3.1-3	Statistical analysis of linear mixed effects models
qwraps2	0.5.2	Data visualisation
rstatix	0.7.0	Data visualisation, statistical analysis
tidyverse	1.3.1	Data handling, data visualisation, statistical analysis

**Appendix Table 2: R packages used in analysis and presentation of all thesis data**